A GEOTECHNICAL CHARACTERISATION OF VOLCANIC SOILS IN RELATION TO COASTAL LANDSLIDING ON THE MAUNGATAPU PENINSULA, TAURANGA, NEW ZEALAND

A Thesis
submitted in partial fulfillment
of the requirements for the Degree
of
Master of Science in Engineering Geology
at the
University of Canterbury
by
Robert Craig Oliver

University of Canterbury
1997

FRONTISPIECE

Landslide at 330 Maungatapu Road

ABSTRACT

Maungatapu Peninsula is a northeast trending peninsula located within the Tauranga Basin covering an area of 1.6km^2. Maungatapu is underlain by a sequence of volcanic tephras, ashes and fluvial deposits derived both locally and from the Taupo Volcanic Zone. In late May 1995 three landslides occurred at 83, 85 and 89 Te Hono Street, and again in late December 1995 at 330 Maungatapu Road. The purpose of this study was to carry out a geotechnical investigation of these landslides, and to establish the mechanisms that produce cliff failure on the Peninsula.

Landslides were identified from aerial photographic interpretation and engineering geological mapping at a scale of 1:5000, and were classified as, 1) probable large scale block failures, 2) piping-triggered block failures, 3) wave erosion triggered block failures, and 4) colluvium/topsoil failures. Geotechnical core logging at a scale of 1:50 identified a number of stratigraphic units including the Post-Rotoehu Ash Tephras, Rotoehu Ash, Palaeosol, Hamilton Ash, Pahoia Tephras, Cross-bedded sequence, Upper Bounding Aquitard, Aquifer, and Lower Bounding Aquitard. The total thickness of the sequences are approximately 15m, and failures in 1995 were associated with a piping failure within the aquifer and lower section of the Cross-bedded sequence triggering a block landslide.

Geotechnical testing involved both field and laboratory testing to characterise the various stratigraphic units present within the logged cliff faces. In-situ shear strength testing indicated variable strength through out the profile, with the Palaeosol demonstrating the highest shear strength, and the Aquifer the lowest. This relationship was also confirmed by unconsolidated undrained triaxial laboratory testing. Clay mineralogy analysis indicated that the main constituent clays present were mixed layer 7 & 10 Å Halloysite and Allophanes. Atterberg Limit testing demonstrated a range of plasticities from low to very high. Direct shear testing indicated low cohesions and high friction angles for the Cross-bedded sequence and Aquifer, and a moderate cohesion and friction angle for the Lower Bounding Aquitard. Dispersion and Erodibility testing showed the Post-Rotoehu Ash Tephras, Rotoehu Ash, and Palaeosol to be non-dispersive and non-erodible, whilst the Cross-bedded sequence was dispersive and highly erodible. Both in-situ and laboratory permeability testing indicated low permeabilities associated with the stratigraphic units of the Peninsula.

From field and laboratory investigations a hydrogeological model was developed to explain the fast lag times delineated by plots of piezometric water level response to rainfall. The hydrogeological model combined components of a "defect controlled permeability model" and a "hydraulic head response model". The "defect controlled permeability model" indicates that these fast lag times can be produced by soakage water permeating through high permeability flow pathways such as exfoliation defects, fractures, and heavy bioturbation structures. The "hydraulic head response model" involves the rapid transferral of a pressure wave along the Aquifer and lower section of the Cross-bedded sequence in response to changes in the hydraulic head of the Peninsula due to recharge within a much larger catchment of approximately 5km^2.

Stability analysis using a non-circular failure mode was conducted for an increasing phreatic surface and landslide block size. The phreatic surface was related to piezometric water levels and showed that with an increase in the phreatic surface there was a decreased in the factor of safety by 0.1 from 1.0 to 0.9. Increasing the landslide block size was undertaken to determine whether larger blocks were likely to fail. From calculations it was concluded that failure of blocks greater than 10m back from the cliff edge were unlikely for the piping triggered model.

Two principal conclusions can be drawn from this study. Firstly a 2H:1V slope line projected back up to the Peninsula's surface from the base of the cliff delineating a geotechnical assessment zone is not a correct representation of the failure types threatening cliff top properties. Therefore, this assessment criteria should be reassessed, and a policy adopted where by any future development on a cliff top property should require a geotechnical report if deemed necessary by the Consents Officer from evidence of slope failures in adjoining properties or other evidence of instability on site. The second conclusion is that it takes approximately two months of double the average rainfall to produce adverse pore water conditions at the cliff edges where a rainfall event can trigger a piping-triggered block slide such.

TABLE OF CONTENTS

LIST OF FIGURES

LIST OF TABLES

Chapter One INTRODUCTION

1.1 PROJECT BACKGROUND

The Maungatapu Peninsula is one of a number of peninsulas situated in the Tauranga City area (Figure 1.1). Over the last 40 years the city of Tauranga has progressively increased in size due to its mild climate and central location within the North Island. This growth has led to many of the productive agricultural areas, such as the Maungatapu Peninsula, being rezoned for residential development. Since the late 1960's major housing development has occurred on Maungatapu Peninsula, gradually infilling the area and resulting in houses being constructed closer to the cliff edge to obtain a picturesque view of Tauranga Harbour.

On the evening of the 29 of May 1995, after a prolonged period of heavy rain, three shallow slips occurred on properties at 79, 85, and 89 Te Hono Street. The property owners contacted their insurers, who in turn contacted the Earthquake Commission. M^{C}larens (International Loss Adjusters) contracted Tonkin & Taylor on behalf of the Earthquake Commission to carry out geotechnical investigations at 85 and 89 Te Hono Street. The Tauranga District Council through its insurers, employed Babbage Consultants to report on the information available concerning the landsliding. In addition to this David Bell (Canterprise) was contracted to review all available information. From the various consultant recommendations three aspects were addressed:

1. The need to conduct a hydrogeological investigation on the eastern part of the peninsula,

2. Elimination of stromwater soakage on the eastern part of the peninsula by reticulating it to the street,

3. The possibility of a thesis to be undertaken to determine the geotechnical properties related to landsliding on Maungatapu Peninsula.

Thesis work commenced December 1995 after approval from Tauranga District Council.

1.2 THESIS OBJECTIVES

The principal objectives of this thesis are:

1. to carry out geotechnical investigations of the Maungatapu Peninsula area involving engineering geological mapping, geotechnical logging of the landslide scarps and borehole core, and sample collection to determine how geology and geomorphology influence landsliding;

2. to develop geotechnical models for the identified slope failure types;

3. to determine the geotechnical properties of the soil materials relevant to landslide assessment;

4. to assess the degree to which the hydrological regime influences failure types, and to develop a hydrogeological model;

5. to examine the hazard assessment guidelines for coastal landsliding, and to reassess these guidelines in relation to Maungatapu Peninsula;

This thesis is intended to provide additional data in conjunction with already existing information, to better aid planning in the future residential developmental use of Maungatapu Peninsula.

1.3 GEOLOGY OF THE TAURANGA BASIN

1.3.1 Regional Setting

a) Location

The Tauranga Basin is a 570 km^2 fluvial/estuarine basin of which approximately 200 km^2 is occupied by a shallow mesotidal estuarine lagoon (Healy and Kirk, 1982). The Tauranga Harbour is 35 km long by an average of 5 km wide, and trends in a northwest to southeast direction along the Bay of Plenty coastline. The harbour is blocked to the sea by a 25 km long barrier island (Matakana Island), and at either end by tombolos at Bowentown and Mt. Maunganui (Figure 1.1). The entrances to the harbour are marked by two rhyolite domes, Bowentown and Mount Maunganui. A number of rivers and streams drain into the harbour, with the Wairoa River being the largest.

b) Physiography and Geological Setting

The Tauranga Basin is bounded on the N to NW side by the Kaimai Range, which has been uplifted by movement on the Hauraki Fault some time after the emplacement of the Waiteariki Ignimbrite at 0.84 Ma. (Kohn, 1973). The Kaimai Range represents a block of Miocene-Pliocene basaltic to rhyolitic volcanic rocks (Briggs et al., 1996).

Southeast of the Kaimai Range is the Whakamarama Plateau, which slopes gently towards the northeast at approximately 3 - 5° (Briggs et. al., 1996). The plateau consists of the Aongatete and Waiteariki Ignimbrites, and forms the local basement of the western Tauranga Basin (Table 1.1). Located within the Whakamarama Plateau are the oldest volcanics in the basin, the Minden Rhyolites at 2.36 - 2.28 Ma.

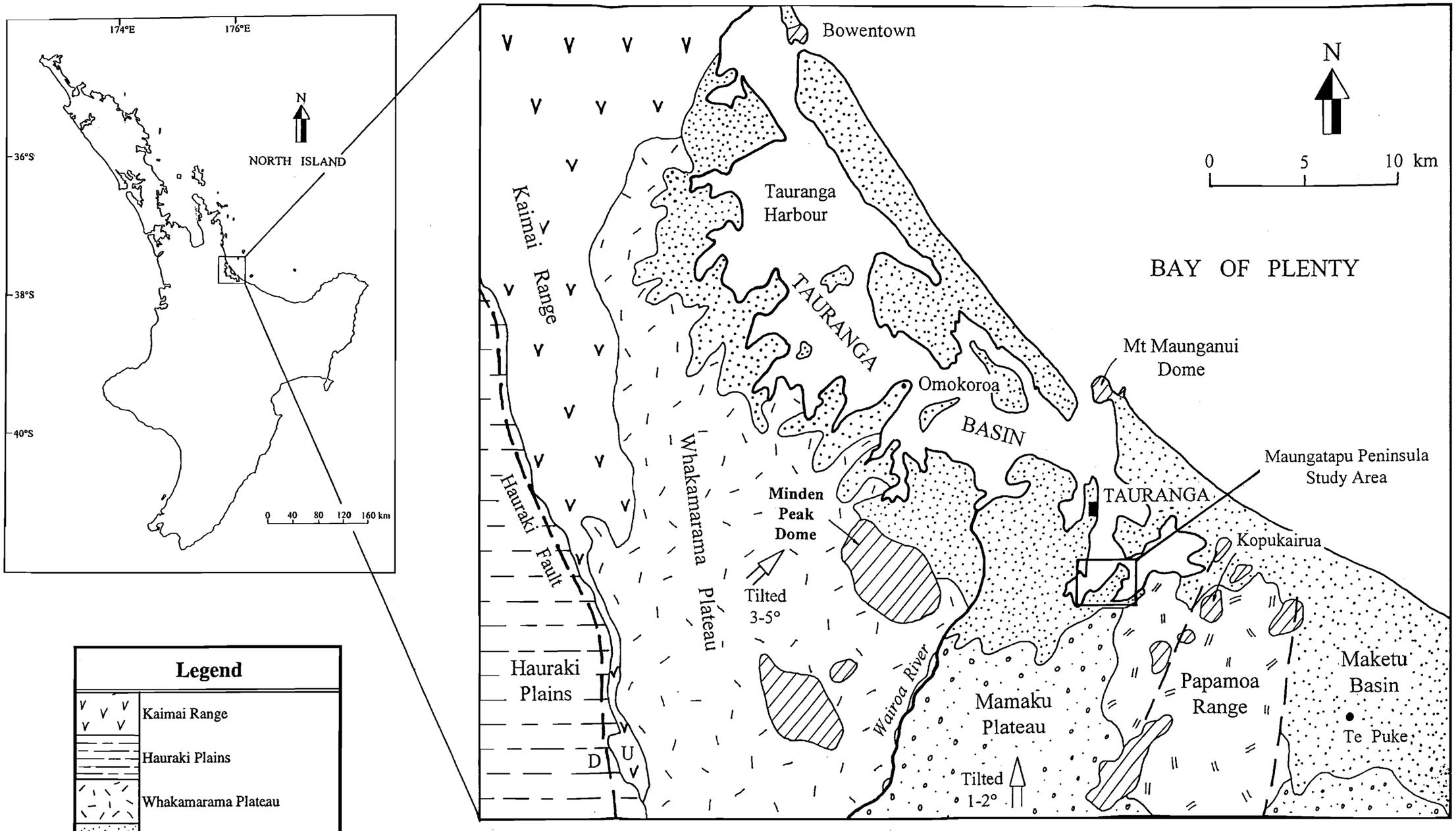

Figure 1.1 Location Map and Main Physiographic Features of the Tauranga Area (From Briggs et al. 1996).

Table 1.1 Generalised stratigraphy of the Tauranga Basin (From Briggs et al. 1996).

GENERALISED STRATIGRAPHY OF THE TAURANGA REGION

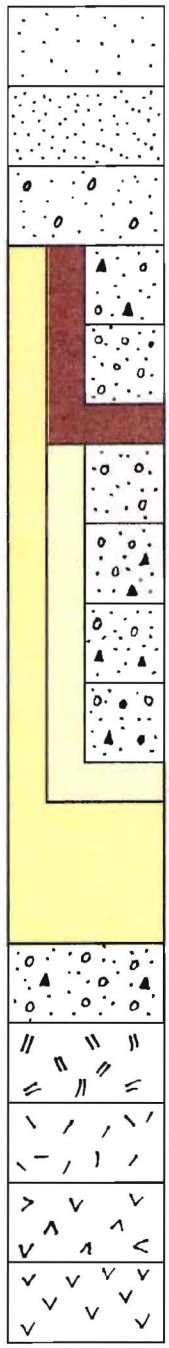

	Age
Holocene alluvium and dunes	
Holocene and Late Pleistocene tephras	< 50 ka
Rotoehu Ash	> c.50 ka
Mamaku Ignimbrite	0.22 Ma
Waimakariri Ignimbrite	?
Hamilton Ash	0.35 Ma - c. 0.1 Ma
Te Ranga Ignimbrite	?
Te Puna Ignimbrite	> 0.78 Ma
Ongatiti Ignimbrite	1.21 Ma
Papamoa Ignimbrite	?
Pahoia Tephras	2.18 Ma - 0.35 Ma
Matua Subgroup (fluviatile sands and gravels, lignites, estuarine sands, lacustrine silts)	c. 2 Ma - c. 50 ka
Waitetariki Ignimbrite	2.18 - 2.13 Ma
Kopukairua Dacite	?
Matakana Basalt	?
Minden Rhyolite	2.36 - 2.28 Ma
Otawa Volcanics	2.95 - 2.54 Ma

The Tauranga Basin is a Pleistocene, predominantly fluvial/estuarine basin partially infilled during a period of rapid subsidence after the eruption of the Waitetariki Ignimbrite (2.18 - 2.13 Ma) (Briggs et al., 1996). The basin sediments consist of volcaniclastic terrestrial and estuarine deposits, as well as a number of welded and non-welded ignimbrites. The ignimbrites, although they have not been sourced, account for a substantial proportion of the basin fill. Several of the non-welded distal ignimbrites which contributed large quantities of volcaniclastic sediment became intercalated with air-fall tephra and sedimentary units (Harmsworth, 1983).

The Mamaku Plateau located to the south of the Tauranga Basin slopes gently towards the north at approximately 1 - 2°. The Mamaku Ignimbrite (0.22-0.24 Ma, Houghton, 1995) is a sequence of thick voluminous fans and lobes of pyroclastic flows which form the Mamaku Plateau. The unit slopes away from its Rotorua caldera source, gradually thinning towards the Tauranga Basin where it is underlain by the Waimakariri Ignimbrite. The plateau has been entrenched by numerous streams and rivers that flow northwards into the Tauranga and Maketu basins (Briggs, et al. 1996).

The Papamoa Range lies to the south east of the Tauranga Basin in between the Mamaku Plateau and Maketu basin. A number of NNE-aligned Pleistocene dacite and rhyolitic domes, and dacitic ignimbrites, have been mapped in the area. In addition to this Healy et. al. (1964) recognised two large NNE-striking faults that are believed by Briggs et. al. (1996) to control the alignment of the volcanic domes.

c) Stratigraphy

From Table 1.1 it can be seen that the oldest units present within the Tauranga region consist of a number of volcanic domes and flows (Otawa Volcanics, Minden Rhyolite, Matakana Basalt, and Kopukairua Dacite) which range in ages from 2.18 Ma to 2.95 Ma.

The Otawa Volcanics are believed to be the oldest unit in the Tauranga region (2.95 - 2.54 Ma) and comprise andesite lavas and volcanic breccias that outcrop in the Papamoa Range. The next oldest unit, the Minden Rhyolite (2.36 - 2.28 Ma) consists of four formations (Kaikaikaroro, Mt. Maunganui, Mangatawa, and Pukunui formations) that contain individual rhyolitic lava domes and flows. The Minden Rhyolite domes are the most prominent landform in the Tauranga Basin, typified by Mt. Maunganui (Briggs et al., 1996). In addition these domes can be seen trending in a NNE alignment along the Papamoa Range (Figure 1.1). The Matakana Basalt (Table 1.1) is a dark grey basalt which occurs as a small flow 30m off shore of Matakana Island. No age relationship has been established due to lack of exposure. The Kopukairua Dacite is a single dome and flow complex situated on the northern parts of the Papamoa Range (Briggs et al., 1996). As with the Matakana Basalt poor exposure has resulted in difficulties determining age relationships.

The Waiteariki Ignimbrite (2.18 - 2.13 Ma) is a large volume welded ignimbrite that forms the Whakamarama Plateau. It is believed to underlie the Tauranga Basin to thickness of 50-150m, and it forms the local basement in the western Tauranga Basin. It is in turn overlain by a thick sequence of pyroclastic, fluvial and estuarine deposits (Matua Subgroup sediments). The Papamoa Ignimbrite is confined to the northeastern section of the Tauranga region outcropping in the foothills of the Papamoa Ranges (Briggs et al., 1996). It has been divided into a lower and upper section by Hughes (1993), with the lower section consisting of five acidic pumice types and one basic scoria type. The upper Papamoa Ignimbrite consists of a single rhyodacite pumice type. The age of the Papamoa Ignimbrite is not known. The Ongatiti Ignimbrite (1.21 Ma) is a welded ignimbrite erupted from the Taupo Volcanic Zone. It outcrops as columnar jointed cliffs in the Wairoa River north of McLaren Falls and stratigraphically overlies the Waiteariki Ignimbrite. The Te Puna Ignimbrite (>0.78 Ma) is a non-welded to partially welded brown ignimbrite containing white to grey fibrous pumice. It is a small volume ignimbrite derived from a local source (unknown) and is confined to the vicinity of the Tauranga Harbour. In turn the Te Puna Ignimbrite is overlain by cross-bedded fluvial pumiceous sands, lacustrine silts

and sands, lignites, and tephras (Pahoia Tephras and Hamilton Ash). The Te Ranga Ignimbrite (age unknown) is a light grey, non-welded, crystal-poor, sandy textured ignimbrite (Briggs et al. 1996). As with the Te Puna Ignimbrite the Te Ranga Ignimbrite is a small locally derived ignimbrite covering most of the area between Maungatapu and the Wairoa River, including parts of Matakana and Motuhoa Islands. It stratigraphically overlies the Te Puna and underlies the Waimakariri Ignimbrite. The Waimakariri Ignimbrite (age unknown) is a brown to light grey pumice-rich, crystal rich, partially welded ignimbrite which is an extensive unit outcropping between the Wairoa River and eastwards to the Papamoa Hills. It stratigraphically overlies the Waiteariki and Te Ranga ignimbrites and is in turn overlain by the Mamaku Ignimbrite. The Mamaku is the youngest Ignimbrite in the Tauranga region (0.22 Ma), consisting of a light grey to light brown to pinkish-purple to purplish-grey, generally pumice-poor, crystal-poor, lithic-poor vapour phase altered welded ignimbrite (Briggs et al., 1996). It is derived from the Lake Rotorua area and forms the upper surface of the Mamaku Plateau, partially covering the southern Papamoa Ranges and parts of the Waimakariri Ignimbrite. The Mamaku Ignimbrite stratigraphically overlies the Waimakariri Ignimbrite.

The Matua Subgroup (c. 2 Ma - c. 50 ka) represents part of the Tauranga Group as defined by Kear and Schofield (1978). It consists of fluvial pumiceous silts, sands and gravels, lacustrine and estuarine muds, lignites and peats, intercalated with airfall tephras and thin distal ignimbrites. The Matua subgroup form a number of terraces of which Maungatapu Peninsula is one. The Pahoia Tephras (2.18 Ma - 0.35 Ma) consist of all tephras older than the Hamilton Ash in the Tauranga Basin, and are thought to be correlatives of the Kauroa Ash Formation (Briggs et al., 1996). The Pahoia Tephras are intercalated with fluvial and other deposits within the Matua Subgroup sediments, and are exposed in coastal sections of terraces such as Maungatapu, Matapihi, Matua, Greerton, and Omokoroa. The Hamilton Ash (0.35 Ma - c. 0.1 Ma) consists of a sequence of strongly weathered, clay-textured tephra beds and palaeosols derived from the Taupo Volcanic Zone which are distributed throughout the Waikato-South Auckland-Tauranga regions. The Holocene and late Pleistocene Tephras consist of the Rotoehu Ash and the Post-Rotoehu Ash Tephras.

The Rotoehu Ash (>c. 50 ka) is a sequence of shower-bedded deposits of younger tephras derived from the Taupo Volcanic Zone. The Post-Rotoehu Ash Tephras consist of a thick cover of younger tephras overlying the Rotoehu Ash (Briggs et al.,1996). The Holocene sediments comprise the tombolos of Bowentown and Mt. Maunganui, which have been joined to the mainland via a system of progradational dune ridges formed during the Holocene and since the post-glacial marine transgression 6500 years ago (Wigley 1990; Munro 1994, in Briggs et al., 1996). In addition low Holocene and late Pleistocene terraces have been formed by river and stream alluvium and peat deposits.

The Matua Subgroup, Pahoia Tephras, Hamilton Ash, Rotoehu Ash, and Holocene and Late Pleistocene Tephras (Post-Rotoehu Ash Tephras) will be discussed in greater detail in Chapter 2 as they are applicable to the development of the slope failure models.

1.3.2 Terraces Of The Tauranga Basin

The Tauranga Basin contains a number of terraces that are generally preserved as peninsulas that trend in a NE or NNE direction (Figure 1.2; Briggs et al., 1996). These terraces are in-turn intersected by broad shallow valleys and generally terminate seawards in low cliffs or steep slopes. Omokoroa, Tauranga City and Greerton, Matua, Matapihi, and Maungatapu are examples of terraces noted by Harmsworth (1983), (Figure 1.2). Several terrace levels have been delineated by Healy et al. (1964) at 80 m, 30-60 m, 12-22 m, 5 m, 0.5-1.0 m above present sea level, most of which dip between 1° and 4° towards the NE or N.

Throughout the Tauranga Basin many of terraces are constructed of sequences of fluvial, lacustrine, estuarine, and lignite deposits of the Matua Subgroup (c. 2 Ma - 0.35 Ma; Table 1.1). These deposits are intercalated with non-welded ignimbrites such as the Te Ranga (age unknown) and Te Puna (> 0.78 Ma) ignimbrites, and airfall tephras such as the

Pahoia Tephras (2.18 Ma - 0.35 Ma). Covering these units is a thick sequence (2 - 5 m) of younger airfall tephras, the Hamilton Ash (0.35 Ma - c. 0.1 Ma), Rotoehu Ash (> c. 50 ka), and a number of Post-Rotoehu Tephras derived from the Taupo Volcanic Zone (< 50 ka).

Harmsworth (1983, figure 1.2), attributed the formation of the terraces to four principle origins (Briggs et. al. 1996):

1. Volcanic constructional surfaces, e.g. the lobes of pyroclastic flow deposits, in particular the Te Puna and Te Ranga ignimbrites, often variably degraded.
2. Volcanic and/or fluvial degradation surfaces modified and covered by airfall tephra.
3. Fluvial terraces formed by aggradation or lateral erosion, and variably degraded.
4. Lower terraces possibly formed by marine aggradation as a consequence of a higher than present sea level.

Hall (1994) concluded that it was difficult to decide on the exact origin of the terraces within the Tauranga Basin. One possible interpretation by Hall related to the age constraints placed on the Hamilton Ash by Kohn et. al. (1992) and Shepherd (1994). From this Hall concluded that the higher terraces could be the result of terrestrial aggradation during an interglacial period which occurred sometime between the deposition of the Waitekariki Ignimbrite (2.18 - 2.13 Ma) and c. 150 ka (deposition of Hamilton H8 Ash, Shepherd 1994). Hall also considered another important factor in the development of the terraces at Tauranga City, Maungatapu and Matapihi was that they were built up during catastrophic events, such as a flood, storm, severe tectonic event or volcanic eruption. These events caused extensive erosion and thus river systems to become choked with sediment, and once the sediment load had decreased rivers downcut through the deposits leaving the terraces seen today as the peninsulas which jut into the Tauranga Harbour.

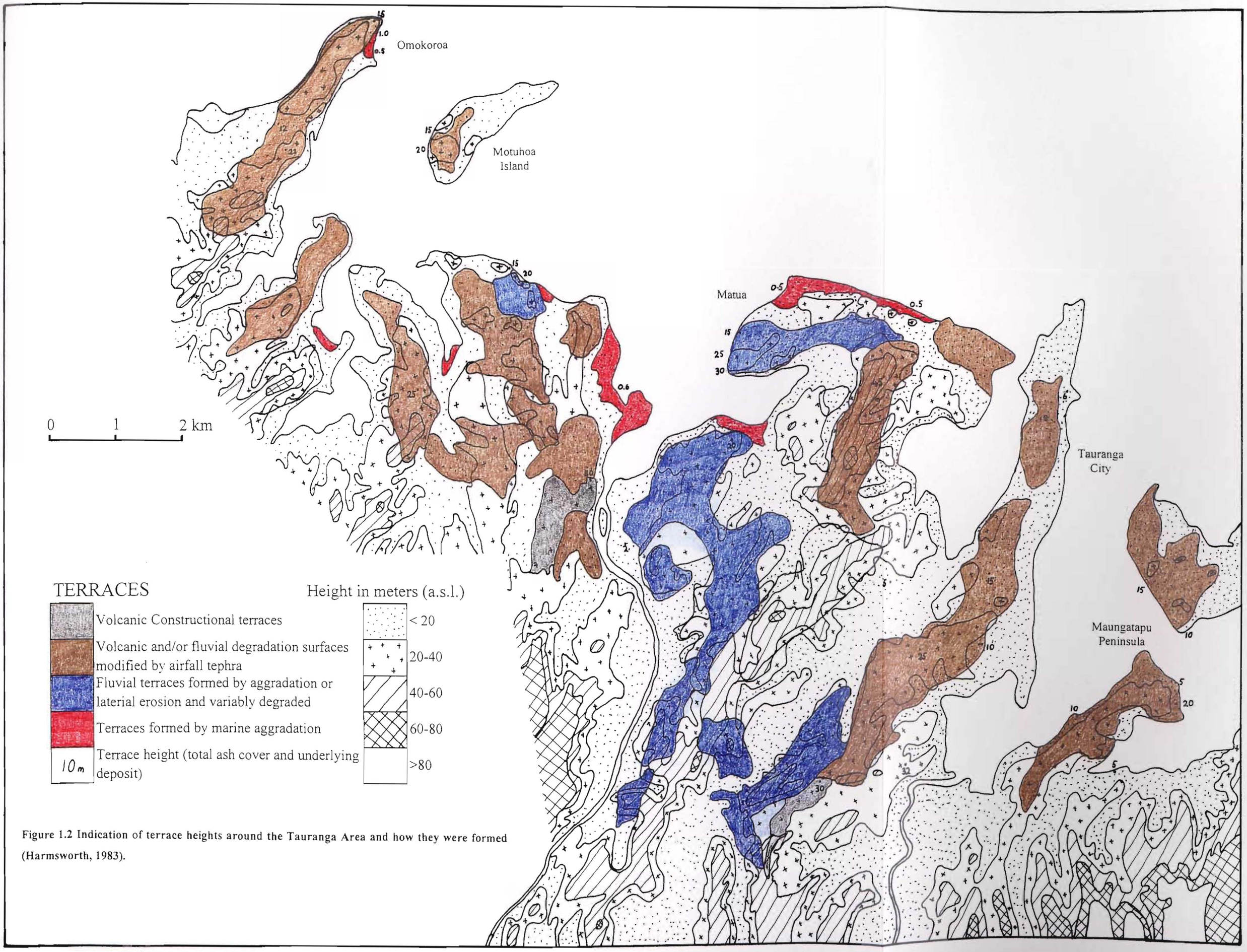

Figure 1.2 Indication of terrace heights around the Tauranga Area and how they were formed (Harmsworth, 1983).

1.4 STUDY AREA

1.4.1 Location and Physiography

Maungatapu Peninsula is a flat topped, 20 to 30 m high cliffed peninsula, located within the Tauranga Basin 4 km southeast of Tauranga's city centre (Figure 1.1). It covers an approximate area of 1.6 km^2 and juts out into the Tauranga Harbour in a northeasterly direction. A number of erosional valleys around the Peninsula edge connect the cliff tops to the harbour below (Map 1, Map Box). Maungatapu Peninsula contains two main road ways, the first a major motorway (SH2 South) which bisects the peninsula connecting north and south Tauranga to Papamoa - Mount Maunganui and the coastal road south to Rotorua, whilst the other (Maungatapu Road) allows access to housing on the peninsula.

1.4.2 Rainfall Records

Rainfall data was obtained from NIWA for station 766204 Waimapu R at Tauranga Aero AWS located approximately 5.5 km north of Maungatapu Peninsula. From information supplied the average yearly rainfall for the period from 1898 to 1978, is 1342 mm. The maximum recorded annual rainfall was in 1916 amounting to a total rainfall of 1897 mm (Figure 1.3). The rainfall for 1995 was 1620 mm, representing an approximately 20 % increase in rainfall. From Figure 1.4, three separate periods of higher than average rainfall can be seen in 1995, March-April, July, and November. April was the most noticeable month with a rainfall of 312 mm representing an approximate 260 % increase above the average for that month (Figure 1.4). If the daily rainfalls for the months March, April, and May (1995) are looked at further (Figure 1.5), no daily rainfall totals are greater than a 1 in 2 year recurrence interval event, which is equivalent to a rainfall of 101 mm for a 24 hour period (Appendix A1). The month of May in which the slips occurred did not have any significant rainfall until the 28 to 29 May (rainfall of 59 and 43 mm respectively), with both of these daily totals well under the 24 hour 1 in 2 year recurrence interval rainfall event of 101mm (Appendix A1). This means that it is the total rainfall for the months of March, April, and May which are the important factors, and not that of a single extreme rainfall event e.g. 1 in 100 year event.

It can thus be concluded that the rainfall leading up to the slips in May of 1995 played a significant part in slipping around the Maungatapu Peninsula. The rainfall for 1979, when a large number of slips were recorded around Maungatapu, was comparable to that of 1995 (Figure 1.6). From Figure 1.6 it can be seen that a two month period of higher than average rainfall occurred prior to recorded slipping in both 1979 and 1995.

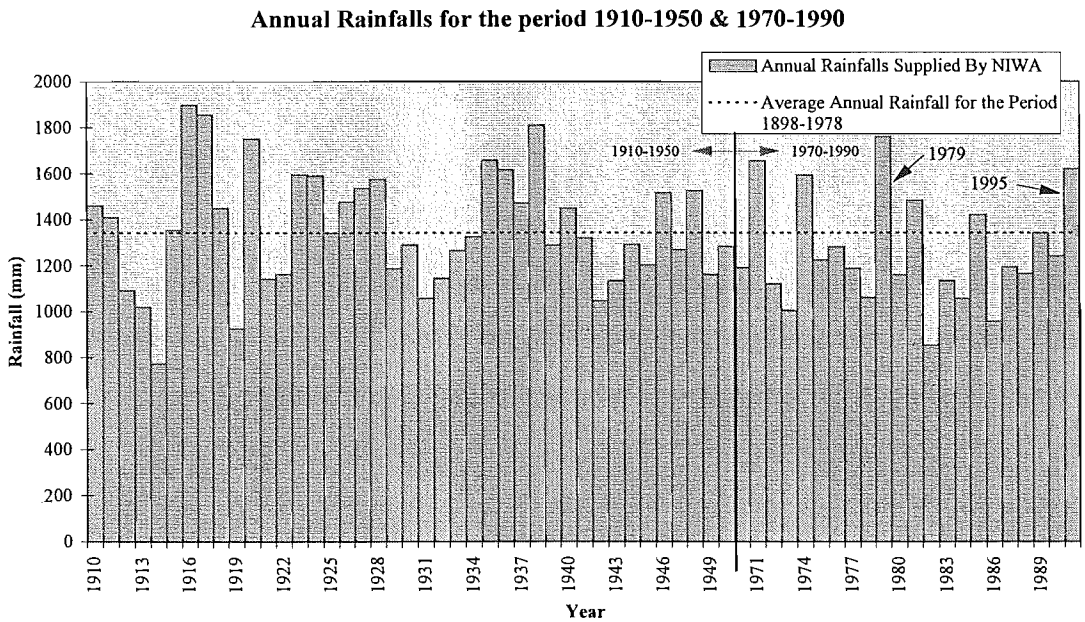

Figure 1.3 Annual rainfall for the period 1910-1950 and 1970-1990, indicating higher than average rainfalls for 1979, and 1995.

The average monthly rainfall data from 1898 to 1978 (supplied by NIWA) was used for comparisons to monthly rainfall data for 1979 and 1995. The montly rainfall data supplied by NIWA (1898 to 1978) covers 80 years, missing the last 20 years from 1978 to 1995. As this was the only data available at the time it was considered that it covered enough of a time period for moderately satisfactory results for making comparisons.

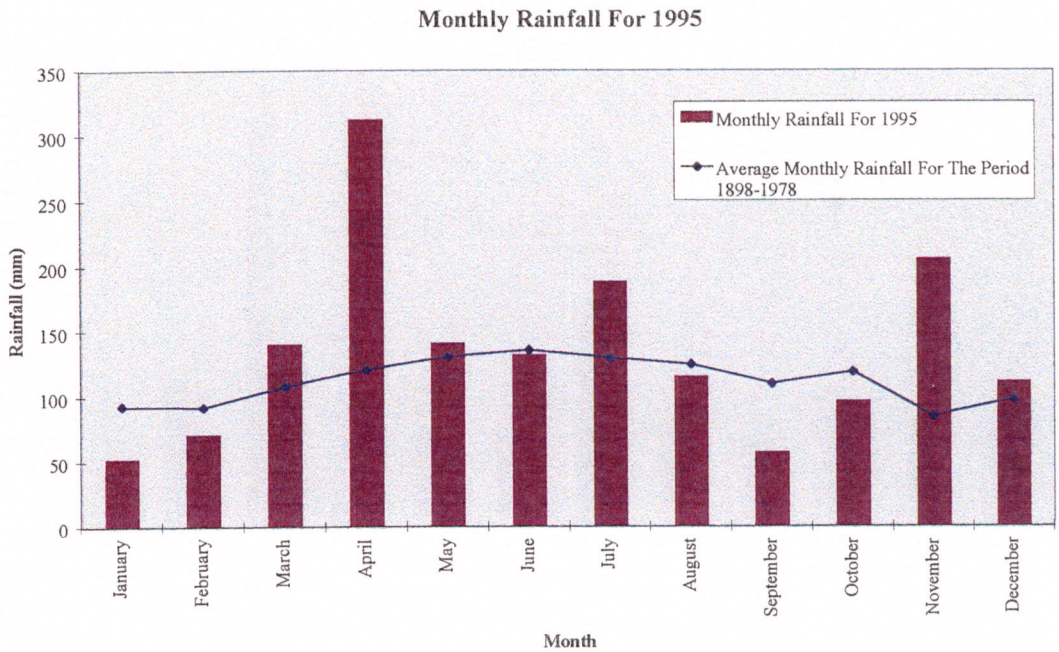

Figure 1.4 Monthly rainfall for 1995 in conjunction with average monthly rainfall for the period 1898-1978 to indicate the higher than average rainfall for the months of March, April and May.

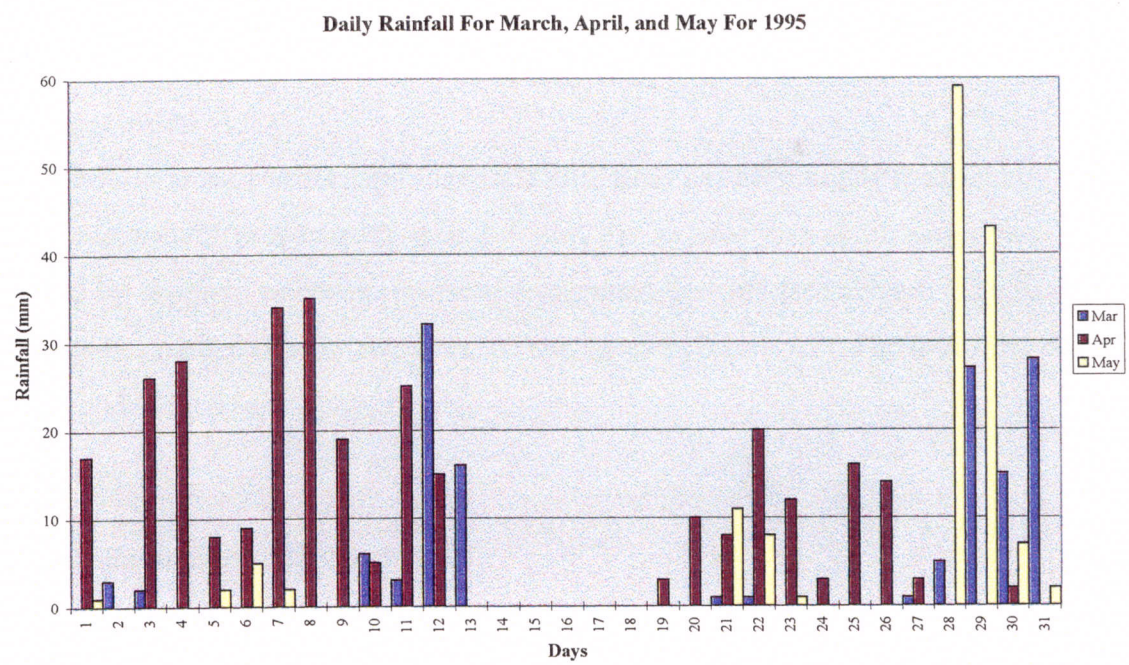

Figure 1.5 Daily rainfall totals for March, April and May for 1995.

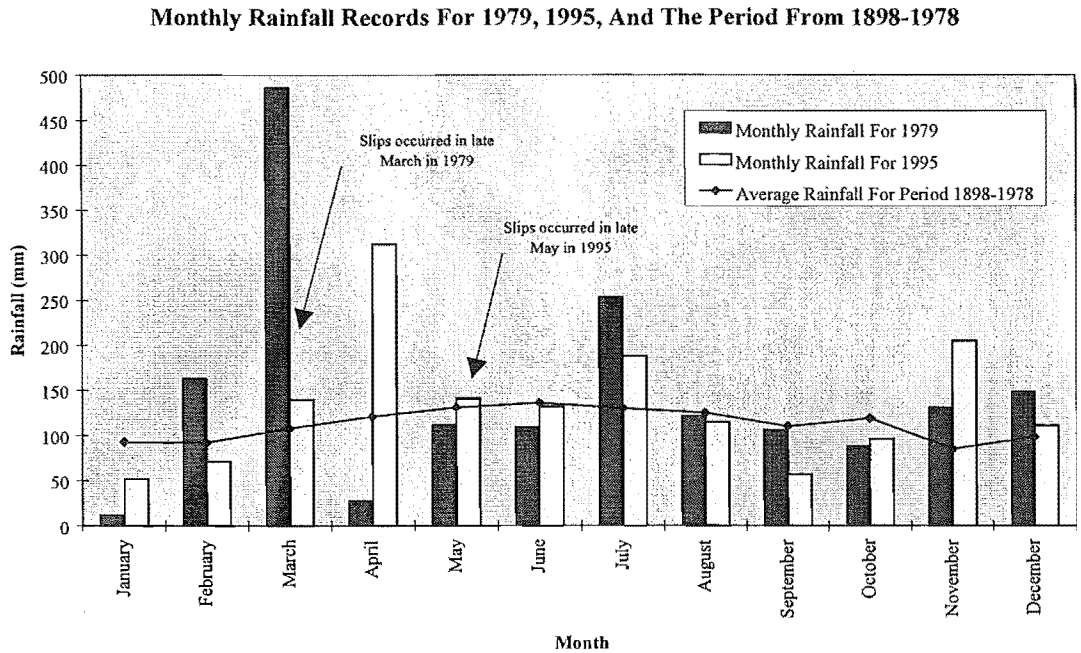

Figure 1.6 Monthly rainfall records for 1979, 1995 and the period from 1898-1978, to indicate months wetter than average.

1.4.4 Vegetation

The vegetation along Maungatapu Peninsula cliff faces has been highly modified by both human and natural processes (Figure 1.7 & 1.8). As tree and shrub cover has been disturbed by slipping, weed species have revegetated the cliff face (Figure 1.8). In other areas man has replanted using more ornamental species (Figure 1.7). The following plants have been identified as existing cover:

a) Native Vegetation

- *Metrosideros excelsa* (Pohutukawa)
- *Cyathea smithii* (Mamaku / Block tree fern)
- *Melicytus ramiflorus* (Mahoe / whiteywood)
- *Hebe species* (Koromiko)

b) Introduced Vegetation

- *Acacia baileyana* (Wattle)
- *Ulex species* (Gorse)

- *Hedychium gardnerianum* (Kahiti Ginger)
- *Leycesteria formosa* (Humsalayan honeysuckle)
- *Cortaderia selloana* (Monterey pine)
- *Passiflora mollissima* (Banana passionfruit)
- *Solanum mauritanum* (Woolly nightshade)
- *Eucalyptus species* (Gum)
- *Agapanthus africanus* (African lily)
- *Sinarundinaria murieliae* (Bamboo)
- *Convolvulus species* (Convolvulus)

Figure 1.7 Vegetation which has been partially altered by human through planting (photograph taken from grid reference 704400, 273800 looking ENE).

Figure 1.8 Cliff face in its natural state with introduced weed species covering some of the native vegetation (Photograph taken from grid reference 705600, 275100 looking SW).

1.4.5 Landuse

Maungatapu Peninsula is a heavily housed sector of Tauranga City, with major residential development commencing in the late 1960's. To date virtually all areas have been urbanised, and most new houses have resulted from dividing an existing property into two separate lots (Infill Housing). Property values lie in the middle to upper echelon of the market, with cliff edge dwellings producing some of the higher prices due to views of the Tauranga Harbour. Because of this, there is a greater demand for building consents for cliff top sections to be approved so houses could be developed on these areas around the edge of Maungatapu Peninsula.

1.5 PREVIOUS WORK

1.5.1 Literature and Thesis Work

Since Cox in 1877 characterised Tauranga sediments as "brown Tauranga sands", a number of works have since been written regarding the geology of the Tauranga Basin and its surrounding regions. Working for the Geological Survey Branch of the Mines Department, Henderson and Bartrum (1913) were one of the first to develop maps that encompass the south-eastern portion of the Tauranga Basin. They divided the volcanics into five main units: Andesite, Dacite, Dyke, Rhyolite Series (subdivided into a younger and older flow and fragmented units), and the Tauranga Beds. The Tauranga Beds, which are synonymous with the Tauranga Group sediments, consisted of a poorly consolidated succession of pumiceous sands including conglomerates, clays, and lignite, all of shallow water origin.

Healy et. al. (1964) published a regional 1:250 000 geological map which extended from the Rotorua district into the Bay of Plenty to include Tauranga. This resulted in a number of new units being defined such as the Waitawheta Dacite, Te Puke Breccias, Minden Rhyolite, Omanhia Andesite, Waiteariki Ignimbrite, and Papamoa Ignimbrite. In 1967 Healy produced an unpublished report prior to the construction of the Kaimai Railway Tunnel. This detailed the surrounding geology of the area and included the Waiteariki Ignimbrite. In addition, Healy (1969) defined a new unit (Aongatete Ignimbrite) during the construction of the Kaimai Railway Tunnel.

Selby et al. (1971) extended the initial work completed by Kear and Waterhouse (1961) on the terraces at Waihi Beach. They differentiated the late Pleistocene Hamilton, Kauroa and Rotoehu Ash, as well as delineating the alluvial, estuarine and dune sands of the Waihi Beach Formation. Chapple (1975) used tephra stratigraphy to try and correlate the terraces at Waihi with other terraces across the Tauranga Basin and Bay of Plenty. He attributed variations in terrace elevation to be the result of warping.

Over the last sixteen years a number of theses have been written by Waikato University graduates regarding the Tauranga Basin. Bird (1981) concentrated on causes of coastal landsliding and strength parameters of the sediments at Maungatapu Peninsula after the 1979 slips. He concluded that failure was the result of high pore water pressure in a lensoidal silty sands/sandy muds above an impermeable clay marker bed. In 1983 Harmsworth completed a thesis looking at the Quaternary stratigraphy, nature and pattern of Tauranga Basin's depositional paleoenvironments. Investigation into the Waitekariki, Waimakariri and Mamaku Ignimbrites was conducted by Morgan (1986) looking at the geology of the northern Mamaku Plateau. To the east Hughes (1993) studied the Papamoa Range lava domes and flows, concentrating on the Papamoa Ignimbrite. The western Tauranga Basin was covered by Whitbread-Edwards (1994) which encompassed the Te Puna Ignimbrite. Around the same time as Whitbread-Edwards, Hall (1994) looked at the south-eastern part of the Tauranga Basin, expanding on limited existing geology information in the area. She studied a variety of volcanic lithologies outcropping as lava domes, flows, and ignimbrites, as well as volcanic-derived sediment forming terrace deposits capped by tephras.

In 1996 an Occasional Report by Briggs et al. (1996) was produced which combined all of the previous geological information present in the Tauranga Basin into one publication. This was done in conjunction with the Bay of Plenty Regional Council and the Institute of Geological and Nuclear Sciences Limited. This publication noted the various stratigraphic units present throughout the Tauranga region providing a summary of the composition, distribution, stratigraphic relationship and age for each stratigraphic unit.

1.5.2 Consultancy Work Held in Council Files

The main body of geotechnical reports held in the council files have been written after the 1979 slips which occurred throughout the Tauranga Basin. These generally consisted of a walk over of the property and a hand-drilled auger hole to approximately four meters. Ground Technology Ltd. undertook geotechnical investigation ground conditions at 413 Maungatapu Road, producing logs to a depth of four meters. Grocott (1988) working for Worley Consultancy Limited produced a report on a proposed building development at 292 Maungatapu Road. He concluded that development was possible if the house was set back by 10.5 m from the cliff edge, and that suitable foundation designs were undertaken. In 1993 Mark Mitchell (Consulting Geotechnical Engineer) reported on a site at 340b Maungatapu Road, concluding that it was not suitable for a house site without extensive excavation and retaining wall construction.

In 1995 M^{C}Larens International Loss Adjusters contracted Bernard Hegan of Tonkin and Taylor LTD to conduct a geotechnical investigation of the slipping at 85 and 89 Te Hono Street. He concluded that cliff face failure was the result of a "blow out" of a loose sand bed by high ground water flow. This left an unstable overhang which failed in a more or less circular failure.

In 1980 two major reports were produced, one by Tonkin and Taylor on the Omokoroa Point landslide of 1979, and the other by Houghton and Hegan on "A preliminary assessment of geological factors influencing slope stability and landslipping in and around Tauranga City". The Omokoroa Point Landslide 1979 report established a similar two month higher than average rainfall prior to the landslides at Omokoroa Point as that found during this study. In addition consultants from Tonkin and Taylor noted that soakholes drilled for domestic waste water discharge (with dimensions 1 m diameter by 12 m deep) were clearly detrimental to the stability of the cliff sections around Omokoroa. Engineering properties of soils were determined by Atterberg Limits, triaxial testing, and

clay mineralogy analysis. Atterberg testing showed that while the liquid limits were high, plasticities were low (liquid limits (LL) = 101 & 76 and Plastic limits 54 and 50 respectively). Triaxial testing of five samples produced a of cohesion (c') = 0 kPa and friction angle (ϕ) = 29.5°, testing of a sample from a failure zone indicated c' = 90 kPa and ϕ = 10°. Clay mineralogy determined that the main constitutent was halloysite. In addition to engineering properties, Tonkin and Talyor developed a failure model for Omokoroa Point (Figure 1.9).

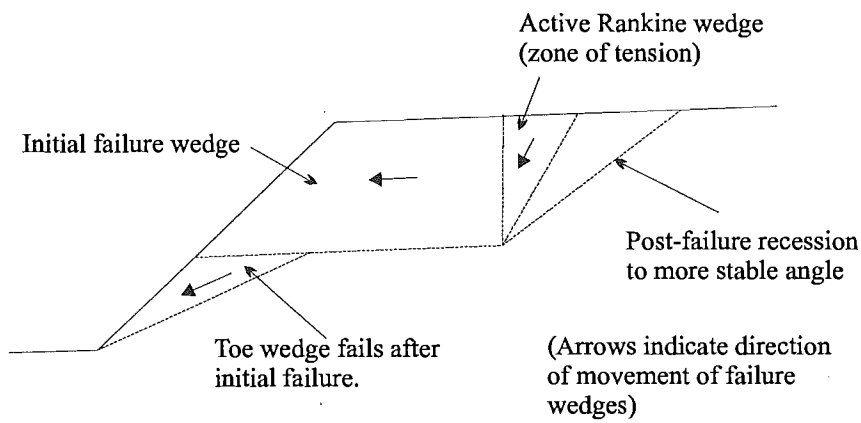

Figure 1.9 Two-dimension model for wedge failure at Omokoroa Point (Tonkin and Talyor, 1980).

Houghton and Hegan (1980) from aerial photograph interpretation mapped deep-seated and superficial failures around Tauranga City. Deep-seated failures were the type experienced at Maungatapu in March of 1979 and Omokoroa in August 1979, while superficial failures were shallow regolith failures (generally less than 2 m) that had occurred when the soil mass had become saturated by water. The main fact to come out of this report was that after the analysis of 17 deep-seated slides at Omokoroa, it was suggested that a buffer zone (hazard zone) developed from a relationship of a height/depth ratio of 2:1 could be adopted. This has since become a guideline for assessing the landslide potential for a given property for the Tauranga District.

1.6 THESIS ORGANISATION

The organisation of this thesis is as follows:

Chapter 2: Geology and Geomorphology of the Maungatapu Peninsula

Within this chapter is a description of the site geology as well as the geomorphological characterisation of landslide types seen around the Maungatapu Peninsula and the failure dynamics of these landslides.

Chapter 3: Field Investigation

Details geotechnical and engineering geological investigations that were carried out, and presents results of geotechnical core logging, hydrogeological investigations, in-situ shear strength and permeability testing.

Chapter 4: Laboratory Data

This chapter presents the laboratory results which are discussed and synthesised to produce geotechnical parameters for use in the development of hydrogeological models and stability assessment.

Chapter 5: Hydrogeological Assessment, Stability Analysis and Implications

Details the development of a hydrogeological model using data obtained from the previous chapters, and assessment of the stability of the cliff sections with an increasing phreatic surface and landslide block. The chapter then further it looks at the implication of these models to hazard zones and mitigation option associated with the Maungatapu Peninsula.

Chapter 6: Summary and Conclusions

This chapter presents the principal results and conclusions, with recommendations for future work.

Chapter Two GEOLOGY AND GEOMORPHOLOGY OF THE MAUNGATAPU PENINSULA

2.1 INTRODUCTION

The Maungatapu Peninsula constitutes one of the many terraces which can be delineated in the Tauranga Basin. It consists of a number of approximately horizontal to gently dipping fluvial and estuarine deposits overlain by tephras, ashes, and colluvium/topsoil. Through a better understanding of the evolution of the Peninsula, a greater idea can be obtained as to how the geology of Maungatapu affects the types of landslides delineated from field investigations. This chapter is divided into two parts, firstly dealing with the geology of the Peninsula looking at the main units that influence the failures seen at properties such as 85 Te Hono Street and other areas. The second aspect looks at the various types of landslides delineated during the field investigation stage of this study, which has been introduced early on in this project to provide a better understanding of the mechanisms that produce failures. Delineation of these failures were based on previous work by Houghton and Hegan (1980), Tonkin and Talyor (1980), Bird (1981) and Hegan (1995), in addition to field investigation techniques undertaken during this study such as aerial photograph interpretation and engineering geological mapping. These aspects are further discussed in Chapter 3. In this study the main emphasis will be on the coastal cliff sediments, which can be divided into four distinctive units (Post-Rotoehu Ash Tephras, Rotoehu Ash, Hamilton Ash, Matua Subgroup sediments; see Table 2.1.

2.2 SITE GEOLOGY

Table 2.1 shows that the stratigraphy of Maungatapu Peninsula can be further divided up into a number of units such as the Post-Rotoehu Ash Tephras, Rotoehu Ash, Palaeosol, Hamilton Ash, Pahoia Tephras, and Matua Subgroup. During the field investigation stage of this project a number of subgroups associated with the Pahoia Tephras (Pahoia Tephra, Upper Bounding Aquitard, Aquifer, and Lower Bounding Aquitard) and Matua Subgroup

Upper Bounding Aquitard, Aquifer, and Lower Bounding Aquitard) and Matua Subgroup (Cross-bedded sequence) were delineated. These subgroups will not be discussed here, but will be dealt with in subsequent chapters. For this section four main sources of information were used, these of Bird (1981), Harmsworth (1983), Hall (1994), and Briggs et al. (1996).

Table 2.1 Generalised stratigraphy in relation to the cliff section at Maungatapu Peninsula.

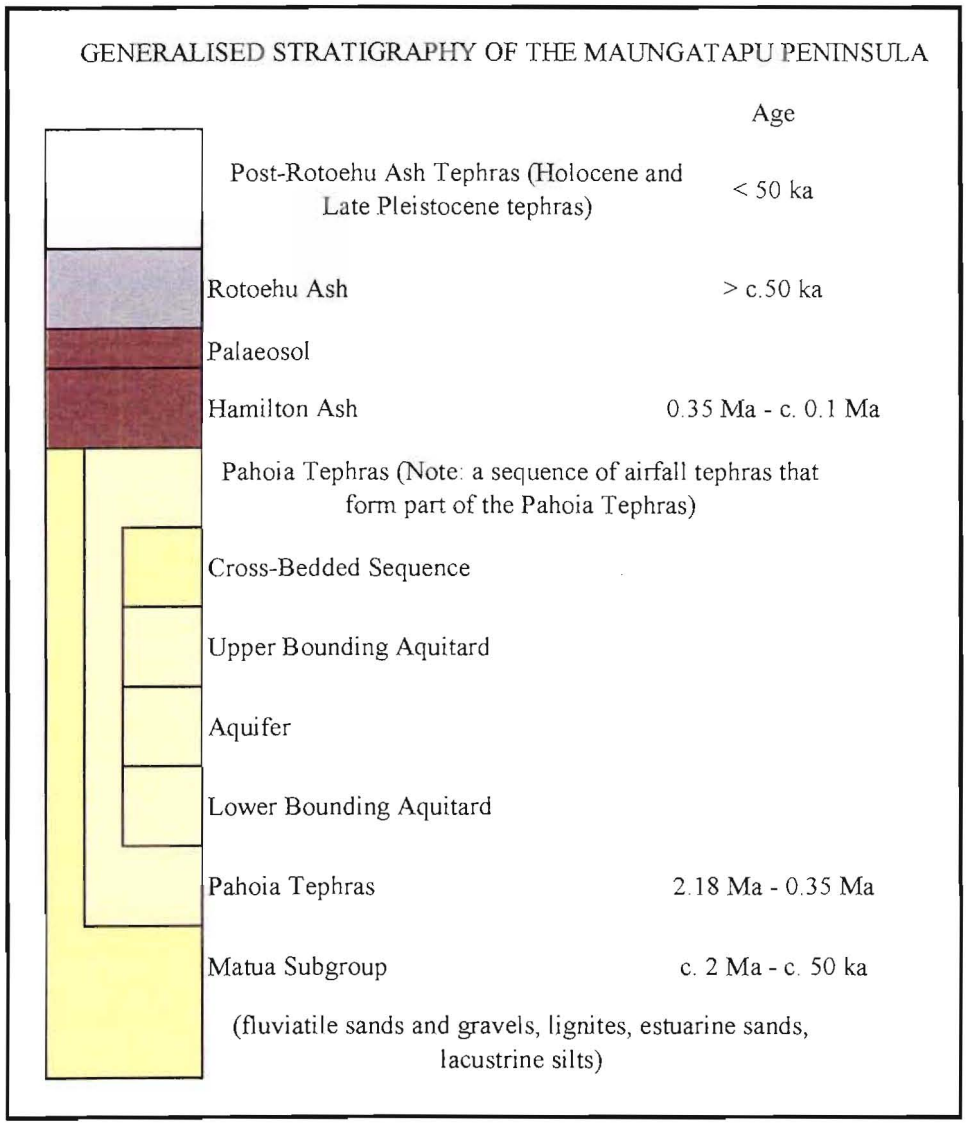

2.2.1 Matua Subgroup

a) Matua Subgroup Sediments

The Matua Subgroup was introduced by Harmsworth (1983) due to the geographical restrictions imposed on the Tauranga Group sediment names then being used in the Tauranga Basin. The Tauranga Group sediments were proposed by Kear and Schofield (1978) to consist of all Late Cenozic terrestrial, estuarine and marine sediments found in the Bay of Plenty, Hauraki and Waikato regions. However, due to the uplift of the Kaimai Ranges by the Hauraki Fault it is impossible to extrapolate these units across into the Tauranga Basin. Because of this Harmsworth introduced the Matua Subgroup to encompasses all terrestrial and estuarine sedimentary deposits formed after the deposition of the Waiteariki Ignimbrite, but excluding recent fluvial regimes (Holocene sediments) delineated by Houghton and Cuthbertson (1989). The Matua Subgroup sediment infilled the Basin to a depth of 150 m and includes a wide range of lithologies from fluvial pumiceous and rhyolitic silts, sands and gravels, lacustrine to estuarine muds, lignites and peats intercalated with airfall tephras and thin distal ignimbrites (Briggs et al., 1996). These sediments display a number of sedimentary structures such as cross-bedding (Figure 2.1), planar stratified and massive units, and post-depositional slump and water escape structures. Most of these sediments were derived from reworked ignimbrites, lava domes and flows, and tephras from the Tauranga region and Taupo Volcanic Zone (Briggs et al. 1996). Harmsworth (1983) informally divided the Matua Subgroup sediments into an upper and lower section. The "Upper" Matua Subgroup sediments basically consist of all Matua Subgroup sediments exposed in coastal cliff sections around the Tauranga region. The "Lower" Matua Subgroup sediments represent the remainder of the sediments not included in these cliff sections. For this study only the sediments from the informal "Upper" Matua Subgroup are seen due to limited exposure in the mapped cliff faces. In the western part of the Tauranga Basin the Matua Subgroup sediments overlie the Te Ranga Ignimbrite and in turn are overlain by the Hamilton Ash Fromation.

b) Pahoia Tephras

The Pahoia Tephras (Pahoia Tuffs of Pullar et al., 1973, which are possibly a correlative of the Kauroa Ash Formation) are intercalated with fluvial and other sediments of the Matua Subgroup (Briggs et al., 1996). Due to this fact, Harmsworth (1983) included the Pahoia Tephras within in the Matua Subgroup. The Pahoia Tephras is a sequence of clay-rich rhyolitic tephras which consist of wide range of grainsizes and structures, including clay, silts, silty sands, and pebbles (Harmsworth, 1983). The Pahoia Tephras range in age from 2.18 - 0.35 Ma, whereas the Matua ranges from *c.* 2 Ma - *c.* 50 ka (Briggs et al., 1996).

Geotechnically the Upper Matua Subgroup sediments and the Pahoia Tephras form the same unit, and can be grouped together within the Upper Matua Subgroup sediments for the purpose of this study.

Figure 2.1 Photo showing cross-bedded structure of part of the Matua Subgroup sediments located in slip face at 85 Te Hono Street.

2.2.2 Hamilton Ash

The Hamilton Ash Formation overlies the Matua Subgroup sediments and underlies the Rotoehu Ash (Figure 2.2). It consists of a number of strongly weathered clay-textured tephra beds and palaeosols which are well represented in the Waikato - South Auckland - Tauranga region (Ward, 1967 & Pain, 1975 in Briggs et al., 1996). The sequence has been divided into eight units numbered H1 (bottom) to H8 (top). However, it is virtually impossible in many situations to decide which unit is present due to extensive erosion of beds and palaeosols. At Maungatapu Peninsula the Hamilton Ash ranges in thickness from < 0.5 m to ~ 6 m in areas of ponding, with an average of 3 m. The Hamilton Ash ranges in age from 0.35 Ma - *c.* 0.1 Ma (Briggs et al., 1996).

Figure 2.2 Hamilton Ash and associated palaeosol at 85 Te Hono Street

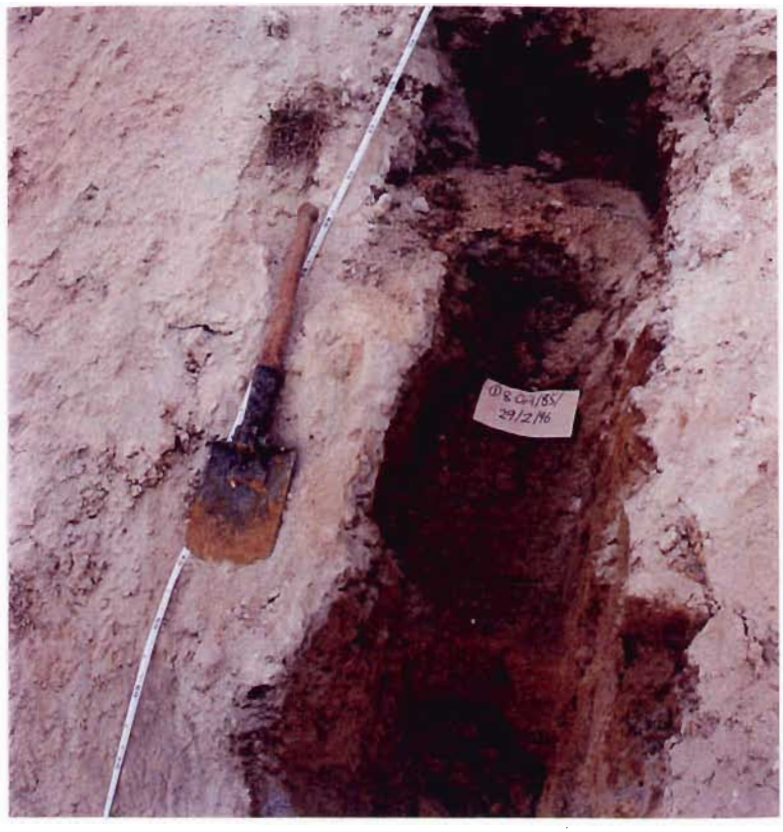

Figure 2.3 Photo showing variation in colour from a dark brown to the more commonly observed orangish brown of the Hamilton Ash at 85 Te Hono Street.

2.2.3 Rotoehu Ash

The Rotoehu Ash is a distinctive sequence of shower-bedded tephras derived from the Taupo Volcanic Zone which cover most of the Tauranga Basin. It is underlain by the Hamilton Ash and in turn is overlain by Post-Rotoehu Ash (Younger Tephras). Individual beds within the 0.3 to 2.4 m thick (Vuccetich and Pullar, 1969 in Briggs et al., 1996) sequence vary between 0.5 - 20 cm in thickness, and are typically white to greyish yellow, and fine to coarse sandy texture. The Rotoehu Ash has an age of > *c.* 50 ka (Froggatt and Lowe 1990; Lowe and Hogg, 1995 in Briggs et al., 1996).

Figure 2.4 Photo showing the planar bedding of the Rotoehu Ash bounded by the Younger Ashes and the Palaeosol.

2.2.4 Post-Rotoehu Ash Taphras (Holocene and Late Pliestocene tephras)

The Post-Rotoehu Ash Tephras consist of a number of airfall tephra deposits sourced from the Taupo Volcanic Zone. These tephras include the Mangaone Tephra (0.6-3m); Kawakawa Tephra (0.3-0.6m); Te Rere Tephra (0.15-0.3m); Okareka Tephra (0.15-0.15m); Rotoura Tephra (0.15-0.45m); Mamaku Tephra (0.1m); Waimihia Tephra (0.1m); Taupo Tephra (0.1m); and Kaharoa Tephra (0.1m). These tephras overlie the Rotoehu Ash in the Tauranga Basin and are useful in the dating of land surfaces and for correlating terrace heights. All tephras except the Tuhua Tephra are derived from the Taupo Volcanic Zone and have an age < 50 ka.

2.3 LANDSCAPE EVOLUTION

The development of the Maungatapu Peninsula and other areas throughout the Tauranga Basin has involved a number of processes from emplacement and erosion of ignimbrites via braided river, to the deposition of airfall tephras and ashes. Harmsworth (1983) has summarised the development of the Tauranga Basin since the middle Pleistocene, roughly dividing the Matua Subgroup into an upper and lower section. The Lower Matua Subgroup begins after the deposition of the Waiteariki Ignimbrite and involves three major episodes. After the deposition of the ignimbrite extensive erosion has occurred through large braided river systems, leaving behind only a small proportion of the ignimbrites. The last ignimbrite to be emplaced was the Waimakariri Ignimbrite which was in turn eroded completely. These processes created a vast amount of reworked fluvially deposited sediment, which was defined by Harmsworth (1983) as the Matua Subgroup.

Harmsworth (1983) further divided the Matua Subgroup into an upper and lower subgroup. The Upper Matua Subgroup has been informally defined as a thick (up to 40 m) sequence of sediments which are represented by subaerially exposed parts of the Matua Subgroup throughout the Tauranga Basin. The bulk of sediment supplied to the Upper Matua Subgroup was derived from unconsolidated pyroclastic deposits: the Wairoa, Te Puna, Te Ranga, and Waimakariri Ignimbrites, as well as rhyolitic air-fall tephra (Harmsworth, 1983). These sediments were in turn eroded by large braided river systems with episodic flooding and deposited into the outer reaches of the Tauranga Basin. At the time of the Upper Matua Subgroup deposition a number of rhyolitic tephras were also deposited (Pahoia Tephras), which became intercalated with the fluvially deposited sediments. This sequence can be seen at Maungatapu Peninsula, where large cross-bedded structures of the Upper Matua Subgroup are overlain by a sequence of tephras related to the Pahoia Tephras. Overlying these sediment are airfall tephras and ashes of the Hamilton Ash, Rotoehu Ash, and Post-Rotoehu Ash (Younger Tephras) Tephras.

2.4 LANDSLIDES

2.4.1 Landsliding History

From Map 1 it can be seen that Maungatapu Peninsula is a progressively eroding headland. During lower stands in sea level during the late Pleistocene, Tauranga Basin was being incised by large braided river systems. This could have produced the larger scale landslides seen at Fantail Drive-Egret Avenue, Maungatapu Peninsula, which formed due to fluvial toe erosion around the base of the cliff scarps. The braided river system of the late Pleistocene abated in the Holocene, resulting in a more stable environment as sea level rise. This in turn decreased the activity of the larger slides, leaving smaller scale slipping around the head scarps of older landslides and cliff sections of the headlands. With the increasing urbanisation of the Peninsula in the late 1960's greater emphasis was placed on the smaller scale coastal slipping. During the period 19 to 20 March of 1979, after a prolonged period of heavy rainfall (Figure 2.4), 51 properties around Maungatapu suffered some form of shallow failure. Most of these shallow failures consisted of colluvium/Topsoil failures involving less than $100m^3$. However, a number of properties situated on the northwestern and notheastern cliff edges of the Peninsula suffered deeper block failures ($\sim 700m^3$), similar to the small scale failures observed at properties like 85 Te Hono Street on 29 May of 1995. These deeper failures during May 1995 also occurred after a prolonged period of higher than usual rainfall in March-April 1995 (Figure 2.5). Most of these failures have become more prominent as vegetation has increased (Figure 2.6). This is because the root mass associated with the vegetation does not allow the free drainage of water from the slope, therefore increasing the pore water pressures within the soils. In addtion, the larger ornamental trees planted around the cliff edge (i.e. Pohutukawa) increase the overall weight, as well as producing a torque on the soil due to their trunk and canopy.

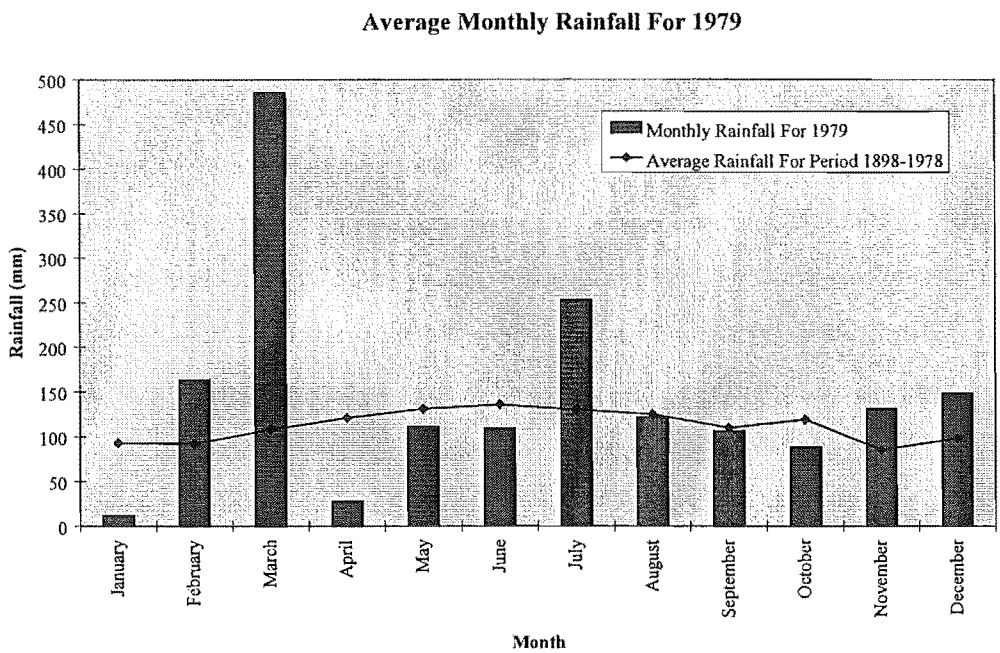

Figure 2.4 Average monthly rainfalls for 1979 indicating the higher than average rainfall for February and March prior to the late March slips.

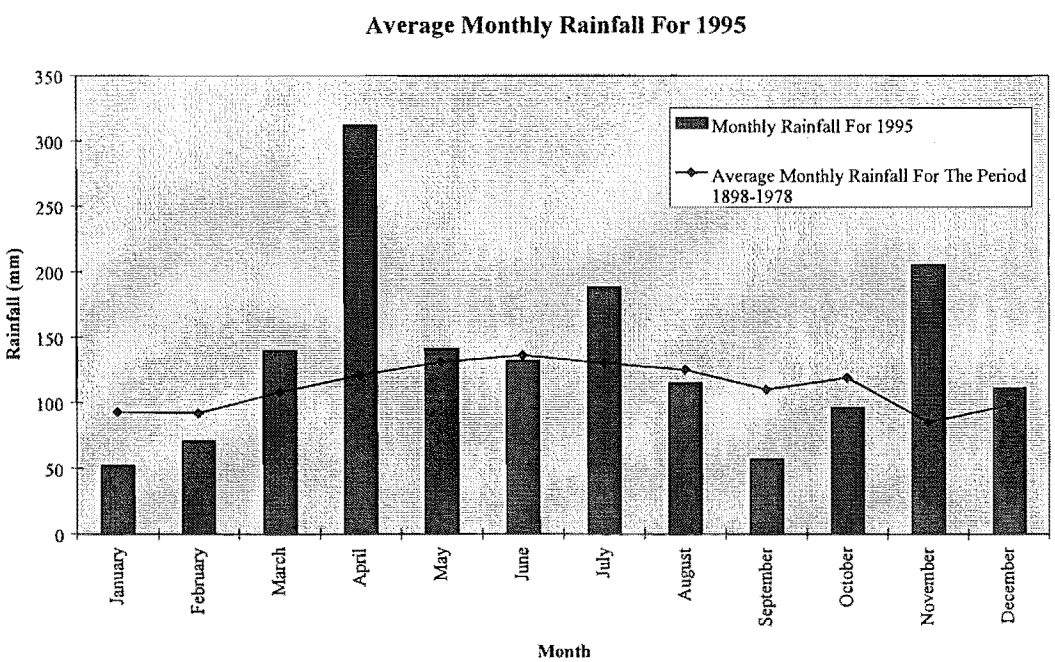

Figure 2.5 Average monthly rainfalls for 1995 indicating the higher than average rainfall for March and April prior to the 29 of May slips.

Figure 2.6 Two shallow failures where the vegetation has become too heavy for the Colluvium/Top soil to support. This can occur after a rainstorm event where the Colluvium/Top soil mass has become saturated. In addition to this the larger trees such as the Pohutukawa on the left hand side of the photograph inpart a torque on the soil mass due to their large size and shallow root mass. This comonly produces these shallow failures seen around the Peninsula cliff sections. Photograph taken at grid reference 705650 275150 looking SE.

2.4.2 Landslide Characteristics

The terminology of Cruden and Varnes (1996) was used to describe the morphology of the various failure types (Appendix A2). From field investigations four major landslide failure types can be delineated: larger scale circular-block, aquifer triggered block, wave erosion triggered block, and colluvium/topsoil failures.

a) Probably Larger Scale Block Failures

From field investigations a number of larger landslides (>1×10^5 m^3) can be identified from the existence of scarp geomorphology (Figure 2.7, and Map 1, Map Box). For example, the scarps (cliff edges) present at Fantail Drive and Egret Avenue indicate that either a moderately large landslide had occurred (~2.5×10^5 m^3), or that a succession of smaller

retrogessive landslides had occurred (Figure 2.7). However, due to high erosion rates in the late Pleistocene and early Holocene, little evidence has remained pertaining to the nature of these larger landslides. From geomorphic evidence such as the long narrow shape of some of these probable landslide features (eg Anchorage Grove, grid reference 704500 274300, Map 1, Map Box), it is suggested that they formed through the downcutting of Peninsula cliff edges by streams draining off the Peninsual surface. As the streams downcut this would produce localised failure around the stream banks. The probable larger landslide features, such as those demonstrated by Fantail Drive-Egret Avenue (Figure 2.7), are suggested to be the result of river downcutting by the two bounding streams present on the SE and NW side of the Peninsula (Map 1, Map Box). This down cutting is suggested to have mainly occurred during glaciation periods of the late Pliestocene to the Otiran glaciation which ended 14 000 years ago. With sea level lowering during these periods downcutting by rivers and streams was greatly increased. These rivers may have eroded away the toe of the cliff producing the geomorphic evidence of these large block landslides. An additional consideration relates to the flat lying geology of the peninsula. This would tend to suggest that if failure occurred it would be in the form of block landslides rather than as circular failures.

b) Piping-Triggered Block Failure

Since urbanisation of the Peninsula this type of failure has produced the most concern as a potential threat to people and property. After prolonged periods of higher than average rainfall, rainwater permeates through the various soil units via erosional structures such as exfoliation defects, fractures, bioturbation (rootlets), and buried stream channels. In addition, soakholes directly inject stormwater into these structures as well as into the stratigraphic units. This in turns recharges an aquifer system located approximately 14m below the Peninsula surface within the Upper Matua Subgroup. The aquifer is thought to extend back up the Peninsula with an approximate slope of 1° into the surrounding hinterland (Hall, 1996), suggesting a reasonably large catchment area (~5 km^2). The porewater pressures within the aquifer increase due to the build up of the hydraulic head within the Peninsula and the low permeability of the aquifer, and the system's ability to

evacuate the water through exit points around the cliff faces decreases. This produces a dynamic system where water infiltration from a prolonged rainstorm can result in a piping-type failure which extends approximately 5m back into the cliff face. This piping failure rapidly expands laterally, thus removing support from beneath the soil mass above. This induces a failure along a single exfoliation defect or a number of defects (evident in the field), with a block sliding downwards and then outwards in a roughly circular path. Internal defects within the slide mass help to break up the block, allowing the contained water to produce a soil flow. Figure 2.8 presents the developmental stages of failure. From Cruden and Varnes (1996) the slide can be defined as a "retrogressive, complex; rapid-extremely rapid, wet, debris, slide-flow".

c) Wave Erosion Triggered Block Failure

Wave erosion-triggered block failures (Figure 2.9) do not appear to be as prominent as other failure types around the Peninsula. Areas most effected tend to be located at the NE end of the Peninsula where wave energy is the greatest. Initially they are started by a small colluvium/topsoil failure at the base of the cliff. Fretting along exfoliation is produced by large root mats related to the vegetation above propagation along defects (Figure 2.9). This fact in conjunction with wave erosion erosion at high tide and rainfall during storm events will produce small (~ $<1m^3$) failures by falling. As the cavity grows the weight of the unsupported block above will shear along either the Colluvium/topsoil-stratigraphic unit boundary, or along an exfoliation defect (Figure 2.9). Difficulties arise in predicting the size of the failure. Potentially if the cavity becomes large enough a reasonable sized block failure could occur. However, in most cases it is surmised that a colluvium/topsoil or shallow block failure will form. A colluvium/topsoil failure is a term used for the failure of either a ($2m^3$ - $200m^3$) section of the colluvium/topsoil (Figure 2.10), or a bigger failure (~ $400m^3$) that involves the colluvium/topsoil and the underlying stratic units (Figure 2.9).

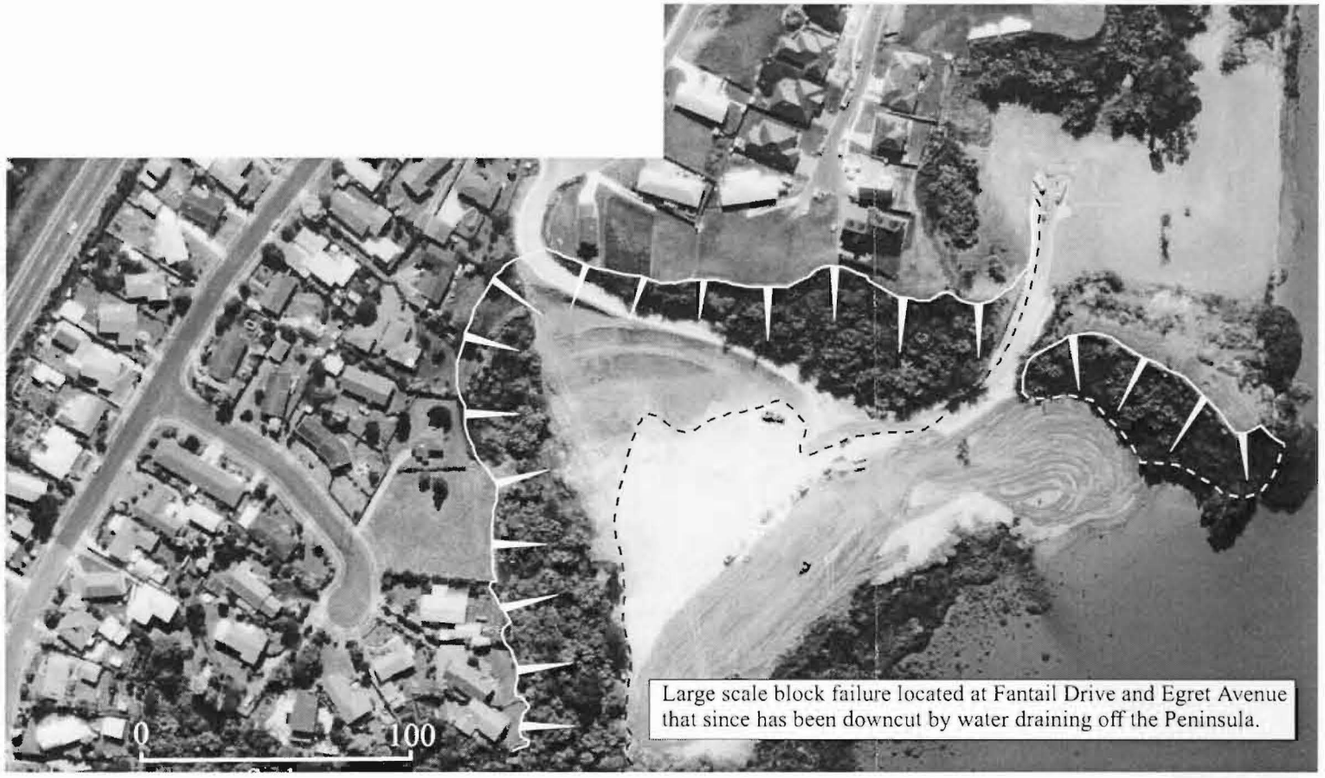

Large scale block failure located at Fantail Drive and Egret Avenue that since has been downcut by water draining off the Peninsula.

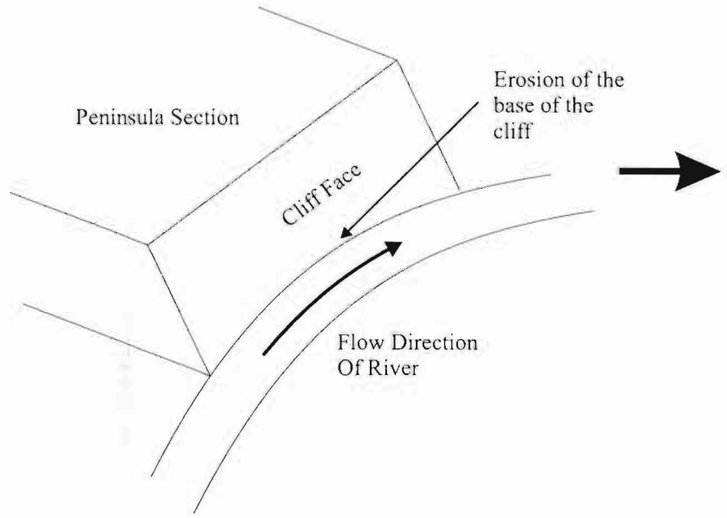

1.) Erosion of the toe of the cliff by the river results in a decrease in the stability of the cliff face.

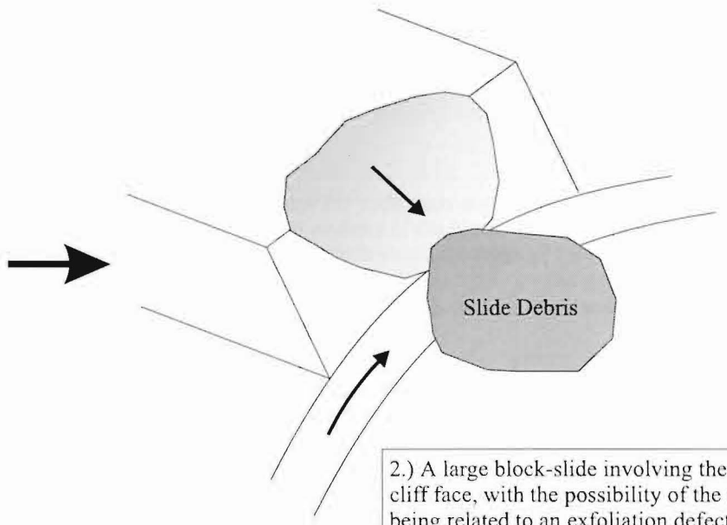

2.) A large block-slide involving the whole of the cliff face, with the possibility of the releasing surface being related to an exfoliation defect.

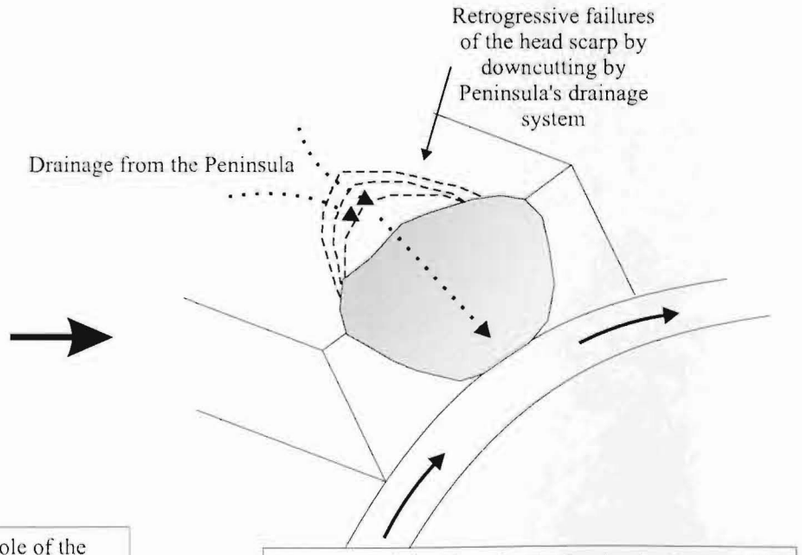

3.) Water draining from the Peninsula slowly downcuts through the soils producing shallow colluvium/topsoil failures that result in expanding the landslide area.

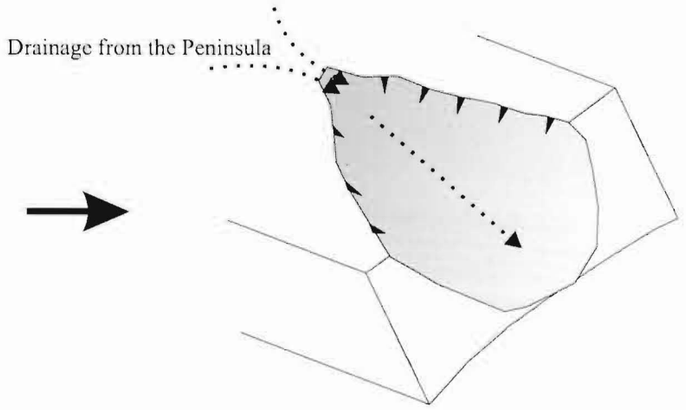

4.) Downcutting by the Peninsula's drainage system produces the geomorphological features seen at Fantail Drive and Egret Avenue.

Figure 2.7 Developmental stages of the "probable larger scale landslides" seen around the Maungatapu Peninsula with an example located at Fantail Drive and Egret Avenue (grid reference 704350 274850).

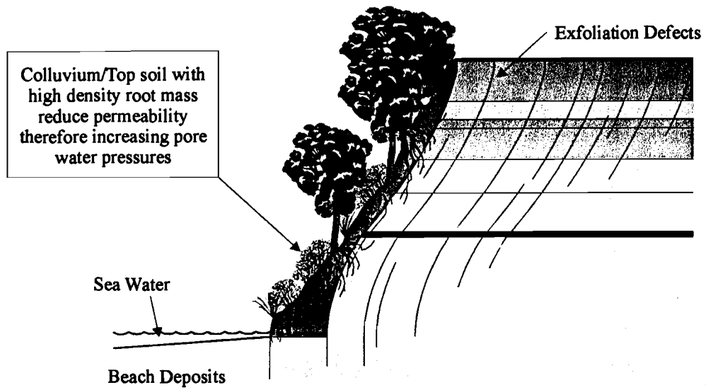

1.) A cliff section showing generalised geology, and vegetation with roots penetrating the colluvium/Top soil. Exfoliation defects which follow the cliff geometry provide possible releasing surfaces for block failure, and are picked up by rootlets near the cliff face.

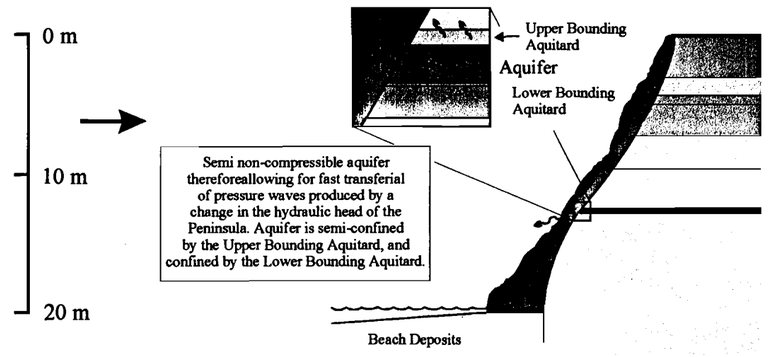

2.) Subsequent to a prolonged period of rainfall the water permeates through the soil mass from the surrounding foot hills and peninsula. Water enters an aquifer ($k=10^{-4}$ m/sec, thickness 15-20 cm) approximately 14 m below the Peninsula surface which is partially confined by two aquitards. Water exits into the colluvium/Top soil of the cliff face where the high density root mass prevents free drainage producing high pore water pressures.

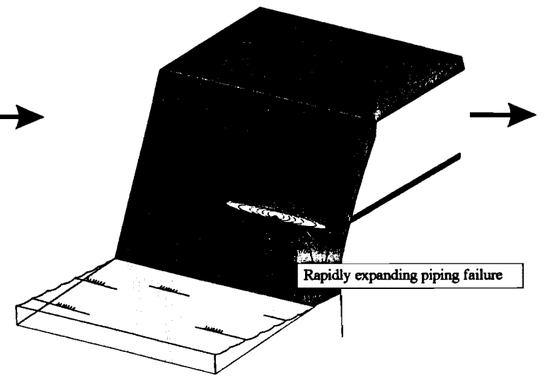

3.) High pore water pressures act on an area of weak Colluvium/Top soil producing a piping failure, which very rapidly expands eroding material.

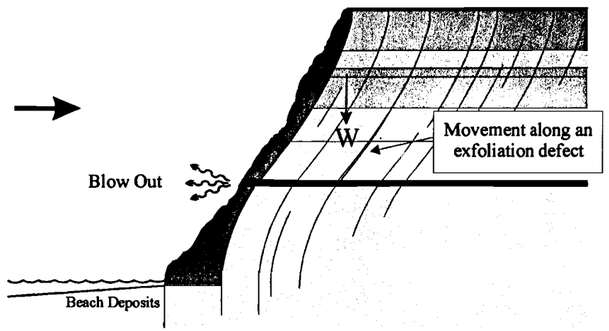

4.) The zone of weakness created by the expulsion of soil via a piping failure allows the weight of the soil mass above to dilate along an exfoliation defect.

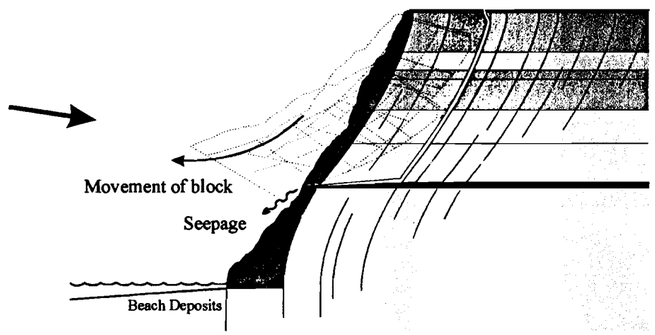

5.) The block slides out under its own weight breaking up along exfoliation defects.

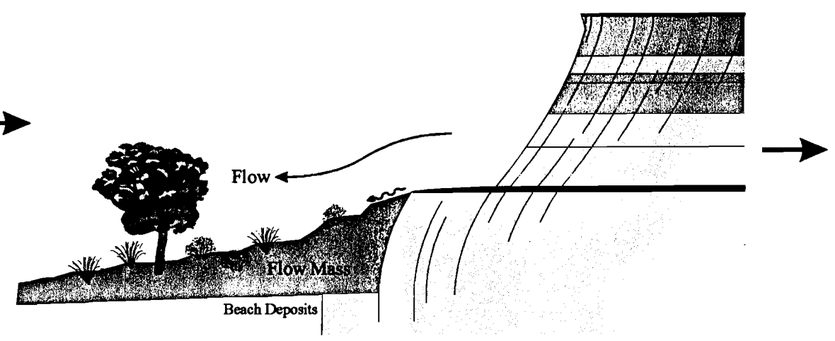

6.) Internal mixing of the slide mass occurs due to inherent water content of the lower sections of the block. This, in conjunction with the possibility that the slide enters the water of the harbour produces a flow. The vegetation that was perviously on the cliff face moves down and out with the slide-flow generally still standing when the flow halts.

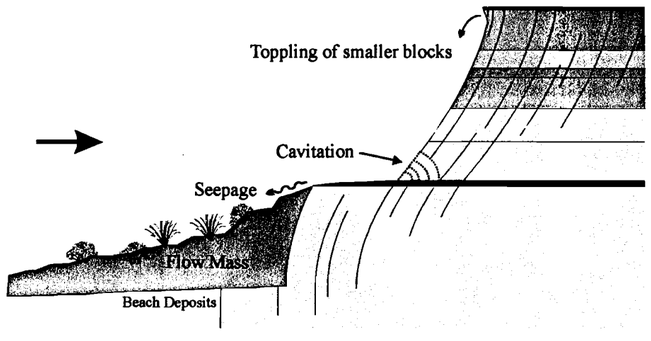

7.) Toppling occurs in overhanging section of cliff top along sub-vertical exfoliation defects. In addition water seeping out of the slope produces minor cavitation particulary around the areas of seepage.

KEY

- Colluvium/Top soil
- Post-Rotoehu Ash Tephras
- Rotoehu Ash
- Palaeosol
- Hamilton Ash
- Upper Matua Group Sediments
- Aquifer

Figure 2.8 Schematic representation of a piping triggered block failure.

Landslide type is influenced by a number of factors such as: water content, aquifer influence, vegetation mass, cliff geometry, size of cavity, and tide height. A suggested situation of moist water content, high vegetation density, reasonably sized cavity (>50m^3), and high tide, could by Cruden and Varnes (1996) terminology be termed a "enlarging, multiple, very slow-slow, dry-moist, earth, fall; complex, very rapid-extremely rapid, moist, debris, slide-flow". Figure 2.9 presents a summary of the developmental stages of cliff failure.

d) Colluvium/Top Soil Failure

Colluvium/topsoil failures are one of the more common types of failures seen around the Maungatapu Peninsula and can involve part or all of the cliff face. Cliff faces tend to be heavily vegetated resulting in a prominent root mass. As in wave erosion-triggered block failures, landslide type is influenced by a number of factors such as: water content, aquifer influence, vegetation mass, cliff geometry, site specific rainfall, and tide height. Rainwater permeating through the colluvium/topsoil mass in addition to aquifer water will increase porewater pressures within the cliff face area. Toe undercutting by wave action will remove support, producing a colluvium/top soil failure at the bottom of the cliff face. Weight from the overlying vegetation and colluvium/topsoil mass will result in the formation of a slide on either an exfoliation defect close to the surface of the underlying soil, or a shear developing between the boundary of the colluvium/topsoil and underlying geologic units. The transition of the failure from a slide to a flow depends on the water content of the colluvium/topsoil and tide height. If the failure mass is saturated, a rapid change will occur between the initial slide and a flow due to partially liquifaction of the soil mass on hitting the bottom of the cliff, especially on entering the harbour water at high tide. From Cruden and Varnes (1996) terminology, the failure sequence can be described as a "complex, very rapid-extremely rapid, moist-very wet, earth, slide-flow". Figure 2.10 presents a summary of the developmental stages of colluvium/topsoil failure. The resulting scarp will undergo additional deformation from rainfall penetration producing rill erosion

therefore producing further smaller (0.5-3m^3) shallow failures. Vegetation and cliff slope will also play an important part in failure. For instance, the steeper the slope the less stable the colluvium/top soil mass is and the more prone to failure when saturated. In addition, vegetation can increase the potential of a failure to occur by increasing weight on the slope, but more importantly will induce a torque on the colluvium/topsoil. This torque is greatest when a large tree (eg Pohutukawa) weight acting downwards induces a moment about the root structure. If the conditions are satisfactory (eg soil mass is saturated) the tree's weight will result in the failure of colluvium/topsoil mass in which the roots are located.

2.5 SYNTHESIS

Soils of the Maungatapu Peninsula are formed by a number of processes varying from fluvial deposition of silts, sands and gravels producing cross and planar beds, to lacustrine and estuarine deposited muds. Intercalated with these deposits are Pahoia Tephras which together form the Upper Matua Subgroup. An aquifer bounded by one semi-permeable aquitard and one non-permeable aquitard, has been delineated from field investigations and is situated within the Upper Matua Subgroup. Overlying the Upper Matua Subgroup in succession are a sequence of ashes and tephras: the Hamilton Ash, Rotoehu Ash, and the Post-Rotoehu Ash Tephras (or Younger Tephras). The Hamilton Ash and associated palaeosol form in part an impermeable barrier between the ashes and tephras above and the Upper Matua Subgroup deposits below. Harmsworth (1983) and Hall (1994) have indicated that the Peninsula deposits extend back into the surrounding hinterland allowing for a larger catchment area (~5km^2) for rainwater to permeate through to the aquifer.

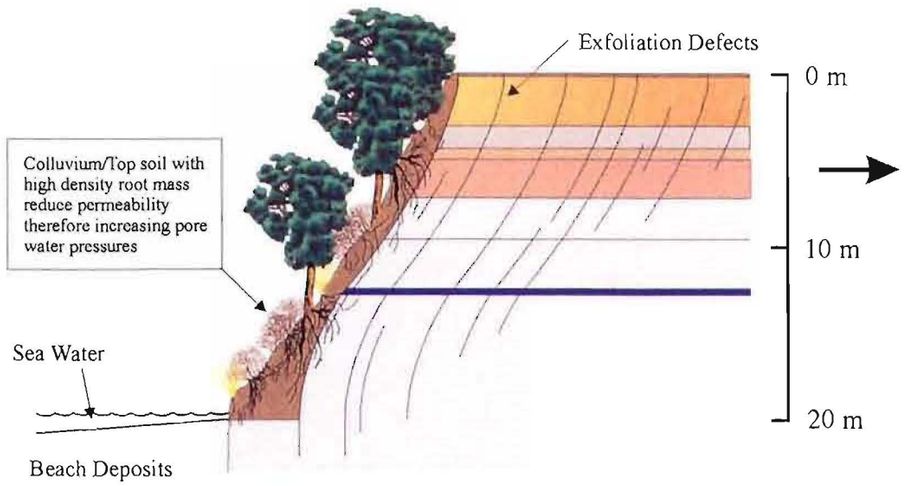

1.) A cliff section showing generalised geology, and vegetation with roots penetrating the colluvium/Top soil. Exfoliation defects which follow the cliff geometry provide possible releasing surfaces for block failure, and are picked up by rootlets near the cliff face.

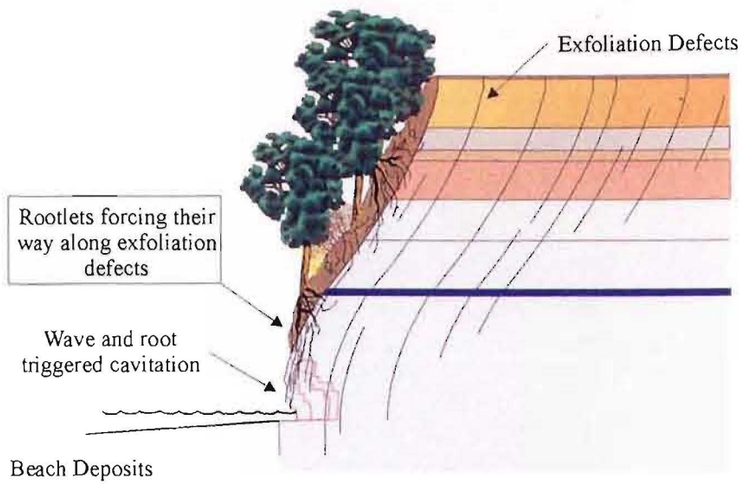

2.) Toe erosion cause initially by a small Colluvium top soil failure at the base of the cliff, producing a fresh surface. Cavitation is caused by a combination of toe erosion by wave action during storm events, and failure along exfoliation fefects by the above vegetation's root mass.

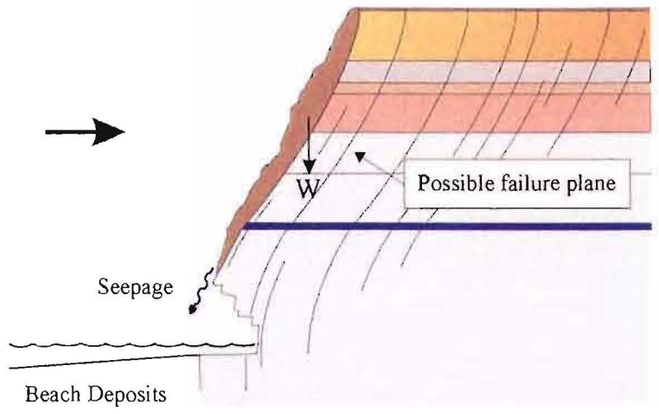

3.)The weight of the above soil mass becomes to great and slides away from the cliff along an exfoliation defect.

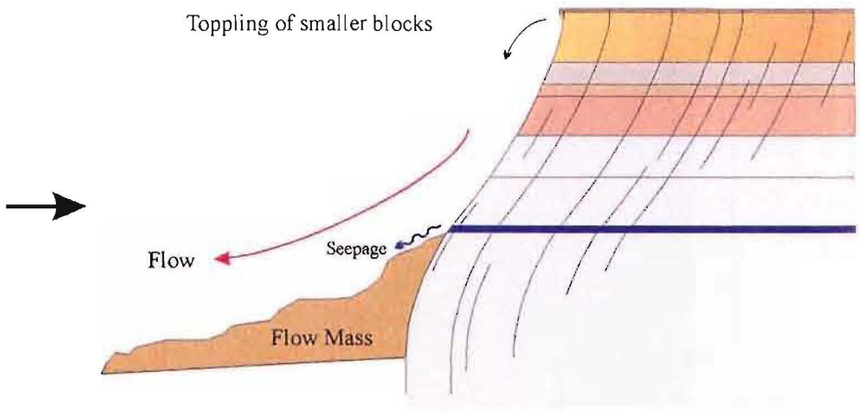

4.) As the block fails internal defects help to break it up as it hits the cliff bottom. With high water content as in aquifer triggered failures or on entering sea water will produce a flow instead of a slide as in the second phase of movement.

Figure 2.9 Schematic representation for a wave erosion triggered block failure. Failure occurs where the toe of the cliff has been removed by erosion producing either a colluvium/top soil failure or a larger block failure. The later stages of failure can be dramatically influences by water content of the soil mass. From Cruden and Varnes (1996) terminology the failure can be defined as a "Retrogressive, complex; very slow-extremely slow, dry-moist, debris, fall; very rapid-extremely rapid, moist-very wet, debris, slide-flow".

The Photograph depicts how the root mass from vegetation above pushes its way through the soil mass along exfoliation defects creating a root mat. This provides a surface on which the soil can fail after it has been undercut by wave action. Failure in this case tends to occur more as falls with debris easily seen accumulated at the bottom of the cliff.

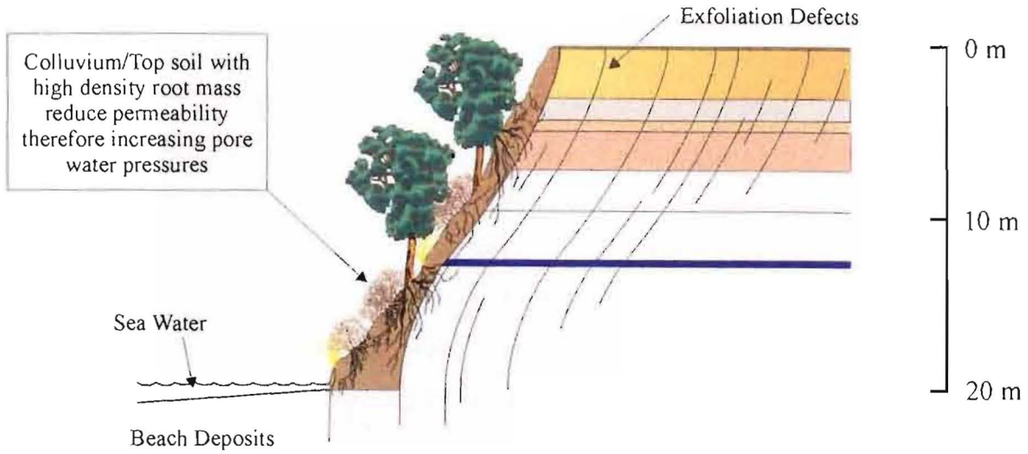

1.) A cliff section showing generalised geology, and vegetation with roots penetrating the Colluvium/Top soil. Exfoliation defects which follows the cliff geometry provide possible releasing surfaces for block failure, and are picked up by rootlets near the cliff face.

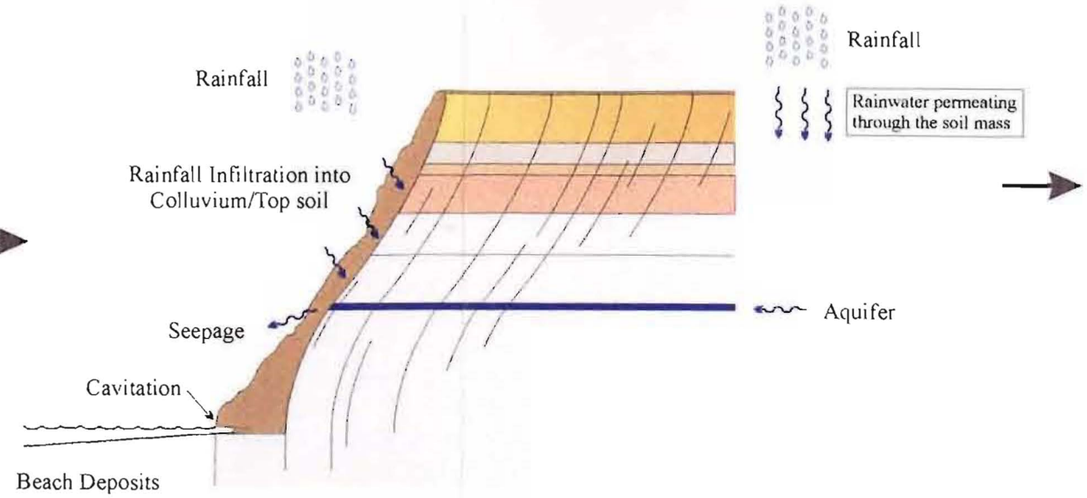

2.) Rainfall entering the soil mass from the surrounding hinterland and Peninsula is transferred to the aquifer which exits at the cliff face. In Addition, rainfall can help to saturate the Colluvium/Top soil mass adding extra weight and increasing pore water pressures. Also erosion by wave action at the base of the cliff can increase the possibility that failure will occur.

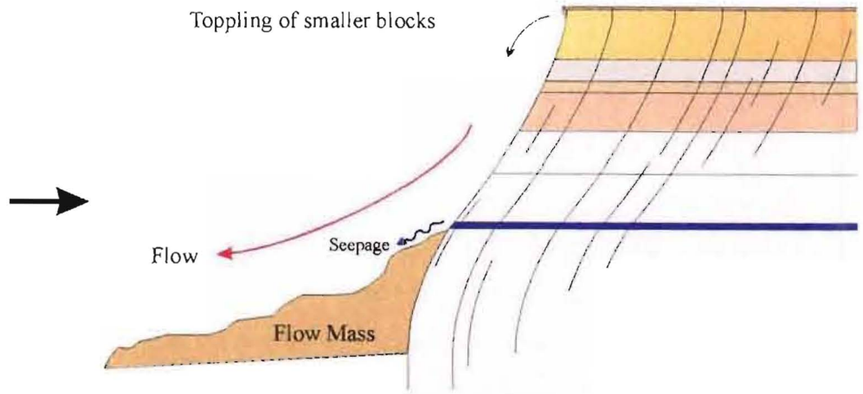

3.) The boundary between the Colluvium/Top soil and underlying geologic units can provide a surface on which a top soil failure may occur. As the top soil slides internal mixing of the soil mass due to the high water content produces a flow. If the flow enters sea water this will increase the effects of the internal mixing and how far the flow will travel. Most of the vegetation tends to survive the failure remaining in a semi-vertical position as on the cliff face.

The Photograph show vegetation root mass in conjunction with Colluvium/ Top soil produces a surface on which failure may occur. Vegetation weight especially larger trees results in a torque placed on the soil mass aiding in production of instability. Sliding has occurred along the interface between the vegetation root mass-Colluvium/Top soil and a shallow exfoliation defect. The debris has subsequently been eroded away by wave action.

Figure 2.10 Schematic representation of a Colluvium/Top soil failure. From Cruden and Varnes (1996) terminology the failure can be identified as a "Retrogressive, complex, very slow-very rapid, dry-wet, debris, slide-flow".

Field investigations defined four major failure types. The first are probably larger-scale block landslides (~$5\times10^5 m^3$) which involve the entire cliff section possibly indicating a triggering mechanism different from that of the other three landslide types. It has been suggested that landsliding is the result of downcutting during glaciation periods where sea level lowering resulted in the rivers bounding the Peninsula on the NE and SW sides have eroded the toe of the cliff sections producing landsliding. An additional consideration relating to the flat lying geology of the Peninsula would tend to suggest the production of block failures more so than a circular failure.

Piping-triggered block failures and colluvium/top soil failures are greatly influenced by rainfall. Historical records indicate that many of these types of failures occur after a prolonged period of higher than average rainfall. Piping-triggered failures tend to occur after two months of higher than average rainfall recharging the aquifer system within the Upper Matua Subgroup. When porewater pressures reach a critical level a piping failure can be occur, which in-turn produces a block failure along an exfoliation defect. colluvium/topsoil failures occur when the top soil mass saturation increases to a point where cohesion between the colluvium/top soil and underlying geology is decreased sufficiently for sliding to occur. Two possible failures can occur involing either the development of a shear between the colluvium and underlying geology, or failure along a near surface exfoliation defect. Vegetation can also produce failure by forcing a root mat along a defect as demonstrated in Figure 2.9. In addition vegetation increases the overall weight on a slope, especially larger trees which will induce a torque on the soil due to their height and canopy. Colluvium/topsoil failures can also be produced by undercutting of the base of the cliff by wave action within the estuary. This creates a small cavity which is expanded by vegetations root mat penetrating exfoliation defect planes resulting in small (~$<1 m^3$) falls (Figure 2.9). The cavity slowly increases in size to a point (>$50 m^3$) where the overlying stratigraphic units can no longer be supported resulting in a colluvium/topsoil failure.

Chapter Three FIELD INVESTIGATIONS

3.1 INTRODUCTION

Engineering geological and geotechnical field investigations involving aerial photograph interpretation, landslide monitoring, in-situ shear strength testing, hydrogeological investigations, in-situ permeability testing, and soakhole investigations are presented in this chapter. The primary aim of this chapter was to obtain an understanding of the components which combined to produce the landsliding seen at properties such as 85 Te Hono Street. Relevant information from field investigations could then be used in conjunction with laboratory testing (Chapter 4) to aid in stability analysis and hazard assessment.

Field investigations involved the use of engineering geological and geotechnical techniques to provide a better understanding of the components which together influence landsliding seen at Maungatapu Peninsula. Numerous methodologies exist to denote investigation stages and objectives from authors such as Fookes (1967), Clayton et al. (1982), Bell and Pettinga (1983), and Bell (1990). Although one system may not be totally appropriate, the general concepts behind these methodologies are the same. For this study the methodology adopted is that denoted by Clayton et al. (1995), and Bell (1990), as shown in Figure 3.1.

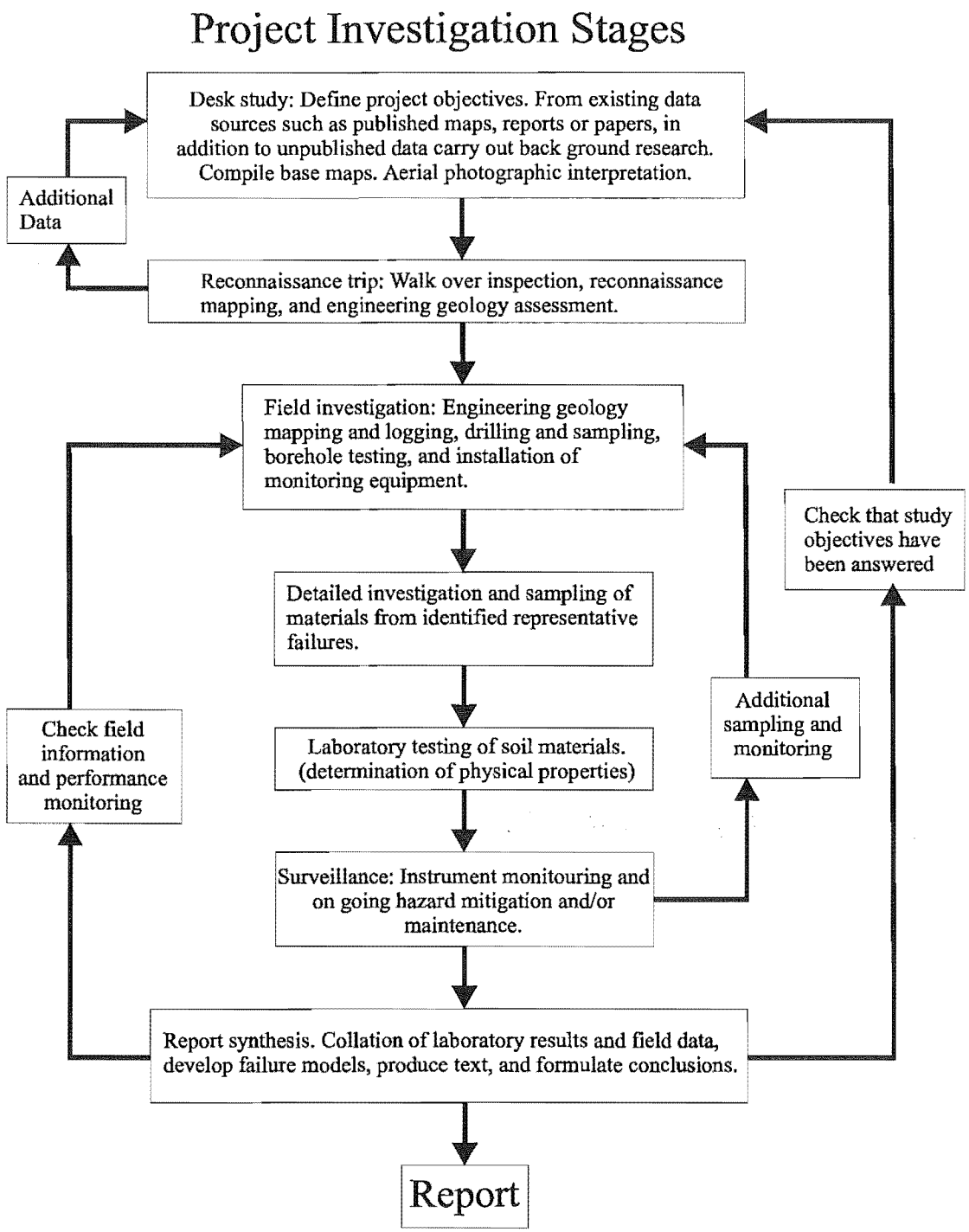

Figure 3.1 Flow chart illustrating the methodology used during this study. The conceptual stages were adopted from Clayton et al. (1982) and Bell (1990).

3.2 DESK TOP STUDY

Existing information such as geotechnical and geological reports, maps, logs, aerial photographs, and theses held by the Tauranga District Council, and other institutes form the available data base used for this project.

3.2.1 Aerial Photographic Interpretation

Aerial photographs were obtained from the Tauranga District Council and Airmaps New Zealand dated 1943, 1975, 1977, and 1992 (Table 3.1). The object of aerial photograph interpretation was to firstly distinguish possible landslide types prior to the site investigation phase; secondly, to assess any progressive regression of the cliff faces around the edge of the peninsula from 1943 to present, and lastly for geomorphic mapping purposes. However, a number of problems arose such as lack of stereo pair cover of the peninsula, and the small air photo scales made it difficult to achieve some of these objectives. For instance, the 1943 photographs only provided stereo pair coverage of the last 400 m, with all photographs from this time period having scales of 1:16 000. This made it difficult to pick up individual evidence of smaller scale failures such as those at properties like 85 Te Hono Street. Comparision between the 1943 aerial photographs at a scale of 1:16 000 with the 1975 and 1992 photographs at a scale of 1:10 000 was not possible due to the differences in scale and hence resolution. While smaller scale failures could be identified on the 1975 and 1992 air photographs they were not distinctive enough to be seen on the 1943 aerial photographs.

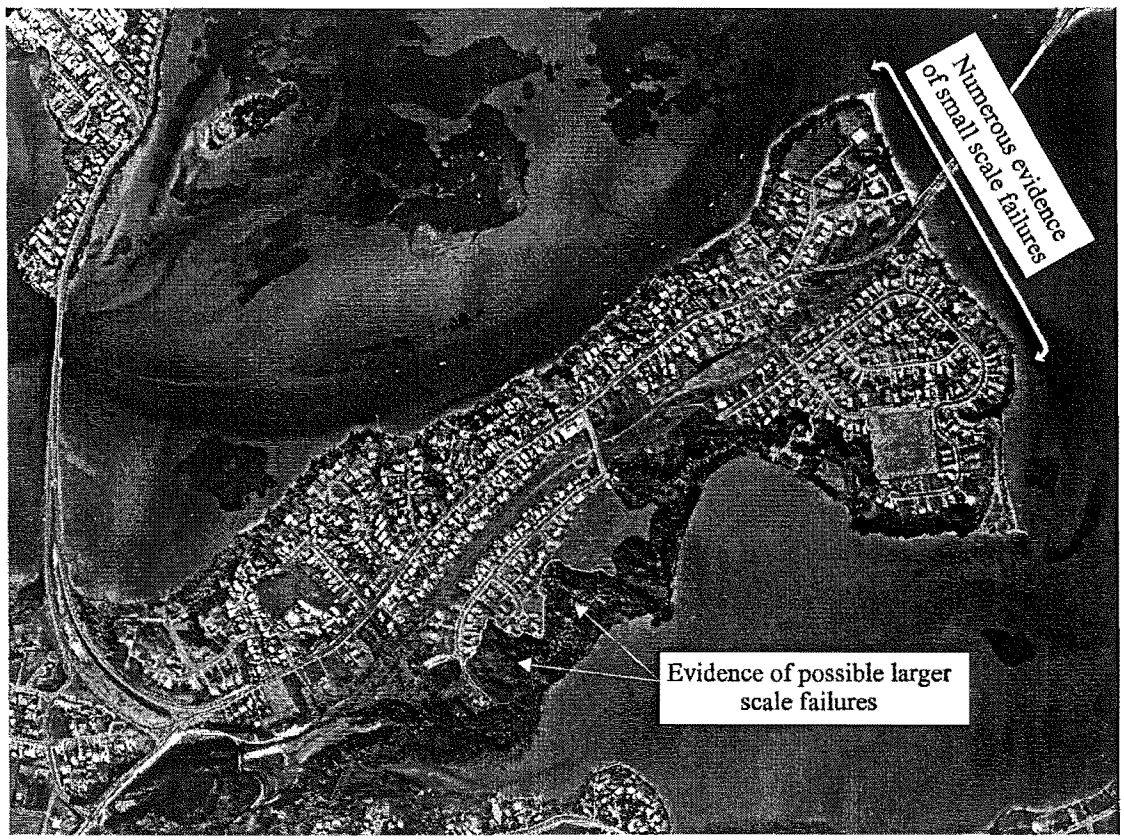

Figure 3.2 Aerial Photograph identifying some of these possible large landslide features as well as a zone where there is numerous evidence of smaller scale failures such as those seen at 85 Te Hono Street.

Table 3.1 List of aerial photographs used in the coarse of this study.

Run Number	Scale	Date taken	Source
501/60 501/61	1:16 000	1943	Tauranga District Council
208761 208762 208765 208766	1:10 000	1975	Tauranga District Council
212251 212252 212253	1:15 800	1977	Tauranga District Council
No Run Numbers	1:10 000	1992	Airmaps New Zealand

The 1977 aerial photographs produced similar problems to the 1943 photographs having a scale of 1:18 000. Air photographs taken in 1975 and 1990 were of most use with scales of 1:10 000. Both runs showed clear evidence of the small scale failures apparent at properties like 85 and 89 Te Hono Street, and the areas where erosion appears to be the greatest occurred at the NE end of the peninsula (Figure 3.2). Because of the small volumes of material which were lost with each slide it became difficult to predict a regression rate from these aerial photographs. Other objectives such as distinguishing landslide types and geomorphic mapping purposes were achievable with these larger scale photographs

3.3 FIELD INVESTIGATIONS

Field investigations involve the use of many techniques such as engineering geological and geotechnical mapping, drilling and sampling, borehole tests, and in-situ geotechnical testing. The field investigation stage can be divided into a number of sections:

1. Engineering geological mapping of the peninsula to further determine landslide types and distribution around the peninsula,
2. geotechnical logging of the landslide scarps at 85 and 89 Te Hono Street, and 330 Maungatapu Road,
3. core logging of bore holes drilled for the installation of piezometers for monitoring ground water behaviour,
4. installation of piezometers to monitor ground water behaviour,
5. a sampling programme initiated in order to collect material for later laboratory testing,
6. in-situ permeability testing to provide some indications of permeabilities associated with the failure zone.
7. in-situ shear strength testing to determine a range of strengths associated with the various soil units found during the logging of the failure scarps,

8. soakhole investigations to try and determine their effect on the hydrogeology of the peninsula.

These aspect are discussed in greater depth further below.

3.3.1 Engineering Geological Mapping

Mapping concentrated on the cliff faces around the Maungatapu Peninsula. Using the G.I.S. data base developed by the Land Information section of the Tauranga District Council a 1:5000 scale base map was produced. Information from aerial photograph interpretation was then transferred to this base map. Mapping mainly concentrated on geomorphic features such as landslide scarps present around the peninsula's edge. This was mainly to determine landslide types and their distribution around the peninsula. In addition to geomorphic information the map provides the location of the piezometers that were installed as well as the positions of the logged landslide scarp faces.

3.3.2 Geotechnical Logging of Landslide Scarps

From the desk top study three landslides were outlined for more detailed investigations, specifically the properties 85 & 89 Te Hono Street, and 330 Maungatapu Road (Map 1, Map Box). The high number of beds associated with the Post-Rotoehu Ash Tephras, Rotoehu Ash, Hamilton Ash, and Upper Matua Subgroup sediments, and little lateral and vertical variation within each bed, resulted in the decision being made not to log the entire face as is normally done. Instead investigations comprised a single geotechnical log that ran longitudinally down the failure scarp (see Face Logs 1-3, Map Box).

Face logs were conducted by abseiling down the cliff face and recording geotechnical information such as a depth below the top of the cliff, soil description using Bell and Pettinga's (1983) engineering geological field descriptions for soil material (Appendix A3.1), a reference number for a bulk or tube samples taken, whether seepage is occurring

and from where, and vane shear strength of the soils. In addition to this, the changes in slope were recorded by a distance and an angle so the log could be later corrected for slope, producing a vertical log (see Face Logs 1-3, Map Box). This information was transferred onto an A1 sheet for easier interpretation (see Face Log 1-3, Map Box).

3.3.3 Geotechnical Core Logging

On the recommendation to the Tauranga District Council by Bell (1995), eight piezometers were installed in March of 1996 to provide better understanding of the hydrogeology of the peninsula. These boreholes were positioned to form a rough grid (Map 1, Map Box), and Perry Drilling was commissioned by Beca Carter Hollings & Ferner Ltd on behalf of the Tauranga District Council to undertake the drilling and installation of the piezometers. The boreholes were drilled using a hydraulic open hole drill rig set up (Figure 3.3), and a 75mm diameter × 750mm long split tube was used to recover the core from the borehole. This provided effective core recovery until the water content of the soil increased, whereupon a 50mm split tube was used. When this proved unsuccessful, a 50mm push tube was driven approximately 750mm in front of the cutting edge of the auger head to provide an undisturbed sample. However, core recovery in these saturated zones proved difficult for two main reasons. Firstly, some samples tended to slide out of the push tube on their way up, and secondarily they liquefy on the addition of water to provide the suction for the push tube. This made it hard to distinguish the aquifer zone that the slotted section of the piezometer was trying to be positioned for.

The boreholes were logged during this study for two main reasons: 1) to ascertain the position of the aquifer in order for the slotted section of the piezometer to be correctly positioned; 2) to provide an opportunity to better constrain the geology of the peninsula. Geotechnical logging of the boreholes consisted of a soil description relative to depth using Bell and Pettinga's (1983) engineering geological field descriptions for soil material

(Appendix A3.1). Data from the logged boreholes was then transferred onto A2 log sheets for easier interpretation (Borehole Log BH1-BH8).

Figure 3.3 Hydraulic open hole drill rig set up. Hallow augers with an internal diameter of approximately 80 mm were used drill a bore hole to a depth where core recovery was inadequate. A 75 mm internal diameter by 750 mm long split tube were used to recover the core using water to create a vacuum. When core recovery became poor a 50 mm internal diameter by 1500 mm long push tube was used.

3.3.4 Piezometer Installation And Monitoring

The piezometers were installed in order to monitor water level responses to rainfall events, and to provide some insight into the hydrogeology of the peninsula. In addition to these piezometer a further two boreholes were drilled by Perry Drilling under contract to Beca Carter Hollings & Ferner and two piezometers in each borehole installed (Piez 9/1, Piez 9/2, Piez 10/1, and Piez 10/2). The piezometers consisted of a 28mm internal diameter PVC tube that contained a slotted length between 0.5 and 2.5m. This slotted section was positioned either within a predicted aquifer zone (located approximately 14-15m below ground surface), or within a perched aquifer located at a shallower depth than the main

aquifer zone (Figure 3.4). The slotted section was sealed by bentonite in order to reduce the influence of water flow from above in the deepest piezometer, and above and below in piezometers located further up the borehole. Table 3.1 indicates the depth of the piezometer as well as the lithological unit in which the slotted section of the piezometer is located. The top of piezometer was surveyed in to obtain a reduced level related to Tauranga's local datum. These reduced levels are present on the borehole sheets as a reference datum, e.g.. BH1 has a reference datum of 23.53m. In addition to this most boreholes contained more than one piezometer, resulting in defining piezometers according to the boreholes they were located in and which piezometer they are, i.e. Piez1/2 means that piezometer 2 is located in borehole 1.

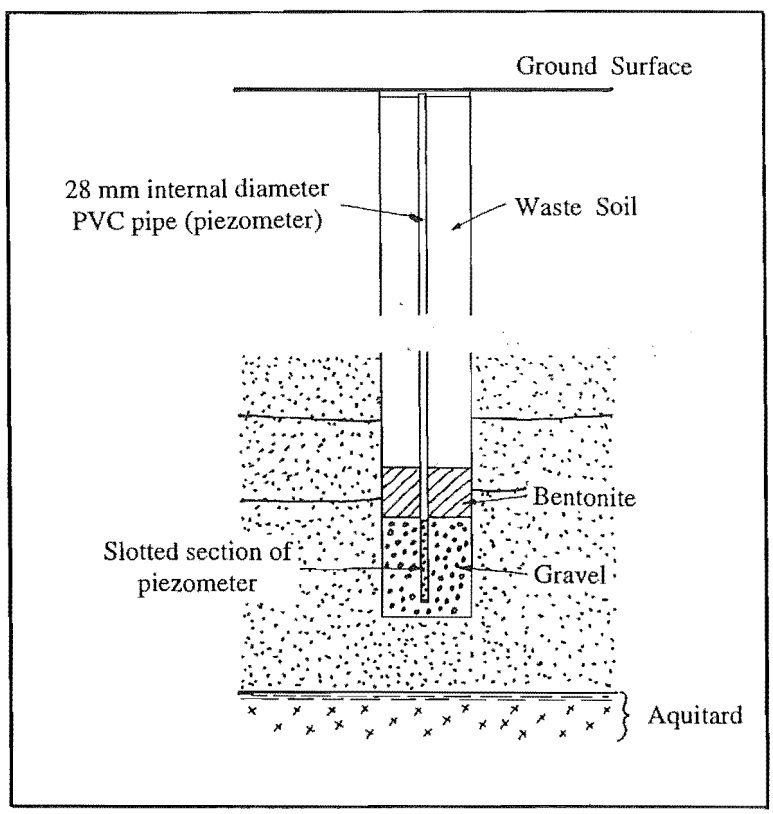

Figure 3.4 shows the typical set up of a piezometer used to measure water level responses from rainfall.

Tauranga District Council contracted Beca Carter Hollings & Ferner Ltd. to monitor the water levels within the piezometers and to provide an assessment of hydrogeology of the peninsula. Monitoring of the water levels was conducted firstly on a daily bases from March to late August 1996, which was reduced to twice weekly from late August to June 1997 on the recommendation of O'Halloran (Beca Carter Hollings & Ferner Ltd., 1996).

Table 3.1 Slotted depths of piezometers and associated soil type within which water levels were measured. Beca Carter Hollings & Ferner drilled a further two bore holes No. 9 & 10.

Bore Hole Number	Piezometer Number	Reduced Level	Depth of Slotted Section From Surface (m)	Lithological Unit	Soil Type
1	Piez 1/1	23.47	16.5-17.0	Upper Matua Subgroup	Bedded Fine-Medium Sands
	Piez 1/2	23.47	13.5-14.0	Upper Matua Subgroup	Cross-bedded fluvial sequence
	Piez 1/3	23.47	10.0-10.5	Upper Matua Subgroup	Pahoia Tephras
2	Piez 2/1	22.16	16.0-17.0	Upper Matua Subgroup	Unknown
	Piez 2/2	22.16	13.5-14.0	Upper Matua Subgroup	Unknown
3	Piez 3/1	20.18	13.0-13.5	Upper Matua Subgroup	Cross-bedded fluvial sequence
	Piez 3/2	20.18	9.0-10.0	Upper Matua Subgroup	Cross-bedded fluvial sequence
4	Piez 4/1	22.46	15.5-16.5	Upper Matua Subgroup	Unknown
	Piez 4/2	22.46	10.5-11.0	Upper Matua Subgroup	Cross-bedded fluvial sequence
5	Piez 5/1	22.74	12.0-15.5	Upper Matua Subgroup	Unknown
6	Piez 6/1	23.98	13.0-14.0	Upper Matua Subgroup	Cross-bedded fluvial sequence
7	Piez 7/1	23.72	11.0-11.5	Upper Matua Subgroup	Cross-bedded fluvial sequence
8	Piez 8/1	24.86	13.0-14.0	Upper Matua Subgroup	Cross-bedded fluvial sequence
9	Piez 9/1	13.77	16.0-18.0	Upper Matua Subgroup	Probably below aquifer zone
	Piez 9/2	13.77	10.0-13.0	Upper Matua Subgroup	Possibly Pahoia Tephras
10	Piez 10/1	16.23	12.5-14.5	Upper Matua Subgroup	Unknown
	Piez 10/2	16.24	6.5-7.5	Upper Matua Subgroup	Unknown

3.3.5 Sampling Program

During the desk top study and initial phases of the field investigation stage a number of tests were identified as being useful in the geotechnical characterisation of the soils associated with the cliff faces. These tests consisted of:

1. Particle size analysis to provide a quantitative classification of the various soils on which geotechnical testing was conducted.

2. Clay mineralogy analyses to determine whether the clays present influenced the behavioural characteristics of the soils.

3. Atterberg limits to provide further geotechnical characterisation of soils, in addition to later usage in stability analysis.

4. Direct shear testing to determine c' (cohesion) and ϕ' (friction angle) parameters for stability analysis (Chapter 5).

5. Triaxial testing for determination of shear strengths and failure mechanisms which could then be compared to what has been identified in the field from in-situ shear strength testing and landslide failure dynamics.

6. Erodibility and dispersion testing to determine how erodible and dispersive the soils were to establish whether the triggering mechanism denoted in Chapter 2 (i.e. piping failure) could occur.

7. Permeability testing to provide a range of hydraulic conductivities for the soil stratigraphy associated with the logged cliff faces for later use in hydrogeological assessment of the peninsula.

Samples were collected from most units, e.g. Post-Rotoehu Ash Tephras, Rotoehu Ash, Palaeosol etc., especially concentrating on the lower section of the cross-bedded sequence, upper and lower aquitards, and the aquifer. Bulk samples that were representative of the unit which they were collected from were obtained for direct shear testing, Atterberg limits, clay mineralogy and particle size analysis. Collecting samples for triaxial, erodibility, and dispersion testing involved carefully pushing into the desired soil material a 38 mm diameter by 100/200 mm stainless steel tube. Collection of samples for permeability testing was performed in much the same way by carefully pushing into the desired soil material a 100 mm diameter by approximately 110 mm long alloy tube. Collected samples were then placed into three heavy duty plastic bags and taped to ensure the in-situ moisture content was maintained. Labelling of the samples consisted of the depth at which they were collected / the number of samples taken at that depth / and the

house number from where they were collected. i.e. 5.8/1/85 indicate that a sample was collected 5.8 m below the top of the cliff, one sample was taken, collected from the cliff face at 85 Te Hono Street. As all laboratory testing was to be conducted at Canterbury University, samples were then placed into boxes that contained polystyrene packing material to provide protection for the journey from Tauranga to Christchurch.

A number of problems arose in obtaining completely undistributed samples because of either the compact nature of the soil or the wide range in grainsize. The Palaeosol and Hamilton Ash proved to be especially difficult to push a sample tube into, so a bulk sample was taken instead. However, even this was difficult as the bulk samples would break along old rootlet structures and fractures within the soils, producing pieces that were too small for an in-situ sample to be used for laboratory permeability testing. This meant that samples on testing had to be broken up and Proctor mould recompaction undertaken in order for permeability testing to be conducted. The recompacted sample would produce a decrease in the permeability due to the absence of rootlet structures and fracturing.

The second problem was that many of the units exhibited a wide range of grainsizes, therefore making inherently difficult to sample and perform tests on. This was especially evident in the Tephras that were associated with the Pahoia Tephras, and situated above the cross-bedded sequence and below the Hamilton Ash. These airfall deposits demonstrated a range of grainsizes between clays and coarse pebbles. In addition to this some areas were predominately sandy and loose compared to areas where large pumice fragments had partially cemented the sands together (Figure 3.5).

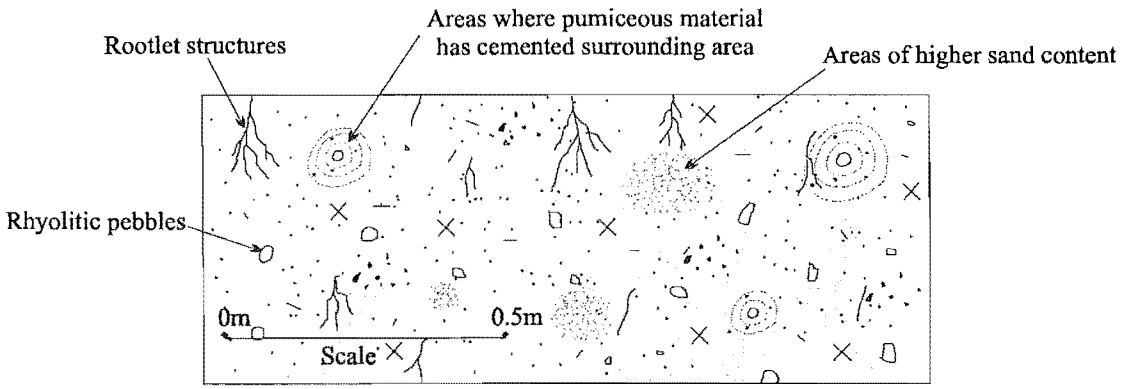

Figure 3.5 Section through a portion of a tephra bed associated with the Pahoia Tephra indicating the wide range of grainsizes, areas of higher sand content, and areas where pumice has cemented grain together.

In addition to the above sampling problems, concern was levelled at the possibility of the water within the saturated samples flowing towards the bottom of the sample, producing an uneven distribution of water within the soil. It is also possible that the samples may be partially disturbed during transport, resulting in the samples no longer truly representing the in-situ conditions at the time of collection. However, how much this weakens the samples is not known. This consideration lead to the turning of the more saturated samples to try and maintain an even distribution of water within the sample in order to reduce this affect.

3.3.7 In-situ Permeability Testing

In-situ permeability testing was conducted using a falling head slug test as outlined by Kruseman and de Ridder (1994) and Fetter (1994). From the suggestion of O'Halloran (Pers. Comn., 1997) borehole BH7 (Map 1, Map Box) was used to conduct an in-situ permeability test during early May 1997 due to its close proximity to a water supply. Methodology, results and discussions will be discussed in a later section (3.4) in this chapter.

3.3.8 In-situ Shear Strength Testing

During geotechnical logging of the landslide scarps a Pilcon Shear Vane was used to determine possible ranges in shear strengths for each stratigraphic unit, i.e. Post-Rotoehu Ash Tephras, Rotoehu Ash, etc. This was done approximately every 0.5m down the slope by pushing a 19mm vane into the desired soil unit to a depth of between 70 and 80 mm, and rotating it at 1 revolution per minute following the manufacturer's instructions. The result was then recorded on the log sheet as a shear strength in kPa, providing a plot of strengths relative to depth.

3.3.9 Soakhole investigations

A soakhole investigation program was undertaken to try and determine the effect that soakholes have on the hydrogeology of the peninsula. They are believed by many people to provide a means where rainwater is directly injected into more permeable soils below the Palaeosol and Hamilton Ash. If this assumption is correct they will have a dramatic effect by increasing the pore water pressures within the aquifer which is located in the failure zone approximately 14 m below the ground surface. Therefore it is important that the determination of the depth or penetration of these soakholes into the underlying stratigraphy is ascertained. From discussions with some of the local property owners around the Te Hono Street end of the peninsula, it was suggested that a drill rig had in fact at one time drilled a number of soakholes through the impermeable Palaeosol and semi-permeable Hamilton Ash, into the Upper Matua Subgroup sediments. Contrary to this, other people such as local builders suggested that soakholes only penetrated to the Rotoehu Ash where upon they stopped on hitting the hard top of the Palaeosol associated with the Hamilton Ash.

To try and quantify the depth that many of these soakholes penetrated to, an investigation was undertaken to locate and record the depths of the soakholes found. However, due to the difficulty in finding soakhole location on properties this was abandoned. Soakholes that were found tended to range in depth between 3 and 4.5m, situating them in the younger ashes (Post-Rotoehu Ash Tephras and Rotoehu Ash). It is therefore concluded that although a majority of the soakholes did not penetrate the Palaeosol, enough qualitative evidence exists to suggest that some clearly penetrated into the Upper Matua Subgroup sediments.

3.4 INTERPRETATION OF FIELD INVESTIGATION DATA

3.4.1 Geotechnical Core Logging

From borehole interpretation the Post-Rotoehu Ash Tephras and Rotoehu Ash are consistent in both thickness and texture with the associated beds blanketing the underlying topography. The Palaeosol varies in thickness from borehole, to borehole altogether disappearing between boreholes BH1 and BH3 (Map Box). Also between these two boreholes the Hamilton Ash thins from 2.7m in BH1 to 0.3m in BH3 (Map Box). This tends to suggest that erosion of these units has occurred by a watercoarse that ran across the peninsula at one time or another. The Hamilton Ash varies in thickness marginally from borehole to borehole, but exhibits a consistent texture. However, the Hamilton Ash does increase considerably in thickness to 6.3m for BH8 (Map Box) around Maihi Crescent. It appears that the hill which trends NE-SW around Maihi Crescent-Te Wati Street is the result of a local thickening of the Hamilton Ash.

The Upper Matua Subgroup units situated below the Hamilton Ash proved difficult to determine a thickness because of poor core recovery. It can be seen when comparing BH1 to BH3, and BH8 to BH1 and Face Log 1 (Map Box) that the boundary between the Pahoia Tephra and the cross-bedded sequence roughly parallels the boundary between the Hamilton Ash and Pahoia Tephra. This means that it can be suggested that the thickness of

the Pahoia Tephra may be reasonably consistent. Consequently it could also be suggested that because the majority of the units and associated beds roughy parallel each other, then the thickness of the cross-bedded sequence will be reasonably consistent.

All units examined showed similar textural characteristics from borehole to borehole, allowing for relatively easy identification of the unit when core recovery was satisfactory. The major problem arose in beds associated with units of interest i.e. the beds situated directly below the cross-bedded sequence (upper and lower aquitard, and aquifer). Core recovery tended to be poor for these beds therefore making it difficult to correlated them across boreholes, in addition to identification of areas for the positioning of the slotted section of the piezometer.

3.4.2 Hydrogeological Investigations

a) Introduction

Piezometric data recorded for the period from 16 March 1996 to 30 June 1997 was obtained from Beca Carter Hollings & Ferner Ltd. The data consisted of rainfall and water level measurements within each borehole. This data was recalculated to produce piezometric water level response plots. The main reason for this, instead of using reduced level elevations (RL), was to make it easier to see piezometric water changes within the plots in response to rainfall events. If reduced levels are used, all that can be seen is a general tend within the data, where individual rises in piezometric water levels in response to rainfall are lost. This was done by using a piezometric water level that was slightly less than the lowest recorded piezometric water level, and subtracting this from the reduced water levels recorded. For instance, if the lowest water level recorded for a year was 22.54m a value of 22m was assigned, and subtracted from the data set for that year producing a piezometric water level response. This response was then plotted against the rainfall and cumulative rainfall data to try and determine any relationship between a

change in rainfall/cumulative rainfall and piezometric water level response (Appendix A3.2).

b) Results

In examining the plots generated for rainfall/cumulative rainfall and piezometric water level response (Appendix A3.2) a clear relationship could be seen. All piezometers exhibited similar water level responses to rainfall, with piezometers in the same borehole roughly paralleling each other (for example Figure 3.6). Figures 3.6-3.9 show the general trend that was exhibited by all rainfall/cumulative rainfall and piezometric water level response plots in Appendix A3.2. From high water levels in 1995 there has been a general decrease in piezometric water levels throughout the summer months to 20 June 1996 where upon they level out until the 16 July 1996 (Figure 3.6 & 3.7). With increased rainfall recorded during late June, July, August, and early September a corresponding rise in piezometric water levels can be distinguished in the period 16 July 1996 to 29 September 1996 (Figure 3.7). As the rainfall decreases from early October 96 to late February 97 a decrease in the piezometric water levels can be seen (Figure 3.7 & 3.8). This downward trend in piezometric water levels tends to occur through to mid June 1997 where upon they level out (Figure 3.8 & 3.9).

In addition to examining the general piezometric water level responses "lag times" can be delineated. The term "lag time" refers to the time it takes for a single rainfall event to produce a corresponding rise in the water level of a piezometer, e.g. lag times for Figure 3.6 and 3.7 have been estimated to range between 12 to 72 hours. Analysis of rainfall/cumulative rainfall and piezometric water level response plots in Appendix A3.2 have indicated that lag times range between 12 and 96 hrs. Further examination of the piezometric responses plots in Appendix A3.2 for the period 1 November 1996 to 30 June 1997 reveals a lag time of approximately a month. For example the piezometric responses plots for Figure A3.11 (Appendix A3.2) indicates a slight rise of 40 mm in late December

1996 to early January 1997. However, it is difficult to distinguish whether this rise has resulted from mid-late November to early December's rainfall, as this would indicate a lag time of approximately a month.

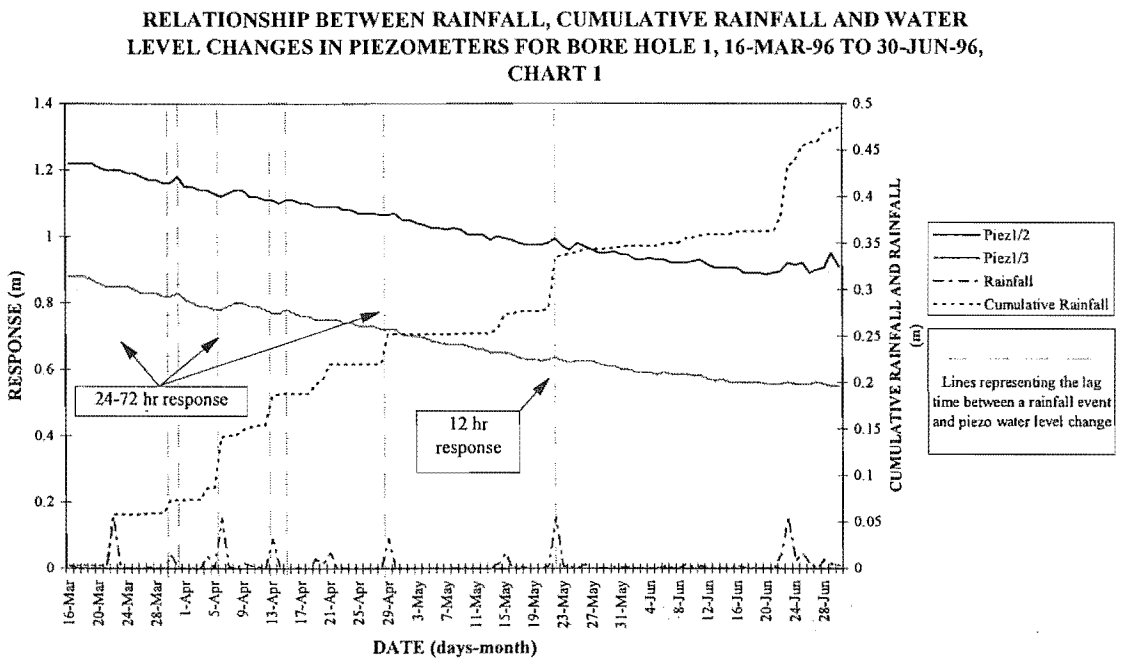

Figure 3.6 Response times between a specific rainfall event and piezometric water response for borehole BH1, 16-Mar-96 to 30-Jun-96. From the plot it can be seen that there is a general decrease in piezometric water levels between the period 16 March and 30 June. In addition to this 12 -72 hour response times can be delineated. Piez 1/2 is measuring a perched aquifer within the Pahoia Tephra located 10.0-10.5m below the ground surface. Piez 1/3 is measuring the aquifer within the lower section of the Cross-bedded sequence located 13.5-14m below ground surface.

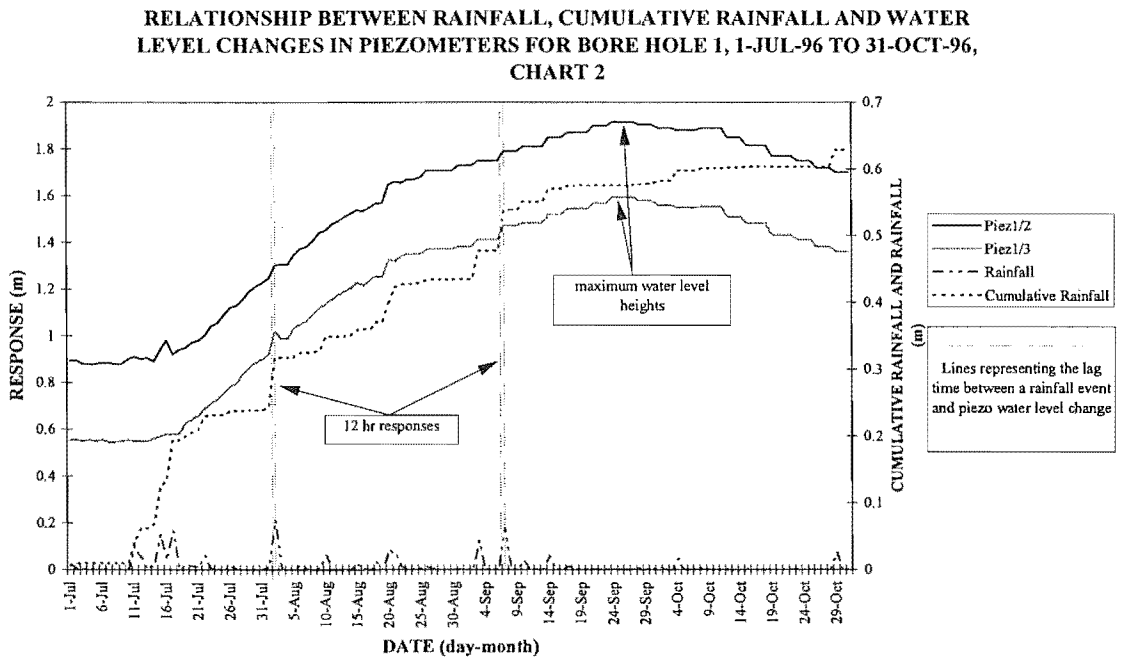

Figure 3.7 Response times between a specific rainfall event and piezometric water response for borehole BH1, 1-Jul-96 to 31-Oct-96. With increased rainfall and low transpiration rates over the winter months, a corresponding increase in the piezometric water levels of approximately 1m can be seen. Conversely with limited rainfall in October a decrease in piezometric water level is distinguished. In addition to this the plot indicates rapid lag times of 12 hours.

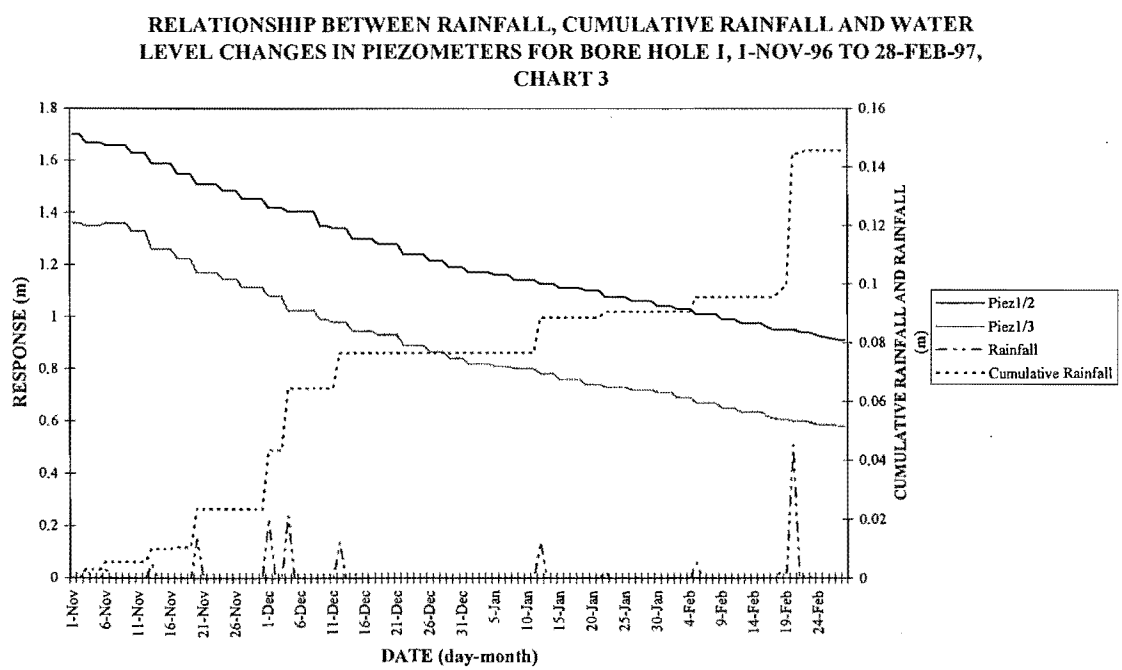

Figure 3.8 Response times between a specific rainfall event and piezometric water response for borehole BH1, 1-Nov-96 to 28-Feb-97. Sparse rainfall and high transpiration rates over the

summer months have resulted in the decline of piezometric water levels. It is possible that when a reasonable rainfall event occurred the soil mass would be dry enough that any quantity of rain water will be absorbed with no piezometric water level response, e.g. 20 February.

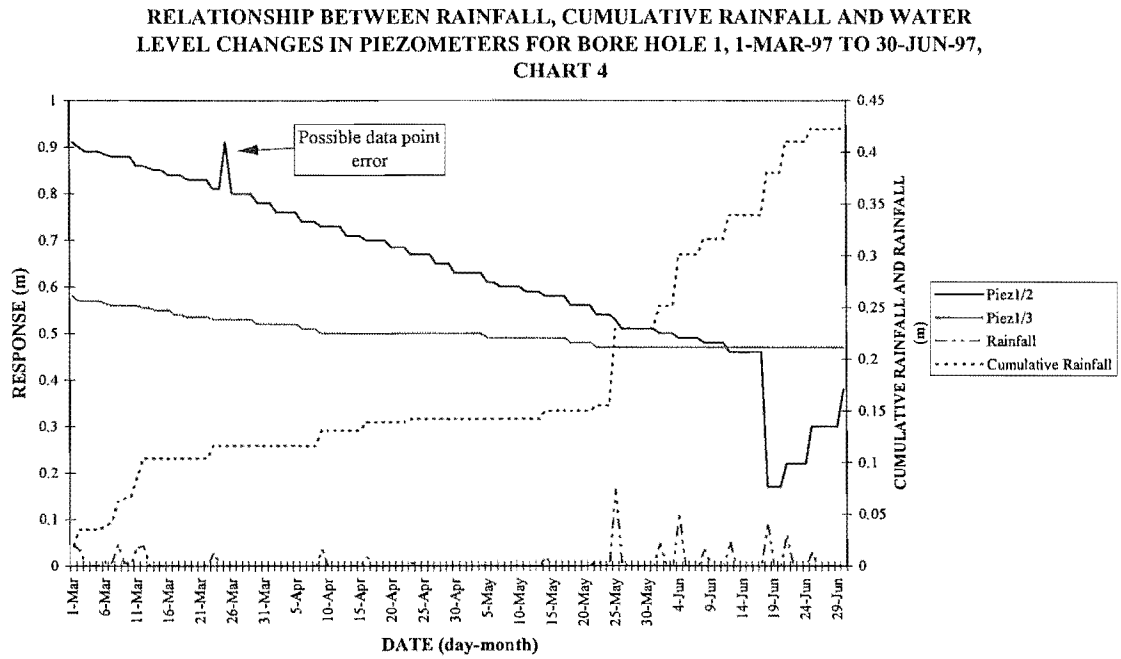

Figure 3.9 Response times between a specific rainfall event and piezometric water response for borehole BH1, 1-Mar-97 to 30-Jun-97. As for figure 3.8 there is a general decrease in piezometric water levels with Piez 1/3 levelling out since early April. The reason for the dramatic decrease in Piez 1/2 around the 17th of Jun is uncertain.

c) Discussion

Results from piezometric water level responses to rainfall plotted up in Appendix A3.2 were interpreted in two ways. The first was to look at the plots as an overview distinguishing seasonal trends. It was found that with increased rainfall over the winter-spring months a corresponding rise in piezometric water levels occurred. Conversely in the summer-autumn months with a decrease in rainfall a corresponding decrease in piezometric water levels occurred.

The second deals with piezometric responses triggered by a specific rainfall event. From this lag times were estimated to range between 12-96 hours. However, rainfall and piezometric water levels were recorded first on a daily basis from 5-6p.m., and then later reduced to twice weekly. This means that because recordings were taken every 24 hours it is impossible to conclude that the plots in Appendix A3.2 demonstrate 12hr lag times. Therefore the minimum possible lag time for the first six months of recording is 24 hours. Consequently this then reduces the range of possible lag times to 24-96 hours. Further reducing recording times to twice weekly means that the minimum lag time increases to 72, hours producing a range of possible lag times of 72-96 hours. Overall these lag times indicate that piezometric water level response to rainfall is quite fast, in that it only takes in many situations 24-96 hours for a body of water or for a pressure wave to be transmitted by head increases in the system to the slotted section of the piezometer.

d) Model 1 (Uniform permeability)

A number of possible scenarios exist that could possibly explain these fast lag times delineated above. The first scenario suggested is that the overall permeability of the stratigraphic units (Post-Rotoehu Ash Tephras, Rotoehu Ash, Palaeosol, etc.) is greater than expected. This means the assumption made during the field investigation stage of the study that the Palaeosol and Hamilton Ash were going to behave like an aquitard was incorrect. The result of this is a hydrological model that suggests that if a volume of water enters the ground at the surface it will permeate through the stratigraphic units to the slotted section located approximately 13-14 m below the ground surface in 24-96 hours (Figure 3.10). Interpretation using this model (Figure 3.10) and the lag times can be taken a step further. For instance, if it takes 24-96 hours to produce a rise in the water of a piezometer after a rainfall event, and say if slotted section of that piezometer is situated 13m below the ground surface, then it can be concluded that an average permeability could be worked out for the stratigraphic unit between the ground surface and the slotted section of the piezometer. In order for this to occur some assumptions have to be made that:

1. The water level responses to rainfall seen in the piezometers are the product of rainwater infiltrating from the surface to the slotted section of the piezometer, and are not influenced by soakholes or aquifer contributions.

2. The soil mass in which the infiltrating water flowed through consists of a uniform matrix where the vertical permeability is equal to the horizontal permeability (k_V=k_H).

3. The water level within each piezometer reflects the water table inherent in the peninsula and is not influenced by aquifer related head-recharge induced water pressures.

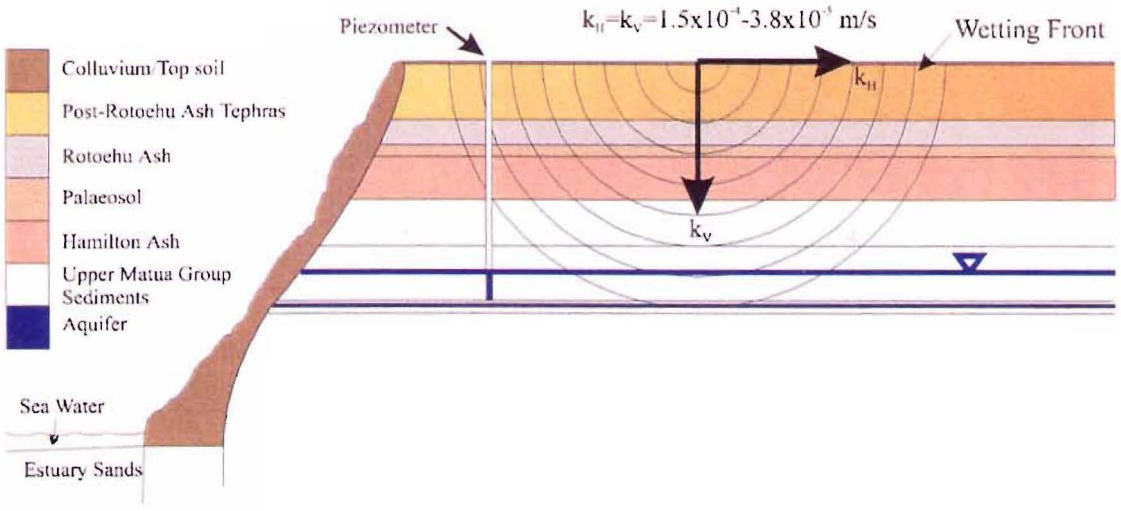

Figure 3.10 Hypothetical soil profile where the vertical permeability is equal to the horizontal permeability through the stratigraphic units.

Therefore using the equation 3.1 the average permeability in m/sec can be calculated using the lag times of 24-96 hours for a volume of rainwater to travel the 13m to the slotted section of the piezometer.

$$\text{Permeability (k)} = \frac{\text{Distance from surface to slotted section of piezometer}}{\text{Lag Time}} \qquad \text{Equation 3.1}$$

$$K_{12hr} = \frac{13m}{12hr \times 60 \times 60} = 3.0 \times 10^{-4}\, m/\sec$$

$$K_{96hr} = \frac{13m}{96hr \times 60 \times 60} = 3.8 \times 10^{-5}\, m/\sec$$

Such calculations produce an average range of permeabilities for the stratigraphic units (Post-Rotoehu Ash, Rotoehu Ash, Palaeosol, Hamilton Ash, Pahoia Tephras, and the cross-bedded sequence) of 3.0×10^{-4} to 3.8×10^{-5} m/sec (Figure 3.10).

e) Model 2 (Defect controlled permeability)

The second scenario suggests that the permeabilities of the various stratigraphic units does not matter in that the infiltrating rainwater flows through high permeability flow paths such as exfoliation defects, fractures, old rootlet structures, and buried stream valleys. These type of structures therefore provide a direct connection between the ground surface and the slotted section of the piezometer producing the fast lag times of 24-96 hours.

f) Model 3 (Head response permeability)

From geotechnical core logging and geological mapping by Hall (1994) which suggests that the stratigraphic units of the Peninsula extend back up into the hinterland. This will have the affect of extending the catchment area of the peninsula. Therefore another

hydrogeological model which could also produce these fast lag times of 24-96 hours is that of a pressure wave that moves along the aquifer (delineated in Chapter 2) induced by a change in the hydraulic head of the peninsula due to recharge from rainfall. This pressure wave could also produce a corresponding increase in porewater pressures at the exit points of the aquifer within the soil mass. These three models are discussed further in Chapter 5 section 5.2.

3.4.3 In-situ Permeability Testing

a) Introduction and Methodology

Borehole 7 was used to conduct an in-situ permeability test during early May 1997 due to its close proximity to a water supply. The piezometer is slotted between 11.0 - 11.5 m from the ground surface, positioning it in the Upper Matua Subgroup cross-bedded sequence (Table 3.1 & Borehole BH7). From piezometric data (Appendix A3.2, Figure A3.25-A3.28) it can clearly be seen to respond to rainfall making it a candidate for permeability testing. Initially a constant head permeability test was conducted but it was found that the flow rate from the house hold hose could not be varied enough to maintain a constant head, consequently a falling head test was carried out. Methodology used was that presented by Kruseman and de Ridder (1994) and Fetter (1994) for Slug Testing. Permeabilities were calculated using the Hvorslev Slug Test and the Bouwer and Rice Slug-Test Methods, Appendix A3.2.

b) Results

Figure 3.12 presents the raw data in graphical form denoting base water level prior to testing, the level to which the piezometer was filled, and the drop in water level compared to time. From two differing methods, the Hvorslev Slug Test and the Bouwer and Rice Slug-Test, two permeability results were obtained. Firstly using the Hvorslev Slug Test a permeability of 8.3×10^{-6} m/sec was calculated, whilst using the Bouwer and Rice Slug-Test produced a permeability of 6.6×10^{-7} m/sec. All calculations pertaining to the two

methods are given in Appendix A3.3. In-situ permeability testing of the cross-bedded section of the Upper Matua Subgroup suggests a possible range in hydraulic conductivities from 8.3×10^{-6}-6.6×10^{-7} m/sec.

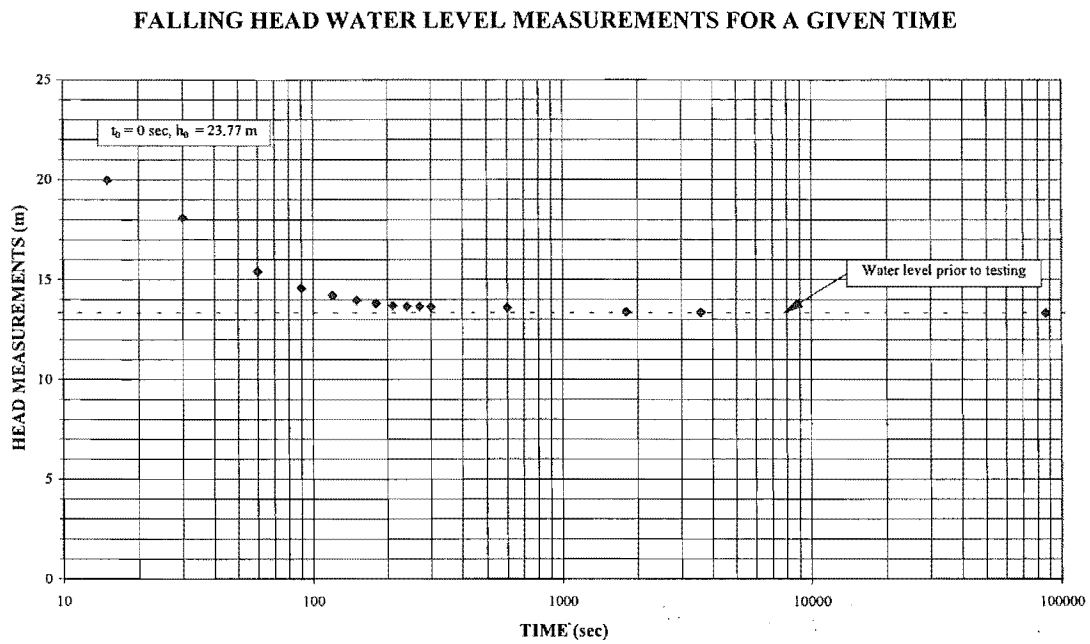

The permeability range obtained from using the Hvorslev and Bouwer-Rice methods (8.3×10^{-6}-6.6×10^{-7} m/sec) compares favourably to that obtained by Bird (1981) of 2.1×10^{-7} m/sec from laboratory testing of a white silty sand (equivalent to the cross-bedded sequence). In addition to this it also comparable to permeabilities that would expected for very fine or silty sands (Table 3.2).

Table 3.2 Permeability and Drainage Characteristics of Main Soil Types (ELE International)

Coefficient of Permeability m/s

	K=1	10^{-1}	10^{-2}	10^{-3}	10^{-4}	10^{-5}	10^{-6}	10^{-7}	10^{-8}	10^{-9}	10^{-10}	10^{-11}	10^{-12}
Drainage Characteristics	Good							Poor	Practically Impervious				
Permeability Classification	High			Medium		Poor			Very Low		Practically Impervious		
General Soil Type	Gravels		Clean Sands			Fissured & Weathered Calys / Very Fine or Silty Sands			Intact Clays				
Test Method – Direct	Constant Head					Falling Head							
Test Method – Indirect			Computation From PSD								From Consolidation Data		

PSD = Particle Size Distribution

These in-situ permeability results (8.3×10^{-6}-6.6×10^{-7} m/sec) do not compare favourably to the range produced by lag time-derived permeabilities ($k_{24}=3.0\times10^{-4}$-$k_{96}=3.8\times10^{-5}$ m/sec). This tends to lend more credence to a mechanisms such as those suggested in models 2 (permeability defect controlled) and 3 (permeability head response) of the prevoius section. As stated in section 3.4.2 this will be explain in more detail in chapter 5 section 5.2.

3.4.4 In-situ Shear Strength Investigations

a) Introduction

The results obtained from in-situ shear strength testing during face logging of the landslides scarps at 85 & 89 Te Hono Street, and 330 Maungatapu Road, produced a range of possible values for each unit, i.e. Post-Rotoehu Ash Tephra, Rotoehu Ash, Palaeosol, etc. When viewing these results it must be noted that the cliff face from which they were collected had been exposed to the elements (sun and rainfall) for nine months prior to logging. This had in part produced some erosion in the form of rills (small channels left by water running down the slope), and had dried out many of the soils in the upper section of the cliff face (i.e. in the top section of the cross-bedded sequence, the Pahoia Tephras, Hamilton Ash, Palaeosol, Rotoehu Ash, and Post-Rotoehu Ash Tephras). This drying out of the soil material could therefore increase the shear strength of the soil. In addition to this Terzaghi, Peck, and Mesri (1996) discuss that in many situations field measurements may differ from actual in-situ shear strengths due to a number of factors including:

1. shear testing does not duplicate the possible modes of shearing along a potential slip surface in the field,

2. mobilisation of shear strengths in the field tend to be over a longer time period than the time it takes to conduct a shear vane test, resulting in recording shear strengths that are higher than actual in-situ strengths,

3. soil disturbance as the vane is pushed in will tend to decrease the shear strength.

Considering these points, it is suggested that units that contain beds with a high silt and clay content have dried out considerably since landsliding has occurred (i.e. Post-Rotoehu Ash Tephra, Palaeosol, Hamilton Ash), and will therefore produce higher shear strengths than actual in-situ values.

b) Results

Figure 3.11 presents plots of depth versus shear strength noting the associated stratigraphic units in which testing was conducted. This data was obtained directly from the face log field sheets before they were recalibrated for cliff face slope angle. It is not the objective of this figure to show that a particular bed will yield a shear strength of this value, but to provide an indication of possible ranges in strengths for each unit as a whole. Because of this it is not necessary for the depths to be adjusted for slope angle as it will make no difference to the shear strengths recorded.

c) Discussion

In-situ shear strength testing is important to determine a range of possible strengths for each stratigraphic unit, i.e. Post-Rotoehu Ash Tephras, Rotoehu Ash, etc. These strengths can then be compared to shear strengths obtained from laboratory investigations. From Figure 3.5 it can be seen that most of the soils are relatively strong, with the majority of shear strengths exceeding 80 kPa. The Post-Rotoehu Ash Tephras demonstrate a wide range of strengths from 20 to 200 kPa. Beds within this unit that were predominantly silty (i.e. beds with a unified soil classification (USC) of ML, refer to boreholes and face logs in Map Box) tended to produce strengths which were greater than 40 kPa. Conversely the more sandy beds (with a USC of SW) yielded shear strengths below 40 kPa. The Rotoehu Ash, like the Post-Rotoehu Ash Tephras, shows a wide range in shear strengths ranging between 20 and 200 kPa. This is not unexpected knowing that this unit comprises numerous airfall deposits with USC of SW,SP, and ML. Overall the Rotoehu Ash is relatively weak compared to other lithologies within the sequence (Figure 3.11).

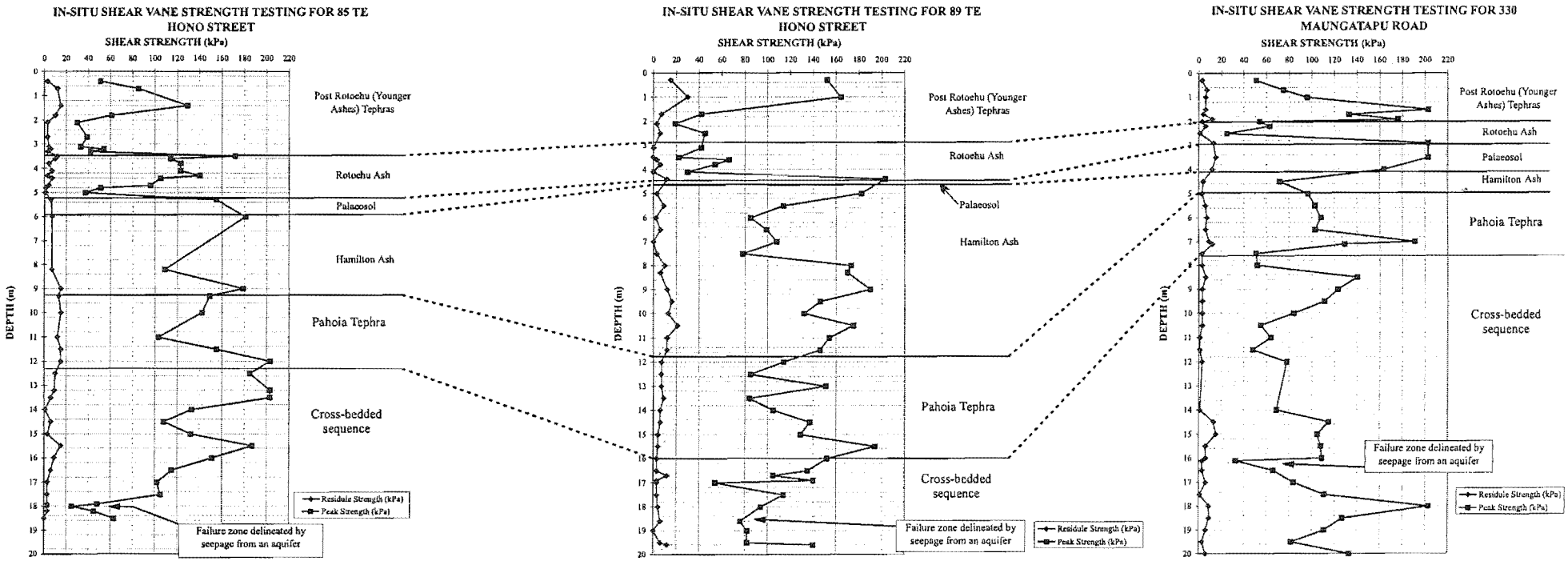

Figure 3.11 Plots presenting in-situ shear strengths for 330 Maungatapu Road, 85 and 89 Te Hono Street tested using a Pilcon Shear Vane during cliff face logging.

One of the strongest units tested is the Palaeosol situated between the Rotoehu Ash and the Hamilton Ash, with shear strengths in excess of 200 kPa. The high strengths reflect the hard to compact nature of the soil, and support many of the arguments that numerous soak holes around the region do not penetrate this unit because of the difficulty in drilling through it. The Hamilton Ash situated directly below the Palaeosol consists of a number of airfall ashes. As in other areas tested the Hamilton Ash indicates variable strengths ranging from 70-190 kPa. Overall the Hamilton Ash demonstrates relatively high shear strength characteristics.

The Upper Matua Subgroup consists of fluvial reworked and estuarine deposited sediment intercalated with airfall Pahoia Tephras (Boreholes BH1-BH8, and Face Logs 1-3, Map Box). The borehole logs indicate the Pahoia Tephras have a USC of SM, SP, and SW, whereas the cross-bedded sequence has a USC of ML, SM, SP, and SW. From Figure 3.5 it can be seen that the Pahoia Tephras have high shear strengths that range between 80 and 200 kPa. The cross-bedded sequence also has a number of beds that exhibit high shear strengths (200 kPa), but overall have a wider range (40-200 kPa). This means that the Pahoia Tephras and the cross-bedded sequence showed similar strong characteristics to those demonstrated by the Hamilton Ash. Conversely, the aquifer (USC of SM, Face Log 1, Map Box) delineated in the failure zone produced very low shear strengths ranging from 20-80 kPa. This was not unexpected as it was very easy to push a finger into the soil mass.

3.5 VISUAL LANDSLIDE MONITORING

Landslide monitoring in the context of this section implies a qualitative assessment of further landslide development. Beca Carter Hollings & Ferner Ltd were contracted by the Tauranga District Council to inspect the landslide at properties 85 and 89 Te Hono Street after the initial failure on 29-30 May 1995. A later failure at 83 Te Hono Street on 6 August 1995 was also included into the inspection program. Council records indicate that

landslides were inspected twice weekly from the start of August to the end of November 1995, whereupon inspections were reduced to once a fortnight until December 1996. After this time inspection consisted of visiting the sites following a major storm event.

Copies of the inspection records can be located in the hazards files of the Tauranga Council, which list all hazards associated with each property. Records indicate that after the initial failure, regression of the cliff faces at 83, 85 & 89 Te Hono Street involved minor block slides confined to the Hamilton Ash and above units. Toppling was also evident in the Post-Rotoehu Ash Tephras. Water was reported to be visibly flowing from the aquifer zone described in Chapter 2 throughout the inspection program, with higher flow rates during the winter periods. In addition water was intermittently report to be seen flowing out of the upper sections of the cliff face. This seepage is more than likely soakhole-related, with water flowing out of the Rotoehu Ash unit. Further failures involving small superficial failure ($<3m^3$) and minor toppling failure within the Post-Rotoehu Ash Tephras were reported to be greater during the winter months especially after a period of prolonged rainfall. Tension cracks seen to be propagating into unaffected cliff areas are possibly the result of unloading caused by landslides on the adjacent properties. Theses cracks will more than likely follow along exfoliation defects inherent in the soil mass.

3.6 DISCUSSION AND SYNTHESIS

Chapter 3 details the various components used in engineering geological and geotechnical field investigations. Engineering geological mapping consisted of the production of a 1:5000 scale map showing the various landslide types as well as their locations. In addition 1:50 scale bore holes and face logs were completed to provide better stratigraphical geotechnical data. Complementing field mapping, aerial photograph interpretation provided good evidence of large scale landslides, but photo scales made it difficult to discern smaller scale failures such as the landslides seen at 85 Te Hono Street.

Additional to engineering geological mapping of the landslide scarps in-situ shear strength testing was conducted to supplement laboratory work, and to provide some indication of strengths throughout the soil mass. The Palaeosol as expected produced the highest shear strengths of about 200 kPa. Conversely areas where seepage was occurring within the Upper Matua Subgroup shear strengths were considerably lower, with a range from ~30-80 kPa. All soils tested demonstrated that in-situ shear strengths can vary from locality to locality, due to the variability of soil itself. Because of this the soil should be viewed as having a range of shear strengths rather than using a specific shear strength for each unit delineated.

On completion of the bore holes piezometers were installed to desired depths determined by geotechnical core logging to better understand the hydrogeology of the Peninsula and how this influences failure. Monitoring of water levels was conducted by Beca Carter Hollings & Ferner firstly on a daily bases and then twice weekly. From the plotted data a clear seasonal change in piezometric water levels of approximately 1m could be seen. The summer-autumn months saw a general decline in piezometric water levels due to low rainfall and high transpiration rates. Conversely the winter-spring months produced increasing piezometric water levels due to greater rainfall volume and low transpiration rates. In addition to the general seasonal change seen, lag time responses of 24-96 hours were produced by comparing piezometric water level changes to rainfall/cumulative rainfall. This lag time was then used to produce a simplistic hydrogeological model (Uniform permeability model) in which average permeabilities of 3.0×10^{-4}-3.8×10^{-5} m/sec were obtained.

These results were then compared to an in-situ falling head permeability (slug) test conducted in borehole BH7. From the data obtained, two methods were used to calculate a permeability, the Hvorslev slug test and the Bouwer-Rice slug test. The Hvorslev method

produced a permeability of 8.6×10^{-6} m/sec, whereas the Bouwer-Rice method produced a permeability of 6.6×10^{-7} m/sec. These permeabilities would suggested that the soil mass adjacent to the piezometer is only moderately permeable. This provides a dilemma as the soil surrounding the piezometer was believed to be one of the more permeable units. This introduced the possibility that another mechanism was responsible for the fast lag times of 24 to 96 hours. Two possible models were suggested, that of a defect controlled permeability model, or a head response model. The defect controlled permeability model suggests that structures such as exfoliation defects, fractures, heavy bioturbation (rootlets), and buried streams provide high permeability pathways for soakage water to flow through. The head response model suggests that a pressure wave induced by changes in hydraulic head of the Peninsula can rapidly move along aquifer increasing the pore water pressures at the aquifer exit points (cliff faces). All of these models are further discussed in Chapter 5 section 5.2.

Chapter Four LABORATORY DATA

4.1 INTRODUCTION

During the field investigation stage of this study 42 samples were collected for geotechnical testing (Table A4.1, Appendix A4). The testing was done so as to provide a geotechnical characterisation of the various soil units throughout the logged cliff faces, and was used in subsequent hydrogeological and slope stability assessments. In addition to this the results obtained in the laboratory were compared to geotechnical data from Bird (1981). Bird had investigated and collected samples for laboratory testing from three landslide sites, one located at the north-eastern tip of Maungatapu Peninsula, and two on the north-western side.

Laboratory testing involved the use of the direct shear box to assess the peak shear strength of various soils by determining phi angles and coefficients of cohesion. Undrained unconsolidated triaxial testing was used to determine peak shear strength so the results could be compared to shear vane data collected in the field but due to equipment problems it was not possible to conduct consolidated undrained triaxial tests to compare to Bird's (1981) data. Other descriptive test such as Atterberg limits, clay mineralogy, and particle size analysis were undertaken, while pinhole and Emerson crumb tests were used to assess the erodibility and dispersive properties of the soils. Falling head permeability testing was conducted on a number of soils throughout the logged cliff faces to produce a range of permeabilities for later hydrogeological analysis, and for comparison with the field results discussed in Chapter 3.

4.2 PARTICLE SIZE ANALYSIS

4.2.1 Introduction

The objective of particle size analysis was to provide a quantitative description and classification of the various soils on which geotechnical tests were subsequently conducted. Sampling of each bed associated with a particular stratigraphic unit proved impossible, as there could be more than 10 beds per metre down the cliff slope. This was especially evident in the Rotoehu Ash where 15 beds alone could be seen within 0.5m, resulting in many beds within each unit not being sampled. This meant that sampling had to concentrate on the most important features of each unit in relation to the objectives of the project. The main objectives in relation to particle size analysis were to:

Collect a sandy sample from the Rotoehu Ash, as this has been indicated to be the major drainage unit for soak water related to soakholes.

Collect samples from the Palaeosol and Hamilton Ash, as these were believed to form an aquitard separating the Post-Rotoehu Ash Tephras and Rotoehu Ash from the underlying Upper Matua Subgroup sediments.

Collect samples from the Upper Matua Subgroup sediments (Cross-bedded sequence, aquitards, and aquifer) to determine particle size for characterisation and correlation with other geotechnical tests.

From a representative bulk sample for a particular soil unit, wet sieving was conducted to the 4ϕ (boundary between silt and sand) with the sample retained on the sieve dried, and dry sieving performed. The wet sample from the collection tray was then transferred to a measuring cylinder for pipette analysis. All methodology followed that set out by Lewis & McConchie (1994). Data obtained from wet particle size analysis is given in Appendix A4.2. Table 4.1 shows the percentages of clay using a 9ϕ (<0.002mm) boundary as described by NZ Geomechanics Society Scheme (Appendix A4.2).

4.2.2 Results

a) Rotoehu Ash

All samples (as perviously noted chapter 2) are derived from airfall deposits and/or fluvial reworked volcaniclastic sediments (close to source), and as expected are well to moderately graded. The Rotoehu Ash from field descriptions (Face Logs 1-2, Boreholes BH1-BH8, Map Box) is a sequence of shower-bedded airfall deposits comprising a range of sandy and silty units. Particle size analysis for this study was only performed on a proportion of the sample used for permeability testing. This was due to the impossible task of analysing all the beds within the Rotoehu Ash, as well as the other stratigraphic units. Particle size analysis of the 4.6/1/85 (Figure A4.1, Appendix A4.2) indicates that the largest proportion represented was sand at 96 % (Table 4.1). The sand fraction can be further be divided up into 38 % medium, 37 % coarse, 12 % fine, 8 % very coarse, and 5 % very fine sand. The sample can be defined as MEDIUM - COARSE SAND. The coarse grainsize and low silt-clay content will allow rapid infiltration of water through this unit. However, this unit only comprises one of many beds that make up the Rotoehu Ash, with other beds composed of finer grainsize fractions, e.g. silts and clays.

b) Palaeosol

The Palaeosol (5.8 / 1 / 85) represents a compact soil associated with the underlying Hamilton Ash. During grainsize analysis it was difficult to disaggregate the sample into its constitutent fractions resulting in a very low clay content (10 %) and a very high sand percentage (58 %; Table 4.1). Textural analysis of the sand fraction when examined under a binocular microscope was composed of numerous aggregates of silt and clay. It was difficult to estimate the percentages of these fractions due to the dark colouring of the aggregates. Lewis and McConchie (1994) suggest breaking up the aggregates using a mortar and pestle, but this would also produce abnormal results. Two possible answers are firstly, to use plasticity as and indicator of clay content in that the higher the clay content the higher the plasticity, and secondly, to use the field descriptions as they are probably the most accurate result.

d) Pahoia Tephras

The Pahoia Tephra as the name states is a number of airfall deposits, and so has an extremely wide range of grainsizes from medium pebbles to clay. In addition the variation in structure, with some areas showing bedding while others were more massive, made it difficult to obtain a representative sample. It was decided that because it was impossible to obtain a sample that accurately represented the soil mass, the best solution was to use the soil descriptions collected during field investigations (Face Logs 1-2, Borehole BH1-BH8, Map Box).

e) Cross-Bedded Sequence

The cross-bedded section of the Upper Matua Subgroup consists of fluvially reworked ignimbrites, tephras and ashes. As a result a wide range of grainsizes are present, producing the very well graded particle size distribution curves in Appendix A4.2. Using the four particle size distribution curves in Appendix A4.2 an envelope can be constructed to indicate the likely grainsize distribution curves (Figure 4.2). However, the envelope wholly depends upon the accuracy of the data set in that consideration has to be given to the highly variable grainsizes possible in the field. Examining Table 4.1 from an engineers perspective of a 9ϕ (<0.002mm) cut-off for the clay-silt boundary, the composition of sand ranges between 27-46 %, compared to 37-50 % for the silt fraction. The clays range between 17-22 %, producing an average grainsize distribution of 38%:sand, 42%:silt, and 20%:clay. Plotting the 8$\phi$and 9ϕ data onto a textural triangle the unit can be referred to as either a silty SAND with some clay or a sandy SILT with some clay (Figure 4.1).

Table 4.1 Particle distribution table 9 ϕ set showing the samples tested

PARTICLE SIZE DISTRIBUTION OF SAMPLES TESTED							
Sample		Pebble	Granula	Sand	Mud		
	%	0.24	0.59	96.19	2.98		
4.6 / 1 / 85 Rotoehu Ash		Sand					
		Very Coarse	Coarse	Medium	Fine	Very Fine	
	%	7.77	37.27	37.96	11.75	5.26	
Sample	ϕ	Percentage	Pebble	Granule	Sand	Silt	Clay
5.8 / 1 / 85 Palaeosol	9	%	0.00	3.10	57.88	29.03	9.99
8.2 / 1 / 85 Hamilton Ash	9	%	0.00	0.29	29.48	33.82	36.41
15.1 / 1 / 85 (1) Cross-bedded Sequence	9	%	0.00	0.00	35.07	42.78	22.15
15.1 / 1 / 85 (2) Cross-bedded Sequence	9	%	0.00	0.00	27.03	50.75	22.22
15.1 / 1 / 85 (3) Cross-bedded Sequence	9	%	0.00	0.08	46.15	37.08	16.70
15.6 / 1 / 85 Cross-bedded Sequence	9	%	0.00	0.00	43.46	39.78	16.76
17.1 / 1 / 85 Aquifer	9	%	0.00	0.08	77.67	16.54	5.72
18.075 / 1 / 85 Lower Bounding Aquitard	9	%	0.00	0.30	46.99	33.66	19.05
18.075-18.08 / 1 / 85 Lower Bounding Aquitard	9	%	0.00	0.55	26.24	20.75	52.46
18.08-18.095 / 1 / 85 Lower Bounding Aquitard	9	%	0.00	0.00	14.41	21.91	63.68
18.08-18.095 / 1 / 85 Check Lower Bounding Aquitard	9	%	0.00	0.00	13.59	25.51	60.90
18.095-18.10 / 1 / 85 Lower Bounding Aquitard	9	%	0.00	0.00	15.12	30.78	54.10
18.10-18.11 / 1 / 85 Lower Bounding Aquitard	9	%	0.00	0.00	46.15	17.95	35.90
18.11-18.12 / 1 / 85 Lower Bounding Aquitard	9	%	0.00	0.00	75.28	15.36	9.36
18.12-18.23 / 1 / 85 Lower Bounding Aquitard	9	%	0.00	0.00	31.33	28.25	40.42

f) Aquifer

The sample tested from the aquifer zone (17.1 / 1 / 330) produced predominantly higher percentages of sand, compared to the silt and clay fraction (Table 4.2). This would categorise the aquifer as a MEDIUM - COARSE SAND with grainsizes ranging from clay to granule. The sample that was collected was in a zone of continual seepage, where it was evident that the finer particles (silts and clays) were being carried out of the cliff face in suspension by the soakage water. Therefore it is likely that the clay and silt percentages reflected here are not truely representative of the in-situ size distribution, and the clay and

silt content within the aquifer may be as high as 10% and 20% respectively. This higher interpreted clay and silt content will decrease the permeability characteristics of the soil.

Table 4.2 Particle distribution table for the 9 phi data set for the Aquifer 17.1 / 1 / 330

SAMPLE COMPOSITION FOR AQUIFER 17.1 / 1 / 330									
			SAND						
		GRANULE	Very Coarse	Coarse	Medium	Fine	Very Fine	SILT	CLAY
9 phi	%	0.08	2.62	21.15	32.57	14.50	6.82	16.54	5.72

g) Lower Bounding Aquitard

The lower aquitard consists of a sequence of shower bedded airfall deposits which form the lower bounding surface to the aquifer delineated during field investigations (Chapter 3), and which vary considerably in their particle size distributions. Plotting these distributions curves (Figure A4.9-A4.16, Appendix A4.2) together, an envelope is produced that indicates a possible range of grainsize distributions for this unit (Figure 4.3). When this is compared to Figure 4.2 it can be seen that the envelope is predominantly larger, while the main concentration of curves within the envelope indicate a higher clay content than the above stratigraphic units. This is also demonstrated in Table 4.1 and Figure 4.1. From Table 4.1 the 9ϕ percentages of clay for the lower bounding aquitard range between 9 and 64 % compared to 15-34 % and 15-75 % for the silt and sand fraction respectively. Averaging this data produces a particle size distribution (clay = 42%, silt = 24%, and sand = 34%) which clearly shows that the aquitard has a higher clay content than other soils throughout the stratigraphic column. This would result in the lower bounding aquitard being practically impermeable. This fact coupled with the proposed continuous extension of this unit back up the peninsula towards the foot hills would provided an impermeable barrier to soakage water infiltrating through the soil mass.

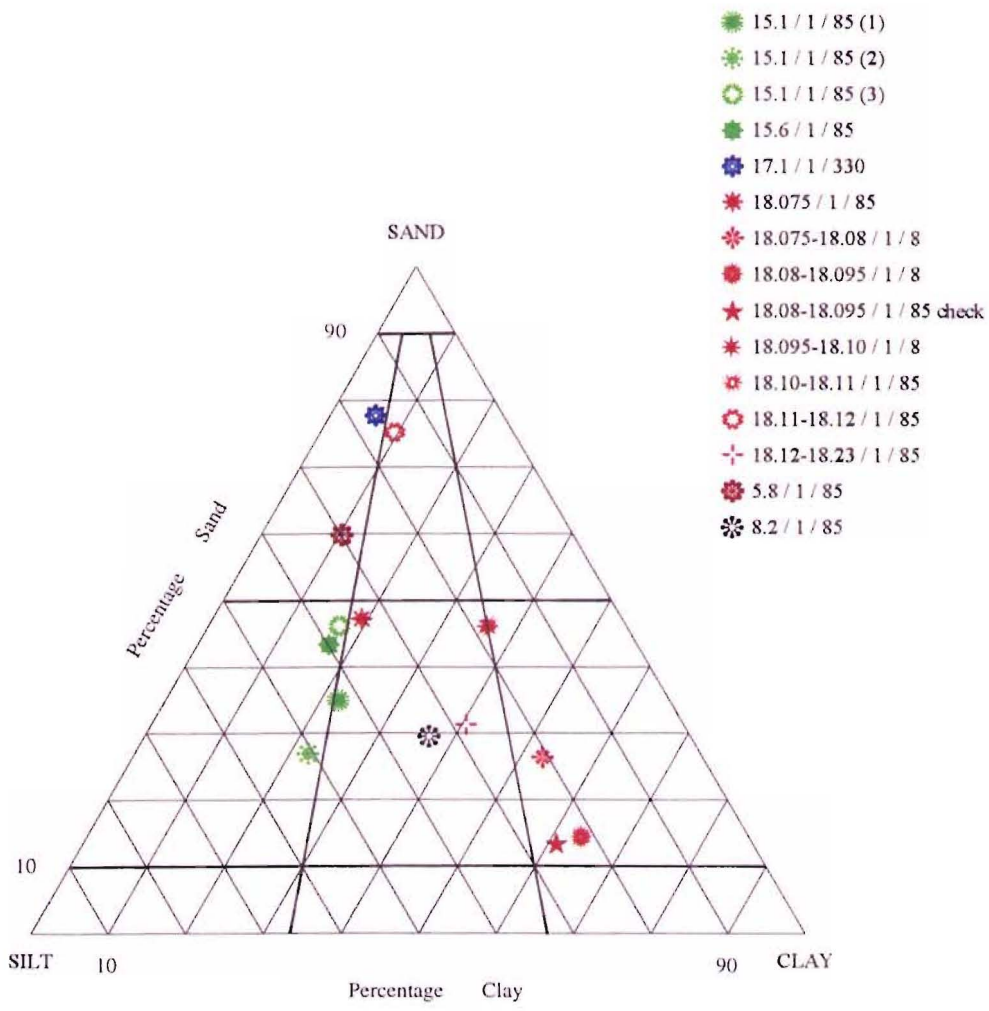

Figure 4.1 Textural triangles for the 9 phi data set for the samples tested

COMBINED GRAINSIZE DISTRIBUTION CURVES FOR CROSS-BEDDED SECTION OF THE UPPER MATUA SUBGROUP

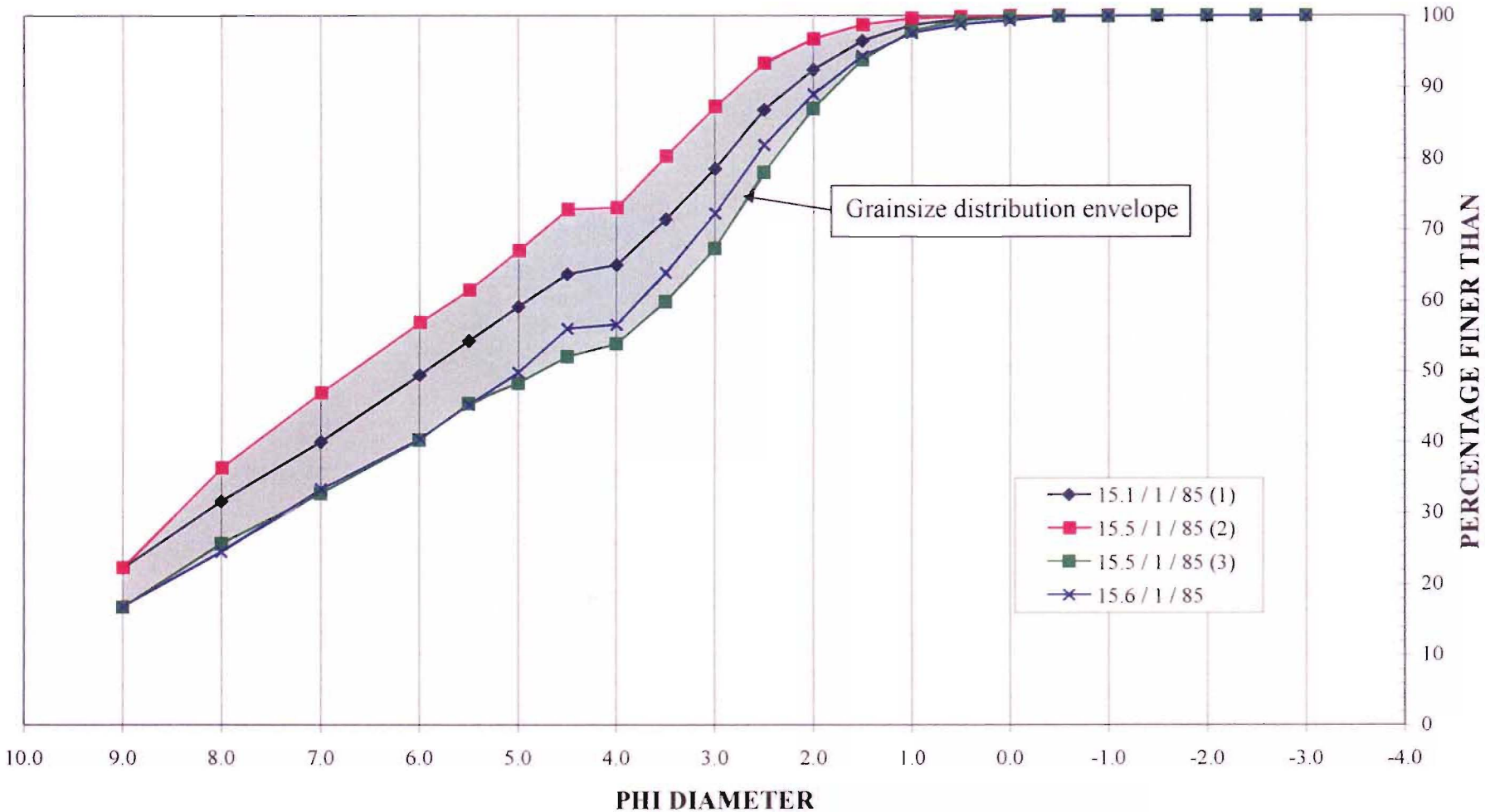

Figure 4.2 Grainsize distribution envelope for Cross-bedded section of the Upper Matua Subgroup

COMBINED GRAINSIZE DISTRIBUTION CURVES FOR THE LOWER AQUITARD LOCATED WITHIN THE UPPER MATUA SUBGROUP

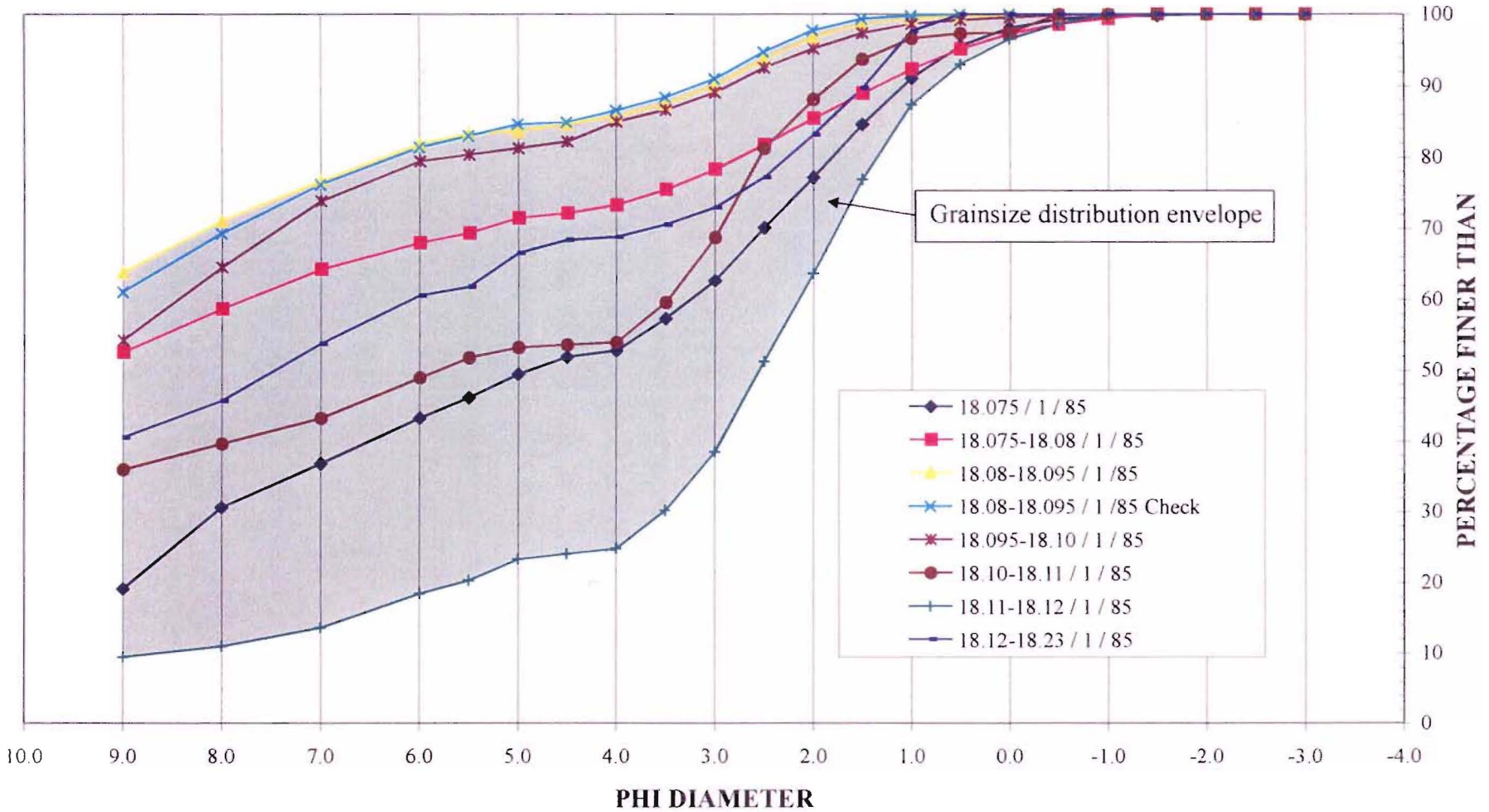

Figure 4.3 Grainsize distribution envelope for the lower aquitard located within the Upper Matua Subgroup

4.2.3 Discussion

As with all grainsize analysis a sampling error has to be considered when assessing the validity of the data sets and resultant grainsize distribution curves. In addition to this few samples were tested compared to the numerous beds that exist throughout the stratigraphy. During field investigations bulk samples were collected as carefully as possible so that a representative sample could be obtained for grainsize analysis. In addition to the difficulty involved in sampling were the textural and compositional problems associated with the soils themselves. Numerous glass shards and pumice grains had a tendency to break up during testing especially dry sieving, which would decrease the grainsizes relative to the more sandy soils.

a) Rotoehu Ash

The Rotoehu Ash is believed to represent the most permeable unit and so should exhibit beds with high sand content and low silt and clay percentages. This fact was demonstrated by particle size analysis of sample 4.6/1/85 with 96% sand (Table 4.1). From field investigations beds are evident within the Rotoehu Ash that contain higher clay and silt contents, which dramatically reduce the permeabilities of such beds, and giving the unit markedly varying composition and resultant flow anisotropy.

b) Palaeosol

The Palaeosol due to its compact nature did not produce a grainsize distribution that was deemed likely when compared to what was seen during field investigations (Face Logs 1-3, borehole BH1-BH8, Map Box). It was found from binocular microscope work that many of the grains were composed of aggregates of silt and clay particles. It is suggest that because the Palaeosol is associated with the underlying Hamilton Ash, a good assumption would be that the grainsize distributions for these two units would be similar. This means that the Palaeosol would have a grainsize distribution of approximately 30% sand, 30%

silt, and 40% clay. If this was so it would almost provide a very low permeability soil and in conjunction with the Hamilton Ash would form an aquitard separating the Post-Rotoehu Ash Tephras and Rotoehu Ash from the underlying Upper Matua Subgroup sediments.

c) Hamilton Ash

The Hamilton Ash with its high clay content will, like the Palaeosol, be a very low permeability soil. From field investigations larger fragments of pumice and rhyolite (pebbles - granules in size) were identified within the unit in quantities of about 1-3% in the soil mass. These fragment were not represented in the grainsize analysis, as the bulk sample only contained one or two of these fragments. Consequently they were not included in the analysis as they would tend to skew the results and not produce a representative grainsize distribution.

d) Cross-Bedded Sequence

The Cross-bedded sequence for the most part contained a substantial amount of clay (~20%), and silt (~40%). This like other units would imply that the unit as a whole would not be particularly permeable. The large wave length cross-beds which showed partial graded bedding also made it difficult to sample. This was compounded by the fact that on closer inspection there appeared to be numerous minute silty layers approximately 2mm in thickness.

e) Aquifer

From field investigations the aquifer is interpreted to have a higher clay and silt content than indicated by grainsize analysis. This will in turn decrease the permability of the soil.

4.3 CLAY MINERALOGY

4.3.1 Introduction

Clay mineralogy is an important aspect to consider when assessing the behavioural characteristics of the soils, and three methods were used to determine the clay mineralogy of the soil samples. Firstly, X-ray diffraction was used to determine whether halloysite was present as suggested by Bird (1981) and Lowe (Pers. Comn. 1997); secondly, X-ray Fluorescences was used to determine the composition of the brownish black, greenish black, and black grains which appeared throughout all of the soils and around old rootlet structures; and thirdly, testing for allophanes was conducted due to the large amounts of volcanic glass associated with the sampled soils. Test methods for XRD and XRF are outlined in Appendix A4.3.

4.3.2 X-ray Diffraction Analysis

a) Introduction

X-ray diffraction analysis was conducted to determine the clay mineralogy of each sample on which testing was conducted for Atterberg limits, particle size analysis, and permeability. The clay mineralogy is an important component when assessing the stability of a slope. If a sufficient quantity of swelling clays are present (e.g. smectites) they will tend to decrease the overall strength of the particular soils in which they are present. This is accomplished by water entering the interlayer space, expanding the mineral reducing interlayer charges and therefore decreasing the strength of the mineral assemblage. If a sufficient amount of clay is present within the soil (>10%) this reduction in the mineral strength will result in decreasing the overall strength of the soil. The methods used for clay mineral XRD analysis are presented in Appendix A4.3.

b) Results and Discussion

Presented below is a summary table (Table 4.3) of the clay mineralogy data obtained from X-ray diffraction analysis. Table 4.3 indicates that throughout the soil mass the major constituent clay is a mixed-layer 10 and 7 Å Halloysite. Halloysite is a member of the

Kaolin subgroup, with the 10 Å Halloysite irreversibly dehydrating to the 7 Å Halloysite at temperatures only slightly above ambient (18-20°C) (Wilson, 1987). Kirkman and Pullar (1978), on investigating the Pahoia Tephras, found that only the hydrated 10 Å Halloysite was present. This suggests that the dehydrated Halloysite found may in fact represent a sample that prior to testing had dried out too much. The Palaeosol and Hamilton Ash samples (Appendix A4.3) were not allowed to dry out significantly to counteract this possible problem. Another possibility is that drying out of the cliff faces prior to sample collection may have partially collapsed some of the 10 Å Halloysite to 7 Å Halloysite producing the mixed layer 10 & 7 Å Halloysite found in all samples tested.

The geotechnical properties of 7Å Halloysite will be similar to those of Kaolinite in that both have a very low swelling index. The swelling index indicates the swell characteristics of a soil by the relationship de/d(logp) where e = voids ratio, p = stress on soil (Mitchell, 1976 in Fell et al., 1992). The hydrated 10 A° Halloysite is suggested to be slightly less stable due to the addition of water in the interlayer. However, with very little information, further geotechnical properties of Halloysite and the implications of these properties was not able to be obtained.

Table 4.3 Summary of the clay mineralogy data obtained from X-ray diffraction

SAMPLE		COMPOSITION
Palaeosol		Mixed layered 10 & 7 A° Halloysite in addition to some Quartz and Oligoclase Feldspar
Hamilton Ash		Mixed layered 10 & 7 A° Halloysite in addition to some Quartz and Oligoclase Feldspar
15.5 / 1 / 85 Cross-bedded section of the Upper Matua Subgroup		Mixed layered 10 & 7 A° Halloysite
15.5 / 1 / 85 retest, fired at 500 °C Cross-bedded section of the Upper Matua Subgroup		Mixed layered 10 & 7 A° Halloysite
15.6 / 1 / 85 Cross-bedded section of the Upper Matua Subgroup		Mixed layered 10 & 7 A° Halloysite
Represents part of the lower bounding aquitard located within the Upper Matua Subgroup	18.0-18.075 / 1 / 85 (8ϕ)	Mixed layered 10 & 7 A° Halloysite
	18.0-18.075 / 1 / 85 (9ϕ)	Mixed layered 10 & 7 A° Halloysite
	18.075-18.08 / 1 / 85	Mixed layered 10 & 7 A° Halloysite
	18.08-18.095 / 1 / 85 (8ϕ)	Mixed layered 10 & 7 A° Halloysite
	18.08-18.095 / 1 / 85 (9ϕ)	Mixed layered 10 & 7 A° Halloysite
	18.095-18.1 / 1 / 85	Mixed layered 10 & 7 A° Halloysite
	18.095-18.1 / 1 / 85 retested, fired at 500 °C	Mixed layered 10 & 7 A° Halloysite
	18.10-18.11 / 1 / 85	Mixed layered 10 & 7 A° Halloysite
	18.11-18.12 / 1 / 85	Mixed layered 10 & 7 A° Halloysite
	18.12-18.23 / 1 / 85	Mixed layered 10 & 7 A° Halloysite
	18.12-18.23 / 1 / 85 retested, fired at 500 °C	Mixed layered 10 & 7 A° Halloysite

4.3.3 X-ray Fluorescences Analysis

a) Introduction

Throughout the soil profile are numerous dark greenish black, brownish black, and black grains which vary from medium sand to granule in size. These occur separately as individual grains or appear to aggregate around old and new rootlet structures. X-ray Fluorescence was conducted on a sample to try and determine composition and therefore mineralogy. The methods used for mineral XRF analysis are presented in Appendix A4.3.

b) Results and Discussions

Results obtained from XRF are presented in Table 4.4. The results were then entered into the XRD inorganic mineral data base to try and produce possible compounds, of which five were found:

1. Sodium Aluminium Silicate,
2. Manganese Iron Phosphate Hydroxide Hydrate,
3. Calcium Manganese Sulphate Hydroxide Hydrate,
4. Aluminium Hydroxide,
5. Zinc Sulphate Hydrate.

Harmsworth (1983) indicated that there were several ferromagnesian minerals present within the Matua Subgroup with which these tested compounds could be associated. However, because the data base contains only inorganic compounds it is likely that none of these compounds represent the sample's true composition, and the sample is in fact an organic derivative. This argument can be supported by the evidence that a large proportion of the material was found around old rootlet structures or in areas which contained a high organic content.

Table 4.4 XRF analytical results presenting percentage chemical composition of sample

Sample	SiO_2	TiO_2	Al_2O_3	Fe_2O_3T	MnO	MgO	CaO	Na_2O	K_2O	P_2O_5	LOI	Total
Number (%)	49.86	0.52	27.53	4.18	3.12	0.15	0.74	1.49	0.79	0.04	10.69	99.12

4.3.4 Allophanes

a) Objectives

Testing was conducted for allophanes to try and explain the unusual behavioural characteristics found during other laboratory tests e.g. Atterberg limits, which are not in keeping with the properties that what would be expected if only halloysite was present.

The methodology used was that outlined by Fieldes and Perrott (1966) for rapid field testing for allophanes. It was not the objective of this test to produce a quantitative or compositional assessment, but to merely indicate their presence or abscence.

b) Methodology

1. Filter paper was treated with phenolphthalein indicator and subsequently allowed to air dry.
2. A small amount of the soil to be tested was smeared on the indicator paper.
3. A small amount (1-5 drops depending on the amount of soil) of saturated aqueous NaF solution (1 M NaF) was added to the soil.

c)..Results and Discussion

Only a small number of representative samples were tested from the Hamilton Ash, Cross-bedded sequence and aquifer, and if allophanes were present within these it could be concluded that they would be present throughout the rest of the soil stratigraphy. Table 4.5 indicates that all samples tested produce a positive result, indicating the presence of allophanes. Fieldes and Perrott (1966) indicate that if a reaction is seen as in this case, it suggests that the Allophanes are in concentrations greater than 10%. This result is not unexpected due to the large volcanic glass content associated with all the soil units noted during field and laboratory testing. It can therefore be inferred that allophanes found during testing are present throughout the soil stratigraphy in concentrations higher than 10%.

Lowe and Percival (1993) indicated that Al-rich allophane is the most dominant form of allophane in New Zealand. However, due to the presence of Halloysite, and the drainage and tephra characteristics of the peninsula and surrounding area, the Si-rich allophane would more probably be the dominant form. However, this aspect has not been investigated, with the recognition of Allophanes being sufficient for this study.

d) Geotechnical Properties

1. Test properties to be expected:

- Oborn (1988) state that Allophanes when undisturbed have a firm friable consistency that breaks abruptly to form a soft paste on remoulded.
- Allophanes are very small, hollow structures, which are generally water filled spherical structures surrounded by tunnel-like pores. When dried these pores tend to collapse preventing water escape (Oborn, 1988). The resulting soil becomes quite hard and is practically non-plastic (Terzaghi et al., 1996).
- Allophanes if allowed to dry show an irreversible change in physical properties such as a decrease in the ability to retain water, and an increase in permeability and erodibility.

2. Behaviour of test soils testes this study

The first two behavioural characteristics of Allophanes were observed during Atterberg limits testing. On mechanical manipulation of the soil during liquid limit testing the sample formed a sticky paste. Consequently when the soil was dried in stages for plastic limit determination it became harder to roll a tread. The samples that were most affected were those from the lower bounding aquitard.

Table 4.5 Allophane test results.

Samples	Stratigraphic Position	Preparation	Results
8.2/1/85	Hamilton Ash	sieved 425μm	strong reaction turning the indicator paper a dark pinkish red
15.0/1/85	Cross-bedded section (Upper Matua	sieved 425μm	moderately strong reaction turning the indicator paper a dark pink
16.5/1/89	Cross-bedded section (Upper Matua	in-situ	moderately strong reaction turning the indicator paper a dark pink
18.0/1/85	Aquifer (Upper Matua Subgroup)	in-situ	moderately strong reaction turning the indicator paper a dark pink

4.4 ATTERBERG LIMITS

4.4.1 Introduction

Atterberg Limit tests were conducted on a range of samples for which grainsize analysis was also performed to provide further geotechnical characterisation of the soil properties. The Pahoia Tephra was not included due to the variable grainsize and soil structure from area to area within the sequence, and also it was not relevant to failures. In addition the aquifer layer was not tested as little clay was able to be obtained from the sample collected. Atterberg Limits can be used to calculate the plasticity and activity of a soil which in turn can be related to the clay content (Lambe and Whitman, 1979). The plasticity and activity parameters were those defined in BS 5930:1981 (Barnes, 1995), however, as the Maungatapu Peninsula consists of numerous airfall, fluvial, and estuarine deposited beds, and with limited test samples, it is difficult to relate the clay content to the plasticity.

4.4.2 Results

Presented in Figure 4.5 are plots of PI, activity, and clay fraction <2μm versus stratigraphic position of the soil within the cliff sequence. Table 4.6 provides an additional summary of Atterberg limits, plasticity, activity, and clay fraction percentage.

a) Palaeosol and Hamilton Ash

The Palaeosol from particle size analysis is predicted to have a clay content around 40% approximately equivalent to the Hamilton Ash. Clay mineralogy analysis indicated the presents of a mixed layer 7 and 10 Å Halloysite, and Allophane in the Hamilton Ash. This mineral composition will also be present within the Palaeosol. Atterberg Limit testing for the Palaeosol produced a high liquid limit (LL=67) and a plasticity index (PI=37), equating to a high plasticity (Figure 4.4). The Hamilton Ash also exhibited a high clay content (36%) and produced an extremely high liquid limit (103). Consequently with a moderate plastic limit (35) the sample produced an extremely high plasticity index (68,

Figure 4.4) and an activity of 1.87 delineating it as being active, (Barnes, 1995). This meant that according to Barnes the clay was equivalent to a montmorillonite or a organic alluvial clay.

b) Cross-Bedded Sequence

With a decrease in the clay content into the Cross-bedded section of the Upper Matua Subgroup a corresponding decrease in the plasticity (16) and activity (0.79) occurs (Figure 4.5). This is not unexpected, with Halloysite believed to be the main clay mineral present. Because Halloysite is a close relative of Kaolinite it is expected that Halloysite will exhibit the same low plasticity and activity.

c) Lower Bounding Aquitard

The samples tested from the lower bounding aquitard that contained high clay contents (36-64%) produced a plasticity index and activity that ranged between 6 and 16, and 0.09-0.4 respectively (Table 4.6). This would indicate samples of low to intermediate plasticity and inactive activity (Figure 4.4). Barnes (1995) suggests that these results would be equivalent to the behavioural characteristics of Kaolinite. Conversely a sample tested from the lower bounding aquitard that contained only 9% clay produced a plasticity index of 49 indicating a extremely high plasticity, and an activity of 5.24 indicating that it is highly active. Barnes (1995) suggests that an activity this high is equivalent to a clay like bentonite. However, as bentonite is not present, Allophanes are the only other clay consitutent with properties that could produce these high plasticities and activities. These types results therefore are opposite to what would normally be expected where an increase in clay content would produce a corresponding rise in plasticity.

4.4.3 Discussion

From XRD results Halloysite was determined to be the main clay mineral present within the stratigraphic units of the Peninsula. With Halloysite being a close relative of Kaolinite it was believed that the same behavioural characteristics of low-intermediate plasticity and inactivity would be exhibited by the samples tested. The samples from the lower bounding aquitard did not exhibit these characteristics, but instead showed that with increasing clay content there was a decline in the plasticity and activity. It was suggested by Lewis (Pers. Comn., 1997) that the behavioural characteristics demonstrated by the samples from the lower bounding aquitard may be in response to the presence of Allophanes in the soils. From clay mineral analysis testing showed that Allophanes were present within the samples tested in concentrations upwards of 10%. Oborn (1988) and Terzaghi et al.(1996) indicate a number of geotechnical properties that are discussed in section 4.3.3 which were observed during Atterberg Limit testing. The influence of Allophanes during liquid limit testing was evident in that on mechanical manipulation the sample formed a paste. This made it difficult to produce a range of cone penetration depths during testing. In addition to this on drying the sample out in stages for rolling of threads during plastic limit testing, probably helped to partially collapse the Allophane structure producing a low plasticity soil. It is evident that with limited samples tested, lack of information on the geotechnical properties of Halloysite, and quantities of Allophanes present in these soils, more testing is required to fully characterise the soils.

Table 4.6 Summary of Atterberg Limits, clay mineralogy, plasticity and activity.

TABLE INDICATING ATTERBERG LIMITS, PLASTICITY AND ACTIVITY							
Sample	Soil Location Within Failure Scarp	Clay Mineral	Percentage finer than 2μm	w_L (LL)	w_P (PP)	PI	Activity
5.8 / 1 / 85	Palaeosol	10 A° Halloysite & Allophanes	assumed to be approx. = 40	67 ±4	30 ±2	37 ±6	0.93
8.2 / 1 / 85	Hamilton Ash	10 A° Halloysite & Allophanes	36.41	103 ±4	35 ±2	68 ±6	1.87
15.1 / 1 / 85	Cross-bedded section of the Upper Matua Subgroup	10 A° Halloysite & Allophanes	20.36	46 ±2	30 ±2	16 ±4	0.79
18.08-18.095 / 1 / 85	Lower bounding aquitard	10 A° Halloysite & Allophanes	63.68	36 ±2	30 ±2	6 ±4	0.09
18.095-18.10 / 1 / 85	Lower bounding aquitard	10 A° Halloysite & Allophanes	54.1	42 ±2	35 ±2	7 ±4	0.13
18.10-18.11 / 1 / 85	Lower bounding aquitard	10 A° Halloysite & Allophanes	35.9	51 ±4	40 ±2	11 ±6	0.31
18.11-18.12 / 1 / 85	Lower bounding aquitard	10 A° Halloysite & Allophanes	9.36	102 ±4	53 ±4	49 ±8	5.24
18.12-18.23 / 1 / 85	Lower bounding aquitard	10 A° Halloysite & Allophanes	40.42	51 ±4	35 ±2	16 ±6	0.4

The Palaeosol is assumed to have a clay content of approximately 40 % in keeping with that of the Hamilton Ash.

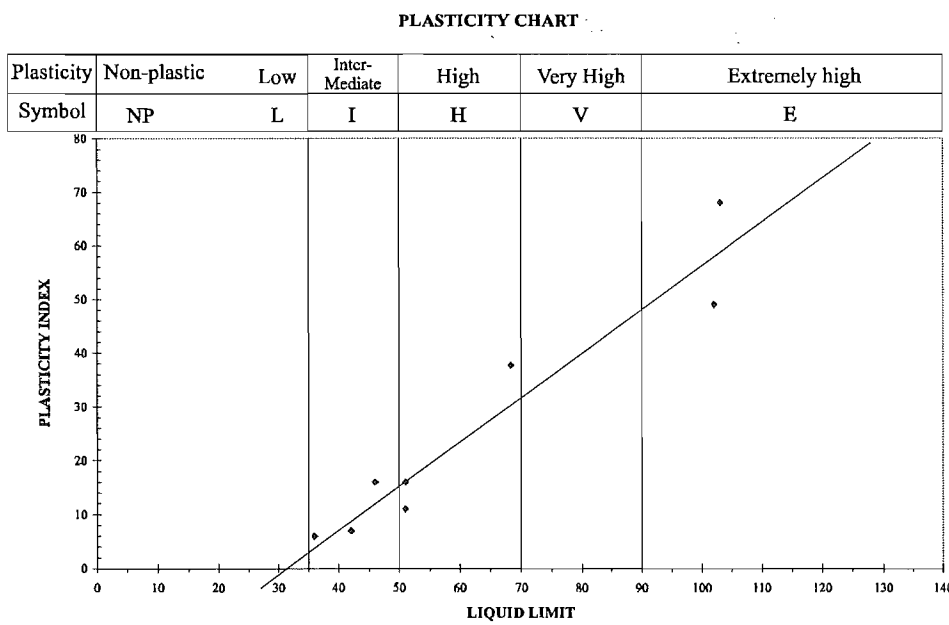

Figure 4.4 Plasticity index verses liquid limit to determine plasticity of tested samples. Modified from BS 5930:1981 in Barnes (1995).

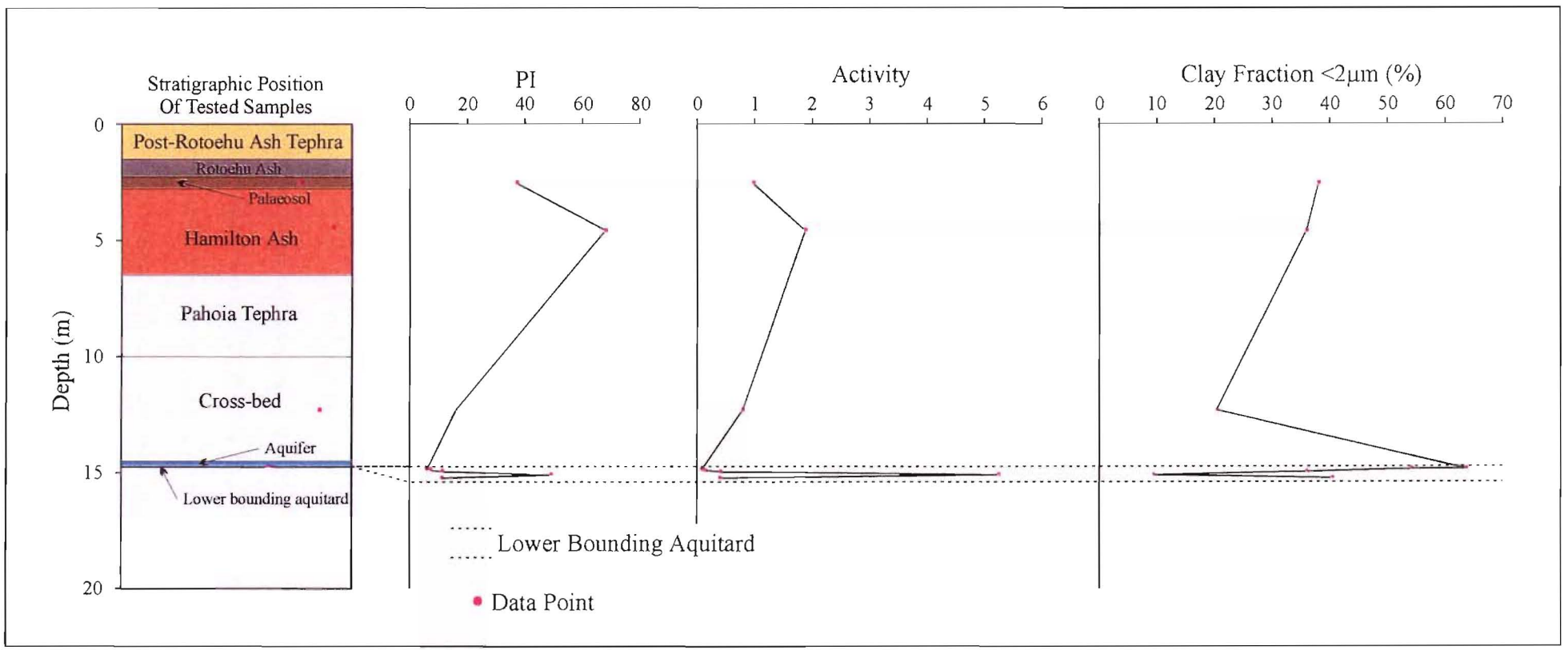

Figure 4.5 Plasticity and activity compared to stratigraphic position and clay fraction. Note Aquifer not tested.

4.5 DIRECT SHEAR TESTING (SHEAR BOX)

4.5.1 Introduction

Direct shear testing provided the opportunity to test the shear strength of a particular layer of interest, as well as providing a means to test more sandy samples that were difficult to test using the triaxial testing setup. Samples used during testing were obtained from either bulk or in-situ sampling in the field. The testing procedure is outlined in Appendix A4.4, with the methodology used being that set out by the manufacturer Wykeham Farrance. For each sample three tests were carried out at differing normal loads of 62, 125, 187, or 249 kPa which equate to a hanger mass of 5, 10, 15, and 20 kg respectively. These normal loads were chosen to simulate a range of overburden weights that compare to an in-situ normal load of 212 kPa representing a hanger arm mass of 17 kg. This provides a range in shear strengths which can be used to calculate Cohesion (c') and friction angle (ϕ'). Shearing rates of 0.120 and 0.80 mm/min were used for the more sandy samples for two reasons. The first was to have a shearing rate that is fast enough that reconsolidation of the sandy soil does not occur during testing, and the second was to use a shearing rate that simulated the fast failure conditions. A shearing rate of 0.024 mm/min was selected for the more silty samples so as not to build-up pore water pressures within the samples, therefore producing a misleading shear strength. At the rates specified failure would could occur between half an hour for the sandy units to 10 hours for the more silty soils.

4.2.2 Results

From plots of shear stress versus displacement, peak shear strength values were calculated for each normal load. These were then plotted in order to obtain an angle of internal friction in addition to a cohesion value. A typical result can be viewed from the plot of shear stress verses displacement and the corresponding plot of normal load versus shear strength in Figures 4.6 & 4.7. All plots of normal load versus shear strength are presented in Appendix A4.5, while a summary table is presented in Table 4.7.

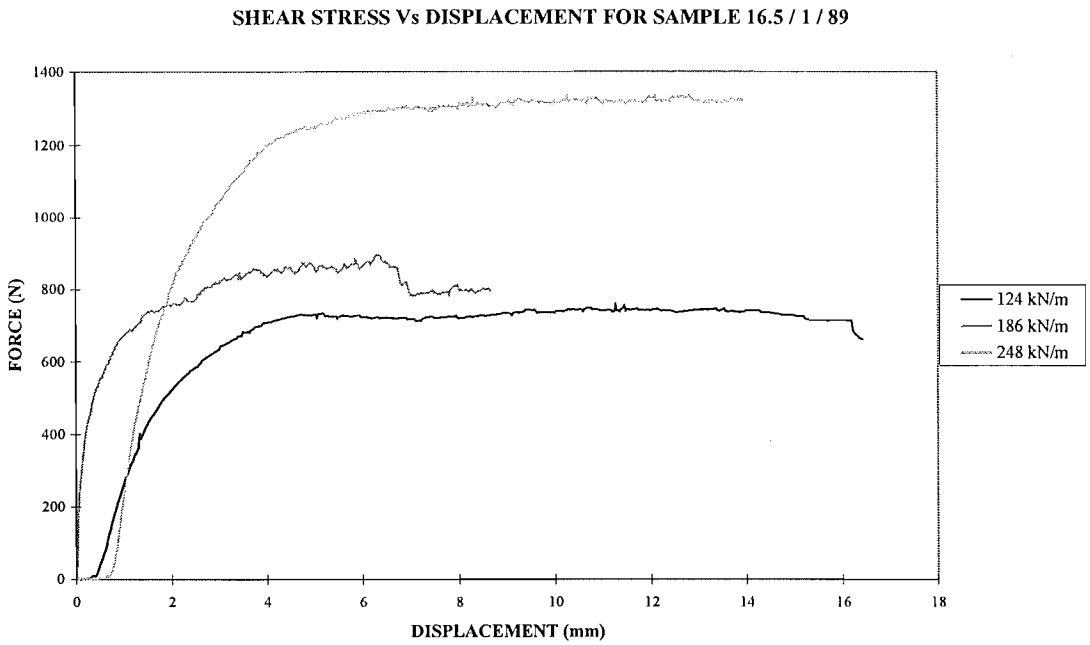

Figure 4.6 presents shear stress verses displacement plot to obtain peak shear strengths for sample 16.5 / 1 / 89, which is part of the Cross-bedded sequence consisting of a sandy SILT with some clay.

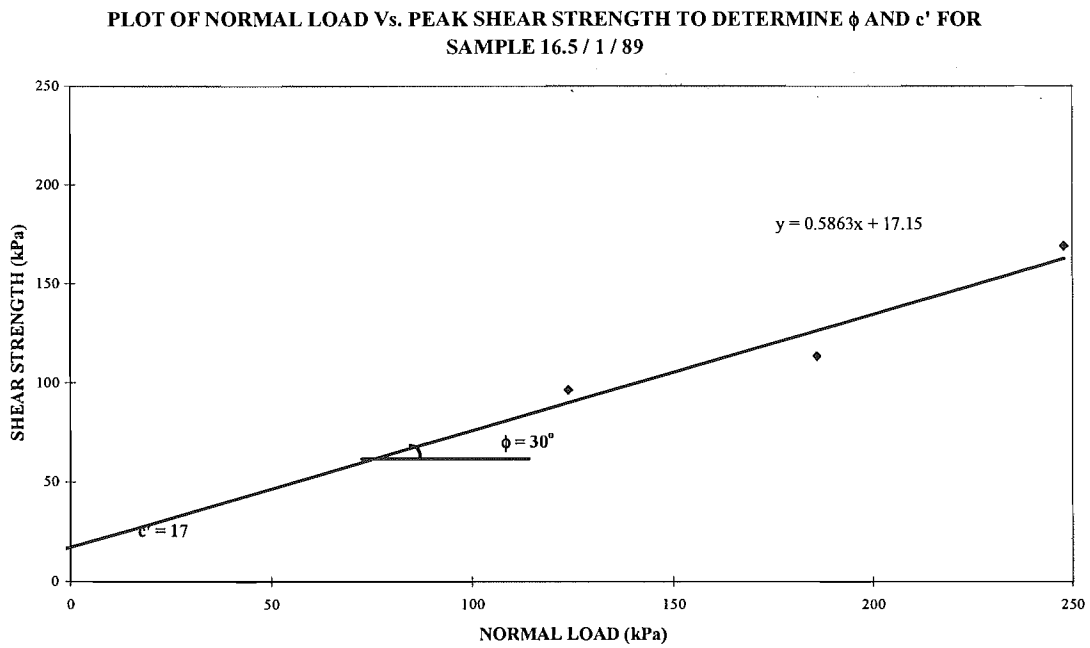

Figure 4.7 plot of normal loads verse peak shear strengths in order to obtain a cohesion of 17 and an internal friction angle of 30°.

Table 4.7 indicates maximum and minimum shear strength values for samples 2.7 / 1 / 85 and 12.4 / 1 / 89, in addition to internal friction angles and cohesion values for the remaining samples.

TABLE INDICATING SHEAR STRENGTH RANGES AS WELL AS COHESION AND FRICTION ANGLE				
Sample	**Shear Strength (kPa)**		**Stratigraphic Unit**	**Soil Type**
	Min	Max		
2.7 / 1 / 85	0	94	Post-Rotoehu Ash Tephras	MEDIUM-COARSE SAND
12.4 / 1 / 89	6	67	Pahoia Tephra (Upper Matua Subgroup)	COARSE SAND with some granules
Sample	**Cohesion (c')**	**Friction Angle (degrees)**	**Stratigraphic Unit**	**Soil Type**
15.6 / 1 / 85	0	36	Cross-bedding (Upper Matua Subgroup)	sandy SILT with some clay
16.5 / 1 / 89	17	30	Cross-bedding (Upper Matua Subgroup)	sandy SILT with some clay
17.0 / 1 / 89	3	37	Cross-bedding (Upper Matua Subgroup)	sandy SILT with some clay
18.6 / 1 / 89	0	42	Situated just above aquiferial zone in the lower section of the Cross-bedded sequence (Upper Matua Subgroup)	sandy SILT
17.1 / 1 / 330	0	35	Upper Matua Subgroup	MEDIUM-COARSE SAND
Sample 11	19	18	Weakest noticeable unit in the field situated within the aquiferial zone (Upper Matua Subgroup)	clayey SILT with with some sand

a) Post-Rotoehu Ash Tephras and Pahoia Tephras

The Post-Rotoehu Ash Tephra and Pahoia Tephra samples used for direct shear testing consisted of coarse sands. On testing with an increase in normal load no corresponding increase in the shear strength was observed. It is considered that the large range in particle sizes, loose compaction and more rounded grains of these pumicious soils resulted in the grains tending to roll when sheared. Increases in shear strength are considered to be the result of a lockup within the soil matrix of individual grains. This lock up of grains could be released by the shearing of the particular grains resulting in an immediate decrease in the shear strength of the sample. Because of this no relationship can be drawn between normal load and shear strength, with the data only being able to be used as an indication of a possible range in shear strengths of these two samples.

b) Cross-bedded Sequence

Cohesion and friction angle for the cross-bedded sequence ranged between 0 - 17 kPa, and 30 - 42° respectively (Table 4.7). Samples that tended to exhibit higher cohesion generally produced the lowest friction angles (e.g. sample 16.5/1/89, Table 4.7). From testing it is suggested that samples that exhibit higher clay contents (such in the case of 16.5/1/89) tend to produce lower friction angles. This was mainly due to the fact that with higher clay contents there is a corresponding relative decrease in sand sized glass shards. If there is comparatively less sand sized glass shards the intra-particle lock up between these glass shards is reduced, resulting in a decrease in the friction angle. Conversely, if there is an increase in the number and size of these sand sized glass shards there will be greater intra-particle lock up within the soil lattice on shearing, therefore increasing the friction angle.

c) Aquifer

The aquifer, being comprised mainly of medium to coarse sand, produce c' = 0 and a ϕ = 35°. The high friction angle and low cohesion was not supprising as the numerous glass shards and little clay would allow the sample lattice to lock up on shearing.

4.5.3 Discussion

a) Affects of Cohesion

From Table 4.7 cohesion values range between 0 and 19 kPa. Cohesion is dependent on the chemical composition as well as the particle size distribution of the soil. This means that soils which are predominantly silts and clays will tend to have higher values of cohesion than silty sands. The soils delineated from field investigations and particle size analysis at Maungatapu Peninsula have a wide range of grainsizes. The sandier beds of the stratigraphic units (e.g. Rotoehu Ash and aquifer) will yield low (e.g. 9 kPa) to 0 kPa

cohesion values. In comparison the silty beds within the stratigraphic units (e.g. Palaeosol, Cross-bedded sequence) produced low to moderate (0-19 kPa) cohesion values.

b) Affect of Friction Angle

From Table 4.7 the angles of internal friction calculated lie between 18 and 42°. The internal friction angle of 18° for sample 11 is indicative of the soft silty clay nature of the soil, which is situated within the upper bounding aquitard of the aquifer zone. Conversely the other friction angles for the rest of the Upper Matua Subgroup range from 30-42° for samples with higher sand contents. These will tend to be higher due to a number of compositional differences. Compositional differences related to texture such as grainsize, uniformity (degree of grading), Roundness, Sphericity, weathering, and void ratio. The two most important factors influencing internal friction angles in this case are:

1. *Grain Size and Uniformity* - with increased particle size there will be a general increase friction angle. In addition an increase in the range of grainsizes present will also increase the internal friction angle. From field investigations and laboratory work during this study many of the soils are composed of a wide range in grainsizes, e.g. the Cross-bedded sequence is a well graded fine sandy MEDIUM SAND with some very coarse sand and silt.

2. *Roundness and Sphericity* - with increasing angularity and decreasing sphericity of grains there will be a corresponding increase in friction angle. The Maungatapu soils consist of numerous low sphericity and angular glass shards which compared to more high sphericity sub angular-sub rounded grains (Lewis and McConchie, 1994). This will lock up the soil lattice therefore producing high internal friction angles. Values of 42° such as sample 18.6 / 1 / 89 can be easily obtained when subjected to high normal stresses as in this case.

These results compare favourably to data produced by direct shear testing by Bird (1981). Bird recorded friction angles which range between 18 to 43° and cohesions from 0 to 24 kPa. From data produced during this study and Bird's, it can be concluded that the soils of the logged cliff face are highly resistant to sliding with the lower friction angle soils tending to exhibit higher cohesive properties.

Bird (1981) performed a number of consolidated undrained triaxial tests on samples associated with soils from the lower and upper aquitard, aquifer, and cross-bedded section of the Upper Matua Subgroup. However, Bird produced a number of negative cohesions which are impossible, therefore making it difficult to compare this data to results obtained during this study.

4.6 TRIAXIAL TESTING

4.6.1 Introduction

Unconsolidated Undrained triaxial testing was conducted to look at various failure modes and to compare the peak shear strengths with those produced in the field by the shear vane. Unconsolidated undrained triaxial testing measures the undrained shear strength of a soil at its in-situ natural moisture content. Field evidence pointed to a rapid type failure, therefore suggesting that an undrained unconsolidated triaxial test (UU) would be better suited to represent the in-situ soil conditions prior to sliding (McManus, Pers. Comn., 1997). In quick UU tests a strain rate of 2% of specimen length per minute (approximately 1.6mm/min) is commonly adopted so that a test can be completed in about ten minutes. However, in this case concern was levelled at the effect that pore pressures within the test sample may have on the shear strength. Because of this McManus suggested that a shearing rate of 0.2 mm/min may not sufficiently allow the build-up of pore pressures within the sample. In addition a range of confining pressures were chosen, 150, 300, 450

kPa to provide a range of shear strengths. These confining pressure represent overburden depths of 10, 20 and 30 m. Testing procedures and results are presented in Appendix A4.6.

4.3.2 Results

The average strength for all samples tested is 22.9 kPa, with a range from 2 - 80 kPa. Individual assessment of test results can be seen below.

a) Palaeosol

The Palaeosol (sample 3.1/1/330) produced the highest shear strength (80kPa), reflecting the compact nature of the in-situ material (Table 4.8). The failed test samples showed clear conjugate shear planes which developed during testing (Figure 4.8). The shear strengths obtained in the field by the use of the Pilcon shear vane were predominantly higher than those seen during laboratory testing, and ranged between 150-200 kPa for the in-situ Palaeosol (Chapter 3). From particle size analysis the Palaeosol was determined to have a clay content of 40%, and as such would be expected to exhibit cohesive properties. Because of this the shear strengths can be classified according to Table 4.9, laboratory determined shear strengths would equate to a soft to firm cohesive soil strength classification. However, shear vane values would equate to a stiff to very stiff cohesive soil strength (Table 4.9). Overall the Palaeosol is suggested to represent the strongest unit within the logged cliff faces.

b) Hamilton Ash

Shear strengths from the triaxial testing of the Hamilton Ash are extremely low due to a pin pick in the rubber membrane that surrounds the sample. This allowed water under confining pressures of 150, 300, and 450 kPa to enter through the pinhole, therefore liquefying the sample. Because of this these results obtained for the Hamilton Ash are meaningless. From field investigation shear strengths ranged between 70 and 190 kPa. It is suggested that because the Hamilton Ash exhibits similar strengths in the field as the

Cross-bedded sequence, the shear strengths produced by triaxial testing in the laboratory for the Cross-bedded sequence will be similar to those that would have been produce by the Hamilton Ash.

c) Cross-bedded sequence

The Cross-bedded sequence proved difficult to sample due to the varying degrees of saturation, grainsize, and soil structure. From particle size analysis the Cross-bedded sequence consists of approximately 40% sand, 40% silt, and 20% clay. Because of the clay content, direct shear results for the Cross-bedded soils produced cohesions around 17 kPa, therefore allowing them to be classified according to Table 4.9 as very soft. It must be noted that cross-bedded soil that are non-cohesive (c' = 0 kPa) can not be classified according to Table 4.9.

Table 4.8 Triaxial test data showing peak shear strengths.

Triaxial Testing Data					
Geologic Unit	Sample	Confining Pressure, σ3 (kPa)	Maximum Deviator Stress, σ1 - σ3 (kPa)	Principal Stress, σ1 (kPa)	Shear Strength (kPa)
Palaeosol	3.1 / 1 / 330	150	160	310	80.0
		300	51	351	25.5
Hamilton Ash	4.9 / 1 / 330	150	12	162	6.0
		300	3	303	1.5
		450	4	454	2.0
Upper Matua Subgroup	16 / 1 / 85 Cross-bedded sequence	150	34	184	17.0
		300	41	341	20.5
		450	23	473	11.5
	1 Upper bounding aquitard	150	37	187	18.5
		300	68	368	34.0
		450	52	502	26.0
	2top Lower bounding aquitard	150	45	195	22.5
		300	30	330	15.0
		450	24	474	12.0
	2bottom Lower bounding aquitard	150	55	205	27.5
		300	51	351	25.5
		450	54	504	27.0
	3top Aquifer	150	62	212	31.0
		300	46	346	23.0
		450	46	496	23.0
	3bottom Lower bounding aquitard	150	43	193	21.5
		300	49	349	24.5
		450	56	506	28.0
	9 Lower section of the Cross-bedded sequence	150	41	191	20.5
		300	69	369	34.5
	10 boundary between the upper aquitard and the lower section of the Cross-bedded sequence	150	41	191	20.5
		300	46	346	23.0
		450	41	491	20.5
				Average Shear Strength (kPa) =	22.9

Shear strength values for sample 16/1/85 (Cross-bedded sequence) ranged between 11.5-20.5 kPa (Table 4.8), indicating the soils to be very soft (Table 4.9). It is believed that this represents the lower end of the scale when compared to shear strengths obtained in the field which ranged between 50-200 kPa, (Chapter 3). Failure generally occurred through a shortening and bulging, with partial rearrangement of the soil structure. This could be the result of porewater pressure partially liquefying the sample during testing. Some horizontal shearing perpendicular to the principal stress occurred, which may also be influenced by pore pressures acting in a more finer confined layer within the specimen. Sample 9 is situated just above the upper bounding aquitard with a particle size distribution similar to that of other sample from the cross-bedded sequence. Shear strengths range between 20.5 and 34.5 kPa, with failure occurring through a shortening and bulging in addition some horizontal shearing.

d) Upper Bounding Aquitard

Sample 10 is located on the boundary between the upper bounding aquitard and the lower section of the Cross-bedded sequence. With a similar composition to that of the direct shear sample 11 (clayey SILT with some sand) it is expected to exhibit cohesive properties. Shear strengths ranged between 20.5-23.0 kPa with failure modes similar to those of sample 3bottom. These very low shear strengths would allow the soil to be classified as a very soft soil (Table 4.9).

Sample 1 is situated within the upper bounding aquitard and consists of numerous small beds 2 to 10 mm in thickness (Figure 4.9). One of these beds can be seen to bulge outwards slightly, indicating a weak zone within the sample. This zone is also present in the lower bounding aquitard. During testing the weak zone was easily compressed, producing a localised failure in the test specimen. The unconfined undrained (UU) plots showed evidence of this by a minor peak around 20 and 40 kPa for the 150 and 300 kPa

tests, respectively (Appendix A4.6). After the small failure the test was continued in order to delineate additional failure behaviour. A set of conjugate shears developed across the various horizontal beds towards the bottom section of the sample. Strengths ranged from 18.5 to 34 kPa, indicating a soft to very soft strength classification (Table 4.9).

e) Aquifer

Sample 3top lies within the aquifer and consists of a silty SAND with some clay. The UU plots (Appendix A4.5) indicate a gradual failure with shear strengths ranging from 23-31 kPa. With the apparent low clay content it is not possible to concluded that sample 3top would show cohesive properties. The sample tested could be divided into two sections, with the top part containing less silt compared to the bottom. The lower section of the sample consisted of a number of fine beds 3 to 10 mm in thickness. During testing shears developed along the boundary of some of these beds, or at a low angle to them.

Table 4.9 Cohesive soil strength from New Zealand Geomechanics Society (1988).

Classification Term	Diagnostic Feature	Undrained Compressive Strength (kPa)
Very Soft	Exudes between fingers when squeezed	< 25
Soft	Easily indented by fingers	25-50
Firm	Indented only by strong finger pressure	50-100
Stiff	Indented by thumb pressure	100-200
Very Stiff	Indented by thumbnail	200-400
Hard	Difficult to indent by thumbnail	400-1000

Figure 4.8 Photograph of conjugate shears which were produced during triaxial testing within the Palaeosol.

Figure 4.9 Photograph of the numerous layering present within sample 1. Also notable is the weak bulging bed towards the top of the sample.

f) Lower Bounding Aquitard

Sample 3bottom lies directly below 3top and represents the boundary between the lower bounding aquitard and the aquifer. Sample 3bottom consists of a clayey SILT with some sand which appears grade into a SILT with some clay and sand. As in sample 1 it is comprised of numerous small beds. From direct shear data the lower bounding aquitard produced a cohesion of 19 kPa indicating that these soils were cohesive. Shear strengths range between 21.5 and 28 kPa, indicating a soft to very soft soil classification (Table 4.9). Failure occurs in the same manner as that of 3top along a number of horizontal to low angle shears similar to Figure 4.8. A possible scenario involves the non-uniform distribution of porewater pressures throughout the sample. When a strain is applied the pore pressures build up within a number of these semi-confined small beds. Once a sufficient pressure is reached within one of these beds a failure occurs along the boundary between itself and the adjacent bed (Figure 4.11).

Sample 2top consists of a clayey SILT with some sand and is situated within the lower bounding aquitard. Shear strength ranged between 12-22.5 (Table 4.8) indicating a very soft soil strength classification (Table 4.9). The 150 and 300 kPa UU plots (Appendix A4.6) showed a gradual failure which reflected the shortening and bulging where as the 450 UU plot indicates a more rapid failure. Apart for these types of failures a number of horizontal cracks appeared alone the boundaries of some of the small beds that exist within the specimens. Sample 2bottom, which consisted of a silty CLAY, was located towards the middle to lower section of the lower bounding aquitard. Both 2top and 2bottom were cut so as to exclude the weaker bed denoted in sample1. Shear strengths for 2bottom ranged from 25.5-27.5 (Table 4.2), indicating a soft soil strength classification. The sample exhibited a more brittle planar type failure orientated at approximately 60-70° from the horizontal (Figure 4.10). The results seam to compare favourably to the in-situ material examined in the field using the classification terms in Table 4.9.

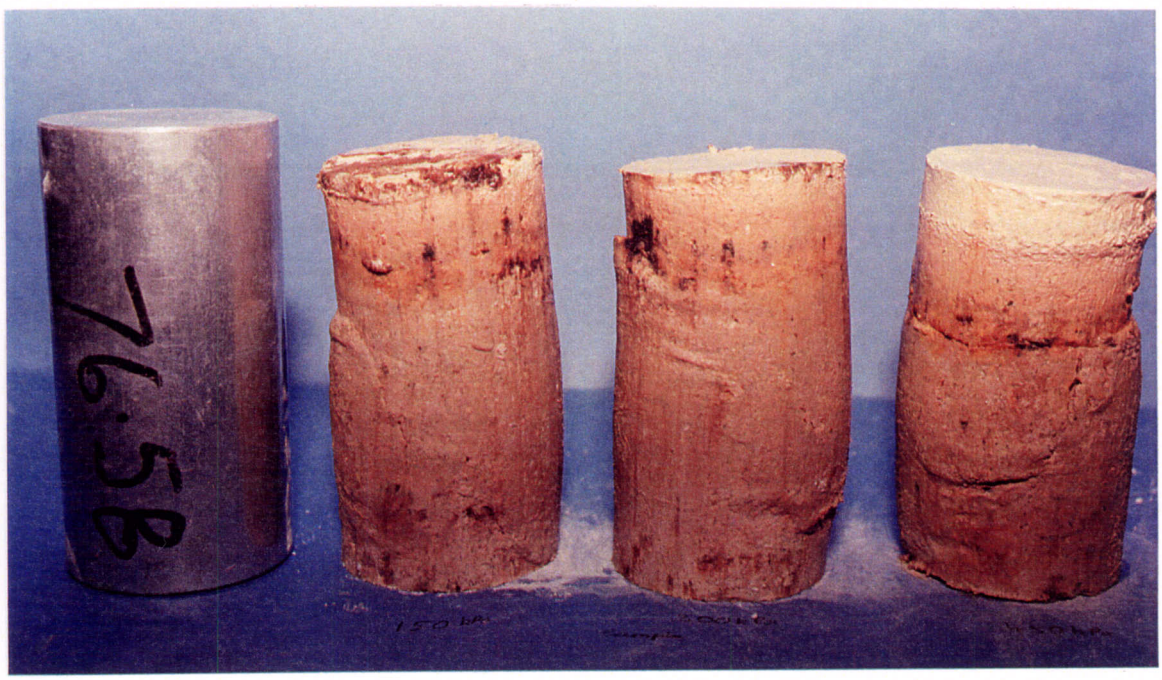

Figure 4.10 Photograph of 2bottom showing a planar failure at about 60-70° from the horizontal.

Figure 4.11 Photograph of 3bottom showing horizontal failures occurring between boundaries of two beds. Also notable are individual beds of weaker silty-clay material which bulge outwards compared to the more sandy beds.

4.3.3 Synthesis

From the test results four main types of failure could be delineated:

1. Conjugate shears,
2. inclined planar failure,
3. planar failure approximately perpendicular to the principal strain direction, most probably the result of porewater pressure concentration with a layer in the sample,
4. shortening and bulging, generally occurred in the more sandy samples where porewater pressure influenced the failure dynamics.

The conjugate shears and inclined planar failures represent brittle types failures, whereas the samples that showed a shortening and bulging are indicative of plastic failures. The horizontal and low angle planar failures can exhibit both brittle and plastic failure dynamics as demonstrated by Figure 4.5. Bird (1981) also noted the differing brittle and plastic failures. These horizontal to low angle failures are suggested to be the dominant form of failure within the upper and lower bounding aquitard and aquifer. This mode of failure is most probably greatly enhanced by the induced porewater pressures resulting from the head-recharge theory presented in chapter 2. Overall the lower bounding aquitard due to it high clay contents is suggested to have very soft soil strengths (Table 4.9).

The number of samples tested cannot be concluded to statistically represent the soils from which they were collected. This is mainly due to the fact that the sample tested only represents an very small proportion of the in-situ soil mass (e.g. 38mm diameter × 80 mm log). Because many of these soils tested have a wide range of grainsizes sampling can never obtain a truly representative sample. To counteract this a large number of samples would used to be collected. As with many sampling programs the logistics of collecting

enough samples, especially in a sequences of volcanics soils, can make this an impossible task. For this study not enough samples have been collected to conclude whether the results obtained from laboratory testing are representative in-situ shear strengths. Overall the laboratory results are generally consistent to the relationship found in the field where the Palaeosol is the strongest unit and while the other units produced a range of shear strengths. It can be suggested that accrual shear strengths for this study will most probably lie somewhere between the triaxial test data and shear vane data.

4.7 DISPERSION AND ERODIBILITY

4.7.1 Dispersion Using The Emerson Crumb Test

a) Introduction

The Emerson crumb test was used to determine the dispersive nature of the clays within the soils used for pinhole testing. A crumb is placed into a beaker of distilled water and the amount of colloidal suspension gives an indication of the degree of dispersion. The degree of dispersion in turn will give a estimation of how easily the clay fraction will go into suspension on the addition of water. If the dispersion is high, the soil will tend to be more prone to erosion as the soil matrix strength is decreased on void saturation. The methodology used is given in Appendix A4.7.1.

b) Results and Discussions

From Table 4.10, the Post-Rotoehu Ash Tephras and Palaeosol were non-dispersive with a classification of Emerson class 1. This was not unexpected and it is reasonable to suspect that these two units (including the Hamilton Ash and some Rotoehu Ashes) will exhibit similar non-dispersive properties. On the other hand almost all of the Upper Matua Subgroup sample showed a strong degree of dispersion, with Emerson classes ranging from 2.5 to 4. This indicates that the clay fraction will easily become entrained and erode provided there is sufficient water velocity. This will decrease the intra-particle bonding, inducing the erosional features seen during pinhole testing (Section 4.7.2).

EMERSON CRUMB TEST			
Sample	**Dispersion Classification**	**Stratigraphic Position**	**Comment**
0.4 / 1 / 330	Class 1	Post-Rotoehu Ash Tephra	Due to the sandy nature of the sample the crumb disintegrated on immersion in water, no perceivable cloud could be seen
4.6 / 1 / 85	Class 1.5	Rotoehu Ash	Slight colloid cloud around the crumb
3.1 / 1 / 330	Class 1 Class 1	Palaeosol	Two tests were performed. On completion of testing very minor disintegration of the crumb had occurred in both cases, with neither crumb showing any signs of colloid suspension
9.8 / 1 / 330	Class 4 Class 4	Cross-bedded	On completion the more sandy crumb had disintegrated, where as the more clayey crumb held together a lot better
10.0 / 1 / 330	Class 4	Cross-bedded	Complete disintegration of crumb
14.0 / 1 / 330	Class 4 Class 3.5	Cross-bedded	Sample can be highly variable with interfingered Clayey Silt, Clayey Sands units. One of the crumbs basically held together (Class 3.5) while the other completely disintegration (Class 4)
14.2 / 1 / 330	Class 3 Class 2.5	Cross-bedded	On completion of testing both crumbs had disintegration
18.0 / 1 / 85	Class 4 Class 3.5	Aquifer	On entering the water filled beakers both crumbs disintegrated. A colloid cloud could clearly be seen in both cases
18.8 / 1 / 85	Class 4 Class 3	Below Aquitard	In both cases the sides of the crumb have slaked off, with one of the samples forming a prominent slurry across the bottom of the beaker (Class 4)

Table 4.10 Emerson Crumb test results for the samples used for pinhole testing.

4.7.2 Erodibility Using the Pinhole Test

a) Introduction

Erodibility testing using the pinhole apparatus was conducted on a number of the soils collected from the stratigraphic units during field investigations to assess the potential for piping failure to occur. The main concern of this study was on the aquifer and cross-bedded sequence, as it is believed that piping failure within these units was the triggering mechanism producing landsliding seen at properties such as 85 Te Hono Street. The Palaeosol from field evidence and laboratory testing demonstrated relatively strong characteristics, therefore it was to be believed to be a non-erodible soil. This would in turn suggest that soakage water slowly permeating through this unit will not scour or erode the soil significantly. Conversely, the cross-bedded section of the Upper Matua Subgroup and associated aquifer showed evidence during the field investigation stage of an erosive nature. This was seen in the failure zone where seepage water exiting out of the aquifer carried a large quantity of material with it down the slope. If these soils were indeed erosive then the piping failure mechanism suggested in Chapter 2 would become more viable. The methodology and data obtained are presented in Appendix A4.7.

b) Results and Discussion

Only one sample of the Post-Rotoehu Ash Tephra was collected during field investigations. Because the main emphasis of testing was not on this unit more samples were not needed. The sample tested consisted of COARSE SAND with some fine pebbles. From Table 4.8 the Post-Rotoehu Tephra is shown to be non-erosive with a erosional class of NE1 or $E_{>1000}$. This low erosional class would not be suggested by the pumiceous coarse grained nature of the soil. One possible explanation for this is that soils with low clay and silt content will allow water to flow freely through them with limited disturbance to the soil matrix when partially confined. Another possibility is that of point to point bonding of the pumice fragments resulting in a stronger soil matrix.

The Palaeosol from particle size analysis has a high clay and silt content (30% sand, 30% silt, 40% clay) content and therefore a low permeability. Pinhole testing produced an erosional class of NE1 or $E_{>1000}$, indicating the soil is non-erodiable.

Table 4.11 Erosional classes determined from pinhole samples tested

EROSIONAL CLASSES FOR PINHOLE SAMPLES TESTED			
Sample	Position within Stratigraphy	Erosional Classes	
		Modified BS	Yetton & Bell (1992)
0.4/1/330	Post-Rotoehu Ash Tephras	NE1	$E_{>1000}$
3.1/1/330	Palaeosol	NE1	$E_{>1000}$
9.8/1/1330	Cross-bedded section of the Upper Matua Subgroup	E1	E_{50}
10.0/1/330	Cross-bedded section of the Upper Matua Subgroup	N/A due to pinhole closure	N/A due to pinhole closure
14.0/1/330	Cross-bedded section of the Upper Matua Subgroup	N/A due to pinhole closure	N/A due to pinhole closure
14.2/1/330	Cross-bedded section of the Upper Matua Subgroup	E1	E_{50}
18.0/1/85	Aquifer located within the Upper Matua Subgroup	E1	E_{50}
18.8/1/85	Upper Matua Subgroup	E2	$E_{180\text{-}50}$

The Cross-bedded section of the Upper Matua Subgroup consists of long wave length fluvially deposited cross-beds, and therefore shows variability in the soil matrix and overall fluvial structures throughout the sequence. The samples (Cross-bedded sequence) used for pinhole testing exhibit a similar grainsize distribution as the Cross-bedded samples from particle size analysis (40% sand, 40% silt, and 20% clay). On testing, samples 9.8/1/330 and 14.2/1/330 from the cross-bedded sequence produced an erosion class of E1 (E_{50}), indicating that they were highly erosive. This was demonstrate by looking at the sample after testing where a large blow out of material had occurred (Figure 4.12). This indicated that a piping failure occurring within the lower section of the cross-bedded sequence was possible.

The other two cross-bedded samples, 10.0/1/330 and 14.0/1/330 (Appendix A4.7), showed a low flow rate exiting the sample. On opening up the sample it was found that the pinhole had closed up either in part or the entire length of the sample. Sample 10.0/1/330 was re-drilled twice but closure of the pinhole stilled occurred. This was not believed to be an indication of the clay fraction swelling, but more so the soil matrix recompacting or moving, blocking the water's flow path through the pinhole. Sample 14.0/1/330 was run for the full 40 minutes to a head of 1000 mm with no appreciable flow rate increase. Because of this the erodibility of the soil cannot be tested due to pinhole closure.

The aquifer located within the Upper Matua Subgroup (18.0/1/85) produced a high erosional class of E1 (E_{50}). This was not unexpected due to field evidence of seepage water exiting from the failure zone containing a high proportion of particles. In addition to this, if the flow rate of the seepage water is high enough through the aquifer unit this will limit the effect of intra-particle bonding, with the clay and silt fraction being transported by the flow of water through this unit.

Sample 18.8/1/85 (situated at the bottom of the lower bounding aquitard) consists of a clayey SILT which belongs to a sequence of airfall deposits situated directly below the lower bounding aquitard. Pinhole testing indicate that the sample was moderately erodible, giving an erosion classification of E2 (E_{180-50}). From field evidence no seepage water was seen exiting below the lower bounding aquitard, therefore indicating that the seepage water was confined to the aquifer and cross-bedded sequence. This suggests that as no hydraulic head would act on these units below the lower bounding aquitard, the blowouts that are possible in the cross-bedded and aquifer soils will not occur.

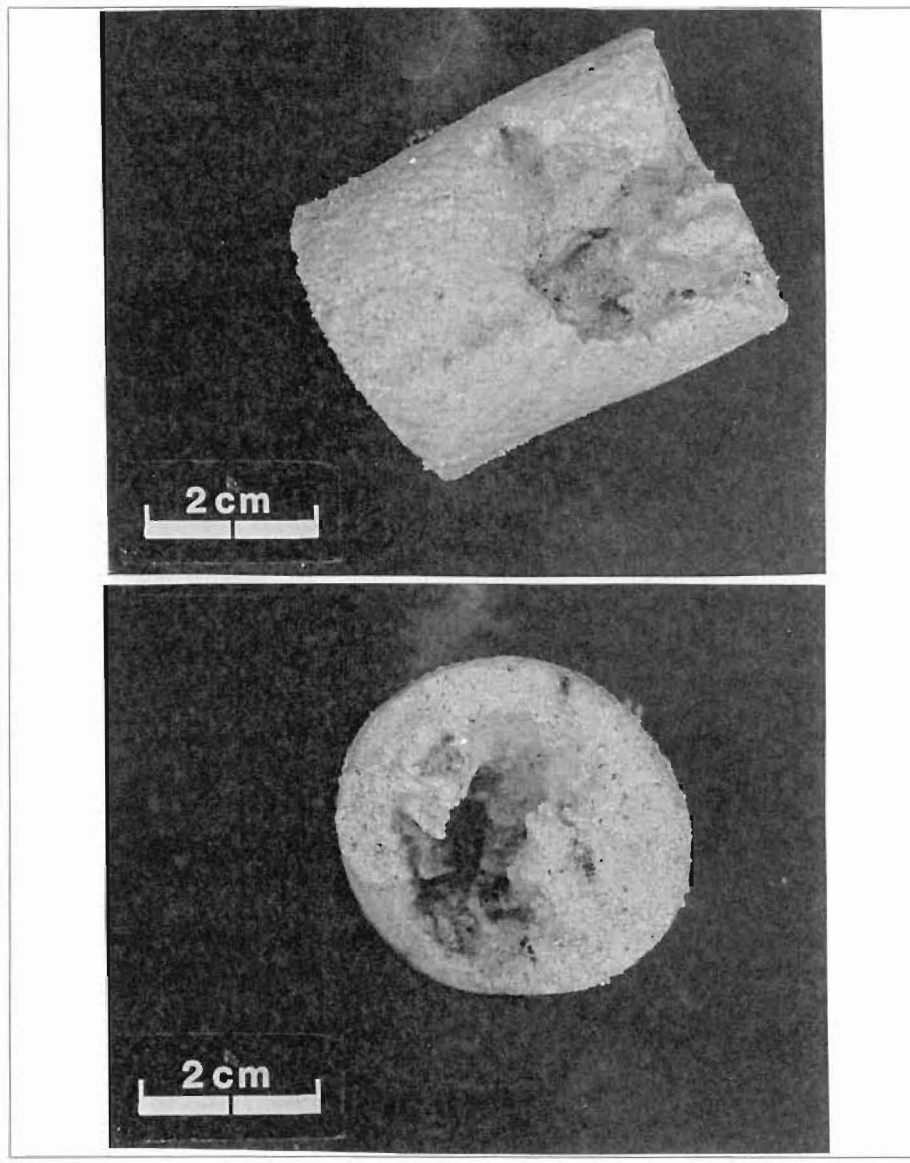

Figure 4.12 Photograph taken of a blowout in sample 14.2/1/330 leaving a large chamber at the end of the sample.

4.6.3 Summary

From erosion and dispersion testing it can be seen that the Palaeosol is a non-erodiable and non-dispersive soil, and this is also true for the most part for the Post-Rotoehu Ash Tephras and Hamilton Ashes. Pinhole testing was not conducted on the Rotoehu Ash due to difficulties in sampling, making it hard to determine its potential erodibility because the unit consists of numerous shower bedded airfall deposits which vary in size from 10 mm

to 20-30 cm. It is believed that overall the Rotoehu Ash will be generally non-erodible, with a suggested erosion class of NE3.

Field evidence from properties such as 85 Te Hono Street indicate the the triggering mechanism for landsliding was that of a piping failure within the aquifer and lower section of the Cross-bedded sequence, therefore suggesting high pore water prior to failure. In order for a piping failure to occur the soils associated with aquifer and lower section of the cross-bedded sequence must exhibit erosive properties. From laboratory testing the aquifer and Cross-bedded units have demonstrated to be both highly erosive and dispersive lending credence to a piping failure scenario out line above.

4.8 PERMEABILITY

4.8.1 Introduction

Permeability testing was conducted in order to obtain a range of permeabilities for the in-situ soil units within the logged failure scarps. Falling head permeability tests were carried out on in-situ (Post-Rotoehu Ash Tephras, Rotoehu Ash, Pahoia Tephras, Cross-bedded sequence, Aquifer, and lower bounding aquitard), and remoulded samples (Palaeosol, and Hamilton Ash), using the method described in Appendix A4.8. To ensure complete saturation of the samples they were left submerged in their permeability cells for 3 to 7 days prior to testing. All tests were conducted according to Wykeham Farrance and Department of Civil Engineering-University of Canterbury guidelines. It is assumed that the vertical permeability (k_V) for the various samples has been tested. Due to the numerous horizontal beds associated with each stratigraphic unit k_V will not be equal to the horizontal permeability (k_H).

4.8.2 Results

All results are present in Appendix A4.8, with a summary table below (Table 4.12). Results and discussions for each unit have been separated out and appear below.

Table 4.12 Falling head permeability results for the various soils tested.

Falling Head Permeability Results	
Sample	Permeability
3.2-3.4 / 1 / 89 Post Rotoehu Ash Tephras	$3.5x10^{-6}$
2.55-2.75 / 1 / 330 Rotoehu Ash	$3.1x10^{-4}$
4.3 - 4.5 / 1 / 85 Rotoehu Ash	$7.5x10^{-7}$
3.1 / 1 / 330 Palaeosol 15 blows	$9.2x10^{-7}$
3.1 / 1 / 330 Palaeosol 27 blows	$1.7x10^{-8}$
3.1 / 1 / 330 Palaeosol 40 blows	$1.4x10^{-10}$
8.2 / 1 / 85 Hamilton Ash 15 blows	$4.6x10^{-6}$
8.2 / 1 / 85 Hamilton Ash 27 blows	$3.3x10^{-8}$
8.2 / 1 / 85 Hamilton Ash 40 blows	$5.8x10^{-7}$
10.3-10.5 / 1 / 330 Pahoia Tephras	$6.1x10^{-8}$
16 / 1 / 85 Cross-bedded sequence	$7.6x10^{-8}$
13 - Sandy unit situated between cross-bedded sequence and upper aquitard	$3.1x10^{-7}$
17.1 / 1 / 330 Located within the aquiferial zone	$3.4x10^{-6}$
Sample 12 Located within the aquitard bounding the lower section of the failure zone	$4.9x10^{-9}$

a) Post-Rotoehu Ash Tephras

The Post-Rotoehu Ash Tephras consist of a number of different shower bedded units which vary in grainsize from coarse sands to sandy silts. Because these beds were only approximately 80mm in thickness, sampling them using an in-situ sampling tube for permeability meant that part of two beds were collected. The in-situ sample tested comprised two roughly equal sections: 1) slightly weathered; moist; soft; light yellowish brown; moderately well graded; silty FINE SAND with some very coarse sand to clay. 2) slightly weathered; moist; loose; light yellowish brown with some black grains; extremely

well graded; MEDIUM - COARSE SAND with some fine pebbles to clay. These two beds produced an average permeability of 3.5×10^{-6} m/s, equating to a permeability classification of poor, (Table 4.13).

b) Rotoehu Ash

The Rotoehu Ash constitutes one of the more permeable sequences which consist of a number of shower bedded deposits. Like other sections of the cliff face the Rotoehu Ash has a wide range of grainsizes from very thin beds of clay (5mm thick) to more coarser beds of coarse sand (150-200mm thick). This fact is reflected in permeabilities obtained during lab testing. Sample 2.55-2.75/1/330 consisted of a FINE MEDIUM SAND with some coarse sand and produced a permeability of 3.1×10^{-4} m/s (Table 4.13). Conversely, sample 4.3-4.5/1/85 which consisted of a SILT produced a permeability of 7.5×10^{-7} m/s (Table 4.12). Therefore the Rotoehu Ash can be classified as containing beds that are of medium to poor permeabilities (Table 4.13).

c) Palaeosol

The compact nature of the Palaeosol made it difficult to obtain an in-situ sample, therefore permeability testing was conducted on three remoulded samples at varying blow counts (Appendix A4.8). From particle size analysis the Palaeosol is suggested to consist of 40% clay, 40% silt, and 20% sand. Table 4.12 demonstrates that as the density increases with a increasing blow count the permeability decreases. Permeabilities of 9.2×10^{-7}, 1.17×10^{-8}, 1.4×10^{-10} m/s were produced for blow counts of 15, 27, and 40 respectively. Therefore with a range in permeabilities form 10^{-7} to 10^{-10} m/sec, the unit can be classified as being poor to practically impervious (Table 4.13).

Table 4.13 Permeability and Drainage Characteristics of Main Soil Types (ELE International)

Coefficient of Permeability m/s

K=1 10^{-1} 10^{-2} 10^{-3} 10^{-4} 10^{-5} 10^{-6} 10^{-7} 10^{-8} 10^{-9} 10^{-10} 10^{-11} 10^{-12}

Drainage Characteristics	Good			Poor	Practically Impervious	
Permeability Classification	High	Medium	Poor	Very Low	Practically Impervious	
General Soil Type	Gravels	Clean Sands	Fissured & Weathered Calys		Intact Clays	
			Very Fine or Silty Sands			
Test Method – Direct	Constant Head		Falling Head			
Test Method – Indirect		Computation From PSD			From Consolidation Data	

PSD = Particle Size Distribution

d) Hamilton Ash

As with the Palaeosol it proved difficult to obtain an in-situ sample for the Hamilton Ash, and so permeability testing was carried out on three remoulded samples at blow counts of 15, 27, and 40. Like the Palaeosol the Hamilton Ash has a high silt and clay content, consisting of 36% clay, 34% silt, and 30% sand, producing permeabilities of 4.6×10^{-6}, 3.3×10^{-8}, and 5.8×10^{-7} m/s for blow counts of 15, 27, and 40 respectively. This indicates the soil has a permeability classification of poor to very low (Table 4.12).

e) Pahoia Tephras

The Pahoia Tephra is an airfall deposit and as such encompasses an extremely wide range of grainsizes from clay to coarse pebbles of rhyolite and pumice, which are randomly distributed throughout the soil matrix. In addition to this lithogically the unit varies from area to area, with some sections comprised of large cobbles of pumice which have essentially constitute cemented areas, and other sections comprising wholly of sand

(Figure 3.5). Also evident is the high content of bioturbation (rootlets) which can be more prevalent in some areas than others. Because of these facts it is extremely difficult to sample and any in-situ samples collected for laboratory permeability testing conducted will only represent one possible permeability value for this unit. The in-situ sample for laboratory testing comprised one of the cemented sections consisting of a silty CLAY, and producing a permeability of 6.1×10^{-8} m/s. This indicates that the unit practically impervious (Table 4.13). It is likely that the more sandy samples will produce permeabilities in the order of 10^{-4} to 10^{-6} m/sec depending on the percentage of silts and fine sands. Other sample were not able to be collected due to lack of sample tubes, and bulk samples tended to fall apart.

f) Cross-bedded Sequence

From grainsize analysis the Cross-bedded sequence consists of approximately 40% sand, 40% silt, and 20% clay. Samples 16/1/85 is situated within the cross-bedded sequence, while sample 13 is situated between the cross-bed section and the upper bounding aquitard in a soil with a similar grainsize distribution to 16/1/85. The reasonably high silt and clay contents produced low permeabilities of 7.6×10^{-8} and 3.1×10^{-7} m/s for 16 /1 / 85 and sample 13 respectively (Table 4.12), indicating a poor to very low permeability classification.

g) Aquifer

Sample 17.1/1/330 is located within the aquifer zone and consists of a high percentage of sand, approximately 78 % compared to 22 % silt plus clay (Table 4.2). However, it has already been suggested that clay and silt contents with the aquifer may be as high as 10-15% and 20% respectively. From testing a permeability of 3.4×10^{-6} m/s was obtained, indicating the soil has a permeability classification of poor (Table 4.13).

h) Lower Bounding Aquitard

Sample 12 consists of a sequence of shower-bedded deposits with high clay-silt contents (e.g. 18.075 / 1 / 85 - 18.23 / 1 / 85, Table 4.1) which together form the lower bounding aquitard to the aquifer delineated in chapter 2. A permeability of 4.9×10^{-9} m/s indicates the sequence has a permeability classification of very low to practically impervious (Table 4.13).

4.8.3 Discussions

a) Post-Rotoehu Ash Tephras

Other beds within the Post-Rotoehu Ash Tephras consist of silty SAND, sandy SILTS with clay and without, which will all produce differing permeabilities. All these differing beds make it impossible to collect samples for each one so only a suggested permeability range can be given. Because of this and the large distribution of grainsizes associated with the tephras, vertical permeabilities (k_V) within the Post-Rotoehu Ash Tephras are suggested to range from 10^{-4} to 10^{-7} m/s. An important aspect to be considered is the influence of heavy bioturbation (e.g. rootlet) present within the unit. This will provide high permeability flow paths through which the infiltrating water will move, therefore a bed that would normally have a permeability of 10^{-7} m/sec will be increased due to the influence by rootlets structures possibly to 10^{-5} m/sec.

b) Rotoehu Ash

The Rotoehu Ash consisting of numerous shower bedded deposits will exhibit a range of permeabilities not too dissimilar to the results produced during lab testing i.e.. 10^{-3}-10^{-7} m/s. It is believed that most of the soakholes around the Maungatapu Peninsula drain into this sequence of beds, and from lab and field evidence the Rotoehu Ash consists of a number of medium permeability beds that will provide adequate drainage. However. there is little evidence of seepage water exiting the cliff face at properties such as 85 Te Hono

Street from the Rotoehu Ash unit. This suggests the soakage water is permeating further through the stratigraphic sequence than the Rotoehu Ash.

c) Palaeosol

From the permeability results the Palaeosol in conjunction with the Hamilton Ash is believed to represent an effective barrier to rapid soakage infiltration without taking into account shrinkage cracks, fractures, exfoliation defects, or soakhole penetration. Field evidence relating to the strength and compact nature of the Palaeosol indicates that these low permeabilities values are likely. However, the test results must consider the fact that the permeability of a remoulded sample tends to be greater than an in-situ sample because the effect of bioturbation (rootlets) has not been introduced. It is difficult to assess the effect that structures such as shrinkage cracks and rootlets have on the permeability, so it is suggested that a permeability of 10^{-8} m/sec should be used to represent the Palaeosol, indicating a very low permeability classification. In chapter 3 it has been suggested that many of the soakholes do not penetrate this unit, but instead drain into the Rotoehu Ash therefore possibly limiting the affect that the soakage water has on the underlying Upper Matua Subgroup sediments.

d) Hamilton Ash

The same factors outlined for the Palaeosol also apply to the Hamilton Ash, therefore a suggested permeability of 10^{-7} m/s can be used to represent the unit, resulting in a permeability classification of poor to very low (Table 4.13). This

e) Pahoia Tephras

The low Permeability of 6.1×10^{-8} m/sec more than likely reflects the lower end of the permeability scale for this unit due to extreme variability in both grainsize and structure. Barnes (1995) suggests that clean sand-gravel mixtures can exhibit permeabilities that

range between 10^{-2} and 10^{-5} m/sec, and very fine sands, silty sands, silts, and stratified clay/silt deposits can have permeabilities that range between 10^{-5} and 10^{-8} m/sec. The Pahoia Tephras from field investigations show a wide range of grainsizes from coarse pebbles to clays with the main consitutent particle size being that of a MEDIUM-COARSE SAND. Due to this the permeability of 10^{-8} m/s has been used as a lower boundary, and a range of permeabilities from 10^{-4}-10^{-8} m/s would be more likely.

f) Cross-Bedded Sequence

The low permeabilities (3.4×10^{-7} and 7.6×10^{-8} m/sec) obtained from testing were not unexpected when viewing the grainsize distribution data (Table 4.1). Permeabilities collected during falling head field permeability testing (8.3×10^{-6}-6.6×10^{-7} m/s) compare favourably to the permeability produced by the laboratory testing. However, field evidence suggests that seepage does occur in the lower parts of this unit just above the upper bounding aquitard. The seepage is not as prevalent as that associated with the aquifer but strong enough to move particles away from the cliff face.

g) Aquifer

ELE international and Fetter (1994) suggest that silty sand like sample 17.1/1/330 can produce low permeabilities such as obtained (3.4×10^{-6} m/sec). This indicates that the permeability of the aquifer is not as high as what was expect when conducting the field investigation portion of this project. From particle size analysis it is suggested that the aquifer does contain a higher percentage of clay and silts than indicated, therefore reducing the permeability. Taking these facts and those outlined in Section 4.8.2 (g), a permeability range from 10^{-4} to 10^{-6} m/sec is likely for the aquifer.

h) Lower Bounding Aquitard

This series of beds below the aquifer (Lower bounding aquitard), and a similar but smaller series situated above (Upper bounding aquitard), semi-confine the aquifer. The lower bounding aquitard produced a permeability of 4.9×10^{-9} m/sec indicaing that it provides an impervious barrier against the infiltration of soakage water through into the stratigraphic units below the aquifer. It is also suggested that the Upper bounding aquitard will exhibit a similar permeability. However, during field investigation stage of this project, seepage water was seen exiting from the lower section of the Cross-bedded sequence indicating that there is partially hydraulic connection through the Upper bounding aquitard.

i) Comparison with Bird's Permeability Data

Bird (1981) conducted a number of constant head permeability tests throughout the sequence to the clay marker bed (which is probably related to the lower bounding aquitard). Permeabilities obtained ranged from 1.5×10^{-3} m/s for the orange sandy ash (Post-Rotoehu Ash Tephras) to 3.5×10^{-8} m/s (Table 4.14). The Red Palaeosol delineated by Bird (1981), which is equivalent to the Palaeosol in this study, produced a permeability of 2.7×10^{-5} m/s (Table 4.14). This permeability is considerably higher than the permeabilities of 9.2×10^{-7}-1.4×10^{-10} m/s obtained from laboratory testing during this study (Table 4.12).

Bird's tests were performed using a constant head apparatus which is mainly used for sandy soils. It is difficult to believe with knowledge of the compact nature, and high silt and clay contents of the soils such as the Palaeosol, how such constant head tests were performed. In addition to this it would be virtually impossible to avoid the clogging up of the constant head outlets tubes by the clay and silt fraction associated with many of these soils.

Table 4.15 Hydraulic conductivity results produced by Bird (1981).

Sample	Depth (m.b.d.)	No. of Tests	Bird's Results, k (m/s)	Thesis Results, k (m/s)
Loose orange sandy ash		7	$1.5x10^{-4}$	$3.5x10^{-6}$
Rotoehu ash palaeosol		6	$4.1x10^{-5}$	$3.1x10^{-4}$ $7.5x10^{-7}$
Red palaeosol	4.1	3	$2.7x10^{-5}$	10^{-8}
Orange mottled tuff	5	17	$6.6x10^{-6}$	10^{-7}
Brown mottled tuff	7	20	$1.9x10^{-5}$	N/A
Yellow brown sand	8.2	5	$1.2x10^{-6}$	N/A
Yellow brown sand	9.2	9	$3.8x10^{-7}$	N/A
White silty sand	9.8	22	$2.1x10^{-7}$	$7.6x10^{-8}$
Clay marker bed	10.2	11	$3.5x10^{-8}$	$4.9x10^{-9}$

j) Stratigraphic Permeability Model and Implications

Table 4.16 presents a stratigraphic permeability model for the units upwards from the Lower bounding aquitard. From Table 4.16 it can be seen that the overall vertical permeabilities (k_V) for the soils are not that high, indicating that it will take considerable time for an element of water to permeate from the ground surface to the aquifer. For example, this time can be calculated by the use of equation 4.1. For an element of water to permeate the Hamilton Ash with a permeability of 10^{-7} m/sec, and a thickness of 3m, will take approximately a year (3m/(10^{-7} m/sec×60×60×24)=347days.

$$\text{Time taken to permeate a unit} = \frac{\text{Thickness of that unit}}{\text{Permeability in m/sec} \times \underbrace{60 \times 60 \times 24}_{\text{To convert to minutes, hours, days}}} \qquad \text{Equation 4.1}$$

Therefore for the element to flow through just the Hamilton Ash will take an extremely long time. When these times are calculated for permeabilities from Table 4.15 they do not compare to the lag times of 24-96 hours discussed in Chapter 3. Because of this it can be concluded that other mechanism apart from just infiltration of water through the soil profile must be occurred in the soil mass to produce these fast lag times. In Chapter 3 it was suggested that high permeability flow structures such as exfoliation defects, fractures, and heavy bioturbation (rootlets), (defect controlled permeability model), and head response permeability model may produce these fast lag times of 24-96 hours. These concept is discussed further in Chapter 5.

4.11 GEOTECHNICAL MODEL

The objective of this chapter was to provide a geotechnical characterisation of the various soils associated with the logged cliff faces. Presented in Table 4.15 is a summary of the laboratory results in addition to some results from Bird (1981). In most cases the statistical accuracy of the laboratory test data is limited to the number of samples tested, the greater the number the greater the accuracy. However, due to the numerous beds identified in the logged cliff faces it was not possible to collect samples for all of these beds. Because of this laboratory testing concentrated on six main units, the Palaeosol and associated Hamilton Ash, the cross-bedded sequence, the upper and lower aquitards, and the aquifer. The other units such as the Post-Rotoehu Ash Tephras, Rotoehu Ash and Pahoia Tephras were only partly tested.

a) Post-Rotoehu Ash Tephras

Clay mineralogy assessment was not conducted, but this result of other stratigraphic units suggest that the halloysite and allophane present in these soils will be present within the Post-Rotoehu Ash Tephras. The Post-Rotoehu Ash Tephras demonstrated a range of direct shear strengths from 0-94 kPa, (Table 4.15). It is believed that the soil strengths will tend to lie towards the upper end of the range denoted by laboratory testing. Bird (1981) tested

one of the more sandy units within the Post-Rotoehu Ash Tephras, obtaining cohesion values of 0 and 1 kPa in addition to friction angles of 41.6° and 40° respectively (Table 4.15). Pinhole and Emerson crumb tests were performed to ascertain the erodibility and dispersion characteristics. The sample tested produce an erosion class of NE1 ($E_{>1000}$), indicating a non-erosive soil and a class 1 dispersion classification denoting a non-dispersive soil. Permeability testing yielded a hydraulic conductivity of 3.5×10^{-6} m/s (Table 4.15). Bird (1981) on the other hand produced a permeability for a more sandy ash within the sequence of 1.5×10^{-4} m/s. It is suggested from permeability testing that hydraulic conductivities will tend to range between 10^{-4}-10^{-7} m/s.

b) Rotoehu Ash

Particle size analysis was conducted on the more sandy sample used for permeability testing, which contained 96% sand, 3% mud, and the remaining 1% pebble and granular material. The lack of time made it difficult to conduct particle size analysis on the silty specimen. Clay mineralogy is interpreted as having the same composition as other soils throughout the stratigraphy, consisting of halloysite and allophanes. The Rotoehu Ash demonstrated low cohesion values and high friction angles, indicating strengths similar to those of the Post-Rotoehu Ash Tephras (Table 4.15). Erodibility, Atterbergs Limits and triaxial testing was not performed due to the difficulty in sampling the numerous beds present within the Rotoehu Ash. It is however believed the more sandy beds will tend to be more erodible than the more silty ones. Dispersion testing was conducted on one of these silty beds producing a dispersion classification of class 1.5 (Table 4.15). This confirm that these beds will be relatively non-erodible. However, more testing would have to be conducted to prove these assumptions correct. Permeability testing yielded hydraulic conductivities of 3.1×10^{-4} and 7.5×10^{-7} m/s for a the sandy (Table 4.10) and silty samples respectively (Table 4.15). These values compare favourably with those obtained by Bird (1981).

c) Palaeosol

The Palaeosol is associated with the Hamilton Ash and is predicted to form an aquitard separating the younger ashes from the underlying Upper Matua Subgroup sediments. From particle size analysis it is likely to have a grainsize distribution of 20% sand, 40% silt, and 40% clay. Clay mineralogy indicated that mixed layer 7 & 10 Å Halloysite, quartz, Oligoclase feldspar, and Allophanes were present. From Atterberg Limit testing a high plasticity and a normal activity was produced. The high plasticity will be the product of the allophanes within the soil more so than the halloysite. From Bird (1981) direct shear data a cohesion of 5.6 kPa and a friction angle of 31° was produced (Table 4.15). This indicates that the unit has a relatively high cohesion as well as friction angle, resulting in a soil that is resistant to sliding. Shear strengths obtained from triaxial testing, which ranged between 25.5-80 kPa, are considerably lower than shear vane values collected in the field of 150-200 kPa (Chapter 3). This suggests that shear strengths will probably lie between these two ranges. Overall the strengths indicate the Palaeosol is one of the strongest units within the cliff face. Pinhole and Emerson Crumb testing determined a erodibility classification of NE1 ($E_{>1000}$) and a dispersion classification of class 1, therefore defining the soil as being non-erosive and non-dispersive. Permeabilities obtained from recompacted samples at blow counts of 15, 27, and 40 produced hydraulic conductivities of 9.2×10^{-7}, 1.7×10^{-8}, and 1.4×10^{-10} m/s (Table 4.17). It has been suggested that an average permeability of 10^{-8} m/s would best represent the in-situ soil conditions. Bird (1981) produced a hydraulic conductivity of 2.7×10^{-5} m/s using a constant head setup. Knowledge of the high silt and clay content and the compact nature of the unit would have made it virtually impossible to conduct constant head tests, and because of this it is difficult to accept Bird's hydraulic conductivity value.

d) Hamilton Ash

Particle size analysis indicated the Hamilton Ash consisted of approximately 30% sand, 34% silt, and 36% clay. The Hamilton Ash produced a similar clay mineralogy to that of the Palaeosol consisting of mixed layer 7 & 10 Å Halloysite, quartz, Oligoclase Feldspar,

and Allophanes. Atterberg limit testing indicated a high liquid limit, producing an extremely high plasticity in addition to an active activity. These characteristics are similar to those activities of montmorillonite and organic clays (Barnes, 1995). This behaviour was not considered to be the result of the more inactive halloysite but the presence of allophanes in the soil. The Hamilton Ash exhibits similar cohesion and friction angles as the Palaeosol, so therefore it is considered to have similar shear strength values (Table 4.15). Erodibility and dispersion tests were not performed but classifications are suggested to be similar to those exhibited by the Palaeosol, i.e. erodibility = E1-E2 and dispersion = class 1. Permeability testing, as for the Palaeosol, involved the recompaction of samples at blow counts of 15, 27, and 40. These densities yielded hydraulic conductivities of 4.6×10^{-6}, 3.3×10^{-8}, and 5.8×10^{-7} m/s respectively, with a representative soil permeability of 10^{-7} m/s. Bird (1981) produced a permeability of 6.6×10^{-6} m/s which compares relatively favourably to the laboratory data. An additional permeability value of 1.9×10^{-5} m/s was denoted by Bird further down in the sequence, which could represent one of the more sandy section of the Hamilton Ash.

e) Pahoia Tephras

The Pahoia Tephras received limited test, with the main concentration involving permeability testing. Like many of the other units the Pahoia Tephra varies considerably both laterally and vertically in grainsize and structure (Figure 4.13), making it extremely difficult to sample. Clay mineralogy will consist of halloysite and allophanes much the same as other units. Shear strengths ranged from 6-67 kPa (Table 4.15), but it is believed that values as high as seen in the Hamilton Ash are possible in some areas. This could possibly represent a range from 6 to approximately 100 kPa, which is still in keeping with what is seen during field investigations. Permeability testing produced a hydraulic conductivity of 6.1×10^{-8} m/s, which most probably lies towards the lower end of the scale. Bird (1981) produced permeabilities in the order of 1.2×10^{-6} and 3.8×10^{-7} m/s. These two permeabilities would also be representative of the Pahoia Tephra.

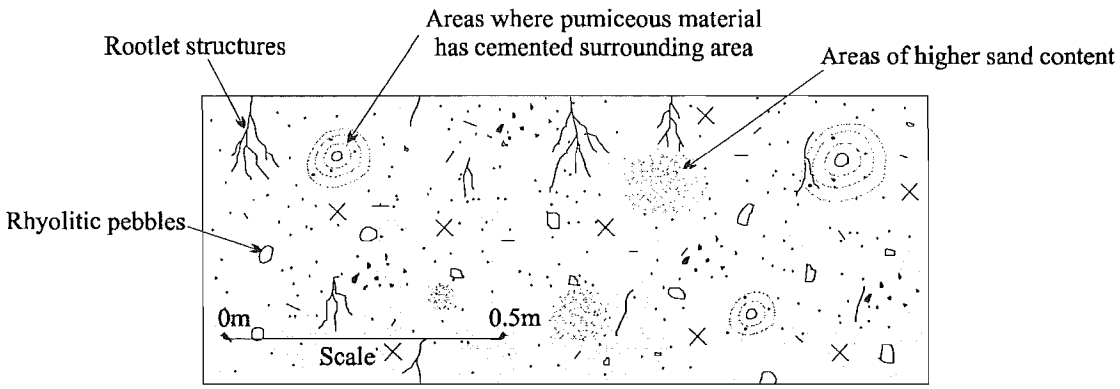

Figure 4.13 Section through the Pahoia Tephra indicating both lateral and vertical variation within the soil matrix.

f) Cross-bedded Sequence

Particle size distribution demonstrates a high percentage of silt and clay equating to approximately 55-65% of the volume (Table 4.1). Clay mineralogy testing found both halloysite and allophanes were detectable in the soils. Atterberg limits show the unit as being of an intermediate plasticity and of normal activity (Barnes, 1995). The cross-bedded section of the Upper Matua Subgroup yielded cohesions which ranged from 0-17.15 kPa and friction angles from 30-43.3° (Table 4.17). This indicates the sequence is quite resistant to sliding. Shear strengths ranged from 11.5-34.5 kPa (Table 4.15), defining a soft to very soft strength classification (Table 4.3). Overall the cross-bedded sequence is suggested to have a soft strength classification. Erodibility and dispersion testing found the unit to be highly erodiable producing an erosion classification of E1 (E_{50}) and a moderate to highly dispersive resulting in a dispersion classification of class 2.5-4. Because of the high clay and silt contents, low permeabilities were produced ranging from 3.1×10^{-7} to 7.6×10^{-8} m/s (Table 4.15). Bird (1981) also found similar permeability values of 2.1×10^{-7} m/s.

g) Aquifer

From particle size analysis the aquifer consists of approximately 78% sand, 17% silt, and 55 clay. It is however suggested that the clay and silt fractions may be higher (Section 4.2). The aquifer as expected has no cohesion and a friction angle of 35°, and shear strengths range between 23-31 kPa (Table 4.15). This compares favourably to shear vane strengths obtained in the field which range approximately between 20-50 kPa (Chapter 3). Pinhole and Emerson Crumb testing demonstrated the aquifer to be highly erosive with a classification of E1 (E_{50}), and highly dispersive with classification of class 3-4. Permeability testing produced a hydraulic conductivity of 3.4×10^{-6} m/s (Table 4.15), equating to a unit that provided good-poor drainage characteristics, and a poor permeability classification.

h) Upper and Lower Bounding Aquitards

Atterberg limits produced some abnormal results with samples which were thought to be moderately plastic in the field due to high silt and clay content, but which in fact demonstrated low plasticities (Table 4.15). The most likely conclusion is that the allophanes in the soils are producing the results, as suggested by Lewis (Pers. Comn., 1997). The upper and lower aquitard comprise beds of similar compositions, and therefore are considered to have the same properties. Direct shear results compare favourably to those of Bird's (1981) with cohesion values of 19 and 24 kPa, and friction angles of 18° and 22° respectively (Table 4.15). This would suggest that the aquitards are reasonably resistant to shearing. Shear strengths range between 12-34 kPa indicate a soft to very soft strength (Table 4.3). This compares reasonably well to assessed strength in the field. The high silt-clay content associated with these soils yielded a low permeability of 4.9×10^{-9} m/s (Table 4.15). This compares to the permeability obtained by Bird (1981) of 3.5×10^{-8} m/s. Therefore it can be concluded from this that the lower aquitard is practically impervious.

Depth Below Surface	Stratigraphic Position		Direct Shear c'=kPa ϕ=degrees	Unconsolidated Undrained Triaxial Peak Shear Strengths (kPa)	Atterberg Limits (LL and PP) Plasticity (PI) and Activities (A)	Clay Mineralogy	Erodibility Pinhole Test	Dispersion Emerson Crumb Test	Permeability, k (m/s)
0 m	Post-Rotoehu Ash Tephras		Shear Strength Range 0-94 kPa c'=0 ϕ=41.6° c'=1 ϕ=40.0°				NE1 ($E_{>1000}$)	Class 1	$3.5x10^{-6}$ $1.5x10^{-4}$
	Rotoehu Ash		c'=0.2 ϕ=41.6° c'=0.3 ϕ=37°						$3.1x10^{-4}$ $7.5x10^{-7}$ $4.1x10^{-5}$
	Palaeosol		c'=5.6 ϕ=31°	Range 25.5-80.0	LL=67, PP=30, PI=37, A=0.97	Halloysite, Allophanes	NE1 ($E_{>1000}$)	Class 1.5	$9.2x10^{-7}$, $1.7x10^{-8}$, $1.4x10^{-10}$
5 m	Hamilton Ash		c'=8.7 ϕ=32° c'=6.1 ϕ=33°		LL=103, PP=35, PI=68, A=1.87	Halloysite, Allophanes		Class 1	$6.6x10^{-6}$ $4.6x10^{-6}$ (15 blows) $3.3x10^{-8}$ (27 blows) $5.8x10^{-7}$ (40 blows) $1.9x10^{-5}$
10 m	Pahoia Tephra		Shear Strength Range 6-67 kPa						$6.1x10^{-8}$ $1.2x10^{-6}$ $3.8x10^{-7}$
15 m	Cross-bedded Sequence		c'=0 ϕ=36° c'=17.5 ϕ=30° c'=3 ϕ=37° c'=0 ϕ=43.3° c'=0 ϕ=42°	11.5-20.5 20.5-34.5 20.5-23.0	LL=46, PP=30, PI=16, A=0.79	Halloysite, Allophanes	E1 (E_{50})	Class 2.5-4	$2.1x10^{-7}$ $7.6x10^{-8}$ $3.1x10^{-7}$
	Upper Bounding Aquitard			18.5-34.0					
	Aquifer		c'=0 ϕ=35°	23.0-31.0		Halloysite, Allophanes	E1 (E_{50})	Class 3.5-4	$3.4x10^{-6}$
	Lower Bounding Aquitard		c'=19 ϕ=18° c'=24 ϕ=22°	12.0-28.0	LL=36, PP=30, PI=6, A=0.09 LL=42, PP=35, PI=7, A=0.13 LL=51, PP=40, PI=11, A=0.31 LL=102, PP=53, PI=49, A=5.24 LL=51, PP=35, PI=16, A=0.4	Halloysite, Allophanes	E2 ($E_{50\text{-}180}$)	Class 3-4	$4.9x10^{-9}$ $3.5x10^{-8}$

■ Laboratory Results

■ Bird's Data

Table 4.15 Summary of laboratory results in addition to data produced by Bird (1981).

4.12 SYNTHESIS

Particle size analysis indicated that along with a varied grainsize distribution many of the stratigraphic units contained beds with high silt and clay contents. Clay mineralogy testing on these clay fractions revealed the present of Allophanes and mixed layer 7 & 10 Å Halloysite. The Allophanes within the stratigraphic units produce tended to produce abnormal results which were especially noted in the samples from the lower bounding aquitard, where an increase in clay content saw a decrease in plasticity. From results obtained during direct shear testing cohesions tended to be reasonably varying from 0-19 kPa. Conversely the friction angles produced were very high ranging between 18-42°. The high friction angles were the result of numerous glass shards the locked up the soil matrix on shearing resulting in a high friction angle. Dispersion and erodibility testing demonstrate that the soils from the cross-bedded sequence and aquifer were highly dispersive and erodiable. This result meant that the piping failure which is suggested to trigger landsliding in Chapter 2 is possible due to the erosive nature of the soils. Permeability testing of beds within the stratigraphic units indicates relatively low permeabilities. This is mainly due to the high silt and clay content present through a lot of the Stratigraphic beds. From the extremely long permeability times produce for an element of water passing through a stratigraphic unit it can be seen they do not compare to the fast lag times produce in Chapter 3 (24-96 hours). This is suggests that the lag times are not produced by soakage water permeating through the soil mass, but by another mechanism such as structure like exfoliation defects, fractures, and heavy bioturbation. This is further discussed in Section 5.2 of Chapter 5.

Chapter Five HYDROGEOLOGICAL ASSESSMENT, STABILITY ANALYSIS AND GEOTECHNICAL IMPLICATIONS

5.1 INTRODUCTION

This chapter interprets the possible regimes that could influence cliff failure at Maungatapu. Based on field observations it was concluded that the block landsliding seen around the peninsula was the direct result of a piping failure, which occurred through a build up of pore water pressures within the aquifer and the lower section of the cross-bedded sequence of the Upper Matua Subgroup. Pore pressure reached a point where it could no longer be confined within these sediments resulting in a piping failure taking with it material from the aquifer, upper bounding aquitard, and lower section of the cross-bedded sequence in conjunction with part of the colluvium/topsoil. This left no support for the material above, producing a block landslide along an exfoliation defect.

This chapter is divided into three section. The first section investigates the possible aspects that influence the hydrogeological regimes that can produce the increased pore water pressures at the edges of the Peninsula, and it examines how much the soakholes influence these hydrogeological controls. The second section involves the use of stability analysis models to assess the influence an increasing phreatic surface and landslide block size would have on the stability of the cliff faces. The factors of safety obtained from increasing the landslide blocks are then compared with to data produced by other people. The third section combines the conclusions from the previous two sections and looks at the geotechnical implications to the 2H:1V slope informally adopted as a geotechnical assessment zone.

5.2 HYDROGEOLOGICAL ASSESSEMENT

5.2.1 Introduction

A hydrogeological assessment of the Peninsula was undertaken to provide a better understanding of the various regimes that could produce the build up of pore water pressures within the Peninsula. This section has been divided into a number of sub-sections, the first dealing with the development of a model to distinguish the various components of soakage, i.e. rainfall infiltration through undeveloped land versus developed land. This is then taken a step further with the results being used in the assessment of soakhole contribution of the Peninsula. Next a hydrogeological model is developed that firstly deals with permeabilities derived from lag times in Chapter 3, which is then expanded with the introduction of actual soil profile data. This considers the effect that varying permeabilities of the multi-layered soil profile will have on a wetting front penetrating the stratigraphic units. Soakholes are introduced to determine how much of an influence they will have in increasing the pore water pressures within the Peninsula. During this sub-section possible mechanisms are considered that provide enough of a hydraulic connection that they could be comparable to the lag times of 24-96 hours obtained in Chapter3.

5.2.2 Rainfall Infiltration

To better understand the hydrogeological regime, consideration has to be given to how much water is entering the system by the various means available. Babbage Consultants (1995) developed a model for the distribution of groundwater soakage in relation to the Maungatapu Peninsula. In the "Babbage Model" infiltration of rainwater could occur in two possible ways;

1. *Through Undeveloped land*, which consists of parks, house-hold gardens, grassed areas, and grassed road verges, etc.; representing approximately 70% of the Peninsula's area.

2. *On Developed land*, equating to the remaining 30%, which can be further divided into

    a) land covered by buildings (and driveways) equating to 20% of the Peninsula's land area, and

    b) land covered by roads equating to the remaining 10%.

Further to this, the "Babbage Model" suggests that 75% of the rainwater falling on the undeveloped land will be absorbed into the ground, leaving the remaining 25% to runoff or evaporate. The rainwater which is collected by the buildings and driveways will be directed into soakholes situated throughout each property. This means that 100% of the rainwater collected will be directly injected into the underlying stratigraphic soil units. The "Babbage Model" was deemed to be a reasonable assessment of distribution of groundwater around the Peninsula and was adopted for this study with a minor adjustment to the percentage of groundwater associated with the developed land. Where the model used for this study ("The Modified Babbage Model") differs from the "Babbage Model" is in the proposed 5% of rainwater falling on the roads which is absorbed into the ground. It is suggested for this study that because the sealed roads are in good condition they will be practically impermeable. Due to this fact it is proposed that all the rainwater falling on the road will be discharged into the road's stormwater system and then out to sea.

Examining the daily rainfall data for 1995 (Figure 5.1), two hypothetical rainfall events (8 and 80 mm) can be used for calculating the proportion of groundwater entering the ground through undeveloped compared to developed land. The 8 mm rainfall event was calculated by averaging the days on which rainfall occurred for 1995, whereas the 80 mm rainfall represents the maximum rainfall to occur in a 24 hour period for 1995. If the area of the Maungatapu Peninsula is taken as approximately equal to 1.6 km^2 the proportional volumes of groundwater can then be calculated as shown below:

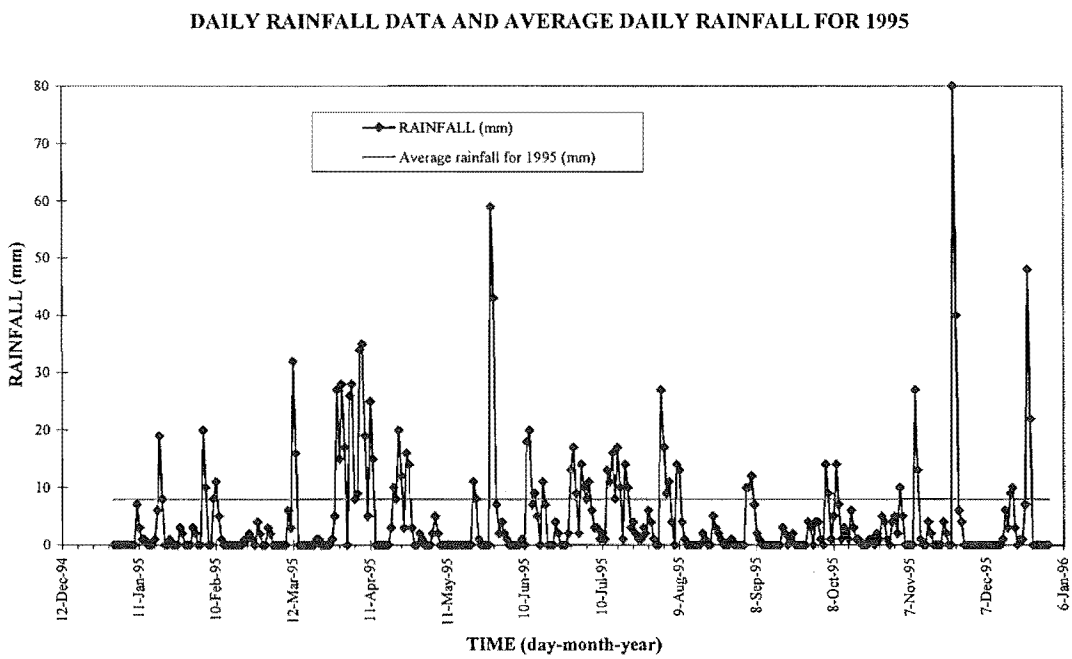

Figure 5.1 Rainfall data for 1995 indicating rainfalls for each day, as well as an average rainfall calculated from days which on rain occurred.

Undeveloped Land:

1. Taking an average rainfall of 8 mm, 75% of this will be absorbed by 70% of the undeveloped land $\Rightarrow$ 75% of 8 mm = 6 mm of rain will be absorbed into 70% of the undeveloped land. The undeveloped land = 1,600,000 m^2 (Peninsula area) × 70% = 1,120,000 m^2. This means the volume of water absorbed into the ground for an 8 mm rainfall event will = 1,120,000 × 0.006 = 6720 m^3.

2. Taking an average rainfall of 80 mm, the volume of water absorbed by the ground is a matter of multiplying the 8mm volume calculated (6720 m^3) by 10. This means the volume of water absorbed into the ground for an 80 mm rainfall event will = 6720×10 = 67,200 m^3.

Developed Land:

1. Developed land = 1,600,000 m^2 × 20% = 320,000 m^2. It is inferred that 100% of the rainwater collected by the buildings and driveways is discharged directly into soakholes on each property. Therefore a rainfall event of 8mm will produce a volume of water which is directly injected into the underlying soil stratigraphy = 320,000 × 0.008 = 2,560 m^3.

2. Developed land = taking an average rainfall of 80mm, the volume of water directly injected into the underlying soil stratigraphy = 2,560×10 = 25,600 m^3.

A summary of volumes of rainwater absorbed into the subsurface for a 24 hour rainfall period can be viewed in Table 5.1

Table 5.1 Groundwater soakage volumes calculated from a 24 hour 8 and 80 mm rainfall event using the modified Babbage Model.

Distribution Of Groundwater Soakage	Volume (m^3)	Percentage Of Total Volume Of Water Absorbed
Rainwater absorbed into the subsurface for a 8 mm rainfall event		
Volume of water absorbed into the soil mass from undeveloped land	6720	52.5
Volume of water discharged into soakholes	2560	20
Total Rainfall	12800	72.5
Rainwater absorbed into the subsurface for a 80 mm rainfall event		
Volume of water absorbed into the soil mass from undeveloped land	67200	52.5
Volume of water discharged into soakholes	25600	20
Total Rainfall	128000	72.5

5.2.3 Soakhole Contributions

From the above calculations approximately 20% of the rainwater is absorbed into the ground via soakholes. This suggests that soakholes can influence the hydrogeology and therefore the cliff failure dynamics of Maungatapu Peninsula. It indicates the importance of the distribution and depth of the soakholes throughout the Peninsula. Chapter 3 suggests that the depth of some of the soakholes may have penetrated through the Palaeosol into the underlying Upper Matua Subgroup sediments. This would result in a more direct connection between the ground surface and the aquifer zone, which is clearly related to landsliding. However, from soakhole investigation it was suggested that the majority of soakholes only appeared to penetrate through to the Palaeosol where upon they stopped. In addition the width of the soakholes varied depending on the type of rig used to drill them. The lager diameter soakholes tended to be of a shallower nature due to the difficulty of drilling with the larger augers especially on reaching the compact Palaeosol. It is however likely that < 10% of all of the soakholes drilled on the Peninsula penetrated the Palaeosol and Hamilton Ash.

By examining the rainwater volumes which discharge into the soakholes, a better understanding of the ability of the soakhole to dissipate the soakage water into the surrounding soil strata can be obtained. In order to do this a number of assumptions have to be made. Firstly, for these calculations a soakhole has been defined as having a diameter of 300 mm and to only penetrate to the top of the Palaeosol at a depth of 4 m. In addition, each property is assumed to have approximately 4 soakholes which collect roof and driveway rainwater. Because of the difficulty including the driveway contribution into the equation due to the variable areas which they cover, they have been excluded from the calculations. This means that only the roof area has been assessed. For these calculations, a roof can be divided into four sections, with each roof section having dimensions of 5 × 10 m, equating to an area of 50 m^2. Each roof section represents an area which intercepts rainwater and consequently discharges it into the relevant soakhole associated with that roof section. Therefore utilising the hypothetical 8 and 80mm rainfalls delineated in Section 5.2.2, daily volumes of water which enter the soakholes can be calculated. When

considering these volumes it is assumed that there will be 100% runoff of rainwater from the roof into the soakhole.

1. Taking an average rainfall for a 24 hour period for 1995 (8 mm) the volume of rainwater entering the soakhole can be calculated:

    - The volume of water collected by the roof = $0.008m \times 50m^2 = 0.4m^3$
    - The soakhole volume with dimensions of ϕ = 300mm, d = 4m, therefore $V=\pi(0.15)^2 4=0.28m^3$
    - Therefore $0.4m^3$ of rainwater has to discharge into a soakhole with a volume of $0.28m^3$.

2. Taking the maximum rainfall recorded for a 24 hour period for 1995 (80 mm) the volume of rainwater entering the soakhole can be calculated:

    - The volume of water collected by the roof = $0.08m \times 50m^2 = 4m^3$
    - The soakhole volume with dimensions of ϕ = 300mm, d = 4m, therefore $V=\pi(0.15)^2 4=0.28m^3$
    - Therefore $4m^3$ of rainwater has to discharge into a soakhole with a volume of $0.28m^3$.

The latter calculation using a rainfall of 80mm produces a large volume of water which has to be absorbed into the soil surrounding the soakhole. On talking to local property owners during the field investigation stage of the project, it was confirmed that no major flooding had occurred on their sections. This demonstrates that soakholes and related soil strata even during large storm events can successfully absorb the roof and driveway derived rainwater.

5.2.4 Hydrogeological Model

a) Definition of Wetting Fronts

A wetting front can be defined as the leading edge of a mass of water which is permeating through a material. The wetting front can be viewed either in three or two dimensions and propagates in a uniformed density sample as concentric rings. For instance, if a volume of water is introduced at a point in a mass of soil, the wetting front will move outwards in much the same way a ripple on a pond does (Figure 5.2).

If this wetting front meets a soil mass of a higher permeability than the one in which it already occurs, the wetting front will undergo a relative step out and become larger due to an increase flow velocity. This is because the water will permeate faster in soil with a higher permeability. Conversely if the wetting front enters a soil of a lower permeability the wetting front will undergo a relative retardation due to a decrease in flow velocity (Figure 5.3).

b) Lag Time Responses (Uniform Permeability Model)

Lag time responses were derived in Chapter 3 from trends in piezometric responses when compared to particular rainfall events. Lag times between 24-96 hours were indicated, which in turn produced equivalent permeabilities of 3.0×10^{-4}-3.8×10^{-5}m/sec respectively. In order for these calculated permeabilities to represent an average hydraulic conductivity for the stratigraphic sequence defined in Chapter 3, a number of assumptions were made:

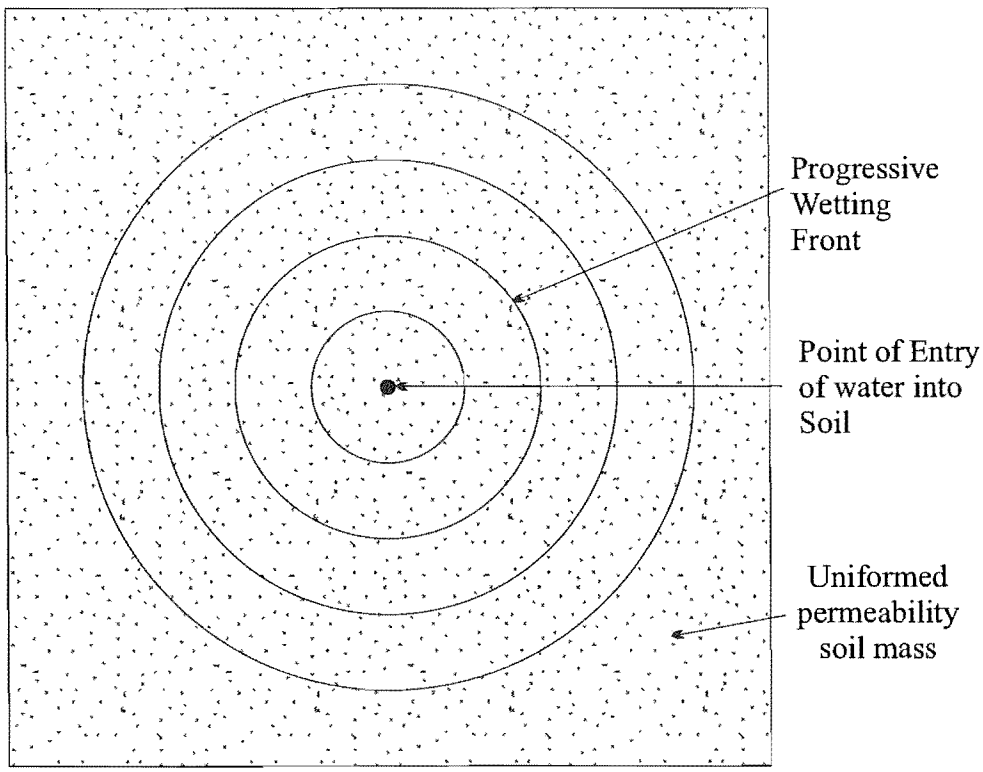

Figure 5.2 Theoretical representation of the progression of a wetting front through a uniformed density soil mass from a central point of entry.

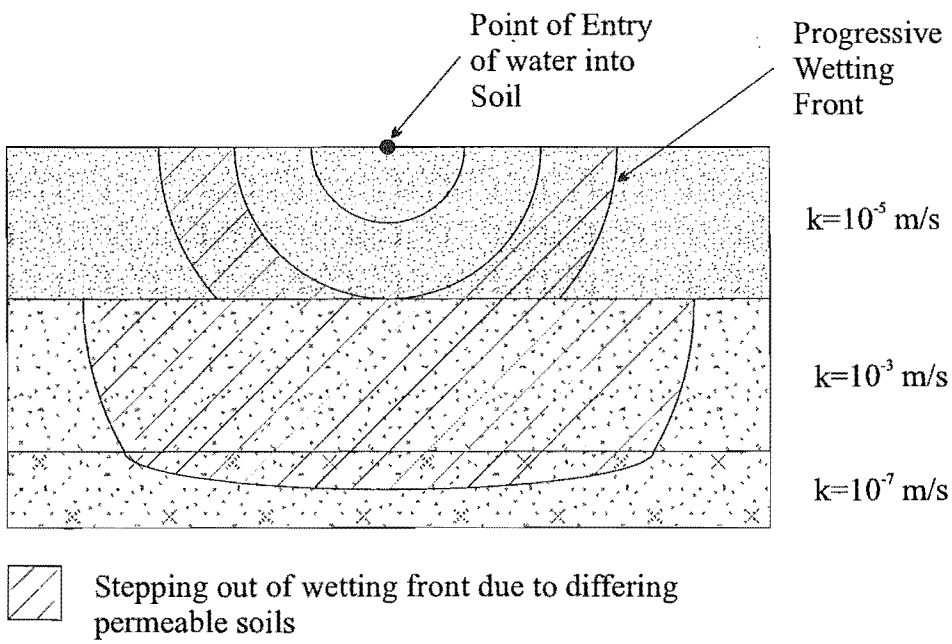

Figure 5.3 Theoretical progression of a wetting front through a number of soils with varying permeabilities. This is a two dimensional schematic in the vertical plane.

1. The water level response to rainfall seen in the piezometers was the product of rainwater infiltrating from the surface to the slotted section of the piezometer, and was not influenced by soakholes or aquifer contributions.

2. The soil mass through which the infiltrating water flowed consisted of a uniform matrix where the vertical permeability is equal to the horizontal permeability ($k_V=k_H$).

3. The water level within each piezometer reflected the water table inherent in the Peninsula, and was not influenced by aquifer related head-recharge induced water pressures.

Considering the above assumptions a diagrammatic representation of the progressive wetting front from a point of infiltration can be constructed (Figure 5.4). This model represents a simplistic approach to the infiltration of a quantity of rainwater through the stratigraphy. The volume of rainwater when introduced at a point moves outwards from a central point as a wetting front in the form of a series of increasing concentric circles (Figure 5.4). However, rainfall does not enter the ground at a central point but uniformly over the entire Peninsula. This produces an infinite number of these "points of entry" resulting in an infinite number of overlapping wetting front circles. Because of this the wetting front instead of showing concentric circles appears as a line parallel to the ground surface moving downwards through the soil mass.

c) Stratigraphic Unit Profile Model

However, the Peninsula does not consist of a uniform density soil matrix but numerous airfall ashes, tephras, fluvial and estuarine deposits of varying permeabilities. This in turn means that the horizontal permeability is not equal to the vertical permeability. In addition, the soakholes and especially the aquifer are suggested to possibly influence the

piezometric responses to rainfall. Because of this the average lag time derived hydraulic conductivities for the cliff face stratigraphy represent an estimation of a response of the hydrogeological system to rainfall. A more representative model would assess the influence of stratigraphy-related soil permeabilities of the logged cliff faces. As presented in Chapter 2, Maungatapu Peninsula consists of numerous ashes and tephras underlain by a sequence of fluvial and estuarine deposits intercalated with airfall deposits. Each major unit can in turn be separated into a number of smaller beds with varying hydraulic properties. From laboratory testing a suggested hydraulic conductivity range of 10^{-4}-10^{-7} m/s was possible for the Post-Rotoehu Ash Tephras. Heavy bioturbation associated with this sequence will tend to reduce the permeabilities, resulting in hydraulic conductivities lying towards the upper end of the range, e.g. 10^{-4}-10^{-6} m/s. The Rotoehu Ash much like the Post-Rotoehu Ash Tephras, is believed to exhibit a range of permeabilities from 10^{-3}-10^{-7} m/s. Bioturbation did not appear anywhere as prevalent as in the overlying Post-Rotoehu Ash Tephras, and therefore does not affect the permeability range to a noticeable extent. Many of the geotechnical consultants in Tauranga have indicated that the Rotoehu Ash is the unit which is aimed for when drilling a soakhole due to its relatively high horizontal permeability, at least in certain beds.

The Palaeosol and associated Hamilton Ash are predicted to have permeabilities of 10^{-8} and 10^{-7} m/s respectively. However, from field investigations these two units show evidence of heavy bioturbation (rootlet structures). These old rootlet structures may increase the permeabilities but to what extent it is difficult to say. It is suggested however, that an increase in permeability in the order of a factor of ten may be possible, resulting in hydraulic conductivities of 10^{-7} and 10^{-6} m/s for the Palaeosol and Hamilton Ash respectively. This is still considerably less than many of the beds within the Rotoehu Ash.

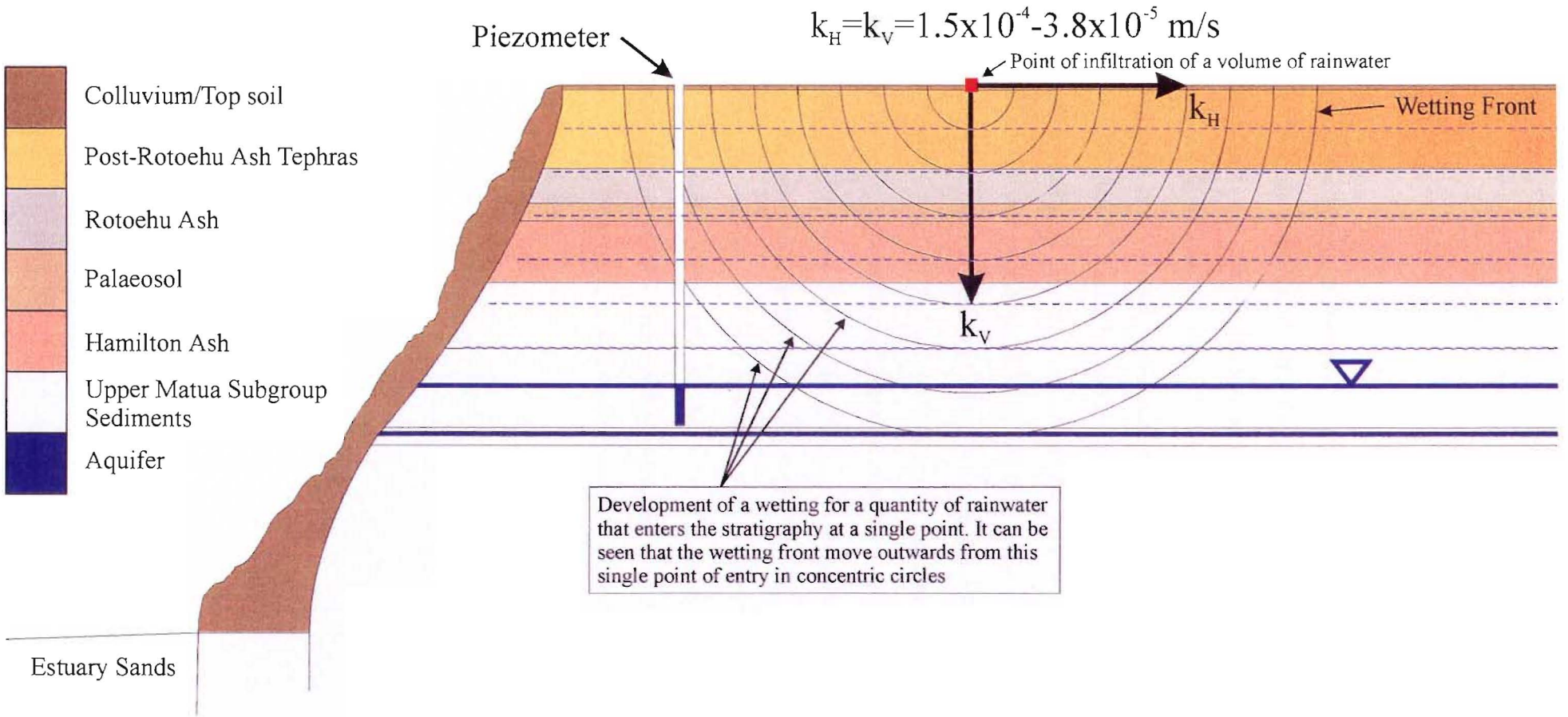

Figure 5.4 Construction of a wetting front from lag time response data in which the vertical permeability of the soil mass is equal to the horizontal.

Underlying the Hamilton Ash is the Upper Matua Group sediments which consist of the Pahoia Tephras intercalated with fluvial and estuarine sediments. The Pahoia Tephra present above the cross-bedded sequence, varies considerably in both grainsize and structure as indicated by Figure 4.13. Because of this it suggested that hydraulic conductivities (k_V) will range between 10^{-4}-10^{-7} m/s from area to area. The cross-bedded sequence was shown during laboratory testing to have a range of permeabilities from 10^{-7} - 10^{-8} m/s. In addition, the lower section of this unit is believed to have a partial hydraulic connection to the underlying aquifer via fracturing or erosion of the upper bounding aquitard. The Upper bounding aquitard is a considerably smaller unit (~50mm) compared to the Lower bounding aquitard (200-300mm), therefore any minor erosion or fracturing will allow water to flow through from the aquifer to the lower section of the Cross-bedded sequence, or *vice versa*. The aquifer yielded a permeability of 3.4×10^{-6}, m/s and taking into account the grainsize distribution, permeabilities could range between 10^{-4}-10^{-6} m/s. Bounding the aquifer are two aquitards, the upper bounding aquitard and the lower bounding aquitard. These two aquitards are suggested to have similar properties, with laboratory testing of the lower aquitard producing a range of permeabilities from 10^{-8}-10^{-9} m/s. Table 5.2 presents a breakdown of vertical permeabilities in relation to stratigraphic position within the cliff face.

Table 5.2 Breakdown of vertical permeabilities relative to their stratigraphic position within the soil profile.

Stratigraphic Unit		Permeability Range (m/s)
Post-Rotoehu Ash Tephras		10^{-4}-10^{-7}
Rotoehu Ash		10^{-3}-10^{-8}
Palaeosol		10^{-8}
Hamilton Ash		10^{-7}
Upper Matua Subgroup	Pohoia Tephra	10^{-4}-10^{-7}
	Cross-bedded sequence	10^{-7}-10^{-8}
	Upper Bounding Aquitard	10^{-8}-10^{-9}
	Aquifer	10^{-4}-10^{-6}
	Lower Bounding Aquitard	10^{-8}-10^{-9}

Behavioural Characteristics of a Wetting Front in Relation To Stratigraphic Constraints

Once a generalised stratigraphy is developed, wetting fronts from a point of infiltration can be used to demonstrate the relationship between the various units within the cliff face. It should be noted that a single entry point source is invalid when considering that rainfall over the Peninsula is basically uniformed, but by looking at a single point source, a clearer picture of the behaviour of infiltrating water can be seen. As stated for the "uniform permeability model" there will be an infinite number of these point sources with a uniform rainfall distribution. If placed on a figure they would obscure any the relationship between the progression of the wetting front in relation to the permeability of the unit. Taking into account that the various units have different permeabilities, the wetting front will exhibit a stepped nature depending on the hydraulic conductivity of the particular bed. Because of this the wetting front constructed for the "uniform permeability model" can be concluded

to be non-representative of the soil profile. Figure 5.5 present a more likely scenario where a wetting front would produce as it travelled through the soil profile.

This type of behaviour can be further investigated by looking at the situation where the Palaeosol forms an aquitard, separating the Post-Rotoehu Ash Tephras and Rotoehu Ash (Younger Ashes) from the underlying Upper Matua Subgroup sediments. These younger ashes are believed to absorb most of the soakage water permeating from the surface. A wetting front model can then be developed to look in finer detail into distribution of the permeating water in the Post-Rotoehu Ash Tephras and Rotoehu Ash (Figure 5.6). As stressed before, this model only shows the relationship between a point source infiltration and bed permeability and not that of a wetting front produced by a uniform distributed rainfall. Figure 5.6 shows the stepped nature of the wetting front as it proceeds downwards through the soil profile. The overall result of this is that soakage water will tend to move laterally along the more permeable soils (e.g. beds with permeabilities of 10^{-3}-10^{-5} m/s) than downwards through the less permeable beds (e.g. 10^{-6}-10^{-8} m/s). On reaching the Palaeosol a decrease in the vertical component of the wetting front velocity will occur due to the low permeability (10^{-8} m/s) of the Palaeosol. This results in the lateral component of the wetting front moving faster along the Post-Rotoehu Ash Tephras and Rotoehu Ash.

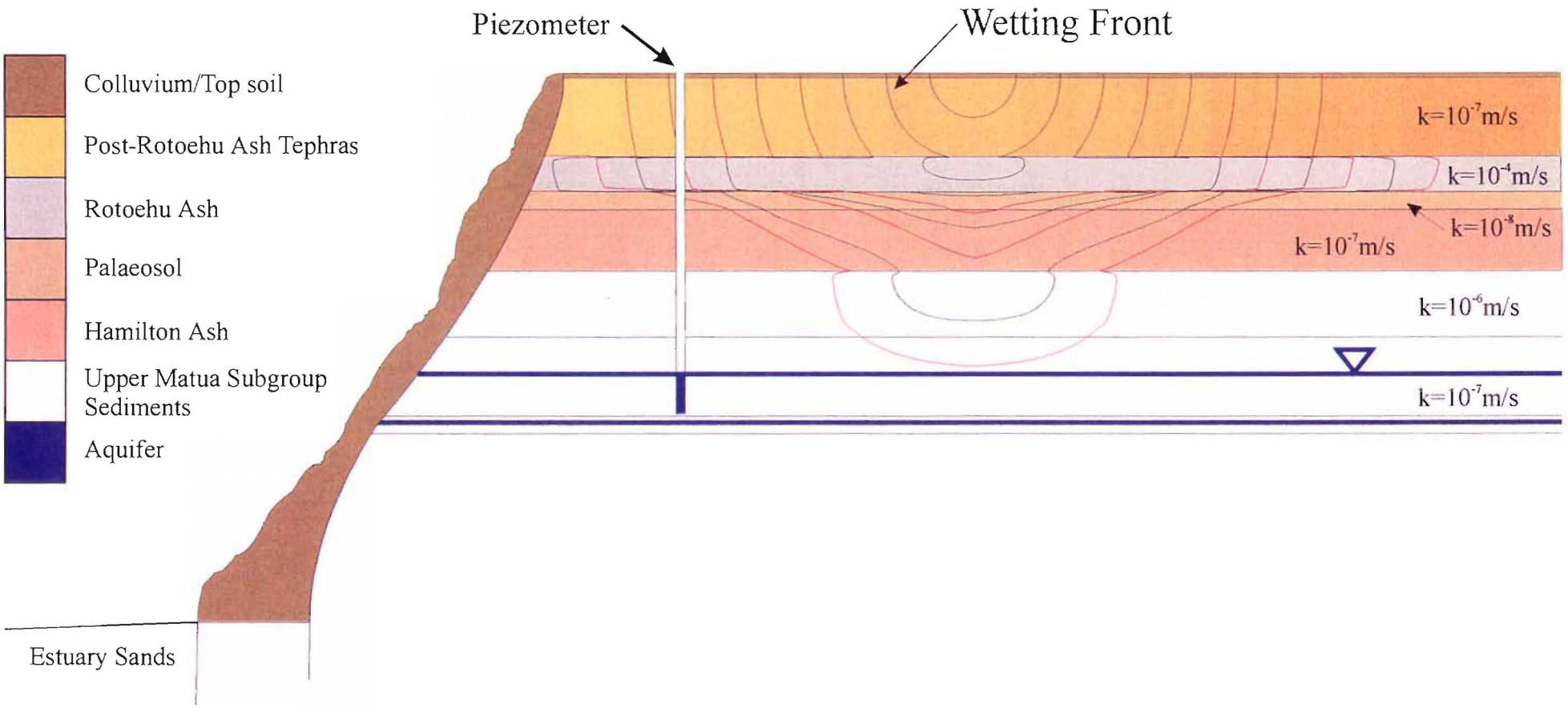

Figure 5.5 Construction of a wetting front related to differing permeabilities for the geologic units of the soil profile. It can be seen that the wetting front moves faster in more permeable units than less permeable. This has the overall affect that lateral movement of soakage water will be greater than the vertical infiltration.

If the permeabilities for the younger ashes are looked at further, an idea can be obtained of the relative times taken for ground water to permeate through the soil profile such as represented in Figure 5.6. Firstly, taking the hydraulic conductivities in m/s and converting them to m/day yields permeabilities such as: 10^{-3} m/s=86.4 m/day, 10^{-4} m/s=8.64 m/day, 10^{-5} m/s=0.86 m/day, 10^{-6} m/s=0.086 m/day, 10^{-7} m/s=0.0086 m/day, etc. These relative permeabilities indicate that the top part of Post-Rotoehu Ash Tephra would allow the slow infiltration of water into the subsurface. This concept can be further expanded to include the whole of the soil profile of the logged cliff face. From permeabilities obtained during laboratory testing (Chapter 4) it is seen that the hydraulic conductivities of the soils below the Hamilton Ash are quite low, 10^{-6}-10^{-8} m/s (=8.6×10^{-2}-8.6×10^{-4} m/day). This means that for soakage water to infiltrate through to the aquifer in the failure zone would take a considerably long time. For instance, if for argument sake the aquifer is situated approximately 15 m below the ground surface, and assessing the average permeability for the soil profile to be approximately 10^{-6} m/s (or 0.0864 m/day), the time it takes for a volume of water to permeate from the surface to the aquifer can be calculated by dividing the distance to the aquifer by an average permeability for the soil profile = 15m / 0.0864m/day = 174 days. In addition, if the average permeability for the soil profile was instead 10^{-5} m/s (=0.864 m/day) the time taken for water to permeate the 15 m = 17.4 days. This only provides a general indication, as the infiltrating soakage water will follow a more complex path as demonstrated by wetting fronts discussed previously. Estimate an average permeability for the soil profile can be difficult, in that units of low hydraulic conductivities as in the cross-bedded sequence, will slow the movement of soakage water considerably, therefore reducing the average permeability of the soil profile. However, the average permeability is certainly not likely to be greater than 10^{-5}m/sec, therefore the result obtained above can then be compared to lag time responses. These indicate response times of 24-96 hours (or 1-4 days) between a rainfall event and a corresponding rise in piezometric water level. If it is assumed that the infiltrating water is not affected by factors like soakholes, jointing and/or erosion of the Palaeosol and Hamilton Ash etc., it can be

concluded that rainwater infiltration through the soil profile from the ground surface can not be responsible physically for changes in the piezometric water levels.

As seepage is recognised exiting the aquifer at the logged cliff faces in greater quantities after rainfall, it suggests that there is some hydraulic connection between the younger ashes and the Upper Matua Subgroup. Possible reasons for this will be addressed in the following section on the implication of soakholes.

d) Implications

Soakholes

As stated in earlier sections, soakholes are suggested to penetrate through to the Palaeosol whereupon they stop. The Palaeosol being relativity impervious will only allow soakage water to drain into the Post-Rotoehu Ash Tephras and Rotoehu Ash. For example, if the Palaeosol is considered to be continuous with an approximate thickness of 0.5m and a permeability of 10^{-8} m/sec, the time taken for a volume of rainwater to permeate this unit can be calculated. Therefore, using equation 4.1 (Section 4.8.3, Chapter 4) it will take approximately 1.6 years for a volume of water to travel the 0.5m of the Palaeosol. This indicates that the flow velocity of the wetting front within the Palaeosol will be extremely slow.

Unlike the situation previously suggested where rainwater has to permeate through from the surface, a soakhole will directly inject the soakage water into the younger ashes. Therefore, when a wetting front is constructed for a soakhole it will look somewhat different from that of Figure 5.6. Figure 5.7 shows a generalised wetting front where soakage water is allowed direct access to the more permeable beds immediately. As in

Figure 5.6, beds with higher permeabilities will show greater infiltration of soakage water than less permeable beds. This creates the staggered wetting front seen in Figure 5.7.

From Figure 5.7, it can be seen that the Rotoehu Ash provides the best soils for drainage. Many of the geotechnical consultants such as O'Halloran (Pers. Comn. 1996) and drillers Perry (Pers. Comn. 1996) indicate that the Rotoehu Ash is the major unit which was aimed for when drilling soakholes around the Peninsula. Some of the beds within the Rotoehu Ash produce permeabilities around 10^{-3}-10^{-4} m/s (=86.4-8.6 m/day), therefore soakage water should be seen exiting soon after a storm event in areas where the Post-Rotoehu Ash Tephras and Rotoehu Ash are exposed (logged cliff faces at 85 and 89 Te Hono Street). However, 1-7 days after periods of heavy rainfall no appreciable discharge is observed in these areas. The only seepage seen can be attributed to the aquifer associated with the failure zone which increases in flow rate after a storm event. This lack of discharge has resulted in the identification of three possibilities.

The first is that the average permeabilities are lower in the Rotoehu Ash than has been interpreted, resulting in considerably slower movement of soakage water through the younger ashes. This would create a mounding affect of the soakage water around the soakholes, with a slowly expanding wetting front and decrease in water height within the soakhole. However, evidence from both volumetric calculations presented earlier in section 5.2.3, and the lack of surface flooding resulting from overtopping of soakholes, would suggest a second possibility exists.

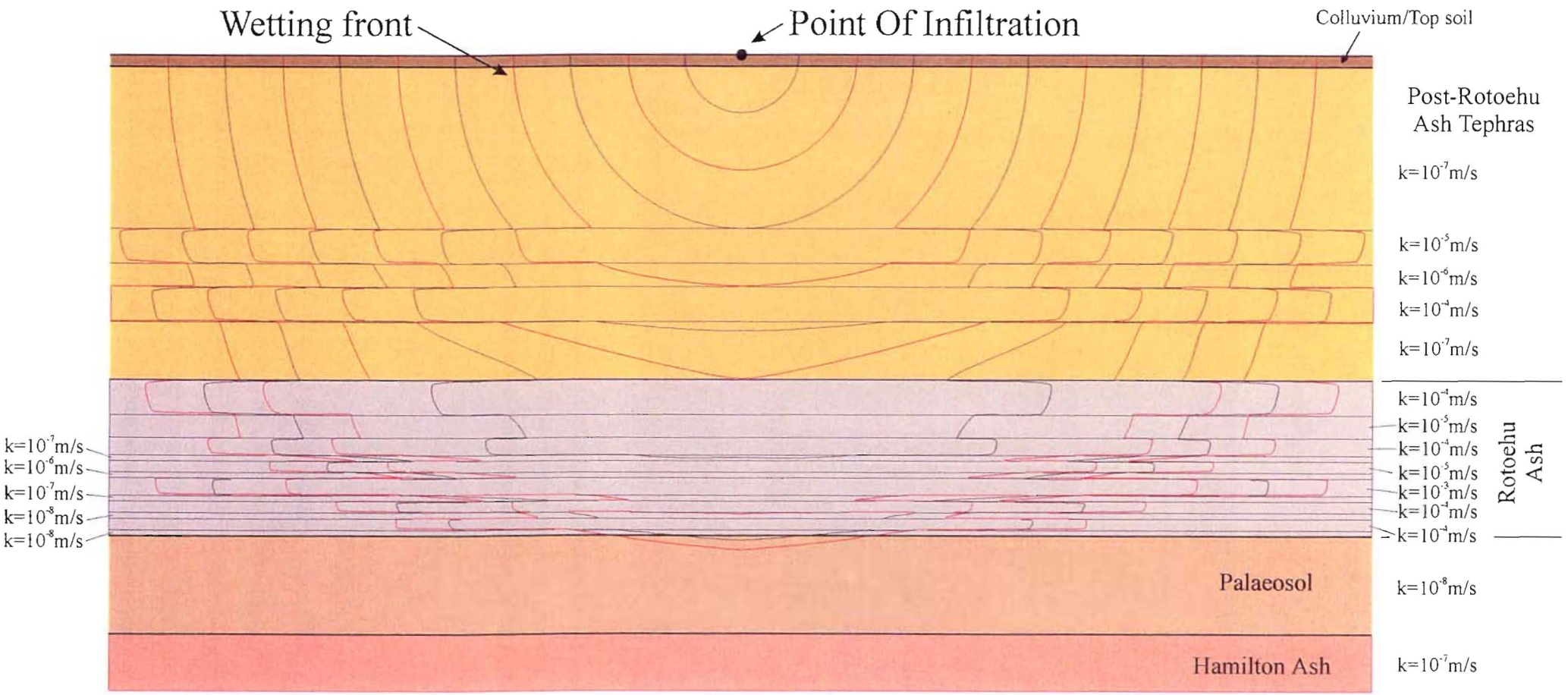

Figure 5.6 A schematic representation of permeabilities associated with the beds of the Post-Rotoehu Ash Tephras, Rotoehu Ash, Palaeosol, and Hamilton Ash. The diagram represents the behaviourial characteristics of a volume of water as it infiltartes the soil mass by the use of a wetting front model. The wetting front can be seen to be stepping out in beds with a higher permeability compared to those with a lower permeability. The result of this means that there will be greater lateral flow within the more sandy-higher permeability beds.

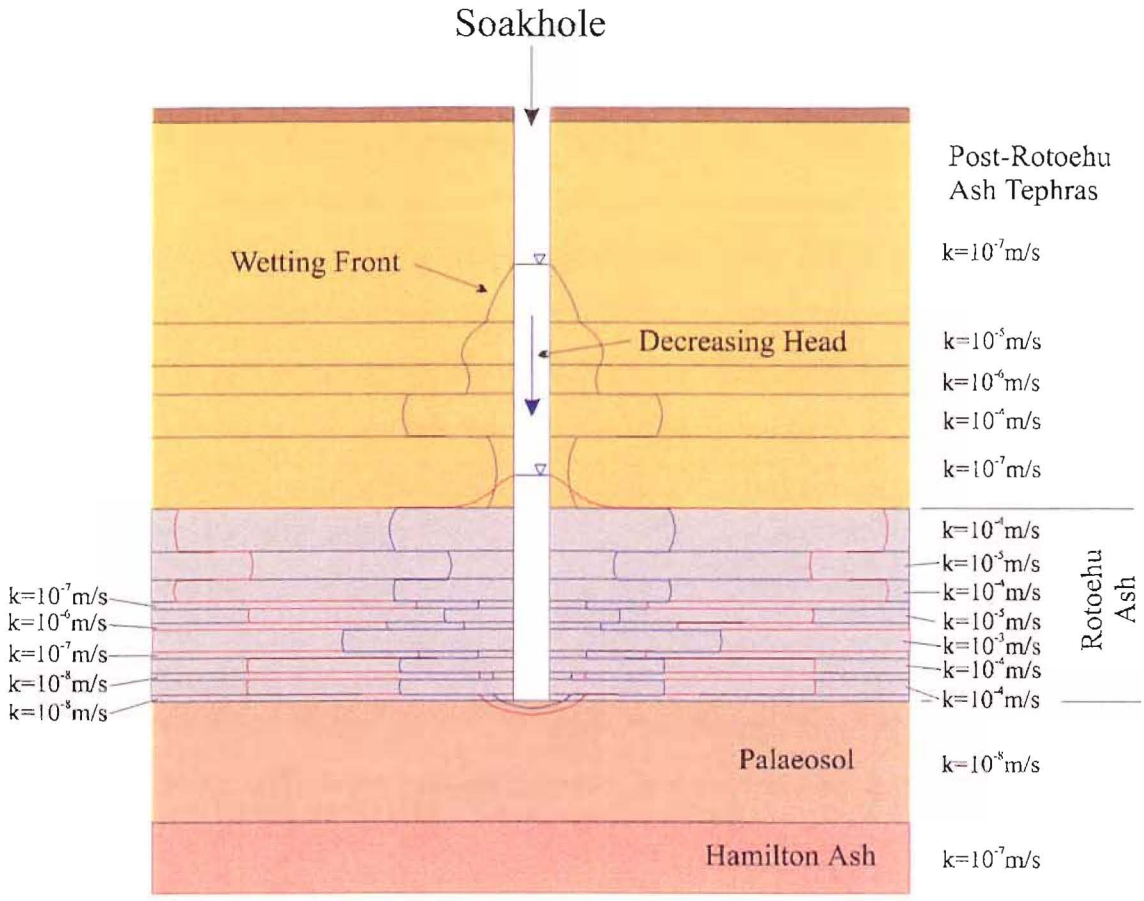

Figure 5.7 Demonstrated how the soakholes provides direct access for the soakage water to enter the various beds of the Post-Rotoehu Ash Tephras and Rotoehu Ash. This means the soakage water will tend to flow laterally along the higher permeability beds which is represented in the construction of a wetting front.

The second possibility is that the soakage water is exiting along areas which are not visible e.g. areas covered by colluvium/top soil and vegetation. It is difficult to detect seepage exit points within steep heavily vegetated sites such as those around Maungatapu therefore lending credence to this possibility. One of the major problems with this is that the logged cliff faces (85 and 89 Te Hono Street) are at the end of Peninsula down the hydraulic gradient and would represent one of the major exiting points for soakage water. Because of these facts it is difficult to discount or to prove this possibility.

The third possibility relates to soakage water permeating through the Palaeosol and Hamilton Ash into the underlying Upper Matua Subgroup sediments. This possibility in turn can be divided up into a number of factors that could allow a hydraulic connection between the younger ashes above the Hamilton Ash and Palaeosol, and the units below. The first consideration is that many of the soakholes were drilled through the Palaeosol into the Upper Matua Subgroup sediments, allowing direct injection of rainwater. Field investigations provided some indication that a few of the soakholes around the peninsula had in fact been drilled through the Palaeosol and Hamilton Ash into these underlying sediments. It is however believed that the majority of soakholes stopped at the Palaeosol (i.e. probably >90% in total).

The next possibility relates to hydraulic connection through exfoliation defects, fracturing within the soil profile, buried stream channels, and bioturbation. Exfoliation defects will be situated around the cliff edges of the Peninsula where unloading is occurring, and decrease in size further inland (Chapter 2). These exfoliation defects will provide preferential high permeability paths for soakage water to flow through, allowing direct injection of soakage water into the Upper Matua Subgroup sediments close to the cliff edges. Soakholes that intersect these exfoliation defects may allow a greater rate of infiltration to occur (Figure 5.8). Other possibilities that will increase the permeability of the soils in localised areas, and as a whole would increase the overall hydraulic conductivity of all the units, include buried stream channels. These buried stream channels can provide partial connection where they have eroded away the Palaeosol and Hamilton Ash. However from laboratory investigations the underlying beds of the Upper Matua Subgroup appear to have similar permeabilities to those exhibited by the Hamilton Ash (Figure 4.16). This means that the downward soakage component of the flow velocity may not increase dramatically, compared to the Hamilton Ash. This in turn means that the effectiveness of buried streams does not influence the overall permeabilities of the soil profile. Therefore the main structures which will affect the infiltration times at the edges of

the Peninsula will be those of exfoliation defects, fracturing within the soil mass and heavy bioturbation (rootlets).

Many in-situ soil tests demonstrated hydraulic conductivities that were very low, i.e. around 10^{-7} m/s (=8.64×10^{-3} m/day), as shown in Table 4.16. When these permeabilities are compared to the corresponding grainsize distributions, it is found that the soils contain a high percentage of silt and clay, suggesting that these hydraulic conductivities are quite reasonable. This can be taken a step further by looking at the time it would take for a volume of water to travel through a 3 m thickness of the cross-bedded sequence that has an average permeability of 10^{-7} m/s (=8.64×10^{-3} m/day). The time taken = 3 m / 8.64×10^{-3} m/day = 347 days, or almost a year for the soakage water to travel the 3m. The cross-bedded sequence only comprises part of the soil profile, indicating that the time it will take for the soakage water to reach the aquifer will be considerably longer than expected. In addition when this figure is compared to lag times in piezometric responses of 24-96 hours, it can be clearly seen that they do not agree. This means that either exfoliation defects, fracturing of the soil profile, deeper soakholes, etc., considerably increase the overall permeability of the units, or another mechanism must be producing these rapid lag time responses delineated in Chapter 3.

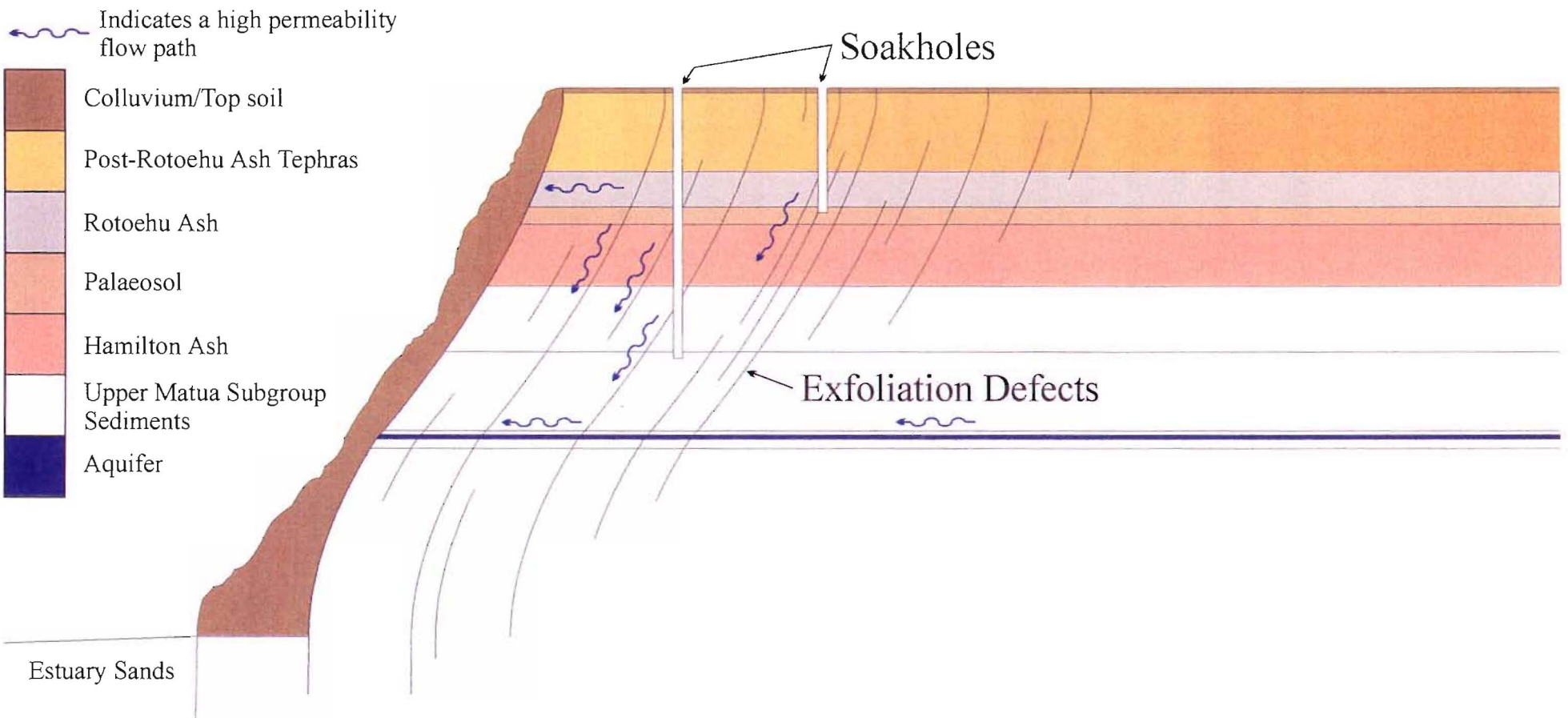

Figure 5.8 Exfoliation defects provide high permeability flow paths where soakage water infiltration time will be dramatically reduced close to the cliff edges (i.e. within ~50m).. In addition soakholes will allow direct injection of this soakage water into exfoliation defects and fractures within the soil mass. The deeper the soakholes the greater number of structures that they will intercept, therefore further reducing the infriltration time.

Hydraulic Head-Recharge Induced Pressure Waves

If the structures previously suggested are considered not to increase sufficiently the rate at which soakage water permeates through to the aquifer, then another mechanism must explain the fast lag time responses delineated in Chapter 3. One possible solution that has been hinted at in earlier chapters is that of a pressure wave, induced by an increase in the hydraulic head, due to recharge from rainfall in the foothills and the Peninsula itself. In an already saturated soil this allows the quick transfer of pressure waves along the aquifer resulting in a corresponding build up of pore pressures at the end of the Peninsula causing an increase in discharge rates and exit velocities.

From field investigations the aquifer discharges water continually throughout the year, even during periods of low or no rainfall. This means that either the flow rate of the permeating water is very slow, or the aquifer is being recharged from somewhere other than the local area immediately above. The aquifer and associated aquitards are airfall deposits which blanket the Peninsula and surrounding area, continuing back up into the foot hills with an approximately uniform thickness. Because of this the aquifer is predicted to provide continuous hydraulic connection over the entire length of the Peninsula. With a permeability of approximately 10^{-6} m/s (= 0.0864 m/day), movement of soakage water within this unit will be extremely slow. In addition, the lower and upper aquitard are believed to be basically non-compressible. The aquifer itself is semi-confined between these to units and also moderately non-compressible. Due to this non-compressibility it will therefore allow the relatively quick transfer of pressure waves along the aquifer. This assumption is lent credence by the fast lag time responses seen in Chapter 3 of 24-96 hours.

The pressure waves are produced by soakage water infiltrating along fractures, exfoliation defects at edges of Peninsula, and other high permeability hydraulic path ways up dip of the northeastern end of the Peninsula. This soakage water induces a change in the hydraulic head in these local areas as well as in the foot hills and the Peninsula itself. The pressure waves travelling along the aquifer will in turn increase the pore pressures at the east end of the Peninsula, where soakage water is trapped by the colluvium/top soil. These pore pressures then reach a point where they can no longer be contained within the aquifer, lower sections of the cross-bed sequence, and the colluvium/top soil, resulting in the production of a piping failure along root structures as observed in Chapter 2. This in turns removes the support under a section of the cliff, inducing the block failure.

It should be noted that landsliding, such as that at 85 Te Hono Street is the result of the cumulative affect of the infiltrating rainwater caused by two months of higher than average rainfall. This creates a dynamic hydrogeological system, where rainfall over one or two days can produce a corresponding piping failure. This can be demonstrated by looking at the sequence of events 2 months prior to the landslides in May 1995. During this time considerably higher than average rainfalls were recorded for March and April resulting in the slow saturation of the stratigraphic units associated with the logged cliff faces. Because most of the stratigraphic units have relatively low permeabilities, the soil mass will be virtually saturated all year round. This means that with any additional rainwater, as in the situation of 1995 from March to May, can be enough to produce a dynamic system as suggested above.

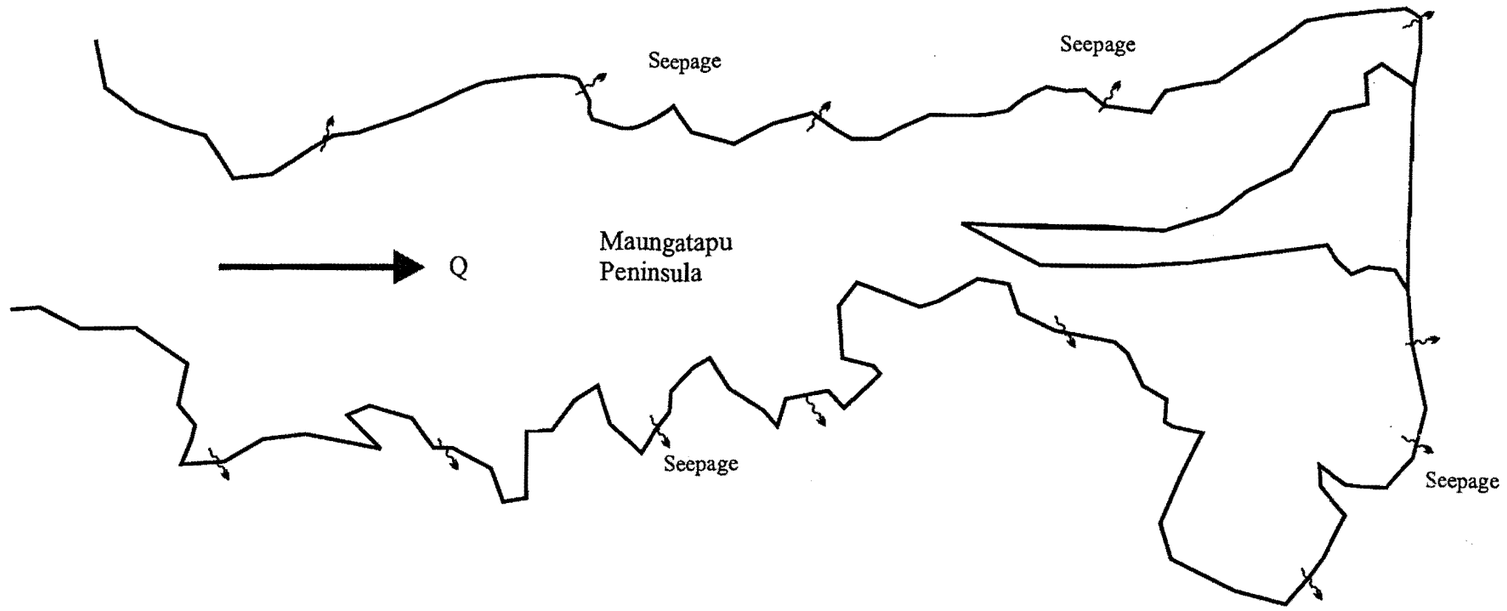

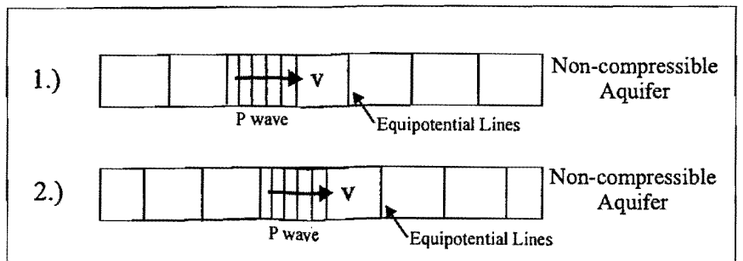

A change in the hydraulic head produces a pressure wave that move rapidly through the non-compressible aquifer zone. This pressure wave behaves in muck the same way as a sound wave, by compressing the air, or in this case the water. This can be presented as a bunching up of equipotential lines representing a pressure wave with a higher velocity than the normal flow rate (Q).

Figure 5.9 Schematical representation of a head recharge model where water permeating through the soil mass induces a pressure wave. This pressure wave can travel rapidly through the aquifer and lower section of the Cross-bedded sequence, resulting in an increase in pore water pressures at the cliff edge.

Piezometers

Eight piezometers were drilled in a rough grid at the end of the Peninsula around the Te Hono Street area where three landslides occurred in 1995. The boreholes were drilled to depths approximately between 15-18m and piezometers inserted with 0.5-1m slotted sections to pick up possible aquifer zones. Most of the piezometers are situated either within the aquifer or just above the upper bounding aquitard within the lower section of the cross-bedded sequence. Beca Carter Hollings and Ferner (1996 and 1997) conducted a hydrological investigation of Maungatapu Peninsula. They found that direction of flow of groundwater was towards the cliff edges. Also denoted in Beca Carter Hollings and Ferner (1996) was a ridge-saddle arrangement around the east end of Maihi (Figure 5.10). Figure 5.10 shows the soakage water flowing away from this ridge-saddle structure towards the cliff edges. Beca Carter Hollings & Ferner Ltd (1996) concluded that the soakage water flowed from this ridge towards 85 Te Hono Street. These type of structures are most probably quite likely but further investigation would have to be undertaken to properly identify such features.

Piezometric water levels can be in response to two possibilities. The first is that they provide a direct indication of the water level within the cliff profile of the Peninsula. However, a number of factors exist that discount this as a possibility. For instance the peninsula consists of numerous beds of varying permeabilities that confine or semi-confine some beds, e.g. the two aquitards that semi-confine the aquifer within the failure zone. In addition to this the soils within the cliff profile of section 5.2.4. are suggested to be virtually saturated all year round therefore also adding credence to discounting this possibility. The best answer is that they represent an indication of the pore pressures related to hydraulic head-recharge from both the exfoliation defect related infiltration, and pressure waves induced by hydraulic head-recharge in the foothills and Peninsula. Because

of this they provide a good indication of the behavioural characteristics of the pore pressures associated with the aquifer and lower section of the cross-bedded sequence.

5.2.5 Discussion and Evaluation

The scenario of head-recharge induced pressure waves relies on the supporting evidence of lag time response data from Chapter 3. In Chapter 3 *"lag time"* refers to the time between a single rainfall event and the corresponding rise in piezometric water levels. This means that changes in piezometric water levels could either be in response to hydraulic head-recharge, or soakhole-related water permeating through the soil profile inducing a physical rise. Analysing the soakhole induced rises in piezometric water levels, a number of conditions have to be satisfied. Firstly, if the majority of soakholes only reach the Palaeosol there has to be some hydraulic connection between the Post-Rotoehu Ash Tephras and Rotoehu Ash and the Upper Matua Subgroup sediments. As all boreholes are located at the end of the Peninsula, hydraulic connection would involve exfoliation defects, fracturing within the soil mass, and bioturbation affects. The most important structure would be that of exfoliation defects allowing high permeability path ways for soakage water to infiltrate into the aquifer within the failure zone. In addition, soakholes will tend to intersect these structures lessening the time for soakage water to reach the aquifer. Therefore soakholes which penetrate the Palaeosol and Hamilton ash to the Upper Matua Subgroup sediments will intersect even more structures lessening the infiltration time dramatically.

Figure 5.10 Schematic diagram showing the direction of flow soakage water between boreholes (from Beca Carter Hollings & Ferner Ltd, 1996).

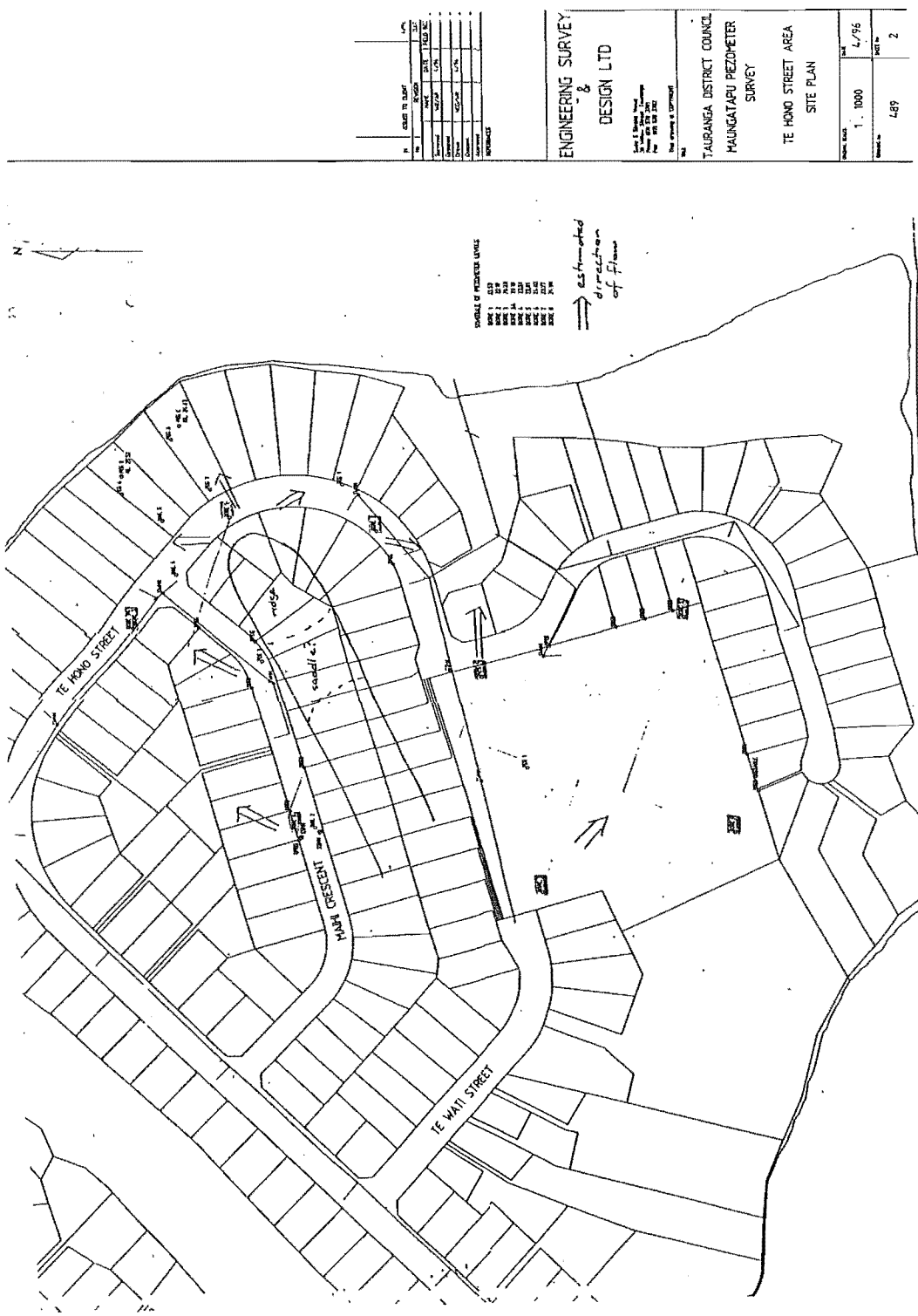

However, as suggested previously in this section and Chapter 3 these deeper soakholes would be few, reducing their influence over the majority of the Peninsula. If there were a number close to the cliff edge they could impart a greater influence by directly injecting rainwater into the fractures and defects within the Upper Matua Subgroup sediments. After a two month period of higher than average rainfall, the cumulative infiltrating water could then create a hydraulic head which increases the pore water pressures at the end of the Peninsula, to a point where a rainfall event can induce a piping failure resulting in a landslide. The factor which does not support this theory is that of the continual seepage present within the failure zone from the aquifer. In other words, soakage water exiting the aquifer must be related to some mechanism other than recharge at the end of the Peninsula. Therefore it can be concluded that the most probable model is a combination of soakhole-defect related hydraulic connections around the edges of the Peninsula and the pressure waves induced by hydraulic head-recharge in the foothills and Peninsula itself. This produces sufficiently high local exit velocities for piping failures to occur at the cliff faces.

5.3 STABILITY ASSESSMENT

5.3.1 Introduction

A stability analysis was undertaken for two main reasons. The first was to determine relative changes in the factor of safety (FS) on the introduction of a varying phreatic surface. The second was to ascertain the affect on the FS that an increasing landslide block would have using a non-circular failure plane and to compare these results to those obtained by consultants like Hegan (1995). One consideration when reading this section is that the stability calculations do not take into account the fact that a piping failure triggered the block landslide. As modelling of this type of scenario of aquifer flow, pore pressures within aquifer and lower cross-bedded sequence and other hydrological aspects, is a complex and large issue within it self, a simplistic approach has been adopted. Factors of safety have been calculated using a non-circular failure circle which differs from

previous stability assessments. In doing this the geometry of the failure circle has a dramatic influence on the factor of safety. Calculations were performed on all face logged cliff sections (Facelogs1-3, Map pocket) using results obtained during laboratory testing as well as some data from Bird (1981).

5.3.2 Previous Stability Assessment

a) Bird (1981)

Bird (1981) looked at the various analytical models available to him at the time to assess the stability of the cliff sections studied. Bird concluded that due to the geomorphology of the surface of rupture, models that considered a circular failure plane were not as applicable as those that considered a non-circular failure plane. Because of this he concluded that the Janbu's Simplified Method of stability analysis was suitable for slopes at Maungatapu. Bird carried out Bishop's Simplified method of stability analysis.

As noted by Hoek and Bray (1981) these two methods of slices are very similar in their approach and can be discusses together. Bird's analysis involved the used of computer programs such as Basic Plus and Jsiter.bas to produce a number of possible iterations for the factor of safety (FS). From idealised soils profiles with cohesions that ranged between 0-8 kPa, friction angles between 30-45°, and unit weights between 11-15 kN/m^3 (Figure 5.11) Bird looked at the effect of changing these values on the factor of safety. As expected he found that as these values increased, a corresponding increase in the factor safety was seen. Bird showed that the factor of safety increased from 0.9 to 1.4 with a corresponding increase in the cohesion from c'=0 kPa to c'=10 kPa respectively.

On the introduction of a phreatic surface Bird noted that the factor of safety dramatically decreased as the phreatic surface was increased in height. Bird also showed that with a 2m increase in the height of the phreatic surface a corresponding decrease of in the FS of at

least 1 occurred, e.g. FS dropped from 1.5 to 0.5 for one test site. Further to his calculations Bird concluded that the biplanar nature of the failure surface was in part due to the cohesive nature of the clay marker bed (lower aquitard), and was unrelated to the intact strengths of the silty sand/sandy mud above the (cross-bedded sequence). In addition, Bird determined that the triggering mechanism for the landslides was related to the high pore water pressures generated at the failure surface.

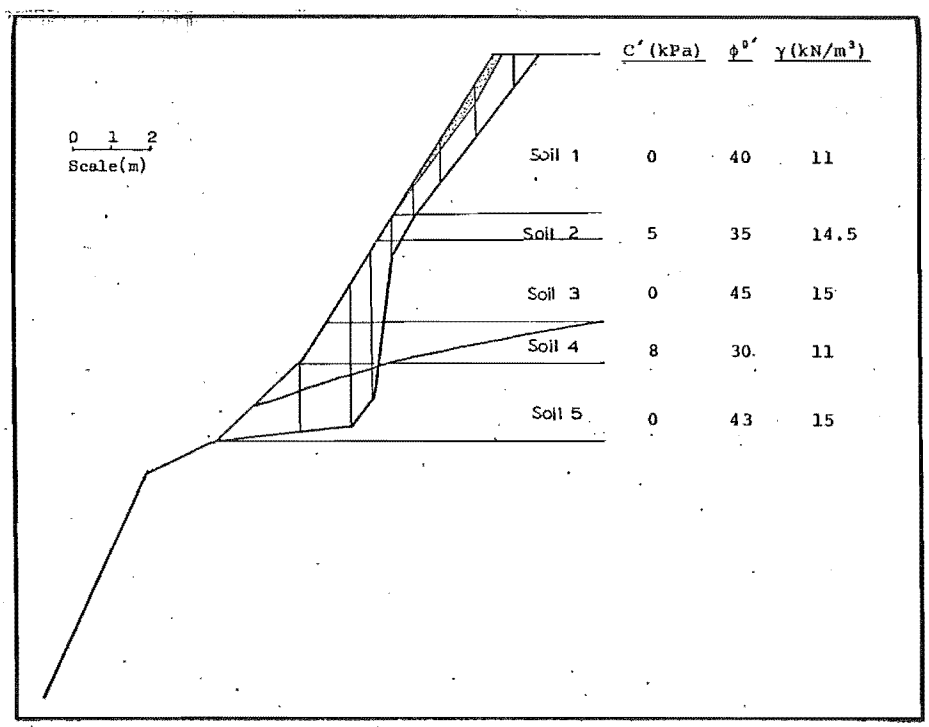

Figure 5.11 Soil profile for stability analysis from Bird (1981).

b) Hegan (1995)

Hegan (1995) produced a number of failure circles for 85 Te Hono Street with Factors of Safety ranging from 1 for the failed landslide to 1.25 and 1.40 for failure circles that project upwards to the conservatory and front of the house respectively (Figure 5.12). Due to the lack of laboratory data, assumptions were made on the relative strength parameters

of the soils associated with the stratigraphy of the cliff faces (Figure 5.12). In addition, it was assumed that the sand unit TG3 (Cross-bedded sequence) was fully saturated. Using the slope stability program UTEXAS 2 in conjunction with the defined strength parameters, factors of safety were calculated for three failure surfaces that projected upwards from the bottom of TG3 (Figure 5.12). Hegan (1995) believed that failure was initiated by a "blow out" in the loose sands (Unit TG3) which then undermined the slope above, resulting in a more or less steep circular failure within the above materials. He also suggested that the clay situated below Unit TG3 acted as an aquiclude, confining the loose sand from below, and that TG3 was possibly prone to fluidization when disturbed. The initiation of the "blow out" was concluded to be the result of increased groundwater pore pressures and/or seepage pressures, with vegetation impairing drainage conditions and further aggravating the problem.

c) Oldham (1995)

Oldham (1995), looking at the residential development of a property on the north-western side of Maungatapu, conducted site investigations involving geotechnical logging of the underlying soils. Strength parameters derived for stability analysis resulted in bulk densities that ranged between 14-16 kN/m^3, cohesions and internal friction angles for the younger to older (Pahoia Tephras) ashes ranging between 2-4 kPa and 32° respectively, with the Tauranga Beds (Cross-bedded sequence) predicted to have a cohesion of 22 kPa and a friction angle of 36°. Stability analysis involved the use of circular failure planes using Bishop's Simplified method. Originally Oldham projected the failure circle from the toe of the cliff back up behind the cliff edge with a factor of safety of 1.53 (Figure 5.11). However this was drastically revised after a landslide 150 m north of this study site in which another consultant firm (unknown) suggested that a slip had accrued immediately above the upper surface of the clay horizon (lower bounding aquitard). Because of this Oldham recalculated his factors of safety with a failure circle that is projected from this new denoted failure zone back up towards the top of the cliff (FS=1.5, Figure 5.11).

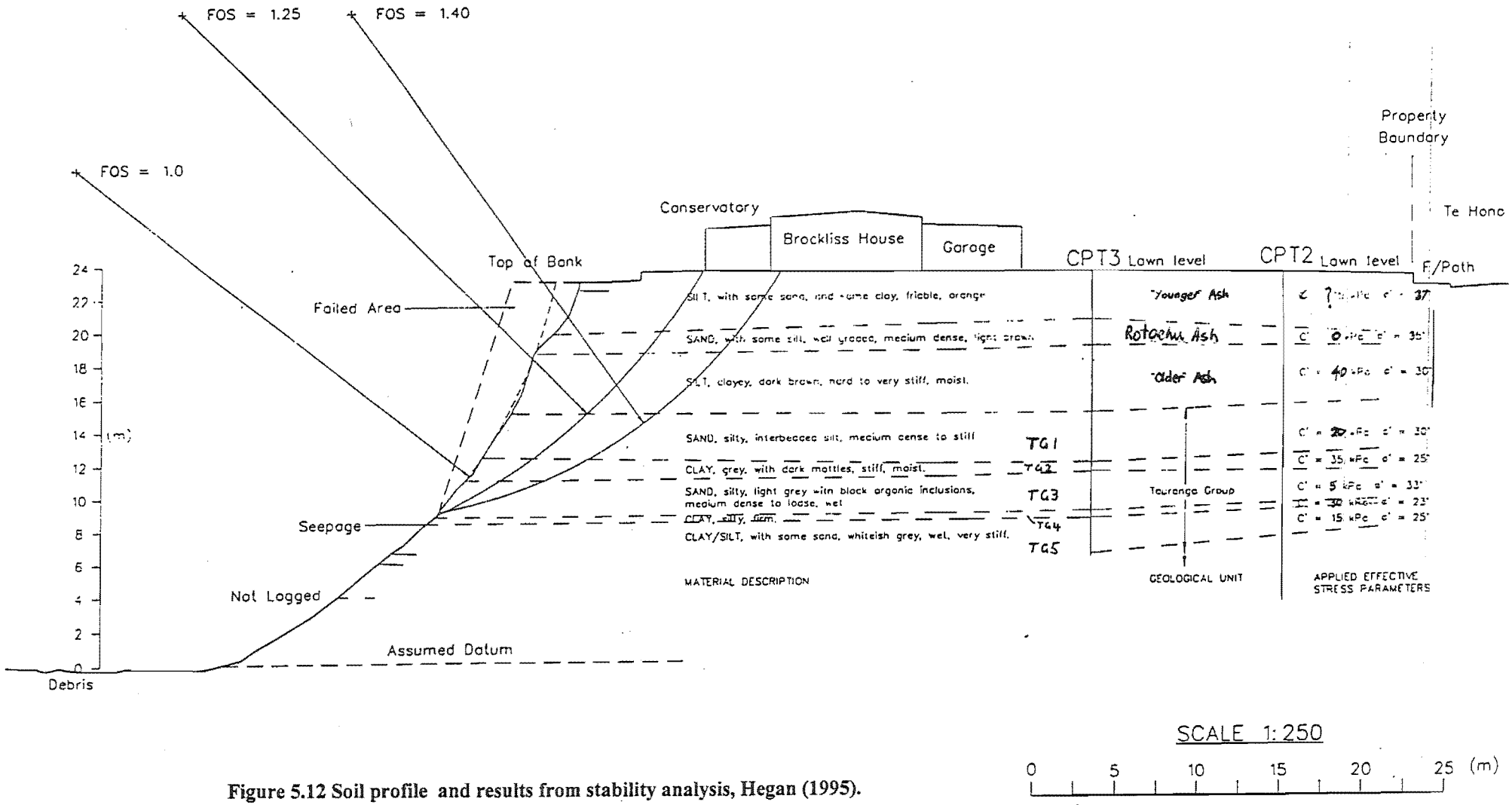

Figure 5.12 Soil profile and results from stability analysis, Hegan (1995).

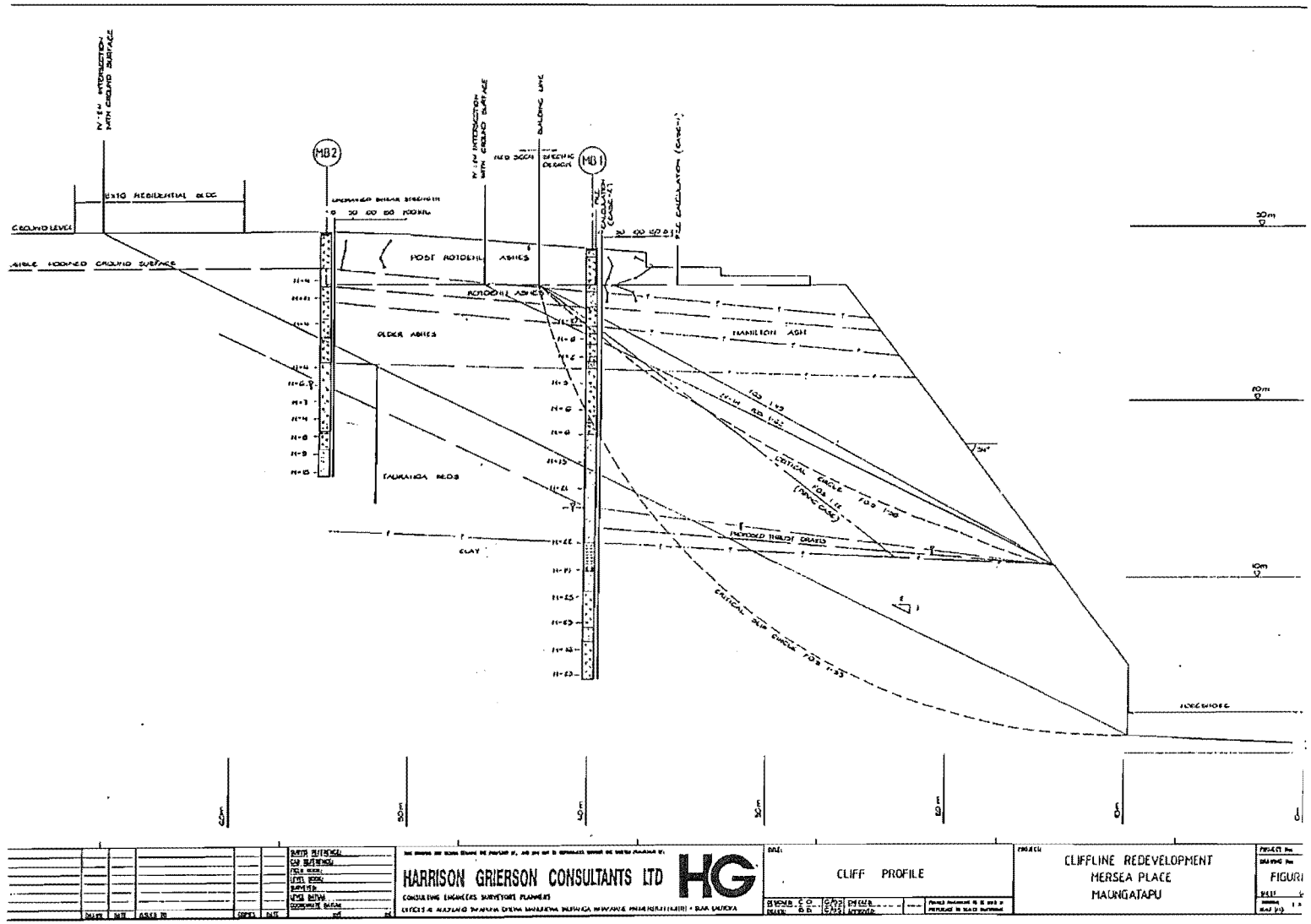

Figure 5.13 Results from stability assessment of a property at Mersea Place, Oldham (1995).

d) Discussion

Bird (1981), Oldham (1995), and Hegan (1995) all derived factors of safety from stability models using circular failure planes (apart from the Janbu's Simplified Method). From field and laboratory investigations during this study it is believed that a piping failure or "blow out" as Hegan (1995) suggests is the triggering mechanism which produces landsliding. This piping failure removes the soil material from the aquifer, upper aquitard, and lower section of the cross-bedded sequence therefore removing the support for the soil material above. This induces a block to slide down and outwards along one or more exfoliation defects, breaking up as it travels down slope. As it is a block failure, it is suggested that a stability failure model should be used that reflects the non-circular nature of the failure surface morphology. Because of this, circular failure surfaces producing FS values of 1.25 and 1.40, such as those delineated by Hegan (1995), suggest to not represent the failure dynamics of the Peninsula as well as a non-circular one. Therefore, it is believed that is these larger circular failures will tend not to occur (Hegan 1995 circular failure with FS=1.40), where as instead smaller block landslides as seen in 1979, and 1995 will in fact occur. However in saying this, a steep circular failure plane roughly orientated along a similar path to an already existing failure plane as indicated by Hegan (1995) for a factor of safety of 1, may provide a reasonable estimation of the factor of safety in many cases. Oldham's (1995) original failure circle calculating a FS=1.53 does not represent the actual morphology of the landslides around the Peninsula and should not be used.

5.3.3 Stability Analysis

a) Introduction

A stability analysis was performed in this project for a number of reasons. The first was to reassess factors of safety for particular cliff areas, such as those at 85 and 89 Te Hono Street, taking into account the actual geometry of the failure surface as determined within this study. The second was to estimate how much of an influence the introduction of an

this study. The second was to estimate how much of an influence the introduction of an increasing phreatic surface will have on the factor of safety. The third reason was to assess how much the factor of safety changes when considering progressively increasing landslide blocks (Figure 5.14). An increasing phreatic surface was introduced in stability analysis in response to the evidence of varying piezometric water levels within the Peninsula. From piezometric water levels interpretations in Chapter 3, showed the water levels varied by approximately 1m from early July to late September. For analysis these water levels were interpreted as representing a specific phreatic surface. An increasing landslide block was used to determine factor of safety values to evaluate the possibility of larger landslide blocks than those seen at of properties such as 85 Te Hono Street, and to compare these results obtained to the data of Hegan (1995).

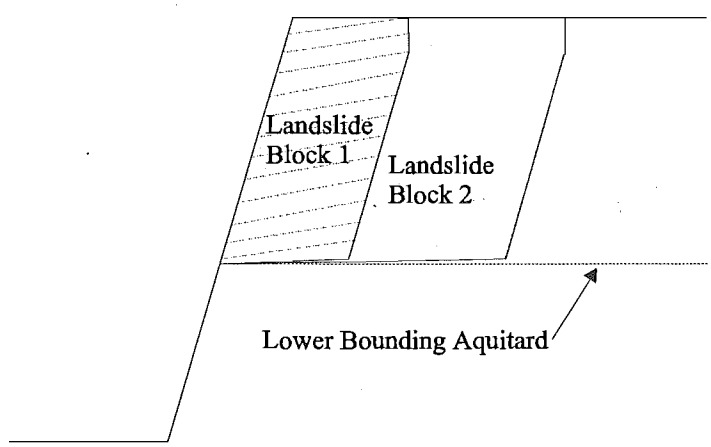

Figure 5.14 Schematical representation of differing sized landslide blocks used to determine how much the factor of safety increases with increasing block size.

There are various methods available which can be used to analyse the stability of a slope. These include Bishop's Simplified methods of slices, Janbu's Simplified method, and Sarma's method. A review these methods can be obtained in any geotechnical publication like Anderson and Richards (1987) or Spangler and Handy (1982). During the field investigation stage of the project three face logs were produced (FL 1-3-map pocket). Face

logging demonstrated that the geomorphology of the failure planes was non-circular (Figure 5.13). This meant that the best method of stability analysis would have to be able to consider non-circular failure planes. For ease of processing and reproducibility of results, a slope stability program "Galena version 2" was used as produced by BHP Engineering Pty Ltd. (1991-1994). Galena provided a number of options from calculating factors of safety to back analysis using either one method or a combination of the three from Bishop's Simplified method (suitable for circular failure surfaces), Spencer-Wright method (suitable for circular and non-circular failure surfaces), or the Sarma method (suitable for more complex problems particularly where non-vertical slice boundaries (such as faults) are significant). Methodology for running Galena can be viewed in the users' guide. For this study the Sarma method was used for stability analysis. Data used in the analyses was obtained from laboratory testing completed during this study as well as some results from Bird (1981).

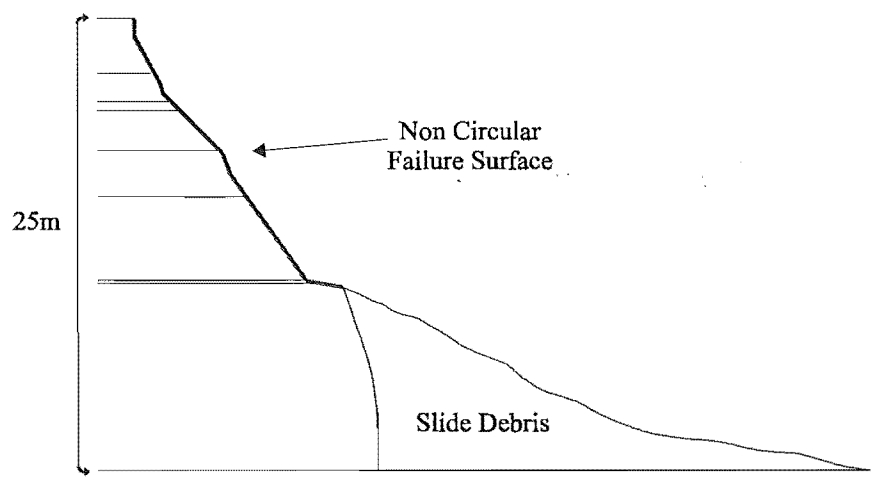

Figure 5.15 Schematic representation of a non-circular failure surface from 85 Te Hono Street.

b) Idealised Soil Profile

Due to the numerous beds associated with the Post-Rotoehu Ash Tephras, Rotoehu Ash, Hamilton ash, and the Upper Matua Subgroup the soil profile has been divided into 10 units. These are given in Table 5.3 with cohesion, friction angles, unit weights, and plasticities (as specified for stability analysis by BHP Engineering) which were obtained

from laboratory testing. If these values are compared to Hegan's (1995) predicted values (Figure 5.12) it can be seen that they differ from the laboratory data obtained during this study, and that of Bird (1981). Hegan has used cohesion values which have a greater range (0-40 kPa), whereas the data used for stability calculations for this study range from 0-22 kPa (Table 5.4). Hegan's data will have the effect of increasing the factors of safety for the slope. However, this is not to say that cohesion and friction angle data predicted by Hegan are necessarily incorrect, as it is believed that certain beds will exhibit higher cohesion than indicated during this study. Conversely, friction angles obtained from laboratory testing demonstrated higher angles than those predicted by Hegan (1995), indicating that there are still a number of unresolved issues in relation to stability analysis in Tauranga.

Table 5.3 Data used in stability analysis consisting of cohesion, friction angles, unit weights, and plasticities obtained from laboratory testing.

Unit 1	Stratigraphic Unit		c'	ϕ	γ	PI
1	Post-Rotoehu Ash Tephras		1	40	13	N/D
2	Rotoehu Ash		0.3	37	14	N/D
3	Palaeosol		5.6	31	15	37
4	Hamilton Ash		8.7	32	15	68
5	Upper Matua Subgroup	Pohoia Tephra	0	38	16	N/D
6		Cross-bedded sequence	0 / 22	36	17	16
7		Upper Bounding Aquitard	19	18	17	N/D
8		Aquifer	0	35	20	N/D
9		Lower Bounding Aquitard	24	22	17	N/D
10	Stratigraphy Below The Lower Aquitard		8	38	18	N/D

Table 5.4 Comparison of c' and ϕ' data from Hegan (1995) to the data used for this study.

Hegan Data			Study Data		
Stratigraphic Unit	c'	ϕ'	Stratigraphic Unit	c'	ϕ'
Younger Ash	?	37	Post-Rotoehu Ash Tephras	1	40
Rotoehu Ash	0	35	Rotoehu Ash	0.3	37
Older Ash	40	30	Palaeosol	5.6	31
			Hamilton Ash	8.7	32
TG1	20	30	Pahoia Tephra	0	38
TG2	35	25			
TG3	5	33	Cross-bedded Sequence	0 / 22	36
			Upper Bounding Aquitard	19	18
			Aquifer	0	35
TG4	30	23	Lower Bounding Aquitard	24	22
TG5	15	25	Lower Stratigraphic Units	8	38

c) Results

Factors of safety were calculated by varying the phreatic surface, block size, and cohesion of material 6 (cross-bedded sequence), for the logged cliff section at 85 Te Hono Street using a non-circular failure plane (Figure 5.16). Varying the cohesion of material 5 from 0 to 22 kPa produced FS of 1.3 and 1.5 respectively (Table 5.5), and with the introduction of a phreatic surface situated 9.3m below the ground (which related to the maximum piezometric level seen in Piez 1/3 (Chapter 2)), the FS decreases by 0.3 to 1.0 and 1.2 for c'=0 and 22 kPa (Table 5.5). Decreasing the phreatic surface further so it is situated within the cross-bedded sequence approximately 12 m below the ground surface (Figure 5.16), a corresponding increase in the FS of 0.2 was seen with FS = 1.2 and 1.4 for c'=0 and 22

kPa. If the phreatic surface is set at the top of the aquifer, FS are equivalent to those values obtained when no water is present within the soil profile (Table 5.5).

In addition to factors of safety being calculated for phreatic surfaces, they were also produced for increasing block size. If the landslide block is increased in size by 1m (Figure 5.17) the FS increased by 0.1 to 1.4 and 1.6 for c'=0 and 22 kPa respectively. Further to this if the block is increased 5m the FS increases to 1.7 and 1.9 for a c'=0 and 22 kPa respectively. For comparison of FS data to that obtained by Hegan (1995) a landslide block was extended back from the cliff edge by 15.1m (equivalent to that of a FS=1.4, Figure 5.10), using a non-circular failure geometry (Figure 5.17). Factors of safety of 2.3 and 2.4 were obtained for c'= 0 and 22 kPa respectively. The result obtained from stability analysis of a 15.1m landslide block shows a factor of safety a lot higher than that obtained by Hegan (1995) of 1.4 (Figure5.12).

The factors of safety for the logged cliff section at 89 Te Hono Street produced values that were 0.3 lower than the calculated FS for 85 Te Hono Street (Table 5.5). A phreatic surface was also located approximately 9.4m below the ground (Figure 5.18) equating to FS of 0.9 and 1.1 for c'=0 and 22 kPa respectively. These values were 0.1 lower than those calculated for 85 Te Hono Street. On lowering the phreatic surface to 11.1 m below the surface no change in the FS occurred (Table 5.5). Further lowering it to 13.2 m, and to the top of the aquifer the FS increased to 1.0 and 1.2 respectively (for a c'=0 and 22 kPa). Increasing the possible landslide block by 1m saw a increase in the FS of 0.1 as that demonstrated by 85 Te Hono Street to 1.1 and 1.3 for c'=0 and 22 kPa respectively (Table 5.5). However, on increasing the block by 5m (Figure 5.19) an increase in the FS of 0.3 was observed (Table 5.5). As with 85 Te Hono Street the block was increased so that it was 15.1m from the cliff edge (Figure 5.19) equating to a FS of 2.0 and 2.3 for a c'=0 and 22 kPa respectively. The non-circular failure surface used in stability calculations for 89

Te Hono Street was the closest to having a circular failure geometry. However, the FS do not coincide to Hegan's calculate FS of 1.4 for 85 Te Hono Street.

Table 5.5 Summary of c and ϕ data for an increasing phreatic surface and landslide block for 85 & 89 Te Hono Street, and 330 Maungatapu Road.

Calculated Factors Of Safety For Logged Cliff Face At 85 Te Hono Street		
	c'=0, ϕ=36°	c'=22, ϕ=36°
No phreatic surface (dry)	1.3	1.5
Phreatic Surface at 9.38 m below surface	1.0	1.2
Phreatic Surface at 12.22 m below surface	1.2	1.4
Phreatic Surface at top of aquifer	1.3	1.5
Increasing the block size by 1 m, no phreatic surface	1.4	1.6
Increasing the block size by 5 m, no phreatic surface	1.7	1.9
Increasing the block so it is located 15.1m back from the cliff edge	2.3	2.4
Calculated Factors Of Safety For Logged Cliff Face At 89 Te Hono Street		
	c'=0, ϕ=36°	c'=22, ϕ=36°
No phreatic surface (dry)	1.0	1.2
Phreatic Surface at 9.4 m below surface	0.9	1.1
Phreatic Surface at 11.1 m below surface	0.9	1.1
Phreatic Surface at 13.2 m below surface	1.0	1.2
Phreatic Surface at top of aquifer	1.0	1.2
Increasing the block size by 1 m, no phreatic surface	1.1	1.3
Increasing the block size by 5 m, no phreatic surface	1.4	1.6
Increasing the block so it is located 15.1m back from the cliff edge	2.0	2.3
Calculated Factors Of Safety For Logged Cliff Face At 330 Maungatapu Road		
	c'=0, ϕ=36°	c'=22, ϕ=36°
No phreatic surface (dry)	1.7	1.8
Phreatic Surface at 4.6 m below surface	1.6	1.7
Phreatic Surface at 6.8 m below surface	1.6	1.7
Increasing the block size by 1 m, no phreatic surface	1.7	1.9
Increasing the block size by 5 m, no phreatic surface	2.0	2.4

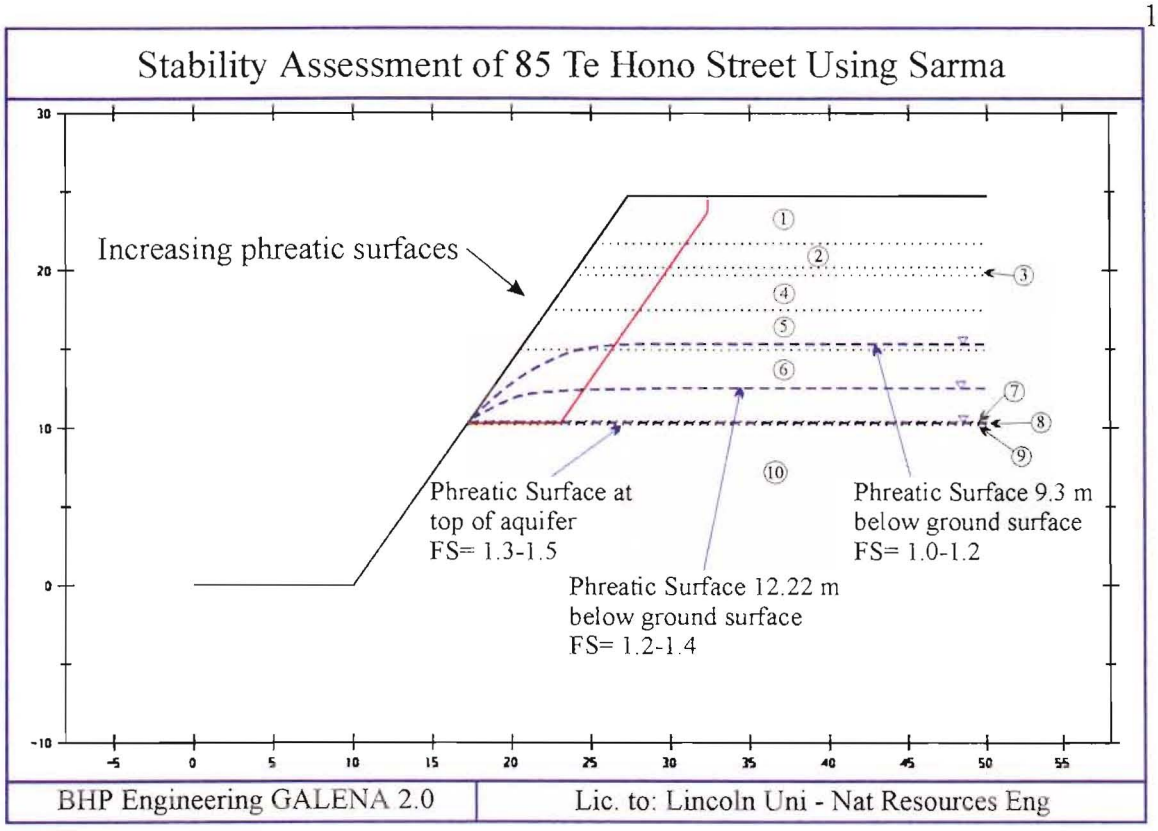

Figure 5.16 Determination of the effect on the factor of safety when an increasing phreatic surface is introduced for 85 Te Hono Street

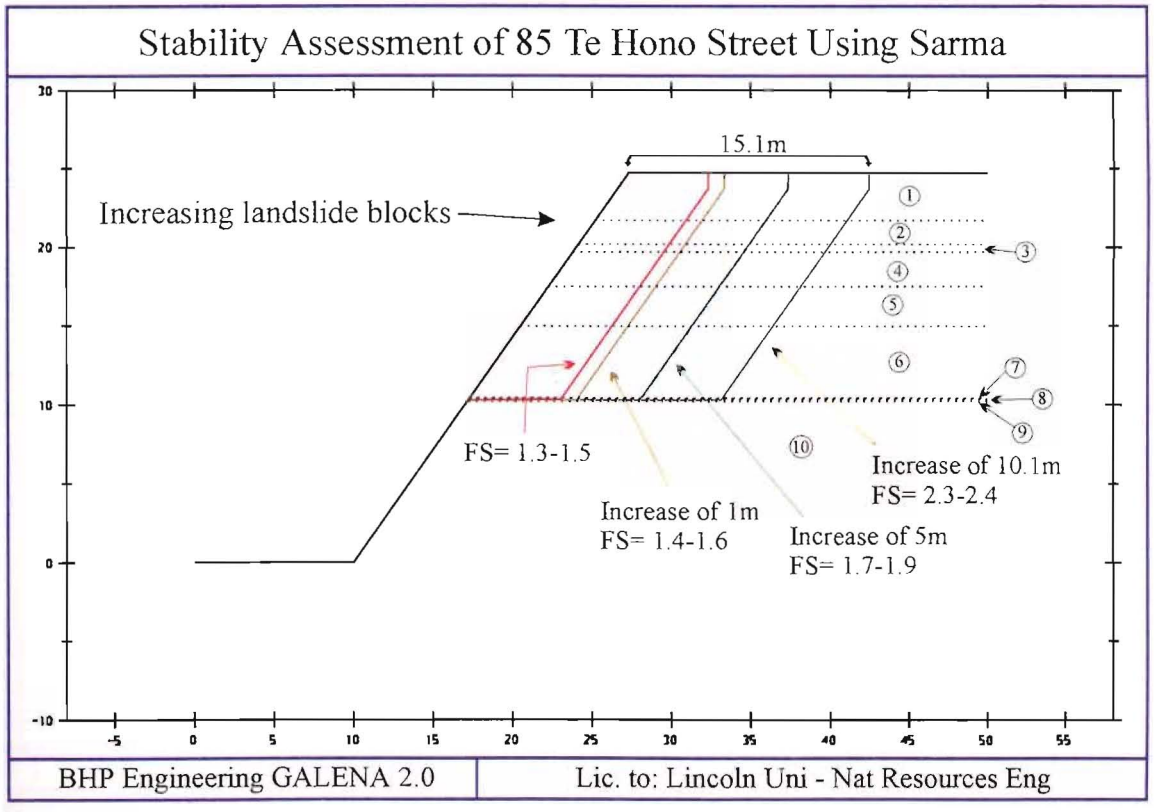

Figure 5.17 Determination of the effect an increasing landslide block size has on the factor of safety for 85 Te Hono Street.

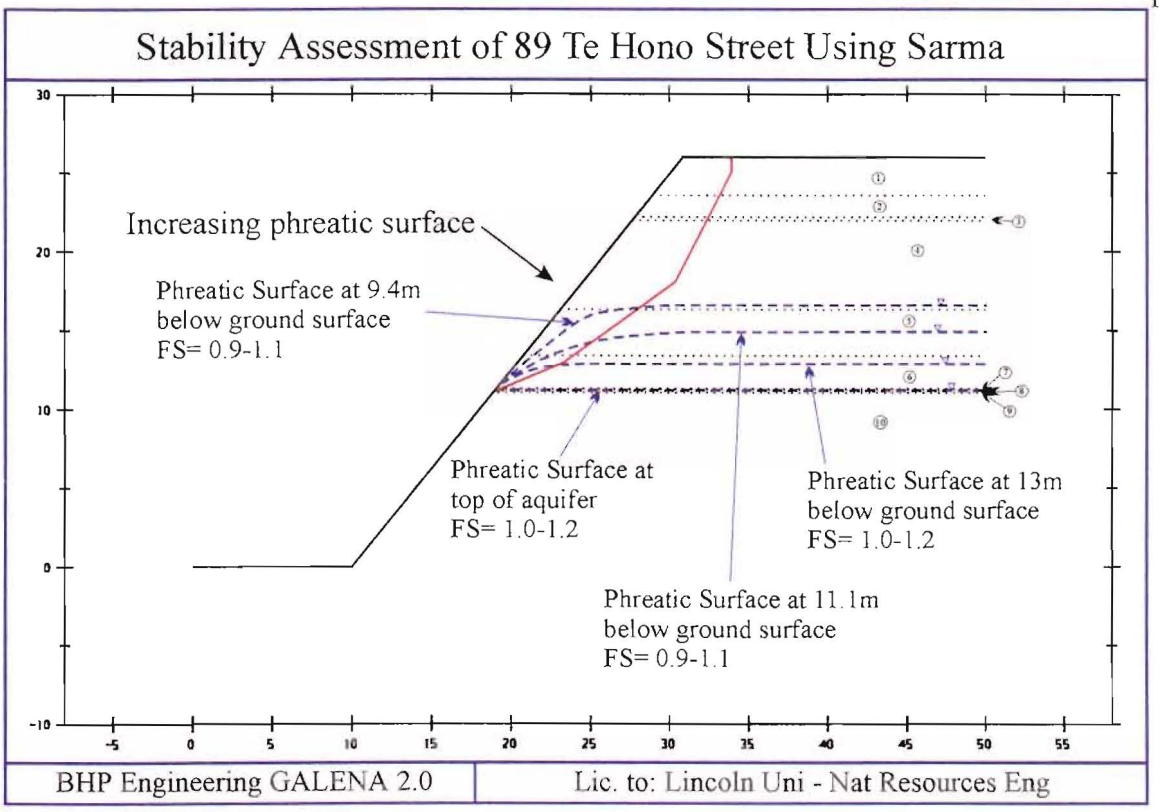

Figure 5.18 Determination of the effect on the factor of safety when an increasing phreatic surface is introduced for 89 Te Hono Street

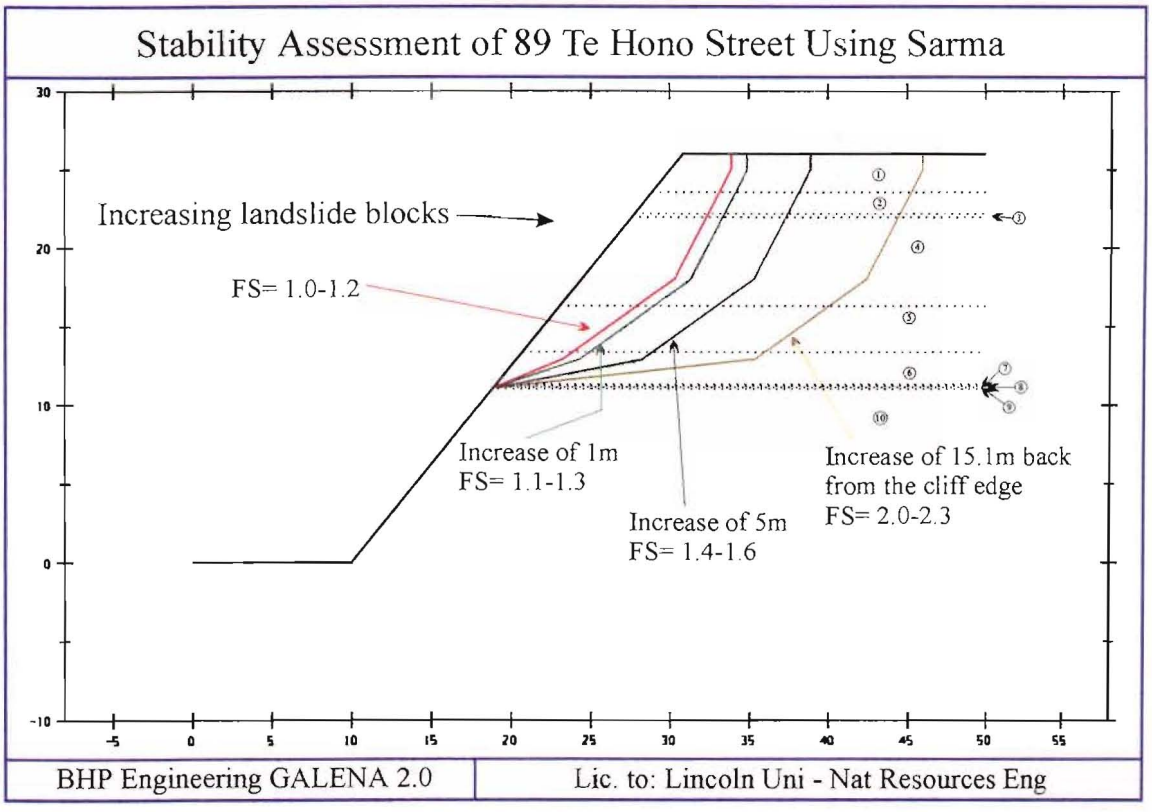

Figure 5.19 Determination of the effect an increasing landslide block size has on the factor of safety for 89 Te Hono Street.

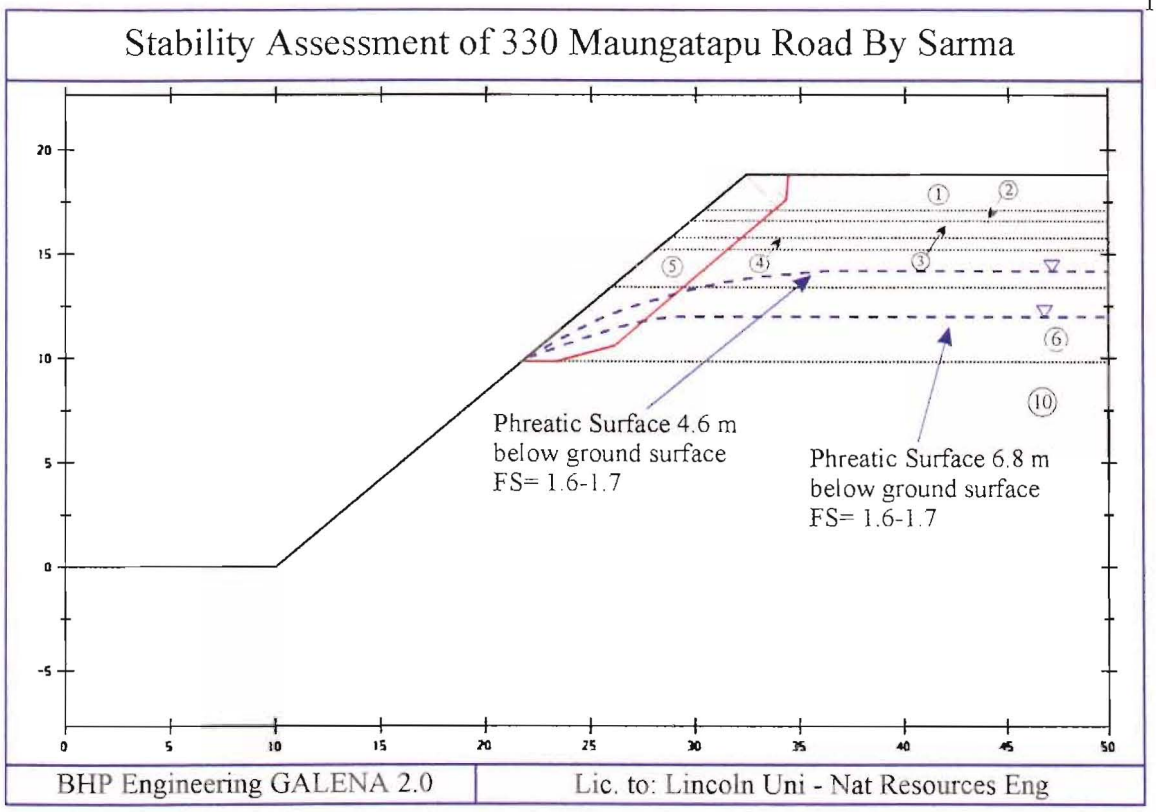

Figure 5.20 Determination of the effect on the factor of safety when an increasing phreatic surface is introduced for 330 Maungatapu Road.

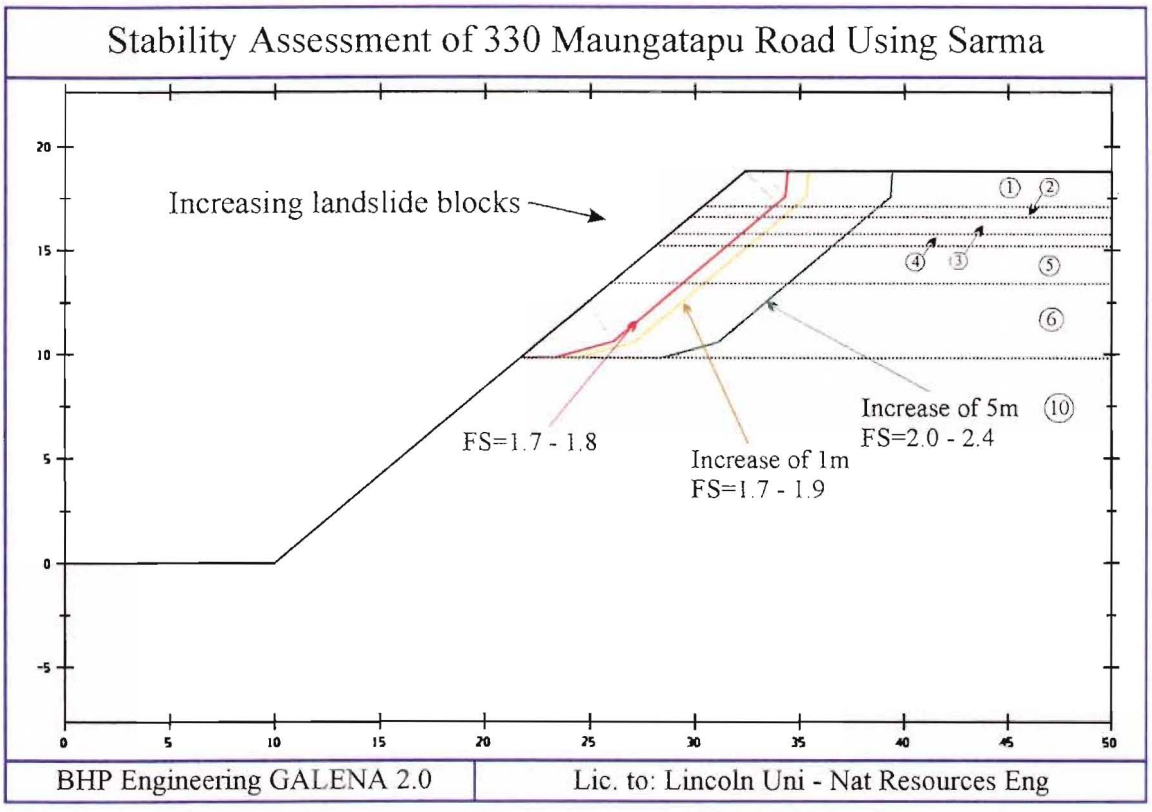

Figure 5.21 Determination of the effect an increasing landslide block size has on the factor of safety for 330 Maungatapu Road.

330 Maungatapu Road is located on the north western side of the Peninsula and is difficult to compare factors of safety with those obtained at 85 and 89 Te Hono Street due to differences in stratigraphy and failure surface geometry. Because the cliff face had been logged after the failure had occurred, it was difficult to extrapolate the unfailed cliff areas on either side across the failed section. This was mainly due to heavy landscape work which had altered the surface geometry of the cliff face before the landslide. This meant that an approximate original cliff profile has been used. Also in the case of the stratigraphy no discernible upper bounding aquitard could be found to separate the lower section of the cross-bedded sequence from the aquifer. It was therefore decided to treat this entire unit as the cross-bedded sequence. Factor of safety calculations for the cliff section with no phreatic surface yielded FS values of 1.7 and 1.8 for c'=0 and 22 kPa respectively. On the introduction of a phreatic surface (Figure 5.20) there was a decrease in the FS by 0.1 to 1.6 and 1.7 (Table 5.5). However on decreasing the phreatic surface no appreciable decline in the FS was observed. Calculations from increasing the landslide block by 1m produced a small change (Table 5.5). Further increasing the block by 5m in size saw a corresponding increase in FS to 2.0 and 2.4 for c'=0 and 22 kPa respectively (Figure 5.21).

5.3.4 Discussion

Results from factor of safety calculations provide a relative indication of stability of a particular cliff soil profile. But it should be kept in mind that these values more than likely do not reflect the complicated multi-layered geology of the Peninsula. In addition to this it has to be remembered that failure of the landslide block, such as that at 85 Te Hono Street, is related to the amount of material removed from the failure zone during the piping failure. This reduces the strength of the supporting material to virtually zero, allowing the block to fail on one of many exfoliation defects which will have c'=0 kPa. Because of this, producing a failure surface through the intact material will not truly reflect the in-situ conditions before failure. However, it is believed that stability calculations will give a

general indication of the influence of the introduction of an increasing phreatic surface and an increasing landslide block size.

From stability calculations, 85 Te Hono Street under dry conditions is more stable than 89 Te Hono Street under dry conditions. If c'=0 kPa for 89 Te Hono Street a FS=1.0 indicating that the slope is on the verge of failing, therefore with the introduction of a phreatic surface the FS decrease to 0.9. However from field investigations, no landslides occurred during the highest recorded piezometric water level for Piez 1/3 in 1996 is equal to a phreatic surface situated 9.4m below ground level. This indicates that the strength of the soils has been underestimated, therefore cohesions can be increased to similar values as indicated by Hegan (1995). At the time the slips occurred in May of 1995 no piezometers were installed to record water levels. This therefore made it difficult to ascertain what a maximum piezometric water level would be needed to produce failure and how sufficiently this would affect the FS.

Using the failure circle geometry denoted from field investigations the landslide block can be increased to ascertain how difficult it would be for a larger landslide to occur. From calculations, increasing the block size by 1m the FS only increased by 0.1. This means that with slightly higher pore water pressures than those that would have occurred in 1995 may be enough to induced failure of a block this size. Further increasing the block size to 5m saw a 0.4 increase in FS. This begins to suggest that in order for a larger block of this size to fail the pore pressures will have to be considerably higher. It is believed that for an approximately 10m block to fail at one time is highly unlikely given the circumstances. Further more Hegan's (1995) calculations for the failure producing a FS of 1.4 (Figure 5.12) is very low when compared to FS of 2.3-2.4 (85 Te Hono Street) and 2.0-2.3 (89 Te Hono Street) obtained using a non-circular failure plane (Figure 17 and 19). This tends to suggest that blocks of this size failing are extremely unlikely. Supporting this is the

evidence from the field that the failing landslide blocks are normally approximately 5m in depth, involving the colluvium/topsoil and part of the underlying units.

To better understand the failure model more analysis has to be directed at the behaviour of the aquifer and lower section of the cross-bedded sequence before a better stability assessment will be more representative of in-situ conditions. This would involve the delineation of peak pore pressures that cause piping failures to occur, and how big an area within the failure zone will see a reduction in strength due to this mechanism. From further in-situ permeability testing and monitoring of piezometric water levels the construction of a flow net will better aid the assessment of cliff stability.

5.4 HAZARD IMPLICATION AND MITIGATION

5.4.1 Introduction

This section mainly deals with how the results presented in the previous two sections can be used to suggest implication to hazard policies and mitigation for Maungatapu Peninsula. Firstly, hazard implications deal with how the results from stability analysis can be used in suggesting alterations to the 2H:1V slope that has been employed as a guideline for ascertaining whether geotechnical evaluation needs to be performed on a property. Suggested hazard mitigation for this study involves looking at decreasing the pore water pressures within the aquifer and lower section of the cross-bedded sequence by reducing the amount of rainwater injected into the soakholes.

5.4.2 Hazard Implications

The landsliding seen around Maungatapu Peninsula represents a potential hazard to both people and property. Because of this the Tauranga District Council has produced a number of hazard maps which indicate where potential areas of instability could occur. These "potentially unstable areas" are derived from an investigation made by Houghton and

Hegan (1980), where after analysis of 17 deep seated failures at Omokoroa revealed a close approximation to a height/depth ratio of 2:1. This has been interpreted to mean by many consultants as a slope of horizontal to vertical (2H:1V), (Figure 5.19). However from Figure 5.19 it can be seen that the projection of this 2H:1V slopes up towards the top of the cliff, positions a hazard zone (Hazard Zone 2) well beyond the largest assessed landslide block. Even if the 2H:1V slope is projected upwards from the failure zone towards the top of the cliff, the hazard zone denoted (Hazard Zone 1) falls well behind the largest landslide block. The 5m and 10.1m landslide blocks produced factors of safety of 1.7-1.9 and 2.3-2.4 respectively, which indicates that property 10-15m back from the cliff face has a relatively lower hazard potential than 5m away which produces a factor of safety of 1.3-1.5.

The implication of introducing a hazard zonation scheme to an already heavily urbanised Peninsula has the effect of reducing the value of the properties around the cliff edge. In this case the projection of a 2H:1V slope upwards from the base of the cliff, creating Hazard Zone 2, is not representative of the failure models discussed in the previous sections and in Chapter 2. The creation of Hazard Zone 2 will result in the devaluation of houses within this zone that are in actual fact quite safe. Conversely even though Hazard Zone 1 reflects the geological constraints and failure dynamics, it would be difficult to define the starting point on the cliff face for the 2H:1V projection line because of colluvium/topsoil and vegetation cover. This means that a hazard zonation scheme should be developed that better reflects the geologic constraints. However, it is believed that instead of redefining the hazard zonation scheme on an already heavily urbanised peninsula such as Maungatapu, the best policy is to deal with each property by means of a site specific geotechnical assessment.

At the moment the Tauranga District Council uses an unofficial policy, where each consent is dealt with on its own merits. In order for this to be successful the expertise of

the Consents Officer has to be such that if he/she suspects that a hazard is associated with the site, then a geotechnical evaluation of the property must be undertaken. This statement within itself has further implications in that all hazards associated with an area have to be recognised in order for the Consents Office to perform their job effectively. In addition, the Council has a policy to "flag" a property that has a hazard associated with it. For instance, if a landslide has occurred on a property then that property is denoted as having a hazard associated with it. This is then in-putted into the GIS system as a "Land Hazard Register", and can only be removed if the property owner proves that the hazard no longer exists through a geotechnical evaluation. It is therefore recommended that the current policy be continued whereby each cliff top property is evaluated on its own merits.

5.4.3 Hazard Mitigation

The term "hazard mitigation" is used in this study to indicate possible means that will reduce the effect of geological and hydrogeological processes on people and property. The type of failure seen at properties such as 85 & 89 Te Hono Street occurred last time in 1979 and again in 1995, suggesting an occurrence interval of approximately once every 15-20 years. This figure is purely speculative as no information is available prior to 1979 landslides. At Maungatapu Peninsula the main triggering mechanism that induces landsliding is that of piping failure produced by excessive pore water pressures. Therefore reducing these pore water pressures will see a reduction in the potential hazard to cliff edge properties. The main mitigation technique suggested here involves the reduction of rainwater being directly injected into the stratigraphic units via soakholes.

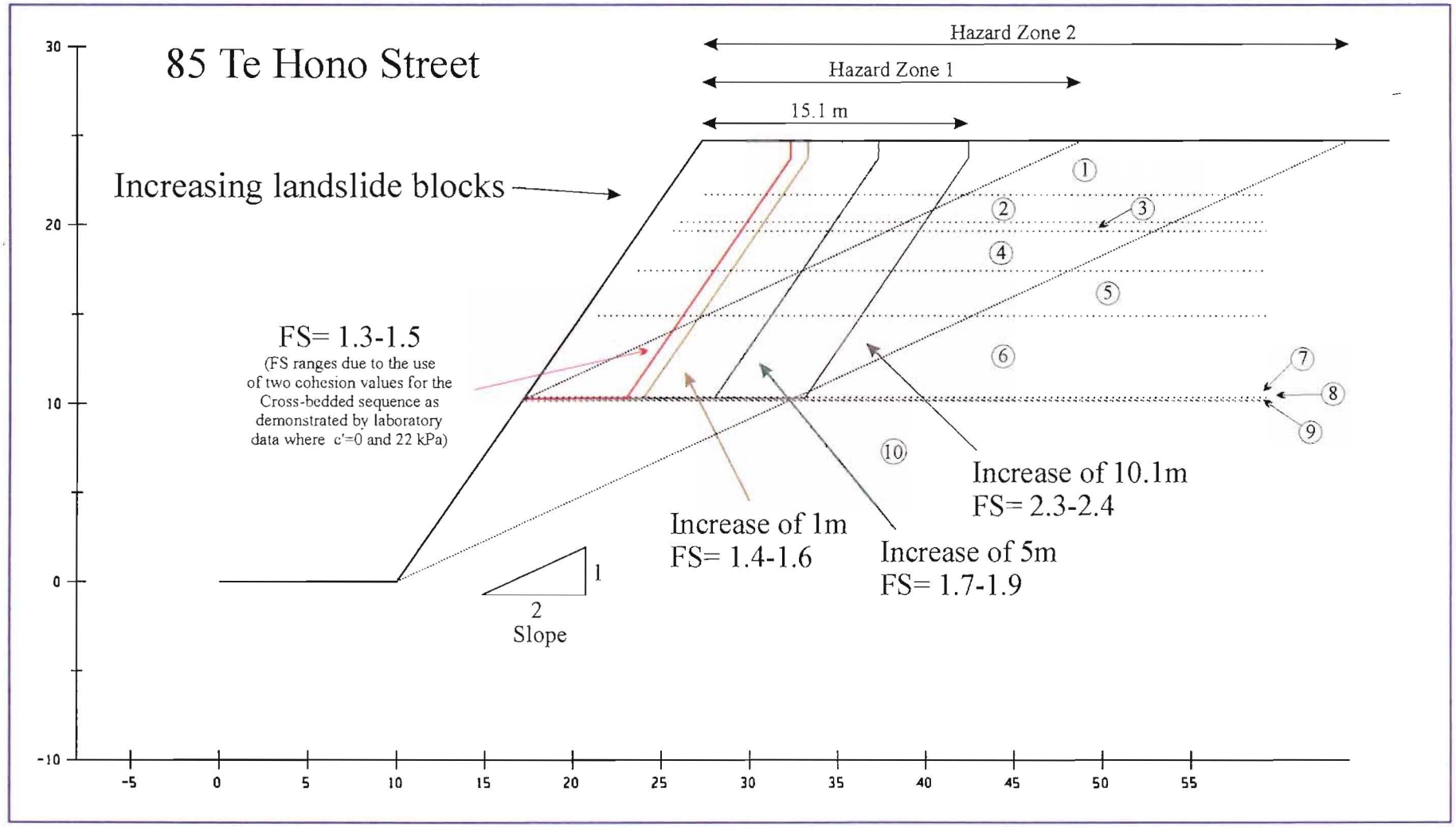

Figure 5.22 Assessment of the validity of the set back distance considering a slope angle of 2H:1V. It can be seen that the 2H:1V slope projected up from the base of the cliff lies approximately 24m inland from the largest proposed landslide block size (15.1m back from the cliff edge). This landslide block yields a FS=2.3-2.4 indicating that the 2H:1V slope is far too conservative a guideline to be used for assessment proposes.

a) Stormwater Disposal

During this study it has been suggested that soakage water is entering the Upper Matua Subgroup sediments such as the aquifer and lower section of the cross-bedded sequence through high flow hydraulic pathways consisting of exfoliation defects, and fractures etc. Bell (1995) recommended that a five stage process of elimination of stormwater disposal via soakage holes on Maungatapu Peninsula. These stages are:

1. Stage 1: Nos. 54-86 on the south-western side of Te Hono Street, as well as Nos. 27-43 on the southern side of Maihi Crescent, as those dwellings are directly up-gradient from the properties presently experiencing landslide damage.

2. Stage 2: Nos. 96-110 Te Hono Street, Nos. 10-40 on the northern side of Maihi Crescent, and Nos. 20-34 Te Wati Street.

3. Stage 3: All dwellings on the estuary side of the Te Hono Street that are not presently discharging to the street or to another approved outfall.

4. Stage 4: All other dwellings located on Te Hono Street, Maihi Crescent, and Te Wati Street.

5. Stage 5: Other parts of the Maungatapu Peninsula in an order of priority to be decided following further geotechnical evaluation.

To date the first three stages have been completed and it is recommended that the fourth stage should be undertaken. This should considerably reduce the potential hazard of landsliding along the Te Hono Street cliff edge. The fifth stage can now be redefined to include properties on the north-western side of the Peninsula from Nos. 300-446 Maungatapu Road, and 2-34 Wikitoria Street. Evidence of landsliding along the rest of the Peninsula would also suggest that progressive reticulation of stormwater should be completed in a number of further stages.

5.4 SYNTHESIS

This chapter was divided into three sections; hydrogeological assessment, stability analysis and geotechnical implications. The objective of the hydrogeological assessment was to understand the possible regimes that could produce the increased pore water pressures at the edges of the Peninsula. Firstly the "Modified Babbage Model" was developed to provide volumetric constraints to ground water soakage in relation to Maungatapu Peninsula. This resulted in estimating that approximately 20% of the rainwater falling on the Peninsula is collected by the roofs and driveways of houses and directed into soakholes. Therefore from a rainfall event of 80mm for a 24 hour period, 67,200 m^3 of rainfall is absorbed into "undeveloped" land while 25,600 m^3 of rainfall is directed into soakholes. This was then taken a step further to try and quantify how effective soakholes are at dissipating the volume of water which enters them. From a soakhole with dimensions of ϕ=300mm and d=4m, for a 24 hour rainfall event of 80mm, it was calculated that the soil soakholes surrounding a soakhole had to absorb $4m^3$ of rainwater into a soakhole with a volume of $0.28m^3$. As no indication during the field investigation stage of this study suggested that surface flooding occurred during these high rainfall events from over-topping of the soakholes, it was concluded that they could dissipate volumes of this magnitude easily.

From this a hydrogeological model was developed using data obtained during field and laboratory investigations. The first consideration involved the lag times derived from piezometric response to rainfall. Lag times between 24 and 96 hours were delineated which equate to permeabilities of 1.5×10^{-4} and 3.8×10^{-5}m/sec respectively. These permeabilities were produced by calculating the time it takes for the infiltrating rainwater to reach the slotted section of the piezometer assuming that in fact direct hydraulic connection existed from the surface. In order for this to occur assumptions were made that the rainwater infiltrated through from the surface, that $k_V=k_H$, and the water level in the piezometers reflects the unconfined water table in the Peninsula.

However, it was also noted that these permeabilities do not truly reflect the multi-layering of the peninsula soil units. Because of this a more representative model was developed called the "Stratigraphic Unit Profile Model". This model assessed the influence of the differing permeabilities of the beds associated with each unit, e.g. Post-Rotoehu Ash Tephras, Rotoehu Ash, etc. It was demonstrated by the construction of a simple wetting front model that the movement of soakage water through the soil profile was complex, with the wetting front moving out faster in areas of higher permeabilities than lower permeable areas. In addition, it was shown that a volume of water infiltrating through from a point on the surface would take a considerable amount of time to permeate to the aquifer. For instance, it would take 347 days for soakage water to travel vertically through a 3m section of the cross-bedded sequence, and this only represents approximately represent 20% of the soil profile depth. Because of this, other mechanism have to occur in order to produce the fast lag times of 24-96 hours.

Such mechanisms that have been suggested are exfoliation defects, fractures (e.g. shrinkage cracks), and bioturbation. It is believed that while fractures and bioturbation will affect the Peninsula as a whole, decreasing the overall permeability of the soil mass, exfoliation defects will provided a high permeability flow path for the soakage water to enter. This will have the affect of decreasing the time it takes for soakage water to be infiltrated through to the aquifer and the lower section of the cross-bedded sequence. However, this does not explain why the seepage out of the aquifer occurs all year around.

The likely scenario is that, in addition to the above defect-controlled infiltration, the aquifer is being recharged from areas outside the Peninsula as well as from rainfall on the Peninsula itself. This introduces the concept of pressure waves that are induced by changes in the hydraulic head in the Peninsula due to rainfall recharge both in the foothills and the Peninsula. This possibility could explain the fast lag times of 24-96 hours seen. It appears

for this system to become a dynamic one, in that a rainfall event is seen to produce a rise in piezometric water levels, it would take approximately two months of double the average rainfall accumulation within the Peninsula. At this time pore pressures at the edges of the cliff faces are at a higher enough level, that a reasonable rainfall event is enough to produce a piping failure resulting in a landslide. Therefore it can be concluded that the piezometric responses are an indication of pore pressures induced by changes in the hydraulic head on both a larger scale as recharge from rainfall in the foothills and Peninsula, as well as smaller scale recharges in relation to exfoliation defects. However, the piezometers do not pick up every rainfall event especially during the summer months when water and piezometric levels are low within the Peninsula. Rainfall at this time of year is absorbed into the Peninsula without a piezometric response.

Soakholes were also examined to try and distinguish how much of an affect they will have in reducing the lag times seen in Chapter 3. For the most part soakholes are believed to stop on hitting the Palaeosol, but there is evidence that a few around the head land of the Peninsula penetrated through the Palaeosol and Hamilton Ash into the Upper Matua Subgroup. Soakholes will have the affect directly injecting rainwater into the substrata, and around the edges of the peninsula into exfoliation defects. This means that around the cliff edges the more the soakholes penetrated the soil mass the more defects that they will intersect, therefore reducing lag times. Because approximately 20% of the rainwater is intercepted by roofs and driveways is directed into soakholes, they may have a significant affect on the stability of the cliff section around the peninsula. This has lead to a staged reticulation of the peninsula which involves taking the rainwater that once discharged into the soakholes and discharging it to the estuary via the roads stormwater system. This will reduce the affect that soakholes will have on increasing the pore water pressures within the aquifer and lower section of the cross-bedded sequence. Another way of reducing these high pore water pressures is through the construction of a retaining wall at the failure zone to allow free drainage of soakage water but not soil material out of the slope.

A hydrogeological assessment stability analysis was undertaken to determine the affect to the factor of safety that an increasing phreatic surface and landslide block would have. An increasing phreatic surface was introduced to the stability analysis in response to the evidence of varying piezometric water levels within the Peninsula, where a specific piezometric water level is interpreted as a phreatic surface. An increasing landslide block was used to determine factor of safety values to evaluate the possibility of the failure of larger landslide blocks compared to those of properties such as 85 Te Hono Street, and to compare the results obtained to the data of Hegan (1995). Analysis involved the use of a soil profile model that was divided up into 10 separate materials that corresponded to the various stratigraphic units. Two cohesions values were used for material 6 (c' = 0 & 22 kPa) which represented the Cross-bedded sequence. This was done in response to results obtained from laboratory testing, where a range of cohesions were produced. From field investigations it was decided that a non-circular failure surface should be adopted, because it reflected the non-circular failure geometry of the failure surface. Most other people who have performed stability analysis in Tauranga have used methods involving a circular failure circle such as Bishop's Simplified method. 89 Te Hono Street, which failure most closely approximated a circular failure, produced the lowest factor of safety for dry conditions of 1.0 and 1.2 for c'=0 and 22 kPa respectively. 85 Te Hono Street and 330 Maungatapu Road produced a relatively higher factor of safety indicating that they were stable under dry conditions. However, when an increasing phreatic surface was introduced the factor of safety decreased by 0.1 to 0.2. When the phreatic surface was set at the highest recorded piezometric water level for 1996 (9.3m below the ground surface), 85 Te Hono Street produced a factor of safety of 1.0-1.2, 89 Te Hono Street produced a FS = 0.9-1.1, and 330 Maungatapu Road had a FS = 1.6-1.7. All of these factors of safety indicate that the cliff section is relatively stable at a high phreatic surface.

Stability analysis of landslide blocks using a failure circle geometry as seen in the field showed that factor of safety for 85 Te Hono Street ranged between 1.3 and 1.5, 89 Te Hono Street FS ranged between 1.0 and 1.2, and 330 Maungatapu Road FS ranged between 1.7 and 1.8. Increasing the landslide block by 1m resulted in a corresponding increase in that FS of 0.1. Further increasing the landslide block by 5m a corresponding increase occurred in the FS of 0.3 to 0.4. These results indicate that failure of a landslide block 10m back from the edge of the cliff was highly unlikely. The increasing the landslide block by 15.1m back from the cliff edge produced a range in the factor of safety between 2.0 and 2.4, which was considerably higher than the FS of 1.4 obtained by Hegan (1995). From these results it is demonstrated that the using a non-circular failure plane as evident in the field, increases the factor of safety considerably and is more representative of in-situ flat lying geology. However it is difficult to properly judge the affect of the high pore water pressures and how these influence the factor of safety due to the complex nature of the hydrogeology.

Using the result obtained from stability analysis of an increasing landslide block size, comparisons can be made to stability data produced by other people, especially that of Houghton and Hegan (1980). Houghton And Hegan (1980) after analysing 17 landslides from Omokoroa, produced a slope of 2H:1V which was informally adopted by the Tauranga District Council for use in assessing the potential cliff instability of a property. The projection of this 2H:1V slope line up from the bottom of the cliff up to the Peninsula surface, produces a geotechnical assessment zone that falls well behind most of the houses situated around the cliff edges. This has resulted in any consents for development of cliff edge property requiring a geotechnical evaluation. However, from analysis during this study it can concluded that the 2H:1V slope does not reflect the non-circular failure dynamics of the landslides such as those that occurred on properties like 85 Te Hono Street. Stability analysis of a landslide block which is situated approximately 10m back from the cliff edge indicates a very low potential for failure to occur with a factor of safety that ranges between 2.0 and 2.4.

Chapter Six SUMMARY AND CONCLUSIONS

6.1 THESIS OBJECTIVES

The principal objectives of this thesis were:

1. to carry out geotechnical investigations of the Maungatapu Peninsula area involving engineering geological mapping, geotechnical logging of the landslide scarps and borehole core, and sample collection to determine how geology and geomorphology influence landsliding;

2. to develop geotechnical models for the identified failure types;

3. to determine the geotechnical properties of the soil materials relevant to landslide assessment;

4. to assess the degree to which the hydrogeological regime influences failure types, and to develop a hydrogeological model;

5. to examine the hazard assessment guidelines for coastal landsliding, and to reassess these guidelines in relation to Maungatapu Peninsula.

6.2 PRINCIPAL RESULTS

6.2.1 Field Investigation Results

a) Engineering Geological Mapping

Engineering geological mapping delineated four types of failure around that Maungatapu Peninsula, these being probable large scale failures, piping-triggered block failures, wave erosion-triggered block failures, and colluvium/topsoil failures. In addition geomorphic features around the Peninsula were mapped at a scale of 1:5 000, indicating that virtually all of the cliff edges had at one time or another experienced some type of block or colluvium/topsoil failure. It appears from engineering geological mapping that the most affected areas are those properties located at the end of the Peninsula on the northeast side of Te Hono Street cliff edge sections. A number of failures were also seen at the end of Maungatapu Road on the northeastern and northwestern side of the Peninsula.

b) Geotechnical Core And Face Logging

From geotechnical core and face logging the site stratigraphy was divided into a number of units; from the top down, - as follows

14-15m

- Post-Rotoehu Ash Tephras (3m)
- Rotoehu Ash (1m)
- Palaeosol (0.5m)
- Hamilton Ash (3m)
- Pahoia Tephras (3m)
- Cross-bedded sequence (3m)
- Upper bounding aquitard (0.005m)
- Aquifer (0.2m)
- Lower bounding aquitard (0.3m)

Upper Matua Subgroup Sediments

The stratigraphic units dip towards the end of the Peninsula at approximately 1°, indicating an almost flat lying structure. There are areas where the Palaeosol and Hamilton Ash have been eroded out, suggesting that erosional processes have occurred throughout the history of the Peninsula's development.

c) Hydrological Investigations

1. Plots of piezometric water level response to rainfall/cumulative rainfall showed seasonal change in piezometric water level of approximately 1-2m from a high in September-October and a low in January-February.

2. Fast lag times of 24-96 hours were delineated from piezometric water level responses to rainfall events. From these lag times a simplistic "uniform permeability model" was developed which was used to calculated an average vertical permeability ($=k_H$) range of 3.0×10^{-4}-3.8×10^{-5} m/sec for the stratigraphic units present (Post-Rotoehu Ash Tephras, Rotoehu Ash, Palaeosol, Hamilton Ash, Pahoia Tephras, and Cross-bedded sequence).

d) In-Situ Permeability Testing

Using the Hvorslev Slug test and the Bouwer and Rice Slug test methods, two permeability values were obtained for the Cross-bedded sequence of k= 8.3×10^{-6} and 6.6×10^{-7} m/sec, which was comparable to the permeability of 2.1×10^{-7} m/sec determined by Bird (1981).

e) In-situ Shear Strength Testing

Shear strengths obtained form a Pilcon shear vane varied throughout the stratigraphy considerably, with the majority of strengths ranging from 20-200 kPa. Beds with a unified soil classification of SM or ML demonstrated for the most part shear strengths between 100-200 kPa. Conversely, beds with a unified soil classification of SW or SP tended to produce lower shear strengths of about 20-100 kPa. Overall the stratigraphic units demonstrated quite high shear strengths, and from Table 6.1 it can be seen that the Palaeosol represents the strongest unit, while the aquifer is the weakest with a shear strength that ranged between 20-80 kPa.

Table 6.1 Summary of in-situ shear strengths test results

Stratigraphic Unit	Shear Strength (kPa)
Post-Rotoehu Ash Tephras	20-200
Rotoehu Ash	20-200
Palaeosol	200
Hamilton Ash	70-190
Pahoia Tephras	80-200
Cross-bedded sequence	40-200
Aquifer	20-80
Aquitard	30-140

f) Soakhole Investigations

Anecdotal evidence indicates that a small number of soakholes were drilled through the Palaeosol and Hamilton Ash into the Upper Matua Subgroup sediments, but that the majority of soakholes stop at the top of the Palaeosol (i.e. at a depth of 4-5m).

6.2.3 Geotechnical Models For Identified Failure Types

a) Probable Large Scale Block Failures

During field investigations some probable large scale block slides were delineated. These slides were also noted by Houghton and Hegan (1980). These larger slides (~2.5×10^5 m^3) are thought to have formed in the late Pleistocene during low sea level stands by toe erosion of the bottom of cliff face by entrenched rivers producing a large block failure. No geotechnical details are available concerning their slides, which are no longer active for which little failed material remains

b) Piping-Triggered Block Failures

The piping-triggered block failures can be defined as a retrogressive, complex; rapid-extremely rapid, wet, debris, slide-flow. The failure occur through a rapidly expanding piping failure which removes a considerable amount of supporting material from under an block size (~800 m^3). This block then fails along an exfoliation defect within the soil mass, resulting in a block sliding down and outwards breaking up as it travels down slope.

c) Wave Erosion-Triggered Block Failures

Wave erosion triggered block failures ($2m^3$-$400m^3$) occur when undercutting occurs by wave action either during a storm or high tide. This becomes enlarged through failures along defects which rootlet mats have penetrated, allowing small blocks to fall from the roof of the expanding cave. The slowly expanding cave decreases the supported underneath the overlying cliff soils, resulting in a Colluvium/topsoil failure.

d) Colluvium/Top Soil Failure

Colluvium/Top failures can vary from small failure of $<1m^3$ to ones that involve the entire colluvium/topsoil of a cliff section (~$250m^3$). They are defined as a complex, very rapid-extremely rapid, moist-very wet, earth, slide-flow. Soil failures can occur through

increased pore pressures due to rainwater infiltration, through toe erosion by wave action, or due to excessive weight of vegetation especially tress which induce a torque on the soil resulting in the failure of the Colluvium/Top soil.

6.2.4 Laboratory Investigation Results

a) Particle Size Analysis

The objective of particle size analysis was to provide a quantitative description of the various soils on which geotechnical tests were subsequently conducted including Atterberg limits, Pinhole erosion, Emerson Crumb, and Permeability. The main units on which were the Palaeosol, Hamilton Ash, Cross-bedded sequence and the lower bounding aquitard, with particle size data summarised in Table 6.2.

Table 6.2 Summary of Particle size analysis results.

Stratigraphic unit	Granule	Sand	Mud	
Rotoehu Ash	1	96	3	
Stratigraphic unit	Granule	Sand	Silt	Clay
Palaeosol ♣	3	58	29	10
Hamilton Ash		30	34	36
Cross-bedded Sequence		38	40	22
Aquifer		78	16	6
Lower Bounding Aquitard		34	24	42

♣Incorrect result due to the granule and sand material were mainly comprised of aggregates.

b) Clay Mineralogy

Clay mineralogy was conducted to assess the behavioural characteristics of the soils. X-ray diffraction identified the presents of a mixed layer 7 and 10 Å Halloysite, and Allophane testing indicated the presents of Allophanes, see Table 6.3.

c) Atterberg Limits

Atterberg testing was conducted on a range of samples for which grainsize analysis was performed to provide further geotechnical characterisation of the soil properties. A summary of results is presented in Table 6.3.

Table 6.3 Summary of results for Atterberg Limits and Clay Mineralogy

Stratigraphic Unit	Clay Mineralogy	Percentage Clay	Liquid Limit	Plastic Limit	Plasticity Index	Activity
Palaeosol	Halloysite / Allophanes	40	67	30	37	0.9
Hamilton Ash	Halloysite / Allophanes	36	103	35	68	1.9
Cross-bedded Sequence	Halloysite / Allophanes	20	46	30	16	0.9
Lower Bounding Aquitard	Halloysite / Allophanes	40	56	39	17	0.4

d) Direct Shear Testing (Shear Box)

Direct Shear testing provided the opportunity to test the shear strength of a particular layer of interest, as well as providing a means to test more sandy samples. The Post-Rotoehu Ash Tephras and Pahoia Tephras showed no corresponding increase in shear strength with an increasing normal load, therefore only a range in shear strengths could be obtained of 0 - 94 kPa for the Post-Rotoehu Ash, and 6-67 kPa for the Pahoia Tephras.

Samples from the cross-bedded sequence were all of similar particle size distributions (i.e. 40% sand, 40% silt, 20% clay), with cohesions that ranged from 0-17 kPa and friction angles from 30-42°. The aquifer produced a cohesion of 0 kPa and a friction angle of 35°, whereas the Upper Bounding Aquitard produced a cohesion of 19 kPa and a friction angle of 18°.

e) Triaxial Testing

Unconsolidated undrained triaxial testing was conducted to look at various failure modes, and to compare the peak shear strengths with those produced in the field by the shear vane. A summary of shear strengths related to each unit is presented in Table 6.4.

Table 6.4 Summary of shear strengths related to stratigraphic unit.

Stratigraphic Unit	Shear Strength (kPa)
Palaeosol	25.5 - 80.0
Hamilton Ash ♣	1.5 - 6.0
Cross-bedded sequence	11.5 - 34.5
Upper bounding aquitard	18.5 - 34.0
Aquifer	23.0 - 31.0
Lower bounding aquitard	12.0 - 28.0

♣ The Hamilton Ash, due to a pin pick in the rubber membrane that surrounds the sample, produced extremely low shear strength that do not represent the strength of the unit.

f) Dispersion and Erodibility Testing

The Emerson crumb test was used to determine the dispersive nature of the clays within the soil used for pinhole testing, while the pinhole erosion test was used to determine the potential erodibility of a number of samples related to particular stratigraphic units to assess the potential for a piping failure to occur.

Table 6.5 Summary of Emerson test dispersion and pinhole erosion classifications in relation to stratigraphic unit.

Stratigraphic Unit	Dispersion classification	Erosional Classes	
		Modified BS	Yetton & Bell (1992)
Post-Rotoehu Ash Tephras	Class 1	N/A	N/A
Rotoehu Ash	Class 1.5	NE1	$E_{>1000}$
Palaeosol	Class 1	NE1	$E_{>1000}$
Cross-bedded sequence	Class 2.5-4	E1	E_{50}
Aquifer	Class 3.5-4	E1	E_{50}

g) Permeability Testing

Falling head permeability testing was conducted in order to obtain a range of permeabilities of particular stratigraphic units for use in the hydrogeological model, and. Table 6.4 presents a summary of these results.

Table 6.4 Summary of permeabilities associated with particular stratigraphic unit.

Stratigraphic Unit	Permeability (m/sec)
Post-Rotoehu Ash Tephras	10^{-6}
Rotoehu Ash	10^{-4} - 10^{-5}
Palaeosol	10^{-8}
Hamilton Ash	10^{-7}
Pahoia Tephras	10^{-8}
Cross-bedded sequence	10^{-7} -10^{-8}
Aquifer	10^{-6}
Lower bounding aquitard	10^{-9}

6.2.5 Hydrogeological Model

The hydrogeological model developed for the Peninsula is a combination of the "defect-controlled permeability model" and the "hydraulic head response model". The "defect controlled permeability model" involves relatively fast movement of rainwater through

high permeability flow paths such as exfoliation defects, fractures, heavy bioturbation, and soakholes. The "hydraulic head response model" involves the rapid movement of a pressure wave along the aquifer and lower section of the Cross-bedded sequence in response to an increase in the hydraulic head due to recharge in both the hinterland and on the Peninsula itself. For the hydrogeological model to become dynamic, where by a rainfall event can trigger a piping failure, takes two months double the average rainfall accumulation.

From the "modified babbage model" 52.5% of rainfall is absorb by undeveloped land and 20% is aborbed by developed land by the way of soakholes.

6.2.6 Stability Analysis

Stability assessment was undertaken to determine the effect on the factor of safety of an increasing phreatic surface and landslide block size. As expected increasing the phreatic surface decreased the factor of safety and therefore the stability of the cliff section. Conversely increasing the landslide block size increased the factor of safety and therefore the stability. A summary of results is presented in Table 6.5.

Table 6.5 Summary of factor of safety results for 85 and 89 Te Hono Street with an increasing phreatic surface and landslide block dimension using a non-circular failure surface.

Stability Analysis Using:	Position	Factor of safety Range for 85 and 89 Te Hono Street
	Dry	1.0 - 1.5
Increasing Phreatic Surface	Top of Aquifer (~15m below ground surface)	1.0 - 1.5
	9.3m below the ground surface	0.9 - 1.2
Increasing Landslide Block	Increase of 1m	1.0 - 1.5
	Increase of 5m	1.4 - 1.6
	Increase of 10m (therefore situated 15.1m back from the cliff edge)	2.0 - 2.4

6.3 CONCLUSIONS

6.3.1 Field Investigation

- Engineering geological mapping showed that Maungatapu Peninsula has suffered substantial landsliding in the past and is likely to in the future. The main landslide types expected will be Colluvium/topsoil failures varying from minor (<1m^3) to larger block failures (~250m^3)), and piping-triggered block failures with dimensions up to 1000m^3.

- Desk top studies and field investigations involving geotechnical core logging suggested that there is continuous hydraulic connection within the aquifer from the end of the Peninsula back up into the hinterland. This therefore increases the catchment size from 1.6 km^2 to ~5 km^2.

- In-situ shear strength testing showed that the aquifer had low shear strengths (20-80 kPa) compared to other stratigraphic units (20-200 kPa). These low shear strengths combined with high pore water pressures will produce a scenario where piping failure within the aquifer and the lower section of the Cross-bedded sequence can occur under extreme groundwater conditions.

- From in-situ permeability testing the conclusion was drawn that due to the low permeabilities of the Cross-bedded sequence, soakage water would take a considerable amount of time (order of years) to permeate through this unit as well as the entire soil profile of the logged cliff faces.

- Soakhole investigations suggested that deeper soakholes only present a minority (<10%), with the majority (>90%) of soakholes stopping at the top of the Compact Palaeosol which forms an aquiclude separating the younger Ashes from the Upper Matua Subgroup. This means the main body of soakage water will not penetrate below the Post-Rotoehu Ash Tephras and Rotoehu Ash, but structures like exfoliation defects, fractures, etc. will allow some additional rapid penetration of water to the aquifer horizon.

6.3.2 Laboratory Results

- From particle size analysis it was demonstrated that the stratigraphic units had a high percentage of silt and clays.

- Atterberg Limit testing produced some anomalous results where beds with high clay contents in the lower bounding aquitard showed low plasticities. The only possible explanation for this was the precense of Allophanes in sufficient amounts to alter the behavioural characteristic of the samples tested.

- Direct shear testing produced very high friction angles (35 - 40°)which is suggested to be the result of a high abundance of glass shards that tend to lock up the internal structure during shearing.

- Unconsolidated undrained triaxial test showed low shear strengths (12-35 kPa) for Cross-bedded sequence, aquifer, and aquitards, compared to in-situ shear vane testing (20-200 kPa) for the sample units.

- Dispersion and Erodibility testing using the Emerson Crumb and pinhole test indicated that the Post-Rotoehu Ash Tephras, Rotoehu Ash, and Palaeosol were non-dispersive and non-erodible, whereas the Cross-bedded sequence and aquifer were highly dispersive and erodible.

- The stratigraphic units overall have low permeabilities (10^{-6}-10^{-7}m/sec) which will limit the rate of infiltration of soakage water through the soil to years.

6.3.4 Hydrogeological Model

- Excessive pore water pressure buildup within the Peninsula especially towards the cliff edges are the main triggering mechanism that causes piping failure, and in turn landsliding.

- From rainfall data it takes approximately two months of double the average rainfall to produce adverse pore water conditions.

- Soakholes account for 20% of the absorbed rainfall in the Peninsula.

- Suggested that <10% of the Soakholes around the Peninsula penetrate the Palaeosol and Hamilton Ash into the Upper Matua Subgroup sediments.

- Hydrogeological model allows for these rapid lag time produced by rainfall events.

6.3.3 Stability Analysis

- An increasing phreatic surface to 9.3m below surface decreased the factor of safety by approximately 0.1, whereas an increasing landslide block by 5m showed an increase in the factor of safety of 0.4.

- The use of a non-circular failure surface was more representative of landslide geometry than using a circular failure.

- It was found during stability analysis that the 2H:1V slope used to define whether a property had the potential for slope instability was not reflective of the actuarial failure types possible around the Peninsula. This was due to the 2H:1V creating a geotechnical assessment zone that included the whole of the cliff top property (a zone >20m back from the cliff edge). Stability analysis indicated that factors of safety for landslide block 10m back from the cliff edge is greater than 1.5, therefore suggesting this 2H:1V slope to be very conservative in its evaluations of potential cliff instability.

6.4 RECOMMENDATIONS

6.4.1 Field Investigations

- Boreholes should be positioned along the length of Maungatapu Road at 150 to 200m spacing to constrain the geology of the Peninsula better, and to confirm that if the stratigraphic units are continuous throughout the entire length of the Peninsula.

- On completion of the boreholes piezometer should be installed with similar specifications to those at the northeastern end of the Peninsula around Te Hono Street

to further evaluate the "hydraulic head response model" and the "defect controlled permeability model".

- Continuous monitoring of at least one piezometer and rainfall gauge around the northeastern end of the Peninsula via a continuous data recording system should be carried out to determine maximum piezometric water levels, and more accurate lag time response data to be used in early warning systems and the determination of a threshold rainfall triggering piping type landslides.

- In-situ permeability testing of one borehole be staged so that each stratigraphic unit can be assess for permeability.

6.4.2 Geotechnical Assessment

- The 2H:1V assessement criteria should be reassessed, and a polict adopted where by any future development on a cliff top property should require a geotechnical report if deemed necessary by the Consents Officer from evidence of slope failures on adjoining properties or other evidence of instability on the site.

6.4.4 Mitigation

- The staged reticulation of soakhole water to be discharged into to the harbour should be continued with stage 4 all other dwellings located on Te Hono Street, Maihi Crescent, and Te Wati Street, and the next stage to concentrate on the northeastern end of Maungatapu Road.

ACKNOWLEDGEMENTS

I would like to thank the following people for there knowledge and assistance in the production of this thesis. Firstly I would like to thank the staff of the Tauranga District Council especially Bruno Petrenas for providing me with this thesis and funding, where without it, I would have not been able to undertake this project. To Ralph Gillard and Collins Mills for there input and help it was invaluable. To all the friends that I made during my stay in Tauranga thanks for providing me with a social life while away from home. Also I would like to thank Bernard Hegan for his suggestions concerning my project and lending an ear to bounce ideas off; Marianne O'Halloran for her help with many aspects of this project; Ian Shaw for all his abseiling help, without it I would have fallen down the cliff faces.

I would also like to extend my thanks to my supervisor David Bell for organising my project and reading my chapters, this was a tremendous help. Thanks to Cathy Knight for helping me with laboratory work and putting up with my mess in the laboratory; Arthur Nicholas for last minute orders for test equipment; Steven Brown for his all his help concerning clay mineral identification; Michelle Wright for keeping tabs on my research grant and providing the means to photocopy a tree of papers. I would like to extend a special thanks to John Southward for all his help concerning computing, and providing enough inkjet paper to print my diagrams. To the rest of the staff of geology for putting up with me for some of my many years of study.

I would like to thank the staff at Waikato University for their help in providing information relevant to my project, especially Dr David Lowe for his help regarding clays minerals within my field area. NIWA for providing me with rainfall data.

To my uncle and aunt, Scott and Barbara Oliver for providing me with a place to stay while up in Tauranga, it was very much appreciated and I enjoyed my self immensely. I

would like to extend a very special thanks to my dad, mum, and sister Craig, Tricia and Sarah Oliver who have supported me patiencely through all my long years of varsity. Also to all my friends out side of varsity for all of their support. I would also like to thank my fellow cell mates; to Ed, the man that has done enough spade work to dig from here to China, the gardening did paid off. Kane who got early parole thanks your help. Aaron, who stayed in the room to almost the bitter end thanks also for all your help it was appreciated.

REFERENCES

Anderson, M. G. and Richards, K. S., 1987. Slope Stability Geotechnical Engineering And Geomorphology. John Wiley & Son. Pp 648.

Barnes, G. E., 1995. Soil Mechanics Principles and Practice. MacMillan. Pp 365.

Bell, D. H., 1990. The Role of Engineering Geologist in Urban Development. New Zealand Geomechanics News. 41:22-31

Bell, D. H. and Pettinga, J. R., 1983. Presentation of Geological Data; Philosophy and metods of investigation used in New Zealand. Proceedings of the Symposium on Engineering for Dams and Canals, Alexandra, IPENZ 94 (g): 4.1-4.36.

Bird, G. A., 1981. The Nature and Causes of Coastal Landsliding on the Maungatapu Peninsula, Tauranga New Zealand. Un published MSc thesis held in the Library, University of Waikato, Hamilton.

Bishop, A. W., and Henkel, D. J., 1962. The Measurement of Soil Properties in the Triaxial Test. Edward Arnold LTD. London, second edition.

Briggs, R. M.; Hall, G. J.; Harmsworth, G. R.; Hollis, A. G.; Houghton, B. F.; Hughes, G. R.; Morgan, M. D.; Whitbread-Edwards, A. R., 1996. Geology of the Tauranga Basin. Depatment of Earth Sciences Occasional Report No. 22, University of Waikato, Hamilton. Published in collaboration with Environment B. O. P., and Institute of Geological & Nuclear Sciences Limited.

Chapple, J., 1975. Upper Quaternary warping and uplift rates in the Bay of Plenty and Westcoast, North Island, New Zealand. New Zealand Journal of Geology and Geophysics 18 : 129 - 155.

Clayton, C. R. I., Matthews, M. C. and Simons, N. E., 1995. Site Investigation. Blackwell Science. Second Edition. Pp. 584.

Cox, S. H., 1877. Report on the country between Opotoki and East Cape. Reports on Geological Exploration, N. Z. Geological Survey (1876-77) 10: 105 - 113.

Cruden, D. M., 1991. A Simple Definition of a Landslide. Bulletin of the International Association of Engineering Geology, No. 43: 27 - 29.

Cruden, D. M. and Varnes, D. J.,1996. Landslide Types and Processess in Turner, K. A. and Schuster, R. L., 1996. Landslides, Investigation and Mitigation, Special Report 247, Transportation Research Board, National Reasearch Council. National Academy Press, Washington, D. C: 36 - 75.

ELE International. Permeability and Drainage Charateristics of Main Soil Types. Civil & Environmental Engineering Test Equipment 9th Ed. Catalogue.

Fell, R., MacGregor, P., Stapledon, D., 1992. Geotechnical Engineering Of Embankment Dams. A. A. Balkema Rotterdam Brookfield. Pp675.

Fetter, C. W., 1994. Applied Hydrogeology, 3rd Edition. Prentice Hall. Pp 691.

Fieldes, M. and Perrott, K. W., 1966. The Nature Of Allophanes In Soils, Part 3 - Rapid Field And Laboratory Test For Allophanes. New Zealand Journal Of Science. 9: 623-629.

Ground Technology LTD., 1985. 413 Maungatapu Road. Held in council files

Hall, G. J., 1994. Volcanic Geology of the Southeastern Tauranga Basin, New Zealand. Unpublished MSc thesis held in the Library, University of Waikato, Hamilton.

Harmsworth, G. R., 1983. Quaternary Stratigraphy of the Tauranga Basin. Unpublished MSc thesis held in the Library, University of Waikato, Hamilton.

Hegan, B. D.,1995. Landslip Damage At 85 & 89 Te Hono Street Maungatapu, Tauranga. Tonkin & Taylor Ltd.

Heagan, B. of Tonkin and Taylor LTD., 1995. 85 and 89 Te Hono Street. Held in council files.

Healy, J.; Schofield, J. C.; Thompson, B. N., 1964. Sheet 5 Rotorua (1st Ed.) Geological Map of New Zealand 1 : 250 000. Department of Scientific and Industrial Research, Wellington, New Zealand.

Healy, J., 1967. Geology of the Kaimai Tunnel Section (abs.). Geological Society of New Zealand Conference, 1967. Unpublished.

Healy, J., 1969. Geological report on the proposed tunnel line, Kaimai Railway Deviation. Unpublished New Zealand Geological Survey Report.

Healy, T.; Kirk, R. M., 1982. Coasts. *In*: Soons and M. J. Selby (eds.) Landforms of New Zealand. Longman Paul, Auckland.

Henderson, J. and Bartrum, J. A., 1913. The Geology of the Aroha Subdivision. New Zealand Geological Survey Bulletin 16.

Houghton, B. F.; Cuthbertson, A. S., 1989. Sheet T14 BD-Kaimai. Geological Map of New Zealand 1 : 50 000. Map (1 sheet) and Notes. Department of Scientific and Industrial research, Wellington, New Zealand.

Houghton, B. F. and Hegan, B. D., 1980. A Preliminary Assessment of Geological Factors Influencing Slope Stability and Landslipping in and Around Taunanga City. New Zealand Geological Survey, Lower Hutt.

Houghton, B. F.; Wilson, C. J. N.; McWilliams, M. O.; Lamphere, M. A.; Weaver, S. D.; Briggs R. M.; Pringle, M. S. 1995. Chronology and Dynamics of a large Silicic Magmatic System: Central Taupo Volcanic Zone, New Zealand. Geology 23: 13-16.

Hughes, G. R., 1993. Volcanic Geology of the Eastern Tauranga Basin and Papamoa Range. Unpublished MSc thesis held in the Library, University of Waikato, Hamilton.

IAEG Commission on Landslides, 1990. Suggested Nomenclature for Landslides. Bulletin of the International Association of Engineering Geology, No. 41: 13 - 16.

International Union Of Geological Sciences Working Group On Landslides, 1995. A Suggested Method For Describing The Rate Of Movement Of A Landslide. Bulletin Of The International Association Of Engineering Geology No. 52: pp 75 - 78.

Kear, D. and Waterhouse, B. C., 1961. Quaternary surfaces and sediments at Waihi Beach. New Zealand Journal of Geology and Geophysics 4: 434 - 445.

Kirkman, J. H. and Pullar, W. A., 1978. Halloysite in late Pleistocene rhyolitic tephra beds near Opotiki, coastal Bay of Plenty, North Island, New Zealand. Australian Journal of Soil Reseach 16: 1-8.

Kohn, B. P., 1973. Some Studies of New Zealand Pyroclasic Rocks. Unpublished PhD thesis held in the Library, Victoria University, Wellington.

Kohn, B. P.; Pillans, B.; McGlone, M. S., 1992. Zircon Fission Track Age for Middle Pleistocene Rangitawa Tephra, New Zealand: Stratigraphic and Paleoclimatic Significance. Paleogeography, Papaeoclimatology, Palaeoecology 95: 73 - 94.

Kruseman, G. P. & de Ridder, N. A., 1994. Analysis and Evaluation of Pumping Test Data, 2nd Edition. ILRI (International Institute for Land Reclamation and Improvement) Publication 47. Pp 377.

Lewis D. W. and McConchie D., 1994. Analytical Sedimentology. Chapman & Hall. Pp197.

Lewis D. W. and McConchie D., 1994. Practical Sedimentology. Chapman & Hall. Pp197.

Michell, M., Consulting Geotechnical Engineer, 1993. 340b Maungatapu Road. Held in council files.

Morgan, M. D., 1986. Geology of the Northern Mamaku Plateau. Unpublished MSc thesis held in the Library, Unoversity of Waikato, Hamilton.

Oboron, L. E., 1988. Canal Failure, Ruahihi Hydro Electric Power Scheme, Bay of Plenty, New Zealand. 5th Australia-New Zealand Conference on Geomechanics, Sydney, 22-23 August: 574-583.

Selby, M. J.; Pullar, W. A.; McCraw, J. D., 1971. The age of Quaternary surfaces at Waihi Beach. Earth Science Journal 5 : 106 - 113.

Shepard, T. G., 1994. Paleoclimatic implications of clay minerals and paleosols within strongly weathered Plio-Pleistocene tephras of the Waikato region, central North Island, New Zealan. Programme and Abstracts, International Inter-INQUA Field Conference and Workshop on Tephrochronology, Loess, and Paleopedology, Hamilton, New Zealand.

Spangler, M. G. and Handy, R. L., 1982. Soil Engineering. Harper & Row, New York. Fourth Edition. Pp. 819.

Takagi, M., 1995. Miocene-Pliocene Arc Volcanism of the Hauraki Region in North Island, New Zealand. Unpublished MSc thesis, held in Library, Hiruzen Research Institute, Okayama, Japan.

Terzaghi, K., Peck, R. B., & Mesri, G., 1996. Soil Mechanics in Engineering Practice, Third Edition. John Wiley & Sons, INC.

Tonkin and Taylor, 1980. Omokoroa Point Land Stability Investigation. Held by Western BOP District Council Corporate Library, Tauranga District Council, Tonkin and Taylor.

Whitbread-Edwards, A. N., 1994. The Volcanic Geology of the Western Tauranga Basin. Unpublished MSc thesis held in the Library, University of Waikato, Hamilton.

Wilson, M. J., 1987. A Handbook Of - Determinative Methods In Clay Mineralogy. Blackie & Son Limited. Chapman and Hall. Pp 308.

WP/WLI, 1990. A Suggested Method for Reporting a Landslide. Bulletin of the International Association of Engineering Geology, No. 41: 5 - 12.

WP/WLI, 1991. A Suggested Method for a Landslide Summary. Bulletin of the International Association of Engineering Geology, No. 43: 101 - 110.

WP/WLI, 1993a. A Suggested Method for Describing the Activity of a Landslide. Bulletin of the International Association of Engineering Geology, No. 47: 53 - 57.

WP/WLI, 1993b Multilingual Landslide Glossary. Bi-Tech Publishers, Richmond, British Columbia, Canada. pp59.

Worley Consultancy Limited, 1988. 292 Maungatapu Road. Held in council files

APPENDICES

APPENDIX A1 Rainfall Data

All rainfall data was supplied by NIWA. Rainfall data was obtained from N. Z. Met. S. Misc. Pub. 163: Rainfall parameters for stations in New Zealand and the Pacific Island. Monthly and average monthly rainfall records were supplied from recording station at Waimapu R Tauranga Aero AWS for the period 1898-1978, and 1970-1990. Also daily rainfall data was provided for 1995. Inaddition to this reaccruence intervals were calculated.

Table A1.1 Reaccruence intervals for storm events in Tauranga calculated from rainfall data collected for Tauranga 37.67S 176.20E.

Reaccruence Intervals From NIWA

HIRDS Version 1.50

High Intensity Rainfall Design System

Table of rainfall depths and standard errors (mm)

Location: Tauranga 37.67S 176.20E

Rainfall Depth (mm)

ARI

(Y)	10m	20m	30m	1hr	2hr	3hr	6hr	12hr	24hr	48hr	72hr
2	11	16	20	30	42	50	68	83	101	125	138
5	15	22	28	41	56	67	91	110	134	166	184
10	17	26	33	48	65	78	106	129	156	194	215
20	20	30	38	56	74	88	120	146	177	220	244
30	21	32	40	60	79	95	129	156	189	235	261
50	23	35	44	65	85	102	139	169	205	254	282
60	24	36	45	67	88	105	143	173	210	261	289
70	25	36	46	68	89	107	146	177	215	266	295
80	25	37	47	70	91	109	149	180	219	271	301
90	25	38	48	71	93	111	151	183	222	275	305
100	26	38	49	72	94	112	153	186	225	279	310

Standard errors (mm)

ARI

(Y)	10m	20m	30m	1hr	2hr	3hr	6hr	12hr	24hr	48hr	72hr
2	1	2	2	3	4	4	6	8	10	12	14
5	1	2	3	4	5	6	7	9	11	14	15
10	2	2	3	5	5	7	9	11	13	17	18
20	2	3	4	6	6	8	10	13	16	20	22
30	2	3	4	6	7	8	11	14	17	22	25

50	3	4	5	7	8	9	13	16	19	25	28
60	3	4	5	7	8	9	13	16	20	26	29
70	3	4	5	8	8	10	14	17	21	27	30
80	3	4	5	8	8	10	14	17	22	28	31
90	3	4	6	8	8	10	14	18	22	28	32
100	3	4	6	8	8	10	14	18	22	29	33

APPENDIX A2 Landslide types and processes

Cruden and Varnes (1996) have expanded on the concept developed by Varnes (1978) to include additional information from more modern sources such as Cruden (1991), IAEG (International Association of Engineering Geology), 1990, and WP/WLI (Working Party on the World Landslide Inventory (International Geotechnical Societies and UNESCO) 1990, 1991, 1993a, 1993b, and other authors. Below is Cruden and Varnes's (1996) terminology used to define the parameters of sliding at Maungatapu Peninsula.

Table A2.1 Glossary for forming names of landslides.

Glossary for Forming Names of Landslides

ACTIVITY		
STATE	DISTRIBUTION	STYLE
Active	Advancing	Complex
Reactivated	Retrogressive	Composite
Suspended	Widening	Multiple
Inactive	Enlarging	Successive
Dormant	Confined	Single
Abandoned	Diminishing	
Stabilized	Moving	
Relict		

DESCRIPTION OF FIRST MOVEMENT			
RATE	WATER CONTENT	MATERIAL	TYPE
Extremely rapid	Dry	Rock	Fall
Very rapid	Moist	Soil	Topple
Rapid	Wet	Earth	Slide
Moderate	Very wet	Debris	Spread
Slow			Flow
Very slow			
Extremely slow			

DESCRIPTION OF SECOND MOVEMENT			
RATE	WATER CONTENT	MATERIAL	TYPE
Extremely rapid	Dry	Rock	Fall
Very rapid	Moist	Soil	Topple
Rapid	Wet	Earth	Slide
Moderate	Very wet	Debris	Spread
Slow			Flow
Very slow			
Extremely slow			

NOTE: Subsequent movements may be described by repeating the above descriptors as many times as necessary.

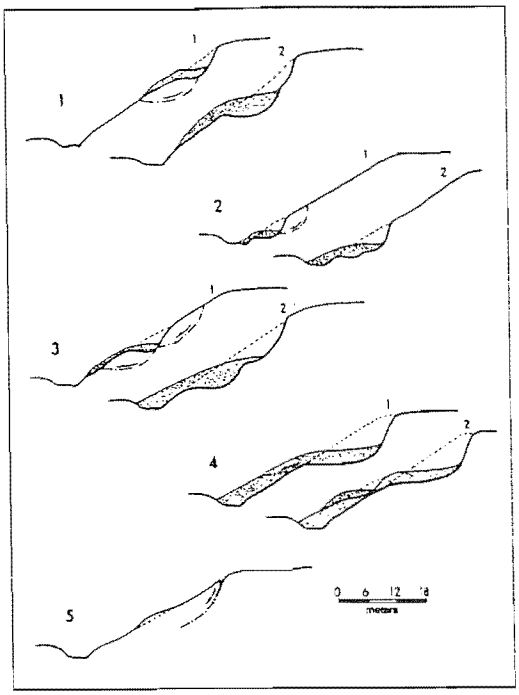

Figure A2.1 Section through landslides showing different distributions of activity:

1. advancing,
2. retrogressing,
3. enlarging,
4. diminishing, and
5. confined.

In 1-4, Section 2 shows slope afer movement on rupture surface indicated by shear arrow. Stippling indicates displaced material.

Velocity Class	Description	Velocity (mm/sec)	Typical Velocity
7	Extremely Rapid		
		$5x10^{3}$	5 m/sec
6	Very Rapid		
		$5x10^{1}$	3 m/min
5	Rapid		
		$5x10^{-1}$	1.8 m/hr
4	Moderate		
		$5x10^{-3}$	13 m/month
3	Slow		
		$5x10^{-5}$	1.6 m/year
2	Very Slow		
		$5x10^{-7}$	16 mm/year
1	Extremely Slow		

Table A2.2 Proposed landslide veolocity scale Proposed landslide veolocity scale form Cruden and Varnes (1996) proposed by International Union of geological Sciences working Group on Landslides.

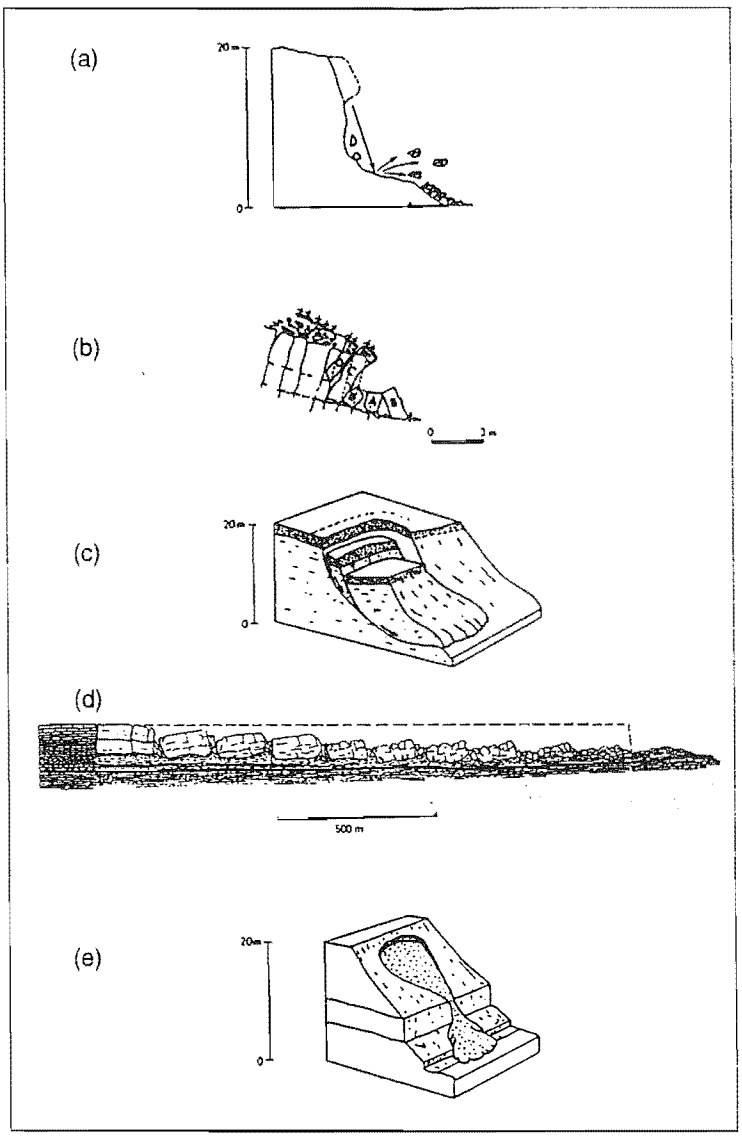

Figure A2.2 Types of landslides: (a) fall, (b) topple, (c) slide, (d) spread, (e) flow. Broken lines indicate original ground surfaces; arrows show portions of trajectories of individual particles of displaced mass (modified from Varnes 1978)

ENGINEERING GEOLOGICAL FIELD DESCRIPTION FOR SOIL MATERIAL

WEATHERING

	TERM	GRADE	SOIL DESCRIPTION
5	Completely Weathered (CW)	V	completely discoloured and altered, no trace of original fabric
4	Highly Weathered (HW)	IV	mostly altered and weakened, little trace of original fabric
3	Moderately Weathered (MW)	III	large discoloured portions of original soil separated by more altered material, significantly weakened
2	Slightly Weathered (SW)	II	minor discolouration of some parts of the original soil, no loss of strength
1	Unweathered (UW)	I	original soil with NO discolouration, loss of strength or other effects due to weathering
0	NOTE * in coarse-grained soils record weathering grade of DOMINANT fraction here and qualify weathering grade of subordinate and/or minor fractions if appropriate		

STRENGTH

	TERM	FIELD CRITERIA
1	loose	can be removed from exposure in disaggregated form by hand
2	compact	only removed from exposure by implement; material readily disaggregated by physical means
3	†cemented	only removed from exposure by implement; material does not disaggregate
4	hard	may be removed from exposure with difficulty by implement or hand; softened on immersion in water and may be remoulded
5	stiff	indented by thumb pressure, but not moulded by fingers; softened on immersion in water, and may be remoulded
6	firm	moulded or indented only by strong finger pressure; easily moulded after immersion in water
7	soft	easily indented or moulded by finger pressure
8	very soft	exudes between fingers when squeezed
9	spongy	readily compressed by finger pressure, but cannot be remoulded

† may require description as rock material

UNIFIED SOIL CLASSIFICATION SYSTEM

			FIELD IDENTIFICATION	GROUP SYMBOL	TYPICAL NAMES
COARSE-GRAINED SOILS	GRAVELS (>50% larger than 2mm)	clean gravels	wide range in grain size and substantial amounts of all interm. sizes	GW	well graded GRAVELS
			predom. one size or a range of sizes with some interm. sizes missing	GP	poorly graded GRAVELS
		gravel with fines	non-plastic fines (see ML below)	GM	poorly graded SILTY-GRAVELS
			plastic fines (see CL below)	GC	poorly graded CLAYEY-GRAVELS
	SANDS (<50% smaller than 2mm)	clean sands	wide range in grain sizes and substantial amounts of all interm. sizes	SW	well graded SANDS
			predom. one size or a range of sizes with some interm. sizes missing	SP	poorly graded SANDS
		sands with fines	non-plastic fines (see ML below)	SM	poorly graded SILTY-SANDS
			plastic fines (see CL below)	SC	poorly graded CLAYEY-SANDS

			SHINE	DILATANCY (1)	TOUGHNESS (1)		
FINE-GRAINED SOILS: SILTS AND CLAYS	LIQUID LIMIT	V.	none to very dull	quick to slow	none	ML	INORGANIC SILTS with slight plasticity
		M.	moderate	none to very slow	medium	CL	INORGANIC CLAYS of low to medium plasticity
		V.	none to very dull	slow	slight	OL	ORGANIC SILTS & CLAYS of low plasticity
		M.	dull	slow to none	slight to medium	MH	INORGANIC SILTS of high plasticity
		V.	very glossy	none	high	CH	INORGANIC CLAYS of high plasticity
		M.	moderate to v. glossy	none to very slow	slight to medium	OH	ORGANIC CLAYS of medium to high plasticity
HIGHLY ORGANIC SOILS			identified by colour, odour, spongy feel and fibrous texture			Pt	PEAT and other highly organic soils

PROCEDURES FOR FINE-GRAINED SOILS OR FRACTIONS (1)

DILATANCY (reaction to shaking) -
1) Prepare pat of moist soil, adding water to make soft - but not sticky
2) Place pat in palm of hand, shake horizontally by striking vigorously against other hand

Positive Reaction: appearance of water on surface of pat, which becomes glossy When squeezed between fingers, water and gloss disappear, pat stiffens and may crumble

TOUGHNESS: (consistency near plastic limit) -
1) Mould sample to consistency of putty, adding water or air drying as required
2) Roll to thin (3mm) thread, fold and reroll repeatedly until thread crumbles at plastic limit
3) Knead together and continue until lump crumbles

Diagnosis: a tough thread and stiff lump indicate high plasticity; a weak thread and lump low plasticity clays

GROUP SYMBOL CODINGS FOR USCS

COLUMN 1		COLUMN 2	
G:1	C:4	W:1	C:4
S:2	O:5	P:2	L:5
M:3	Pt:6	M:3	H:6

BOUNDARY CLASSIFICATIONS specify, enter 0,0

WEATHERING TERM | WATER CONTENT TERM | STRENGTH TERM | COLOUR | FABRIC | SOIL NAME | USCS SYMBOL

WATER CONTENT

	TERM	FIELD CRITERIA
1	Dry	looks and feels dry; fine-grained soils usually hard, powdery or friable; coarse-grained soils may run freely through hands
2	Moist	soil feels cool and may be darkened in colour; particles tend to adhere in coarse-grained materials, fine-grained soils may be softened
3	Wet	soils feel cold and are darkened in colour; free water forms on hands when sample is disturbed
4	Saturated	restricted to wet soils below the water table or the static water level in excavations or drill holes

COLOUR

1: light	1 pinkish	1 pink	
2: dark	2 reddish	2 red	
	3 yellowish	3 yellow	
	4 brownish	4 brown	
	5 olive	5 olive	
	6 greenish	6 green	
	7 bluish	7 blue	
	8 whitish	8 white	
	9 greyish	9 grey	
		0 black	

FABRIC

1: finely layered (< 25 mm)
2: coarsely layered (25-100 mm)
3: massive
4: other (specify)

SUBORDINATE FRACTION

20-50% volume visual estimate

1 coarse	gravelly
2 medium	
3 fine	
4 coarse	sandy
5 medium	
6 fine	
7 silty	
8 clayey	
9 peaty	

DOMINANT FRACTION

>50% volume visual estimate

SOIL TYPE TERM		PARTICLE SIZE (mm)	GRAPHIC LOG
1 coarse	gravel	> 60	
2 medium		20-60	
3 fine		2-20	
4 coarse	sand	0.6-2.0	
5 medium		0.2-0.6	
6 fine		0.06-0.2	
7 silt		0.002-0.06	
8 clay		< 0.002	
9 peat		NA	

MINOR FRACTION

< 20% volume visual estimate

WITH SOME	1 coarse	gravel
	2 medium	
	3 fine	
	4 coarse	sand
	5 medium	
	6 fine	
	7 silt	
	8 clay	
	9 peat	

PARTICLE SIZE

APPENDIX A3.2 Piezometric Water Level Responses To Rainfall

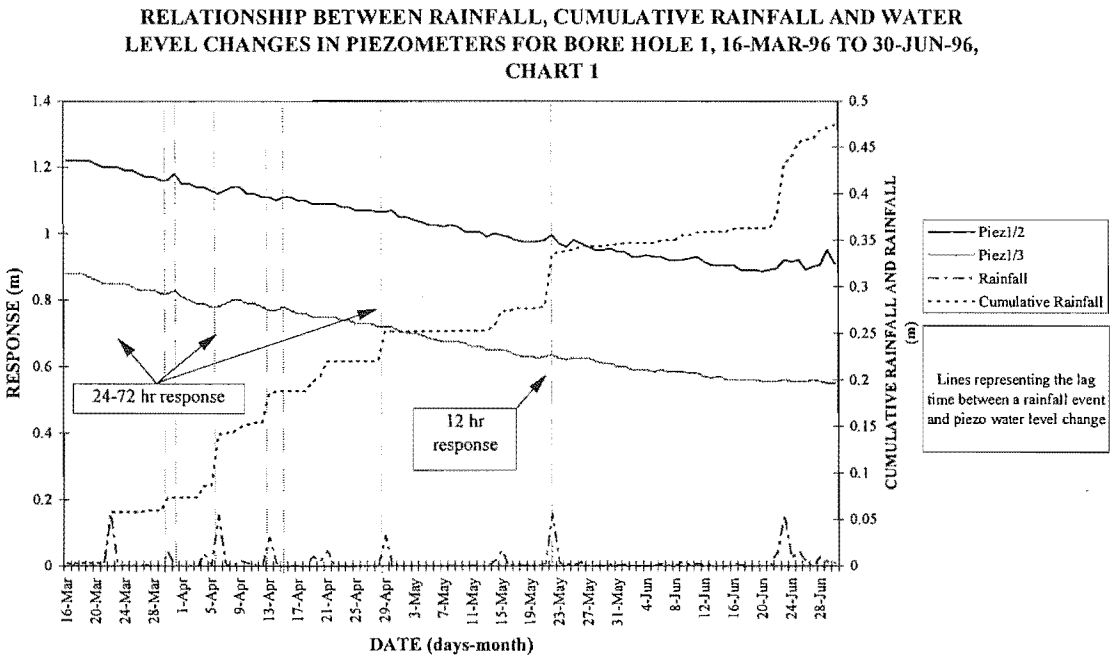

Figure A3.1 Plot of Piezometric water level responses to rainfall for borehole 1, 16 March 1996 to 30 June 1996.

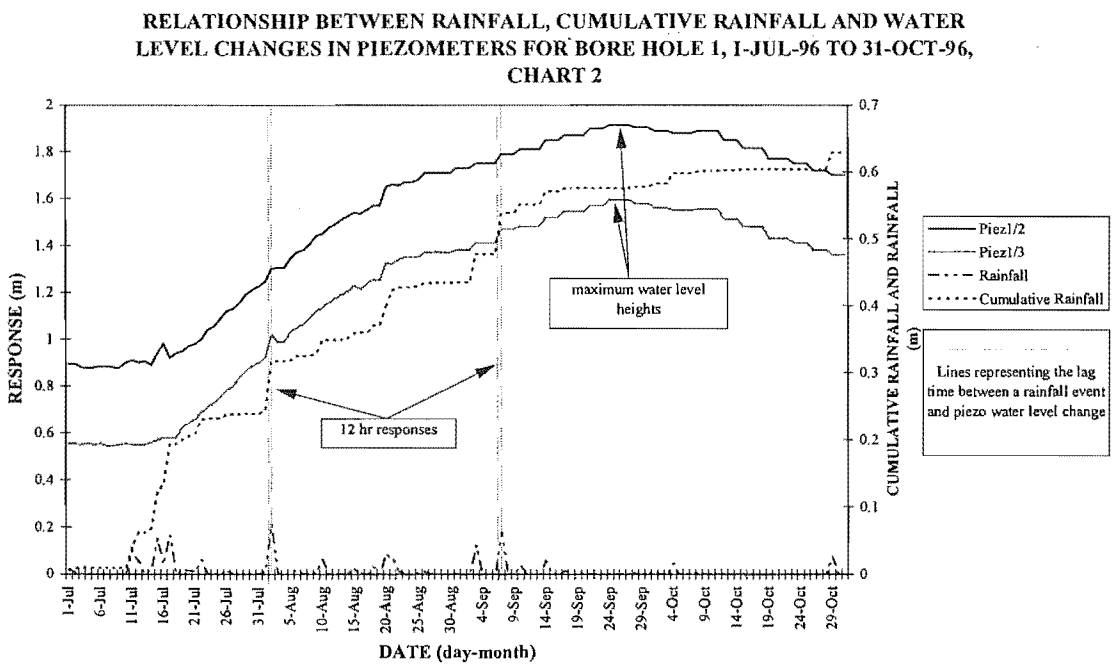

Figure A3.2 Plot of Piezometric water level responses to rainfall for borehole 1, 1 July 1996 to 31 October 1996.

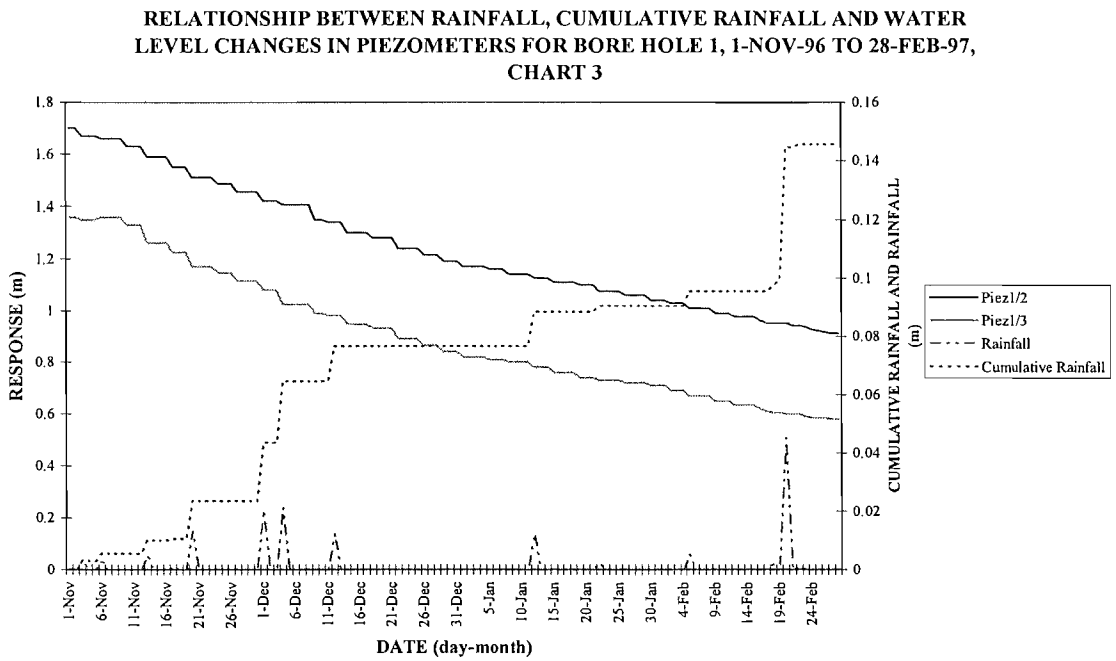

Figure A3.3 Plot of Piezometric water level responses to rainfall for borehole 1, 1 November 1996 to 28 February 1997.

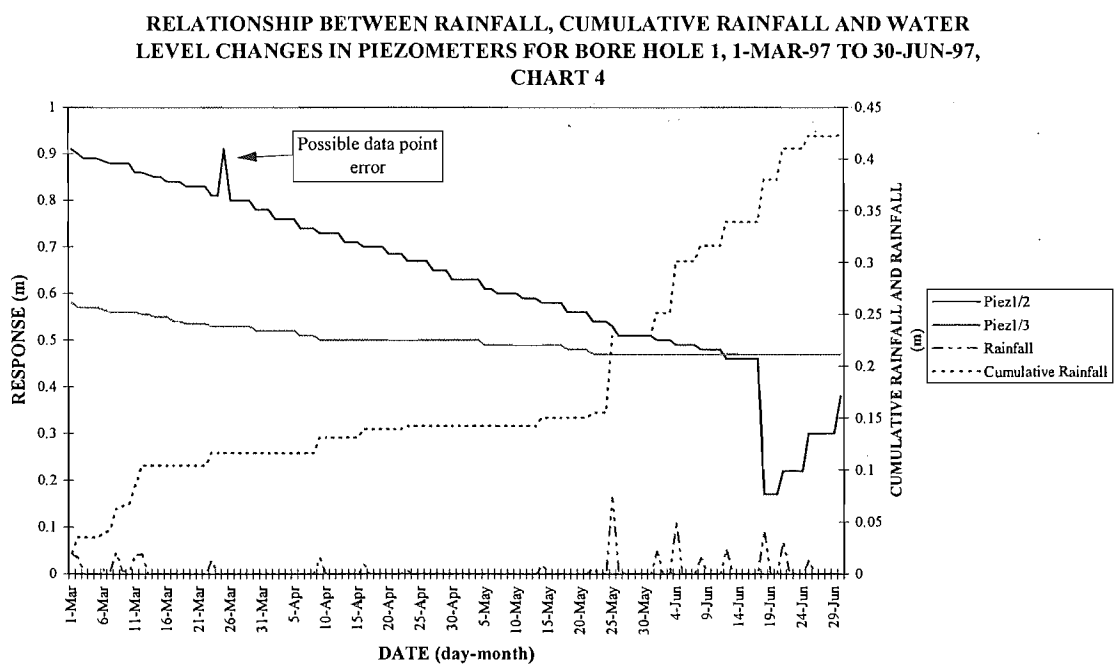

Figure A3.4 Plot of Piezometric water level responses to rainfall for borehole 1, 1 March 1997 to 30 June 1997..

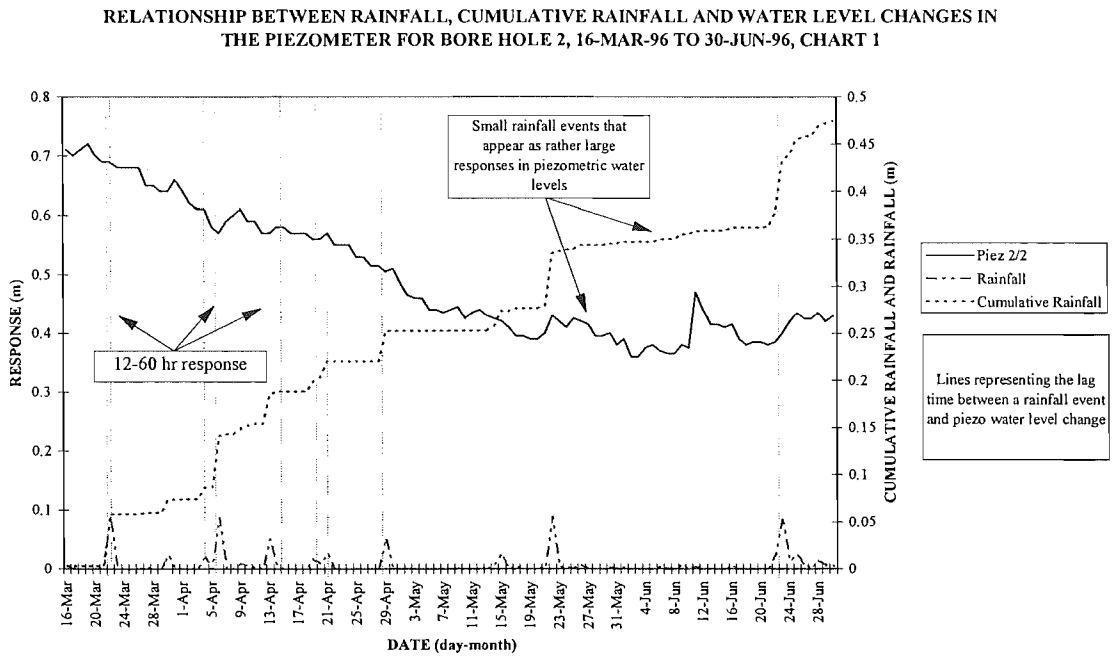

Figure A3.5 Plot of Piezometric water level responses to rainfall for borehole 2, 16 March 1996 to 30 June 1996.

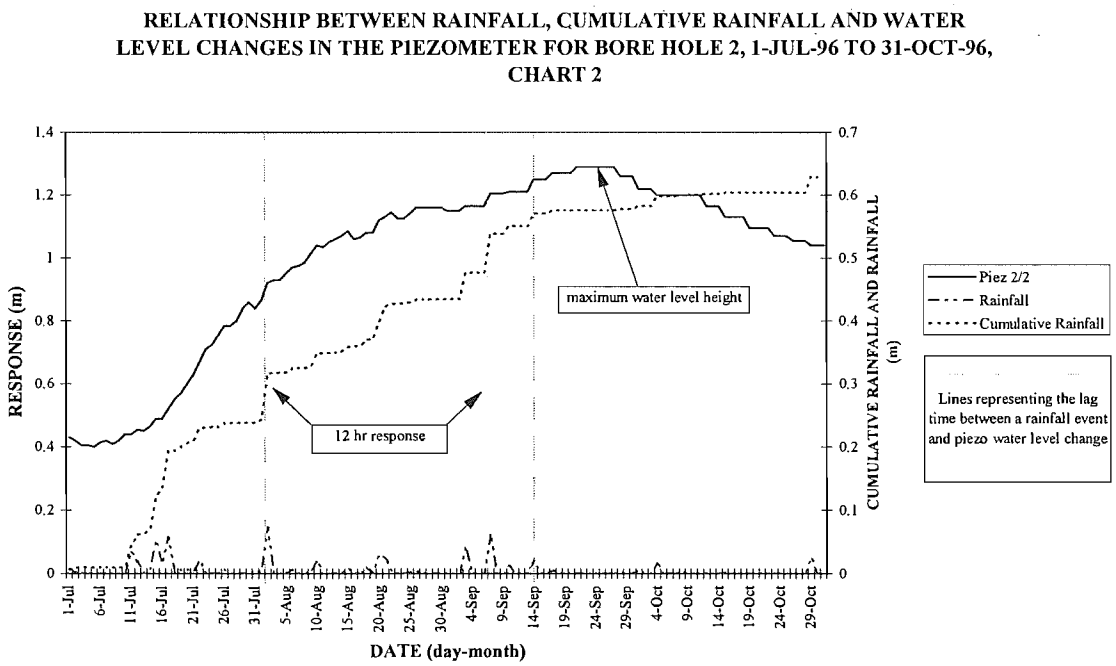

Figure A3.6 Plot of Piezometric water level responses to rainfall for borehole 2, 1 July 1996 to 31 October 1996.

RELATIONSHIP BETWEEN RAINFALL, CUMULATIVE RAINFALL AND WATER LEVEL CHANGES IN THE PIEZOMETER FOR BORE HOLE 2, 1-NOV-96 TO 28-FEB-97, CHART 3

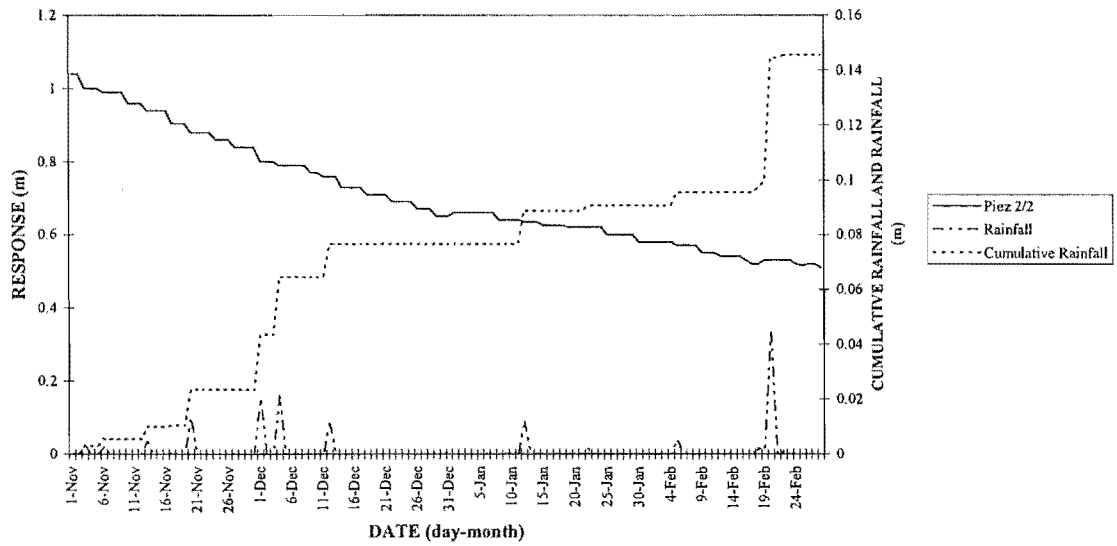

Figure A3.7 Plot of Piezometric water level responses to rainfall for borehole 2, 1 November 1996 to 28 February 1997.

RELATIONSHIP BETWEEN RAINFALL, CUMULATIVE RAINFALL AND WATER LEVEL CHANGES IN THE PIEZOMETER FOR BORE HOLE 2, 1-MAR-97 TO 30-JUN-97, CHART 4

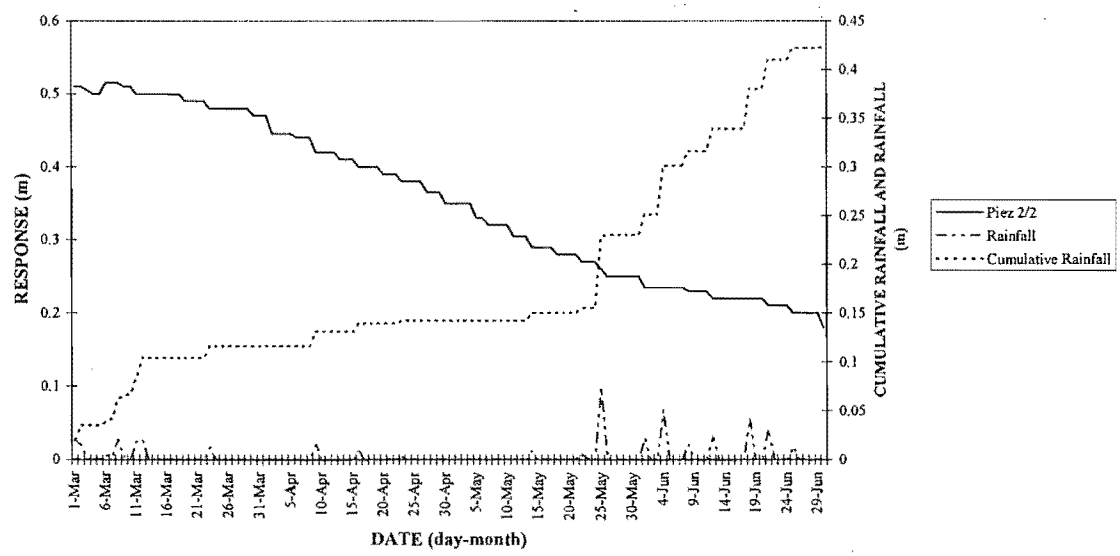

Figure A3.8 Plot of Piezometric water level responses to rainfall for borehole 2, 1 March 1997 to 30 June 1997.

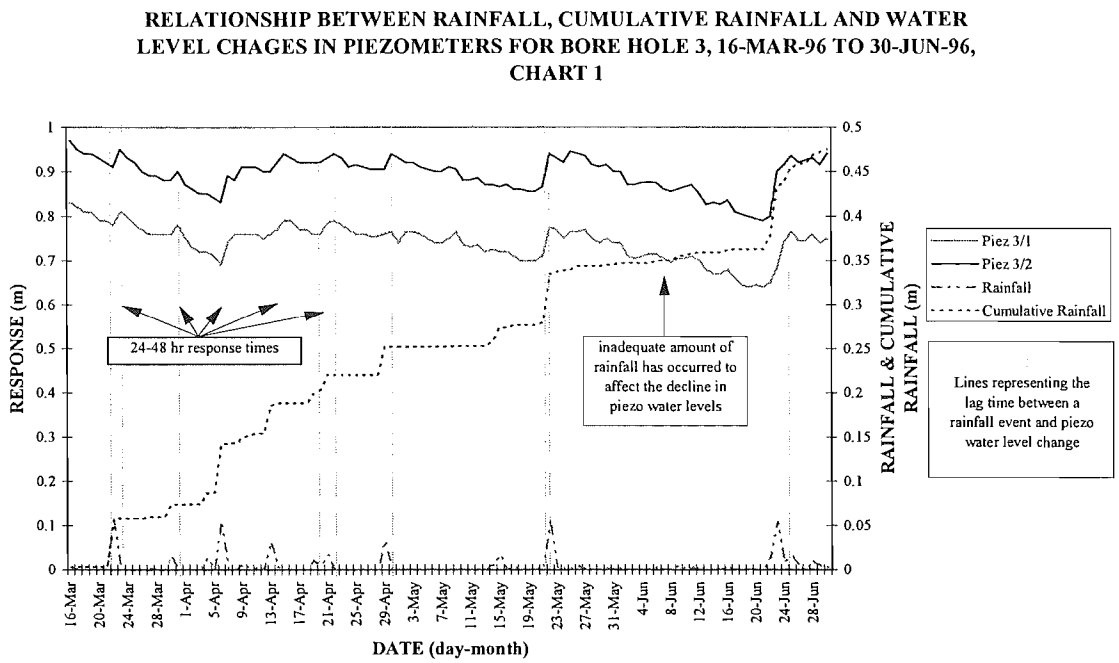

Figure A3.9 Plot of Piezometric water level responses to rainfall for borehole 3, 16 March 1996 to 30 June 1996.

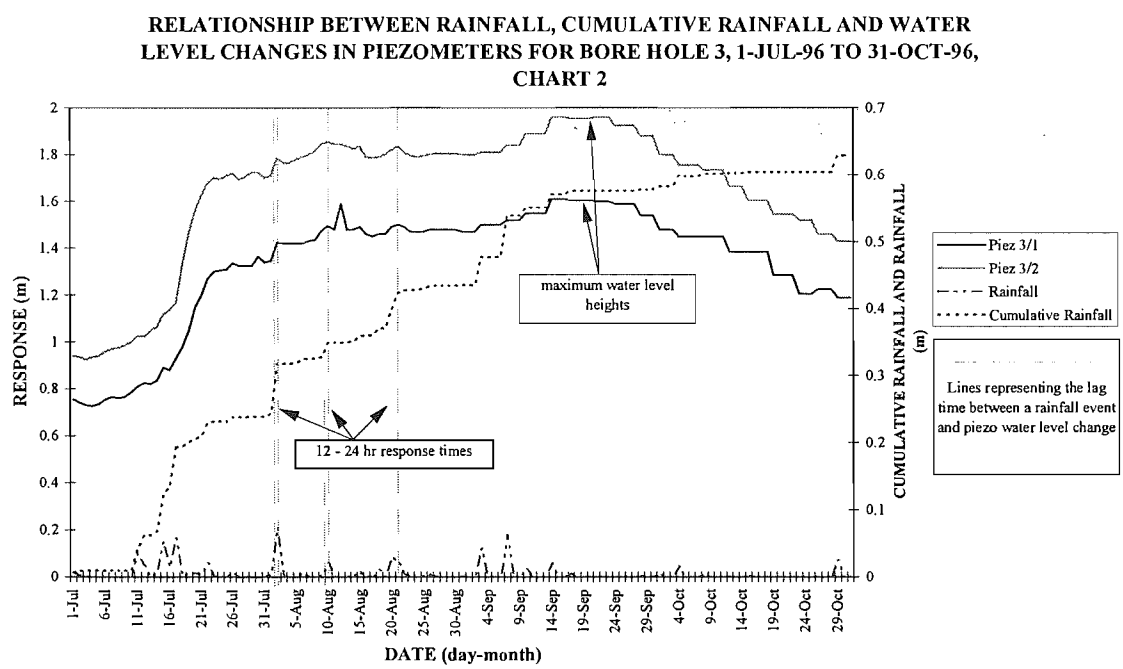

Figure A3.10 Plot of Piezometric water level responses to rainfall for borehole 3, 1 July 1996 to 31 October 1996.

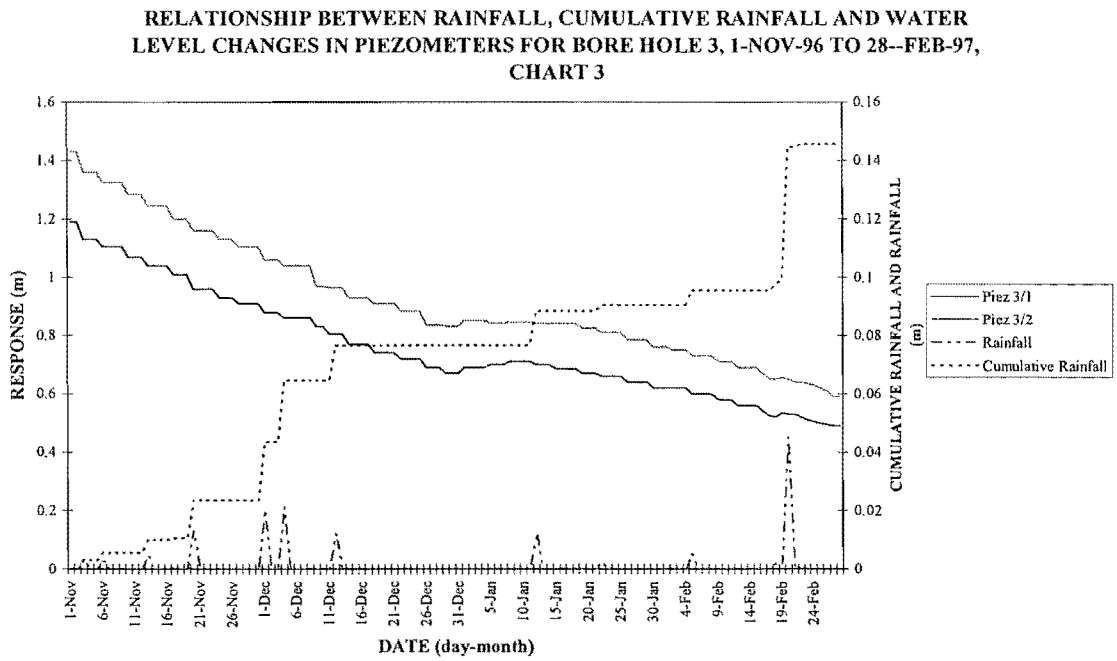

Figure A3.11 Plot of Piezometric water level responses to rainfall for borehole 3, 1 November 1996 to 28 February 1997.

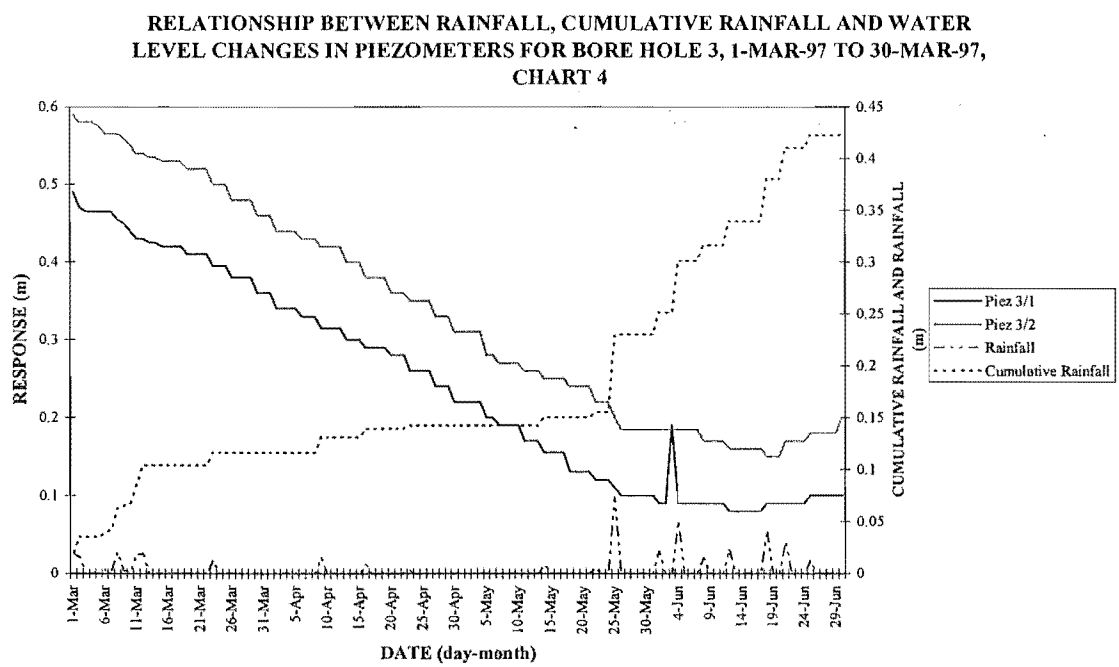

Figure A3.12 Plot of Piezometric water level responses to rainfall for borehole 3, 1 March 1997 to 30 March 1997

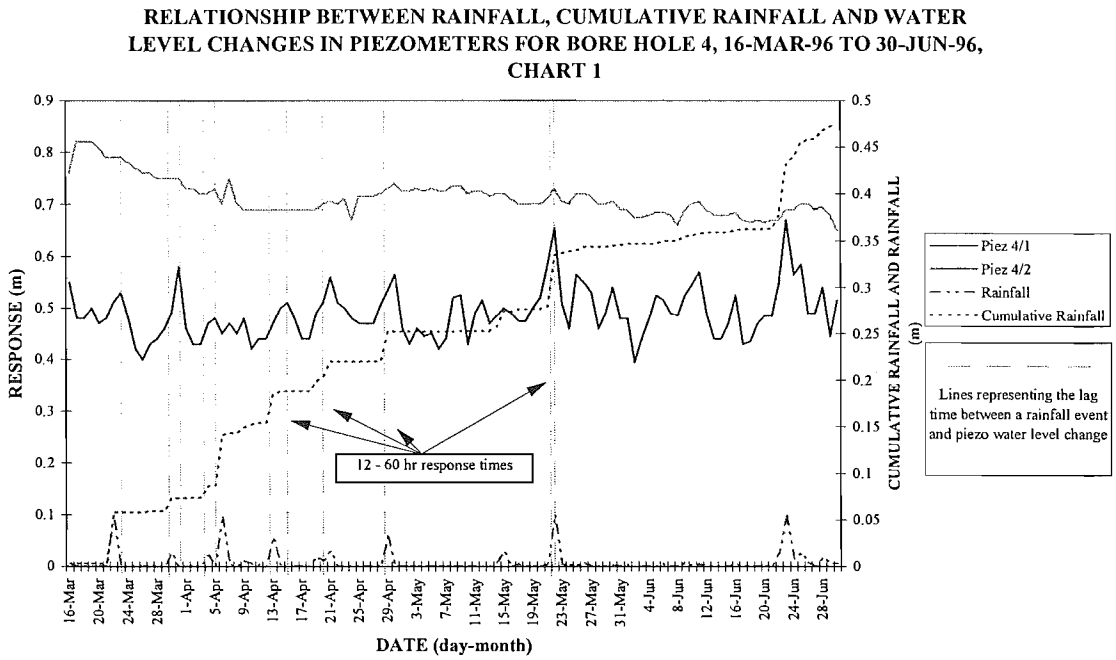

Figure A3.13 Plot of Piezometric water level responses to rainfall for borehole 4, 16 March 1996 to 30 June 1996.

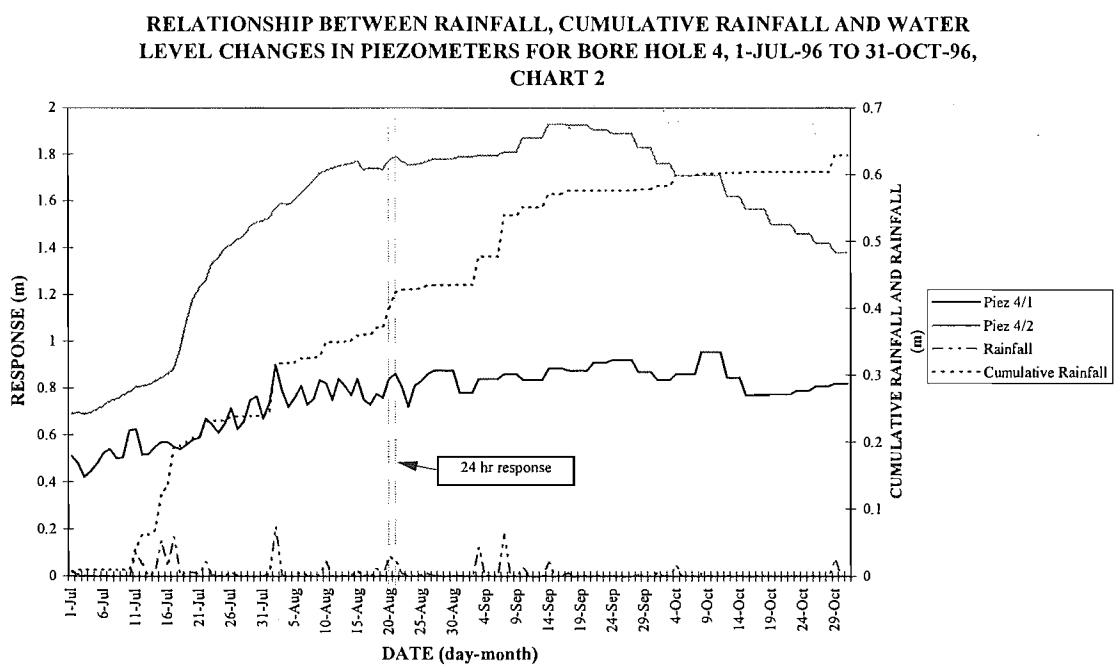

Figure A3.14 Plot of Piezometric water level responses to rainfall for borehole 4, 1 July 1996 to 31 October 1996.

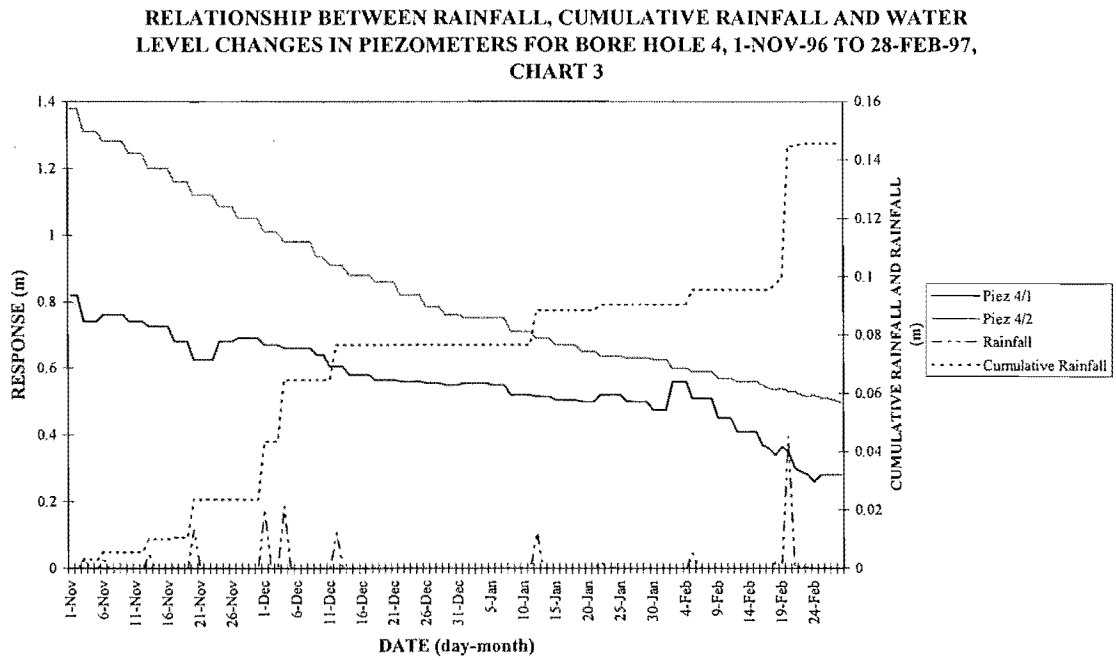

Figure A3.15 Plot of Piezometric water level responses to rainfall for borehole 4, 1 November 1996 to 28 February 1997.

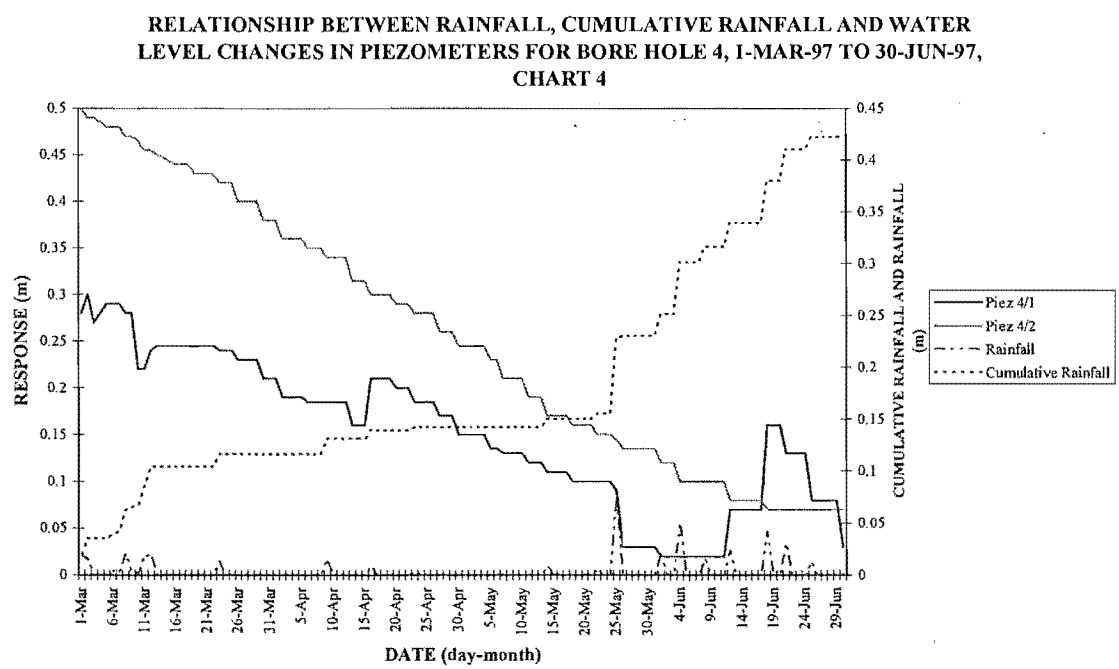

Figure A3.16 Plot of Piezometric water level responses to rainfall for borehole 4, 30 June 1997 to 30 June 1997.

RELATIONSHIP BETWEEN RAINFALL, CUMULATIVE RAINFALL AND WATER LEVEL CHANGES IN THE PIEZOMETER FOR BORE HOLE 5, 16-MAR-96 TO 30-JUN-96, CHART 1

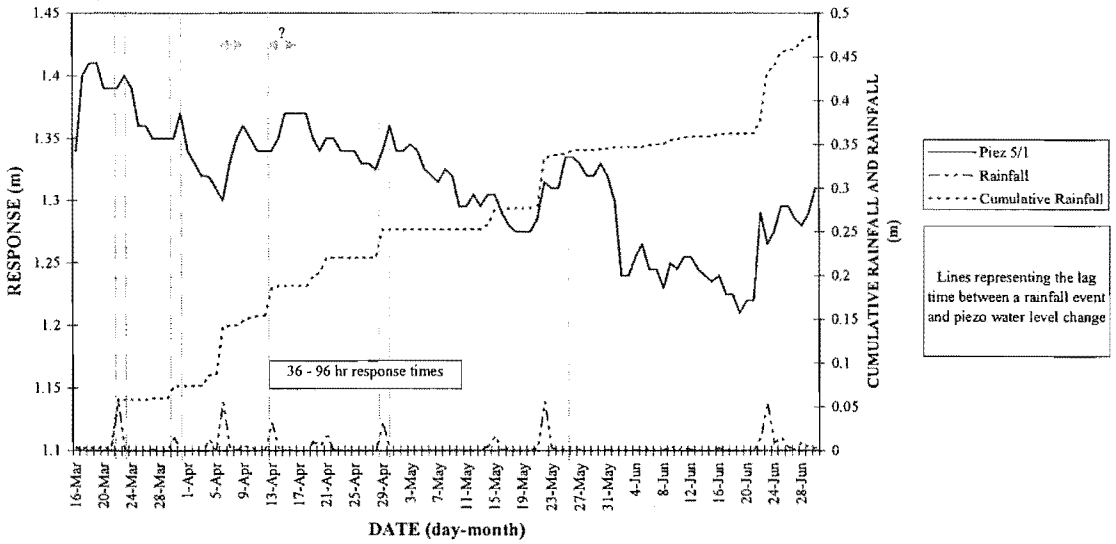

Figure A3.17 Plot of Piezometric water level responses to rainfall for borehole 5, 16 March 1996 to 30 June 1996.

RELATIONSHIP BETWEEN RAINFALL, CUMULATIVE RAINFALL AND WATER LEVEL CHANGES IN THE PIEZOMETER FOR BORE HOLE 5, 1-JUL-96 TO 31-OCT-97, CHART 2

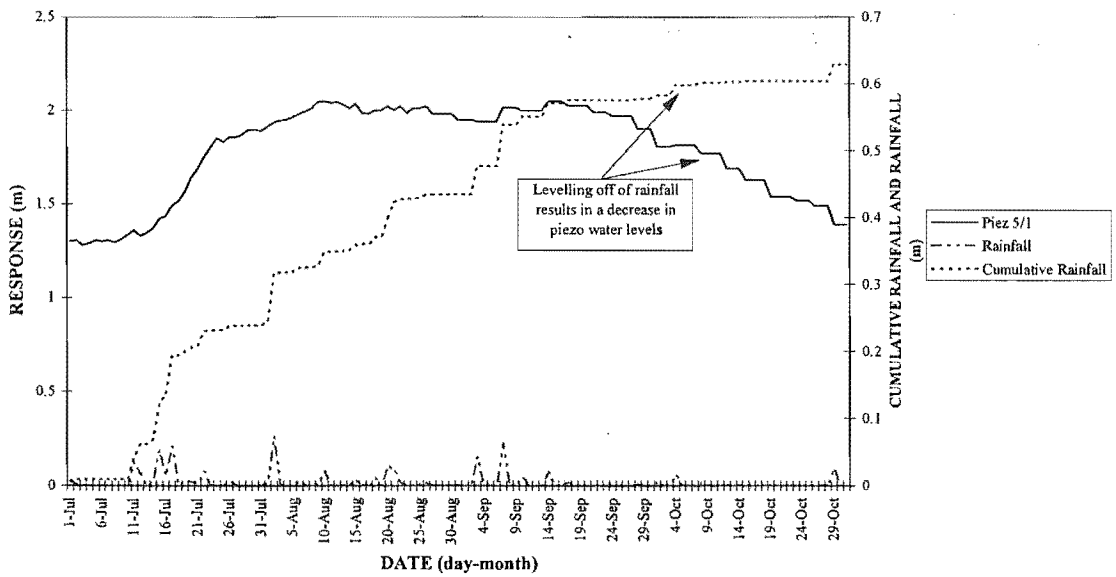

Figure A3.18 Plot of Piezometric water level responses to rainfall for borehole 5, 1 July 1996 to 31 October 1996.

RELATIONSHIP BETWEEN RAINFALL, CUMULATIVE RAINFALL AND WATER LEVEL CHANGES IN THE PIEZOMETER FOR BORE HOLE 5, 1-NOV-96 TO 28-FEB-97, CHART 3

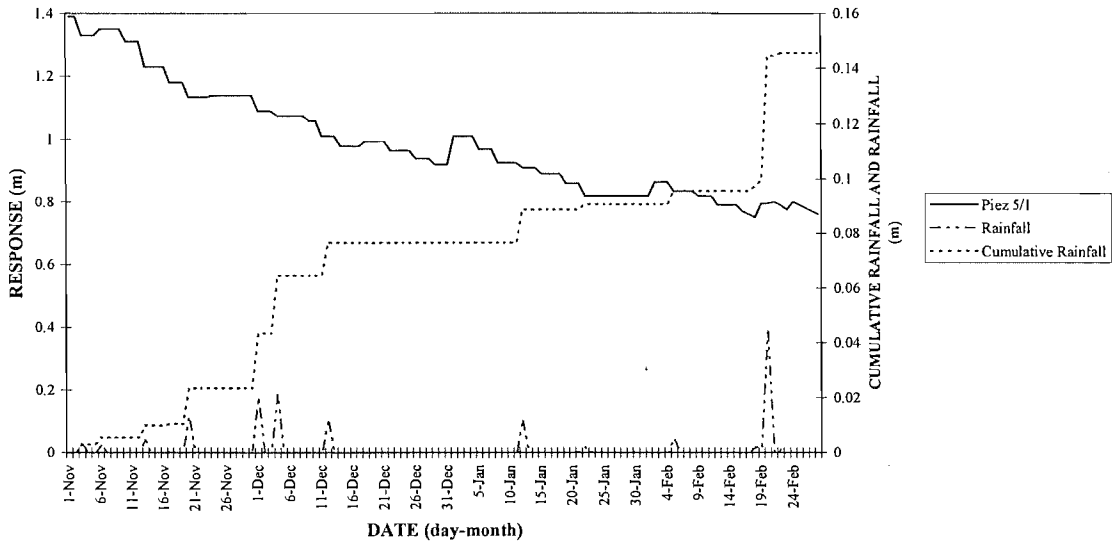

Figure A3.19 Plot of Piezometric water level responses to rainfall for borehole 5, 1 November 1996 to 28 February 1997.

RELATIONSHIP BETWEEN RAINFALL, CUMULATIVE RAINFALL AND WATER LEVEL CHANGES IN THE PIEZOMETER FOR BORE HOLE 5, 1-MAR-97 TO 30-JUN-97, CHART 4

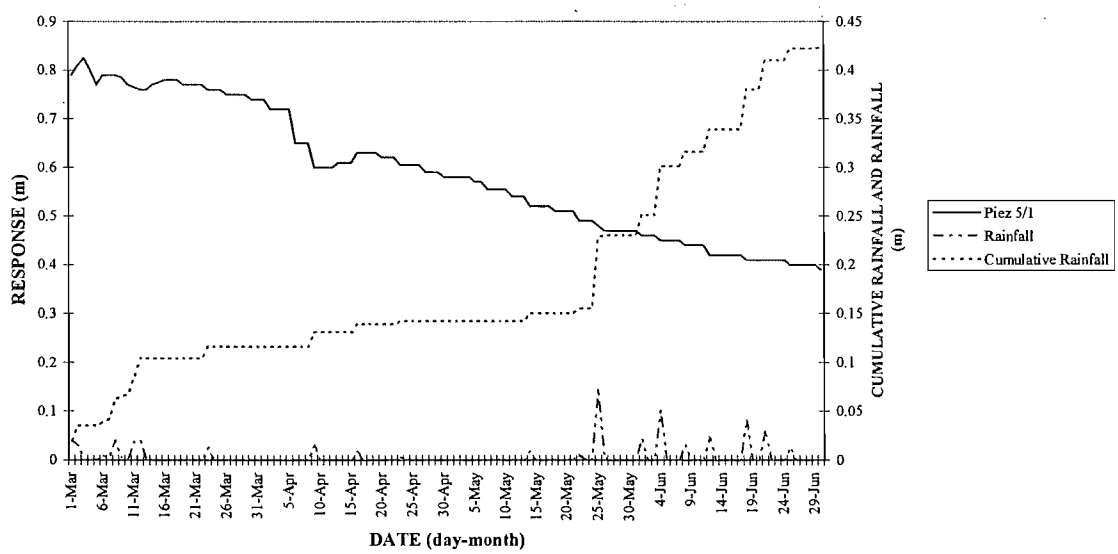

Figure A3.20 Plot of Piezometric water level responses to rainfall for borehole 5, 1 March 1997 to 30 June 1997.

RELATIONSHIP BETWEEN RAINFALL, CUMULATIVE RAINFALL AND WATER LEVEL CHANGES IN THE PIEZOMETER FOR BORE HOLE 6, 16-MAR-96 TO 30-JUN-96, CHART 1

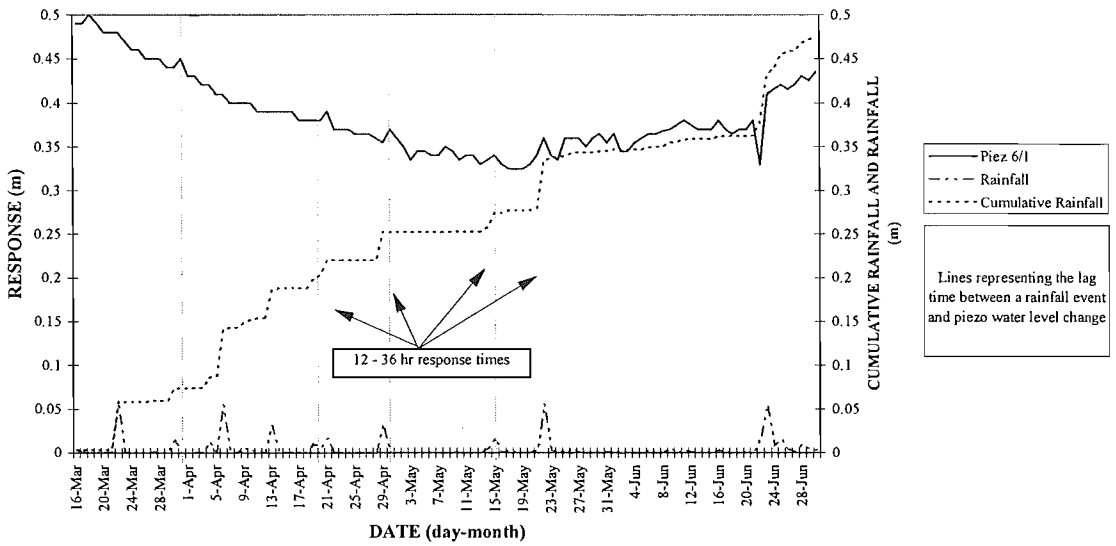

Figure A3.21 Plot of Piezometric water level responses to rainfall for borehole 6, 16 March 1996 to 30 June 1996.

RELATIONSHIP BETWEEN RAINFALL, CUMULATIVE RAINFALL AND WATER LEVEL CHANGES IN THE PIEZOMETER FOR BORE HOLE 6, 1-JUL-96 TO 31-OCT-96, CHART 2

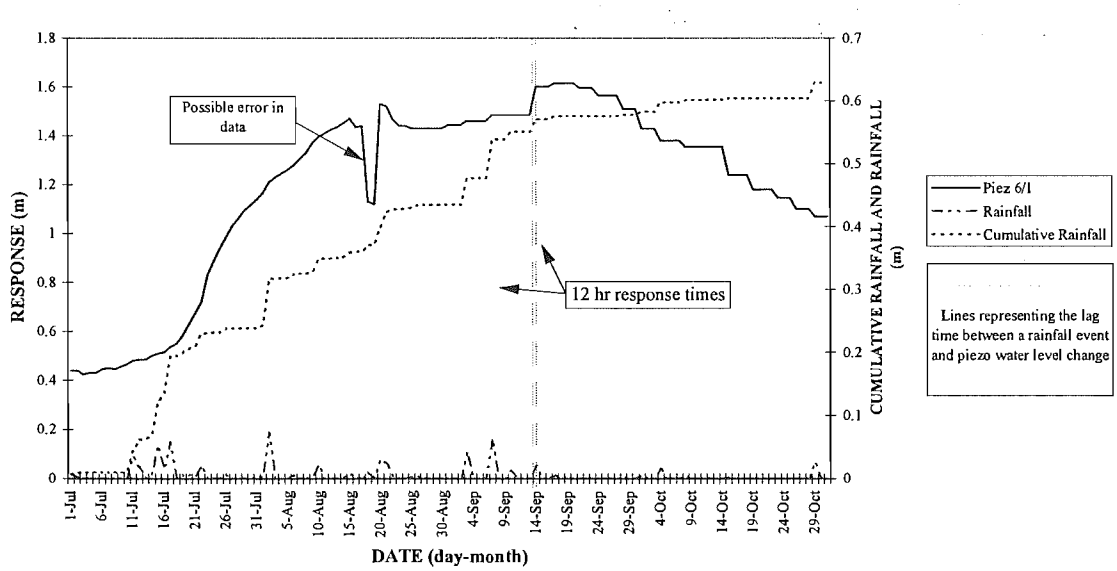

Figure A3.22 Plot of Piezometric water level responses to rainfall for borehole 6, 1 July 1996 to 31 October 1996.

RELATIONSHIP BETWEEN RAINFALL, CUMULATIVE RAINFALL AND WATER LEVEL CHANGES IN THE PIEZOMETER FOR BORE HOLE 6, 1-NOV-96 TO 28-FEB-97, CHART 3

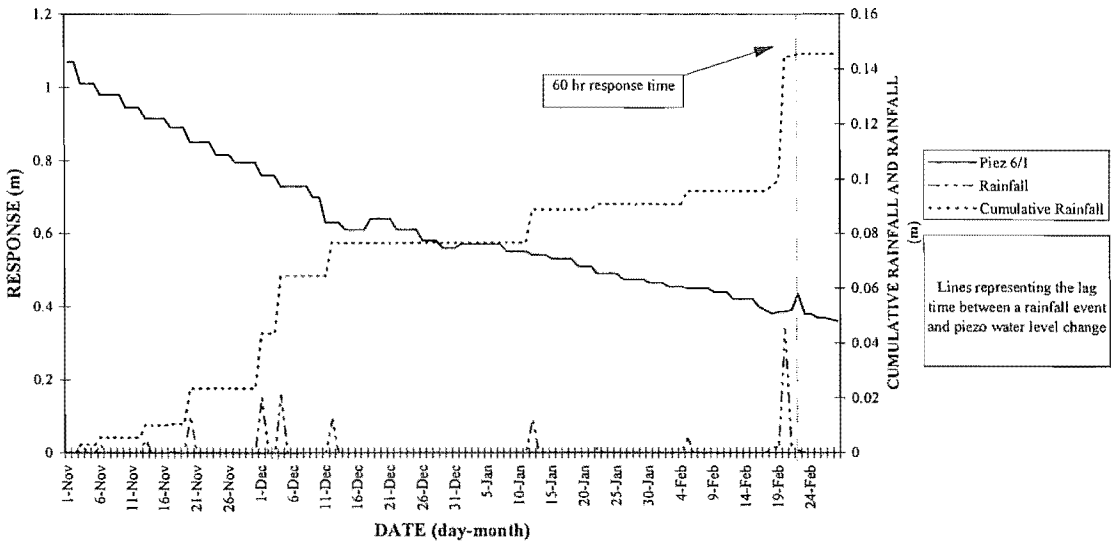

Figure A3.23 Plot of Piezometric water level responses to rainfall for borehole 6, 1 November 1996 to 28 February 1997.

RELATIONSHIP BETWEEN RAINFALL, CUMULATIVE RAINFALL AND WATER LEVEL CHANGES IN THE PIEZOMETER FOR BORE HOLE 6, 1-MAR-97 TO 30-JUN-97, C4

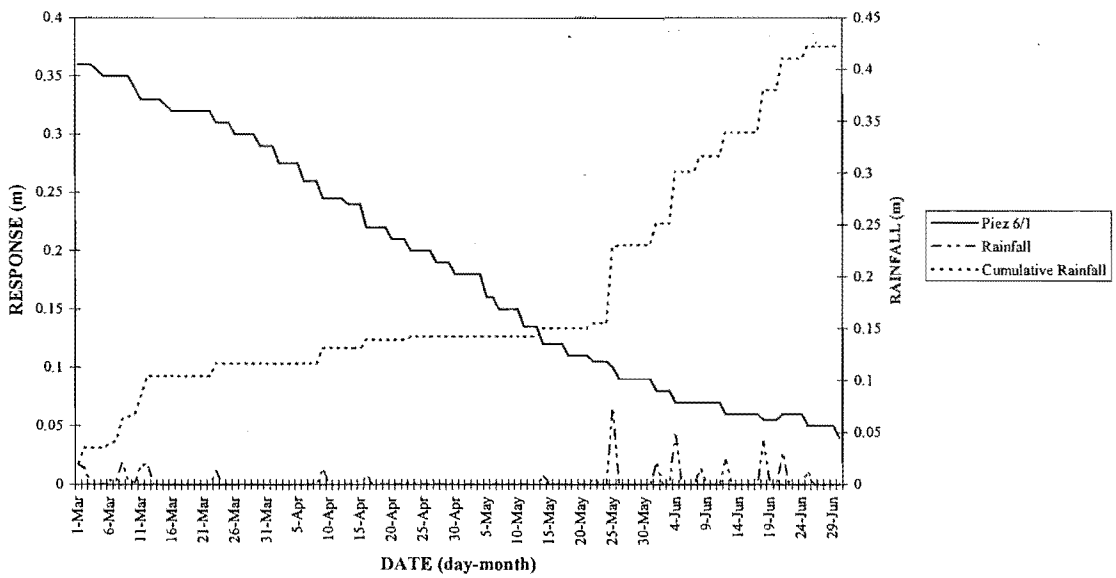

Figure A3.24 Plot of Piezometric water level responses to rainfall for borehole 6, 1 March 1997 to 30 June 1997.

RELATIONSHIP BETWEEN RAINFALL, CUMULATIVE RAINFALL AND WATER LEVEL CHANGES IN THE PIEZOMETER FOR BORE HOLE 7, 16-MAR-96 TO 30-JUN-96, CHART 1

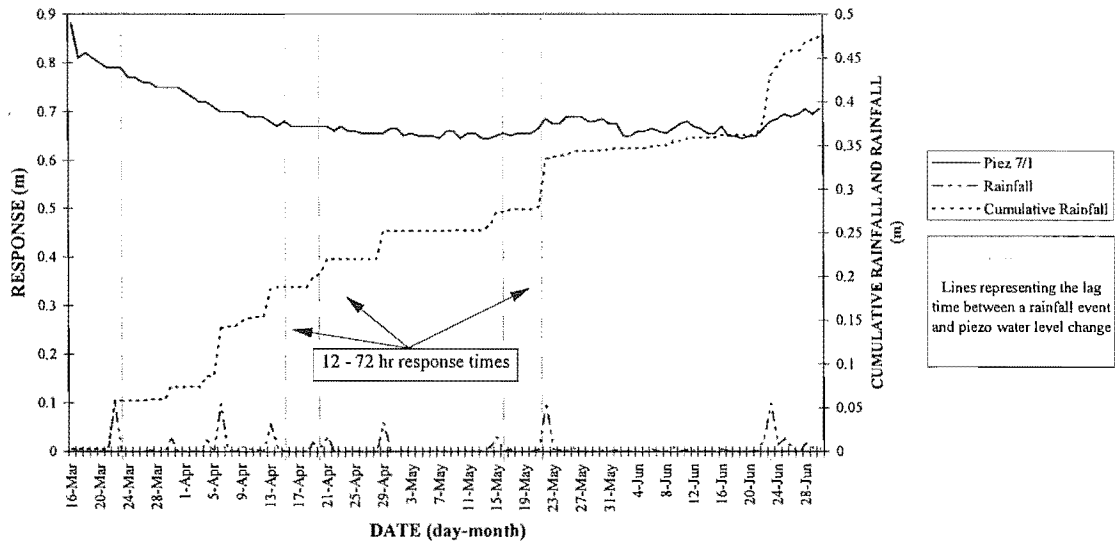

Figure A3.25 Plot of Piezometric water level responses to rainfall for borehole 7, 16 March 1996 to 30 June 1996.

RELATIONSHIP BETWEEN RAINFALL, CUMULATIVE RAINFALL AND WATER LEVEL CHANGES IN THE PIEZOMETER FOR BORE HOLE 7, 1-JUL-96 TO 31-OCT-96, CHART 2

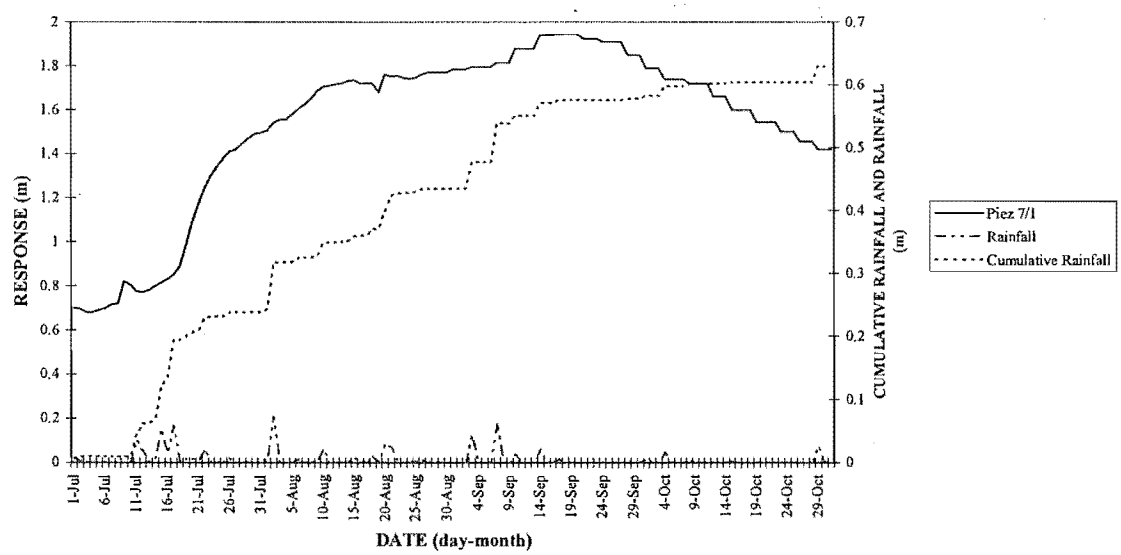

Figure A3.26 Plot of Piezometric water level responses to rainfall for borehole 7, 1 July 1996 to 31 October 1996.

RELATIONSHIP BETWEEN RAINFALL, CUMULATIVE RAINFALL AND WATER LEVEL CHANGES IN THE PIEZOMETER FOR BORE HOLE 7, 1-NOV-96 TO 28-FEB-97, CHART 3

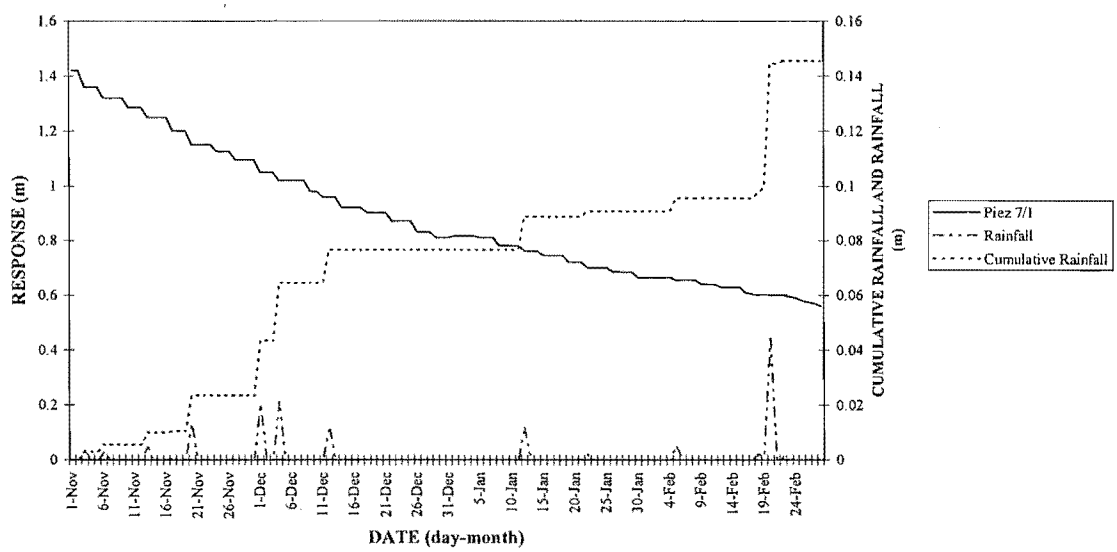

Figure A3.27 Plot of Piezometric water level responses to rainfall for borehole 7, 1 November 1996 to 28 February 1997.

RELATIONSHIP BETWEEN RAINFALL, CUMULATIVE RAINFALL AND WATER LEVEL CHANGES IN THE PIEZOMETER FOR BORE HOLE 7, 1-MAR-97 TO 30-JUN-97, CHART 4

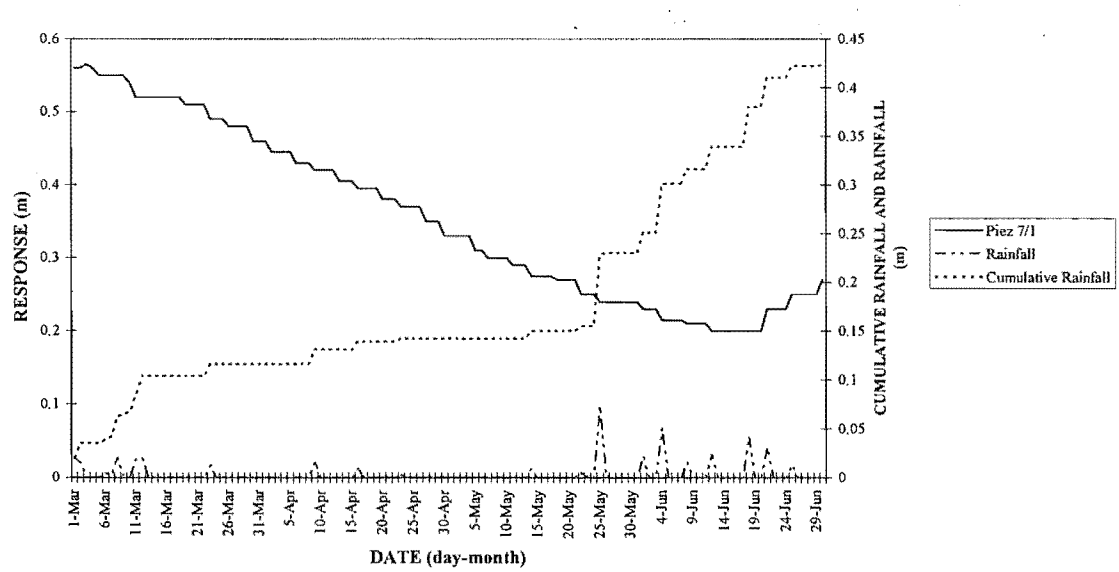

Figure A3.28 Plot of Piezometric water level responses to rainfall for borehole 7, 1 March 1997 to 30 June 1997.

RELATIONSHIP BETWEEN RAINFALL, CUMULATIVE RAINFALL AND WATER LEVEL CHANGES IN THE PIEZOMETER FOR BORE HOLE 8, 16-MAR-96 TO 30-JUN-96, CHART 1

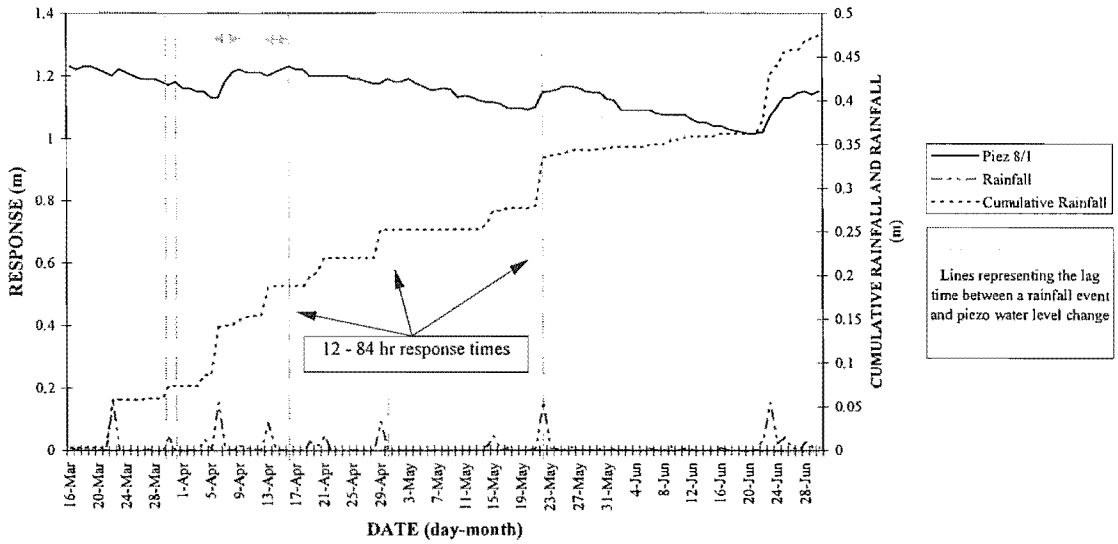

Figure A3.29 Plot of Piezometric water level responses to rainfall for borehole 8, 16 March 1996 to 30 June 1996.

RELATIONSHIP BETWEEN RAINFALL, CUMULATIVE RAINFALL AND WATER LEVEL CHANGES IN THE PIEZOMETER FOR BORE HOLE 8, 1-JUL-96 TO 31-OCT-96, CHART 2

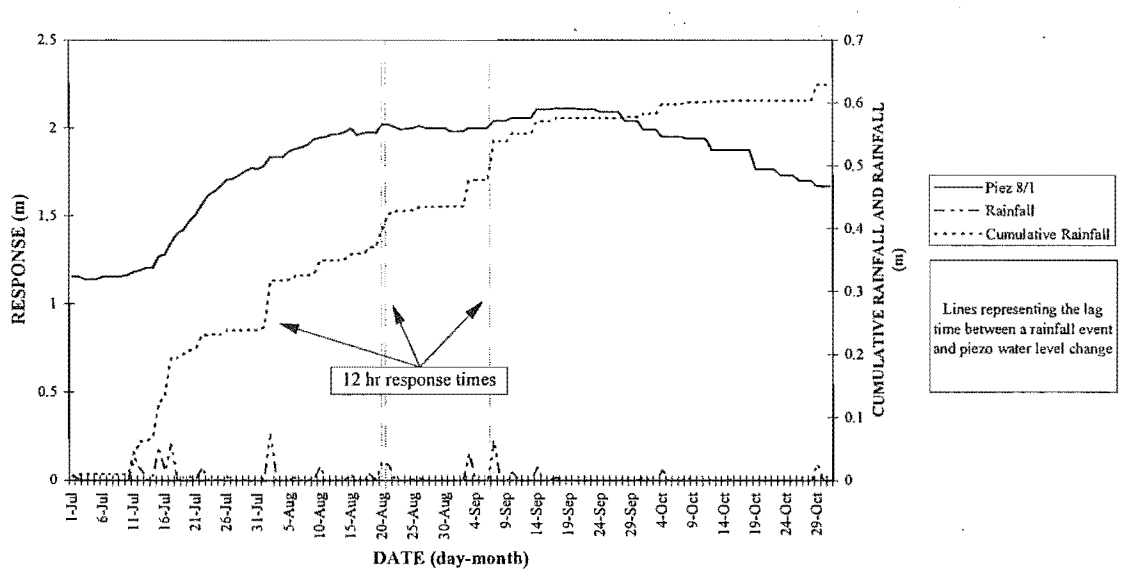

Figure A3.30 Plot of Piezometric water level responses to rainfall for borehole 8, 1 July 1996 to 31 October 1996.

RELATIONSHIP BETWEEN RAINFALL, CUMULATIVE RAINFALL AND WATER LEVEL CHANGES IN THE PIEZOMETER FOR BORE HOLE 8, 1-NOV-96 TO 28-FEB-97, CHART 3

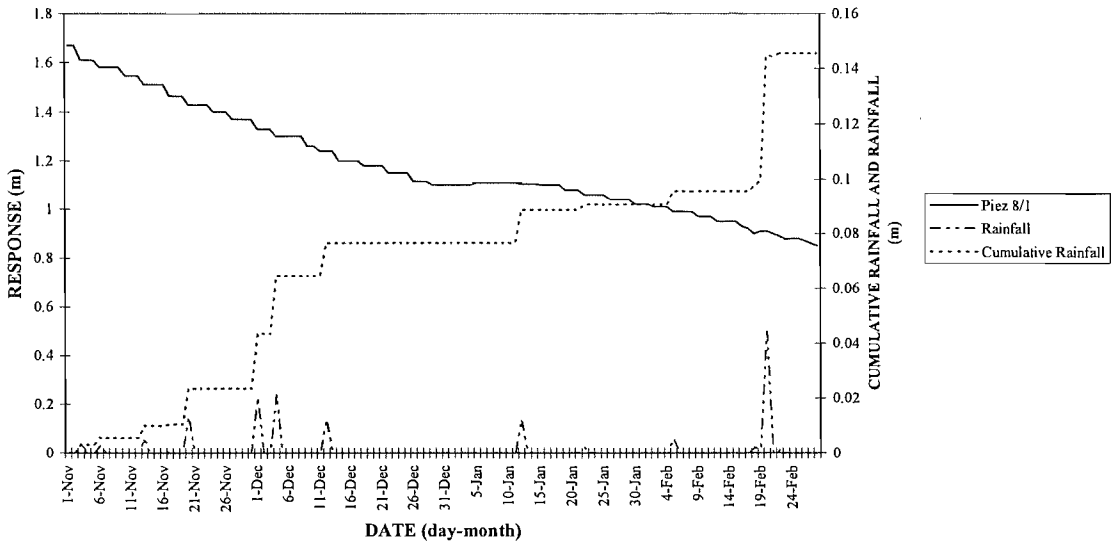

Figure A3.31 Plot of Piezometric water level responses to rainfall for borehole 8, 1 November 1996 to 28 February 1997.

RELATIONSHIP BETWEEN RAINFALL, CUMULATIVE RAINFALL AND WATER LEVEL CHANGES IN THE PIEZOMETER FOR BORE HOLE 8, 1-MAR-97 TO 30-JUN-97, CHART 4

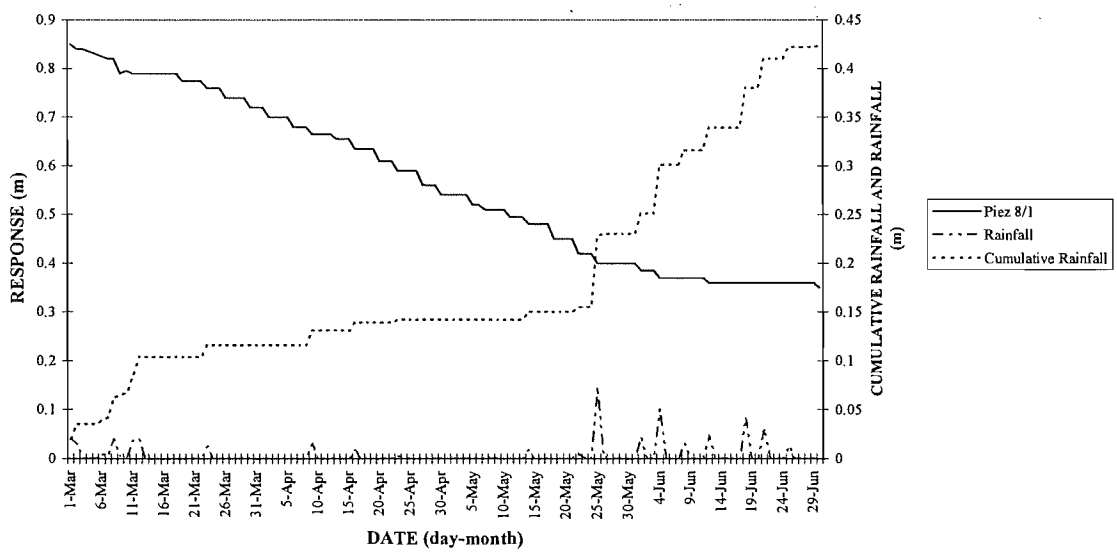

Figure A3.32 Plot of Piezometric water level responses to rainfall for borehole 8, 1 March 1997 to 30 June 1997.

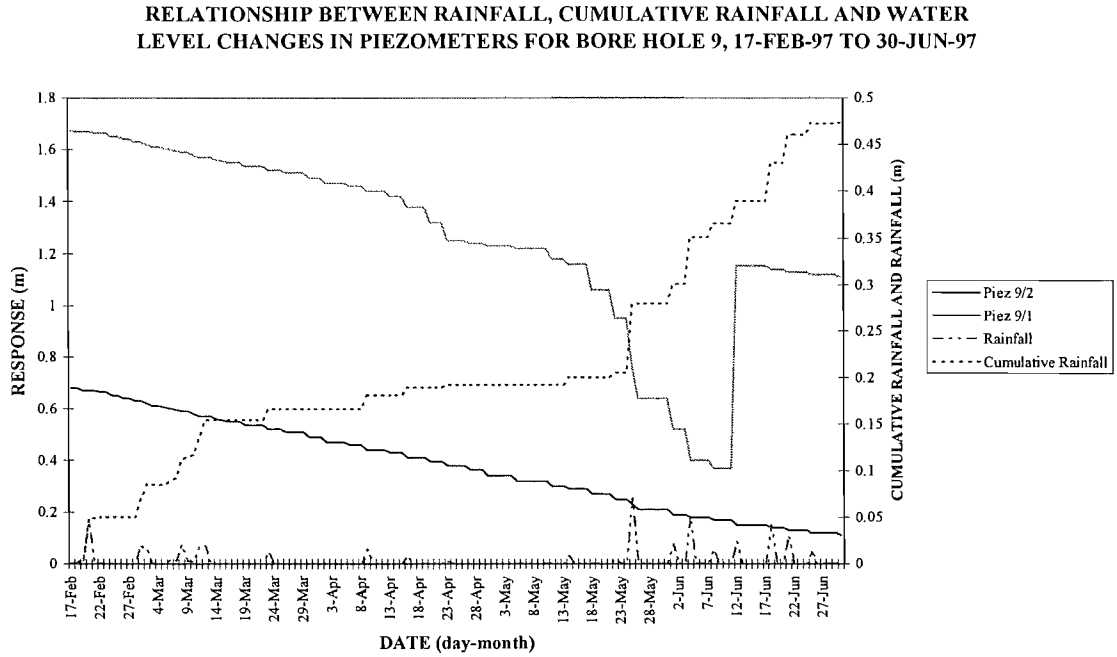

Figure A3.33 Plot of Piezometric water level responses to rainfall for borehole 9, 17 February 1997 to 30 June 1997.

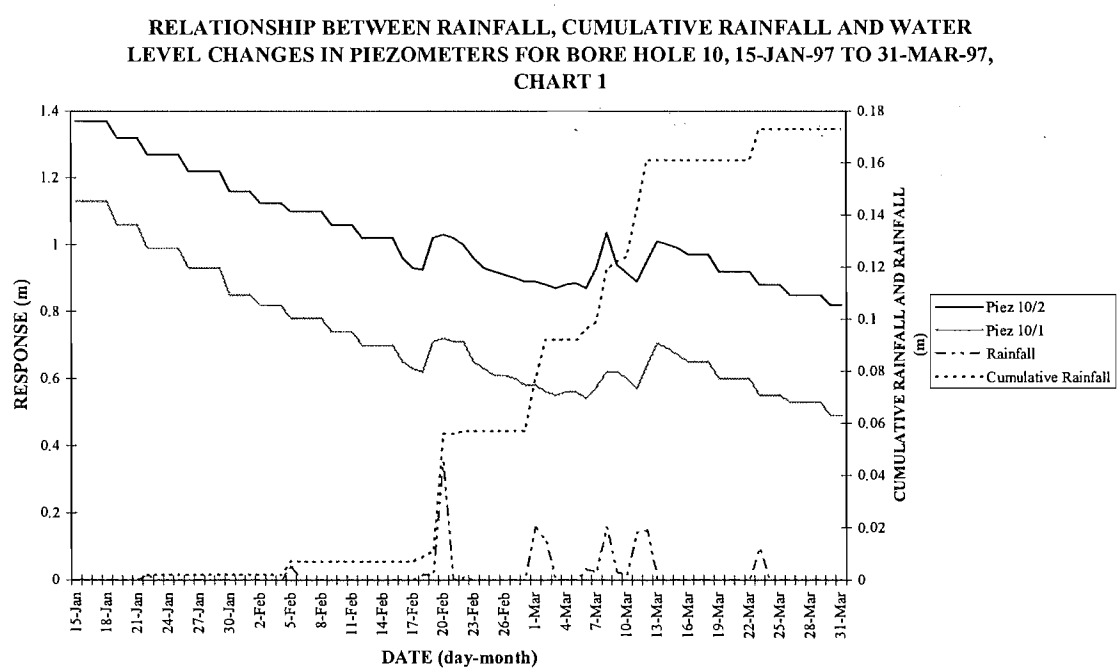

Figure A3.34 Plot of Piezometric water level responses to rainfall for borehole 9, 15 Janurary 1997 to 31 March 1997.

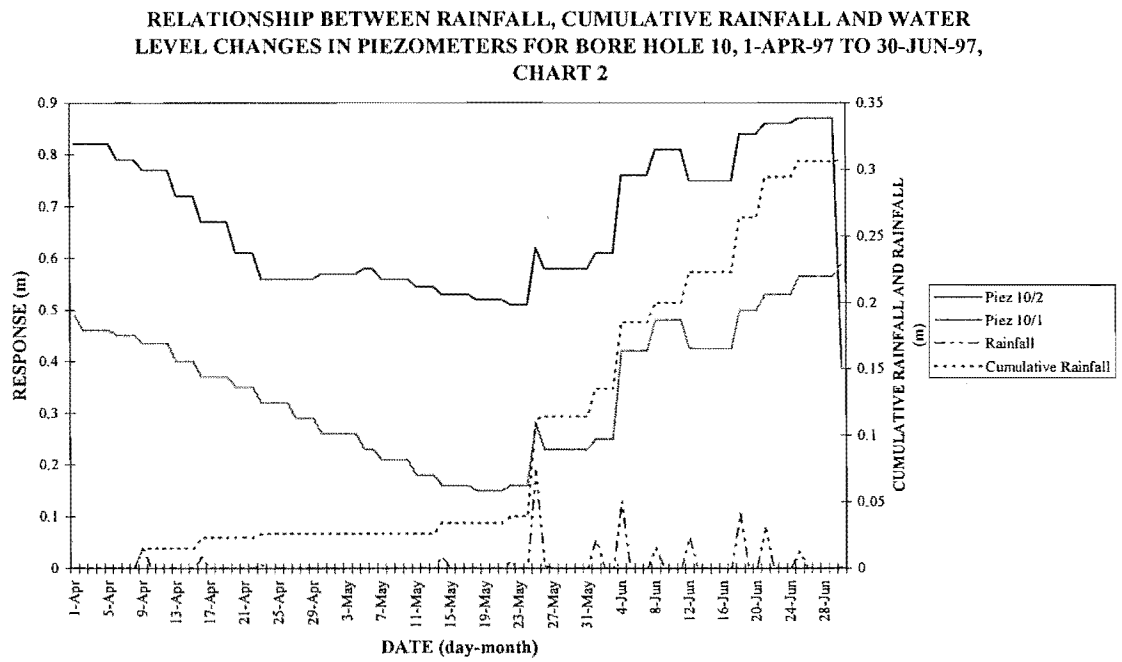

Figure A3.25 Plot of Piezometric water level responses to rainfall for borehole 10, 1 April 1997 to 30 June 1997.

APPENDIX A3.3 Field Permeability Investigations

The Hvorslev and Bouwer-Rice slug test methods were used to calculate permeability's from falling head test data collected from Piez 7/1. Methodology can be obtained from Fetter (1994) or Kruseman and de Ridder (1994).

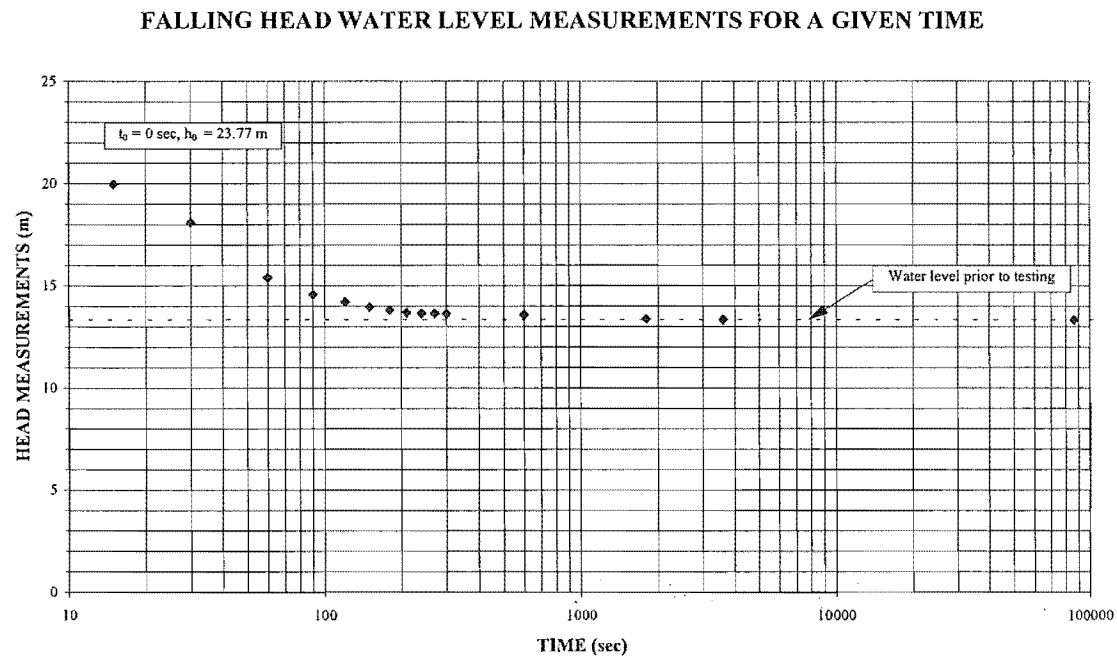

Figure A3.36 Plot showing raw data collected from a falling head permeability test conducted at Piez 7/1.

A3.2.1 Hvorslev Method (From Fetter, 1994)

This method can be used on piezometers and auger holes that do not fully penetrate an aquifer, with a water level above the slotted section of the piezo. Presented below are the steps that were used in the calculation of a permeability. Firstly H/H_0 was calculated from the raw data, Table ?. From here a plot of H/H_0 against time is used to produce T_0 or the time it takes for the water level to rise or fall to 37 % of the initial change, Figure ?. Once complete the permeability can then be calculated from the following expression:

$$K = \frac{r^2 Ln(L_e / R)}{2L_e T_0}$$

where

K is hydraulic conductivity (m/sec)

r is the radius of the well casing (m)

R is the radius of the well screen (m)

L_e is the length of the well screen (m)

T_0 is the time it takes for the water level to rise or fall to 37 % of the initial change

where for Piez 7/1 r = 0.014 m, R = 0.06 m, L_e = 0.5 m, & T_0 = 50 sec

$$K = \frac{0.014^2 Ln(0.5 / 0.06)}{2(0.5 \times 50)} = 8.3 \times 10^{-6} m / \text{sec}$$

Table A3.1 presenting calculations to obtain values for H/H_0.

Bore Hole 7 - Piez 7/1				
Piezometer internal diameter = 0.025 m Reduced Level 23.77 m Slotted Section = 11.0-11.5 m Height of water before testing = 10.45 m Reduced Level of water before testing = 13.32 m				
Time (sec)	Height (m)	RL	Change in Water Level h (m)	H/H_0
Static Water Leve	10.45	13.32		
0	0	23.77	10.45 (h_0)	1.571
15	3.8	19.97	6.65	1.000
30	5.69	18.08	4.76	0.716
60	8.38	15.39	2.07	0.311
90	9.2	14.57	1.25	0.188
120	9.56	14.21	0.89	0.134
150	9.81	13.96	0.64	0.096
180	9.97	13.8	0.48	0.072
210	10.08	13.69	0.37	0.056
240	10.12	13.65	0.33	0.050
270	10.13	13.64	0.32	0.048
300	10.15	13.62	0.3	0.045
600	10.18	13.59	0.27	0.041
1800	10.39	13.38	0.06	0.009
3600	10.43	13.34	0.02	0.003
86400	10.45	13.32	0	0.000

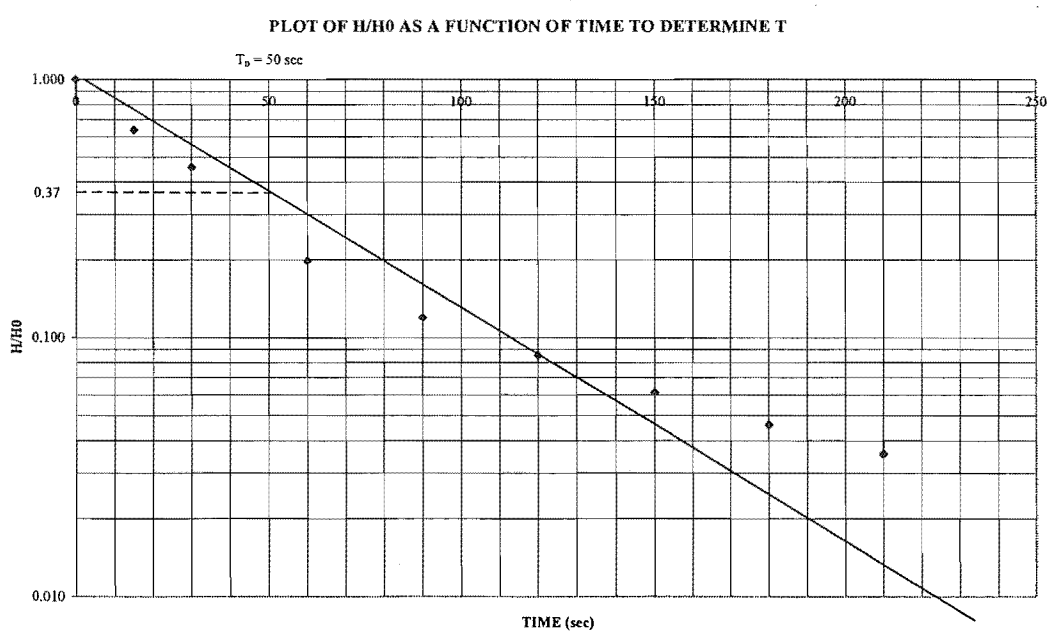

Figure A3.37 Plot to determine T_0.

A3.2.2 Bouwer and Rice Method (From Fetter (1994), and Kruseman & de Ridder (1994)

The Bouwer-Rice method can be used for fully or partially penetrating piezometers. Also the method is applicable for both the addition or removal of water from the piezometer. Permeability is calculate from the relationship:

$$K = \frac{r_c^{\,2} Ln(R_e / r_w)}{2d} \frac{1}{t} Ln \frac{h_0}{h_t}$$

where

r_c radius of the unscreened part of the well where the head is rising

r_w horizontal distance from well centre to undisturbed aquifer

R_e radial distance over which the difference in head, h0, is dissipated in the flow system of the aquifer

d length of the well screen or open section of the well

h_0 head in the well at time $t_0 = 0$

h_t head in the well at time $t > t0$

The geometrical parameters r_c, r_w, and d are shown in Figure ?.

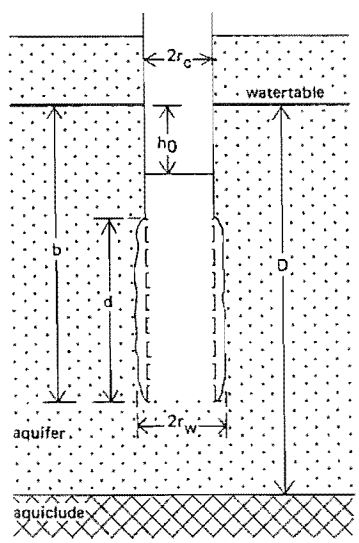

Figure A3.38 An unconfined aquifer, partially penetrated by a large-diameter well from which a slug of water has been removed

In order to calculate K two relationships have to be addressed: $Ln(R_e/r_w)$ and $1/tLn(h_0/h_t)$. The first can be calculated from the expression below where A, B, and D are obtained form Figure ?.

$$Ln\frac{R_e}{r_w}=\left[\frac{1.1}{Ln(b/r_w)}+\frac{A+BLn[(D-b)/r_w]^{-1}}{d/r_w}\right]$$

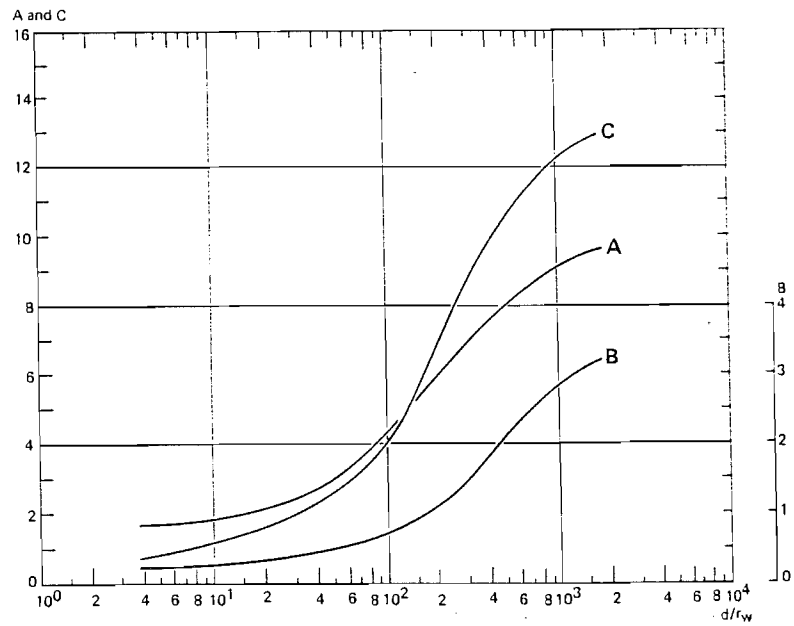

Figure A3.39 The Bouwer and Rice curves showing the relationship between the parameters A, B, C, and d/rw, from Kruseman & de Ridder (1994).

Where A = 1.8, B = 0.25, and C = 1.0, b = 1.05 m, r_w = 0.06 m, and d = 0.5 m, D = 13.25 m, therefore:

$$Ln\frac{Re}{rw}=\left[\frac{1.1}{Ln(1.05/0.06)}+\frac{1.8+0.25Ln[(13.25-1.05)/0.06]^{-1}}{0.5/0.06}\right]$$

$$.....=0.525$$

Secondarly under these conditions where $1/tLn(h_0/ht) = (1/(t_2-t_1))Ln(H_1/H_2)$, $1/tLn(h_0/ht)$ can be obtained from Figure ?.

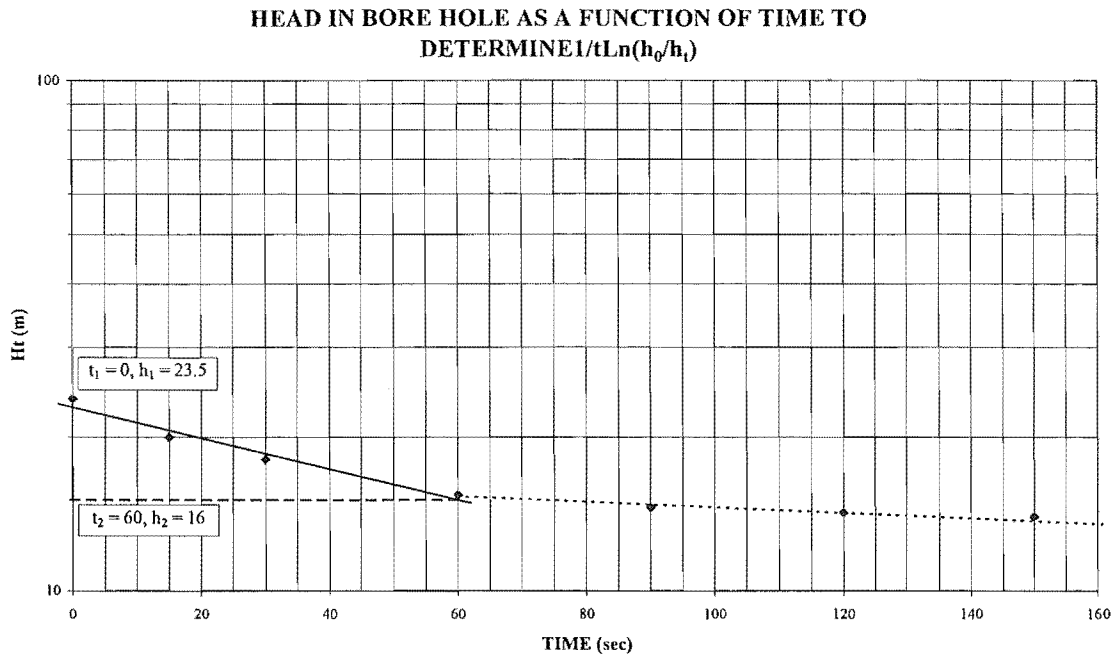

Figure A3.40 Plot to determine the relationship (1/t)Ln(H_0/H_t).

Therefore

$$\frac{1}{t}Ln\frac{H_0}{H_t} = \frac{1}{(t_2 - t_1)}Ln\frac{H_1}{H_2}$$

$$\ldots\ldots\ldots = \frac{1}{(60-0)}Ln\frac{23.5}{16.0}$$

$$\ldots\ldots\ldots = 6.4\times10^{-3}$$

Combining the two relationships the permeability can now be calculated as follows, where r_c^2 = 0.014 m, d = 0.5 m, Ln(R_e/r_w) = 0.525, and (1/t)Ln(h_0/h_t) = 6.4×10^{-3} then:

$$K = \frac{r_c^{\,2}Ln(R_e / r_w)}{2d}\frac{1}{t}Ln\frac{h_0}{h_t}$$

$$\ldots = \frac{0.014^2 \times 0.525}{2\times0.5}\times 6.4\times10^{-3}$$

$$\ldots = 6.6\times10^{-7}\, m/\sec$$

APPENDIX A4.1 Tests Performed On Samples

Stratigraphic Unit	Test Performed On A Sample From A Particular Unit							
	Particle Size Analysis	Clay mineralogy	Atterberg Limits	Direct Shear	Triaxial	Dispersion	Erodibility	Permeability
Post-Rotoehu Ash Tephras				2.7/1/85		0.4/1/330	0.4/1/330	3.2-3.4/1/89
Rotoehu Ash	4.6/1/85					4.6/1/85		2.55-2.75/1/330 4.3-5.0/1/85
Palaeosol	5.8/1/85	5.8/1/85	5.8/1/85		3.1/1/330	3.1/1/330	3.1/1/330	3.1/1/330
Hamilton Ash	8.2/1/85	8.2/1/85	8.2/1/85		4.9/1/330			8.2/1/85
Pahoia Tephras				12.4/1/89				10.3-10.5/1/330
Cross-bedded sequence	15.1/1/85 15.6/1/85	15.1/1/85 15.6/1/86	15.1/1/85	15.6/1/85 16.5/1/89 17.0/1/89 18.6/1/89	16.0/1/85 sample 9	9.8/1/330 10.0/1/330 14.0/1/330 14.2/1/330	9.8/1/330 10.0/1/330 14.0/1/330 14.2/1/330	16/1/85 sample 13
Upper bounding aquitard				Sample 11	sample 10			
Aquifer	17.1/1/330			17.1/1/330	sample 1 sample 3top	18.0/1/85	18.0/1/85	17.1/1/330
Lower bounding aquitard	18.075/1/85 18.075-18.08/1/85 18.08-18.095/1/85 18.095-18.10/1/85 18.10-18.11/1/85 18.11-18.12/1/85 18.12-18.23/1/85	18.075/1/86 18.075-18.08/1/86 18.08-18.095/1/85 18.095-18.10/1/85 18.10-18.11/1/85 18.11-18.12/1/85 18.12-18.23/1/85	18.08-18.095/1/85 18.095-18.10/1/85 18.10-18.11/1/85 18.11-18.12/1/85 18.12-18.23/1/85		sample 2top sample 2bottom sample 3bottom	18.8/1/85	18.8/1/85	sample 12

APPENDIX A4.2 Particle Size Analysis

A wide variety of grainsize terminology schemes are available for the differing needs of proffesional in various areas of experties, e.g. two common ones are, the Udden-Wentworth scale used by geologists, and the New Zealand Geomechanics Society scheme adopted by most engineers within New Zealand. Table A4.1 demonstrates how the two schemes differ in defining the boundaries between variuos grainsizes.

Table A4.1 A comparison between grain size analysis schemes for the Udden-Wentworth scale and the NZ Geomechanics Society scheme.

GRAINSIZE ANALYSIS SCHEMES						
NZ Geomechanics Society Scheme			**Udden-Wentworth Scale**			
Soil Fraction		Particle Size (mm)	Soil Fraction		Particle Size (mm)	Phi Diameter (phi = $-\log_2$ mm)
CLAY		< 0.002	CLAY		< 0.0039	> 8
SILT		0.002 - 0.006	SILT	Very Fine	0.0039 - 0.0078	8 - 7
SAND	Fine	0.06 - 0.2		Fine	0.0078 - 0.0156	7 - 6
	Medium	0.2 - 0.6		Medium	0.0156 - 0.0313	6 - 5
	Coarse	0.6 - 2.0		Coarse	0.0313 - 0.0625	5 - 4
GRAVEL	Fine	2.0 - 6.0	SAND	Very Fine	0.0625 - 0.125	4 - 3
	Medium	6.0 - 20.0		Fine	0.125 - 0.25	3 - 2
	Coarse	20.0 - 60.0		Medium	0.25 - 0.5	2 - 1
	Very Coarse	60.0 - 200.0		Coarse	0.5 - 1	1 - 0
BOULDERS		> 200.0		Very Coarse	1 - 2	0 - -1
			GRANULE		2 - 4	-1 - -2
			PEBBLE		4 - 64	-2 - -6
			COBBLE		64 - 256	-6 - -8
			BOULDER		> 256	< -8

For this project the grainsize terminology scheme which was used in the field investigation section of the thesis was also adopted for the particle size analysis section of the labouratory chapter, Table A4.2. As it can be seen it compares favouribly to the two other schemes. The main reason that this scheme was chosen over the NZ geomechanics society's (as stated in chapter 2) was that it provided greater reproduciable and accurate results in assessing grainsize, than the more subjective estimation of grainsize produced with other terminology schemes. This was due to the grainsize compartive card which provided a pictourial representation of the varoius grainsizes.

In this project the "phi" scale is use as a means to simplify the grainsizes that would normally be given in millimetres, e.g. Table 2. The phi scale (ϕ) was introduce by Krumbein (1934) to avoid dealing with fractions of millimeters and having to use semi-log paper. The phi diameter is related to particle diameter by the relationship phi=-$\log_2$mm, with the most abundant particles, those finer than 1 mm having positive values, Lewis & McMonchie (1994).

Another significant difference between the engineering and geological classification schemes is how they define the boundary between clays and silts. Under such schemes as the NZS Geomechanics society's the clay boundary is set at 0.002 mm compared to 0.0039 for the Udden-Wentworth scale. For this project both boundaries are presented in the tables of grainsize distribution, Tables ?-?.

Table A4.2 Grainsize terminology used in field description of soils (from Department Of Geology, University of Canterbury).

GRAINSIZE ANALYSIS SCHEME			
Soil Fraction		Particle Size (mm)	Phi Diameter (phi = -$\log_2$ mm)
MUD	Clay	< 0.0039	> 8
	Silt	0.0039 - 0.0625	8 - 4
SAND	Very Fine	0.0625 - 0.125	4 - 3
	Fine	0.125 - 0.25	3 - 2
	Medium	0.25 - 0.5	2 - 1
	Coarse	0.5 - 1	1 - 0
	Very Coarse	1 - 2	0 - -1
GRANULE		2 - 4	-1 - -2
PEBBLE	Fine	4 - 8	-2 - -3
	Medium	8 - 16	-3 - -4
	Coarse	16 - 32	-4 - -5
	Very Coarse	32 - 64	-5 - -6
COBBLE		64 - 256	-6 - -8
BOULDER		> 256	< -8

Methodology

The method used to determine the particle size distribution of the various soils of interrest was a combination of Lewis & McConchie (1994) Samples for testing were obtained from

Bulk samples collect during field investigations. Table A4.3 and A4.4 provide a description of the methologies used.

Table A4.3 Example of a standard procedure for pipette analysis of a mud, Lewis and McConchie (1994).

Preparation

1. Obtain a representative subsample that will yield no more than 15–20 g of mud.

2. Fully disaggregate the subsample (see Chapter 5). It may be adequate to cover the sample with a little distilled water plus dispersant (keep track of dispersant added) in a beaker and to use fingers in a rubber glove to break up the sample fully (rinse mud off glove back into the beaker). Alternatively, standardize on a time with an ultrasonic device.

3. Wet-sieve the sample with a *reserved-for-the-purpose* 4ϕ wet sieve. Place the sieve over a large evaporating basin and wash all its fines into the sieve using as little distilled water (usually the standard dispersant solution) as possible—end up with no more than 900 mL of water and mud! (After about 600 mL, let the silt settle out, then use the partly clear water for further wet-sieving; wash finally with clean water.)

4. Transfer all the sand fraction retained on the sieve to an evaporating basin or a beaker, using the wash bottle. Dry the sand fraction, leave to cool for 1 hr, and weigh to 0.001 g. (If there is a significant amount of sand, dry-sieve it before carrying out the pipette analysis, and extract any new mud fraction that may appear after dry sieving.)

5. Transfer all the mud collected in the basin to the 1-L measuring cylinder via a large funnel (label each cylinder).

6. Add 20 mL of prepared dispersant solution to the column if you have not previously used a solution with dispersant in your wash bottle or for disaggregation (see Chapter 5, "Dispersion of Clays"). Between about 0.5 and 1 g of sodium hexametaphosphate ("Calgon") is normally sufficient to prevent flocculation of clays, but this compound may dissolve fine carbonate grains such as foraminifers and may interfere with later X-ray analysis of clays. It is essential to know the exact amount of dispersant in each column for later calculations.

7. Top the column up to 1000 mL with distilled water. Thoroughly stir the column with a brass stirring rod (a disk with holes at the bottom of the tube is designed to generate maximum turbulence).

8. Label, and weigh to 0.001 g, eight (or nine) 50-mL beakers (one for each withdrawal on the pipette data sheet). Arrange the beakers in front of the column.

9. Cover the column with a watchglass and let it stand overnight to check for flocculation before running the pipette analysis. Fill a beaker with tap water and insert a thermometer (preparatory to the next step).

Analysis

Begin pipette analysis early in the morning, because the time between first and last withdrawals is at least 8 hours.

Before beginning, check that no columns have flocculated. Flocculation can be recognized by a curdling and rapid settling of clumps of particles, or by the presence of a thick, soupy layer on the bottom of the cylinder that passes abruptly into relatively clear water above. If flocculation is evident, try adding more dispersant solution or make up a new suspension with a smaller amount of sample. Using a mechanical stirrer for 5 minutes may assist dispersion.

10. Take the temperature of the water in the beaker of tap water and look up the corrected depths in Table 7-2. Note these depths on the pipette schedule, and monitor any temperature changes during the analysis (or ensure constant temperature by air conditioning). Viscosity changes with temperature and settling velocities will change significantly if there is variation.

11. Select a 20-mL pipette (one that empties quickly) with depth graduations. Connect a rubber pipette filler and check that the suction works efficiently. Have a large beaker of distilled water ready on the bench for rinsing.

12. Start the timepiece 1 min before the initial withdrawal (if using an electronic timepiece, set it at 11:59 P.M.). Immediately begin stirring column 1, using a brass stirrer. Start with short, quick strokes at the bottom and stir up all the settled mud, then work up the column with long, vigorous strokes, being careful not to mix air in with the suspension. Precisely at time zero (12:00:00 on the electronic timepiece), withdraw the stirrer. Lower the pipette to 20 cm. At exactly 20 sec, extract a 20-mL sample. Empty it into the respective 50-mL beaker and then rinse the pipette into the same beaker after sucking up 20 mL distilled water (also wash outer part with distilled water from the wash bottle).

This first withdrawal is particularly critical since it represents everything finer than 4ϕ (that is, total mud). Insertion of the pipette for subsequent withdrawals should be made with much more care to avoid creating turbulence.

13. The next withdrawal is for the fraction finer than 4.5ϕ. At exactly 2 min, withdraw 20 mL, empty it into the next beaker, and rinse as before.

Repeat the procedure for all subsequent withdrawals. Efficiency is essential, particularly where multiple samples are to be analyzed. Initially, a withdrawal must be made and the next column stirred within 1 min. Withdrawal and rinsing need to be completed in 30 sec, leaving 30 sec for stirring the next column. (To ensure thorough stirring of every column, carry out a preliminary stir in each one during an earlier spare moment.)

If withdrawal must be made at the wrong depth or time, make a note of the error and use Fig. 7-11 to find the grain size represented.

When there are long periods between withdrawals, cover each column with a watch glass. Any external source of vibration must be eliminated during the analysis.

14. When all withdrawals are completed, put beakers onto trays and oven dry them; it may take up to 48 hr to evaporate all the water. If further analysis of the clays is to follow, do not heat above 65°C.

15. Remove dry beakers from the oven and leave them to equilibrate with the atmosphere for at least 1 hr. Weigh to 0.001 g; record on data sheet.

16. Calculate cumulative weight percentages:

(a) Subtract beaker weights from beaker + sediment weights to get sediment weights.
(b) Multiply the weight of sediment from the 4ϕ sample by 50 and subtract the weight of dispersant in the column. This gives the total weight of mud, e.g., 0.405g (4ϕ sediment weight) × 50 − 1 g (wt. of Calgon in the procedure suggested) = 19.25 g (weight of mud, F).

This value, added to the weight of the sand fraction (S) determined from step 4, provides total sample weight. To test for experimental error, either (1) measure total sample dry weight initially (however, even low-temperature drying may cause problems in subsequent dispersion of the clay fraction); or (2) dry and weigh the suspension remaining in the cylinder after full analysis. If error has crept in to the above calculations, correct as necessary.

(c) Add the sand percentages cumulatively to obtain their cumulative percentages (step 9 of Table 7-1).
(d) Remember that each pipette sample represents material in the column finer than a certain grain size. To obtain cumulative percentages for mud intervals, multiply each mud weight by 50, subtract the weight of dispersant, divide by the total sample weight, and subtract from 100:

cum. % (mud range) =

$$100 - \frac{100 \times (50 \times (\text{pipette sample wt.})) - 1 \text{ (assuming 1g/L dispersant)}}{S + F}$$

A computer program can be constructed easily in standard spreadsheet software packages to process the raw data (all cells other than those for data entry should be "locked"; see also Slatt and Press 1976; Coates and Hulse 1985).

17. Plot results on graph paper as required (see Figs. 7-4–7-7) and proceed to graphical statistical analysis, or process by Method of Moments.

Table A4.4 Example of a standard procedure for sieve analysis of a sand, Lewis and McConhie (1994).

Preparation

1. Disaggregate thoroughly, remove salts and organic matter (see Chapter 5). Select a representative subsample and label a data sheet for it (e.g., Fig. 7-3). Weigh to 0.001 g.

2. (a) For samples with less than about 10% mud and when analysis of the mud is not necessary, dry the subsample at no more than 65°C (to avoid baking clays). Leave to cool and equilibrate with the atmosphere for at least 1 hr before weighing. Then thoroughly disaggregate the sample—for most loose sands, a rubber bung on a piece of glazed paper is adequate.

(b) For samples with a mud fraction to be analyzed, wet-sieving is necessary (see Table 7-3, steps 3 and 4). It is wise to perform a wet-sieving operation on two subsamples—for one, dry both fractions and determine the proportion of mud to sand, whereas for the second only the sand fraction is dried and weighed and the wet mud fraction used for pipette or hydrometer analysis. After wet-sieving, dry the coarse fraction and weigh.

Analysis

3. Select a nest of sieves to cover the grain size range of the sample. If the sample has been wet-sieved, the finest sieve should be 4ϕ; otherwise sieves as fine as 4.75ϕ may be used. For detailed work and where polymodal distributions are present, use 0.25ϕ intervals.

4. Clean the sieves before using them: invert each sieve and tap it gently onto a flat surface or, using your hand, rap the side diagonally to the mesh to knock out any loose grains. Then brush the screen, again diagonally to the mesh, with a soft sieve brush. If any grains are trapped in the mesh, do not attempt to force them out—leave them there (or distortion of the mesh may result). Stack the sieves in order, with the pan at the bottom. If two nests are necessary, use the coarser set first, then transfer the contents of the pan to the finer stack (with another pan under it!).

5. Pour the sample into the top sieve and add the cover (the greatest load on a sieve should not exceed 5 grain-diameter thickness; otherwise mass-trapping effects or mesh distortion will occur). Secure the sieve nest firmly in the sieve shaker. Shake for a standardized time—usually 10 or 15 min.

6. After shaking, invert and clean each sieve as in step 4; retain each fraction on a large sheet of glazed paper, and transfer each to a labeled, preweighed beaker or envelope. If the sample has previously been wet-sieved and mud analysis is to follow, add sediment passing the 4ϕ sieve (pan fraction) to the mud fraction.

7. Weigh the beakers (or envelopes). Retain each fraction in a labeled envelope for future use.

8. Check each fraction for grain aggregates and other properties (e.g., compositional differences, shape properties) with hand lens or under a binocular microscope (there may be significant differences between fractions). If aggregates are common, either disaggregate and resieve, or carefully estimate the percentage of aggregates in each fraction and subtract this percentage of the weight of the fraction from both the weight of the fraction and the total weight of the subsample.

9. Compute the weight percentage of each fraction, then compute cumulative percentages. The weight percent of each sand fraction is:

$$100 \times \frac{\text{weight of sand on sieve}}{\text{total sample weight (sand plus mud)}}$$

Add these percentages incrementally to obtain cumulative weight percentages.

10. Plot the data on a histogram (if desired) and as a cumulative curve on graph paper (e.g., Figs. 7-4–7-7). Consistent "kicks" at the same size grade in cumulative curves for different samples may indicate a defective sieve.

Results

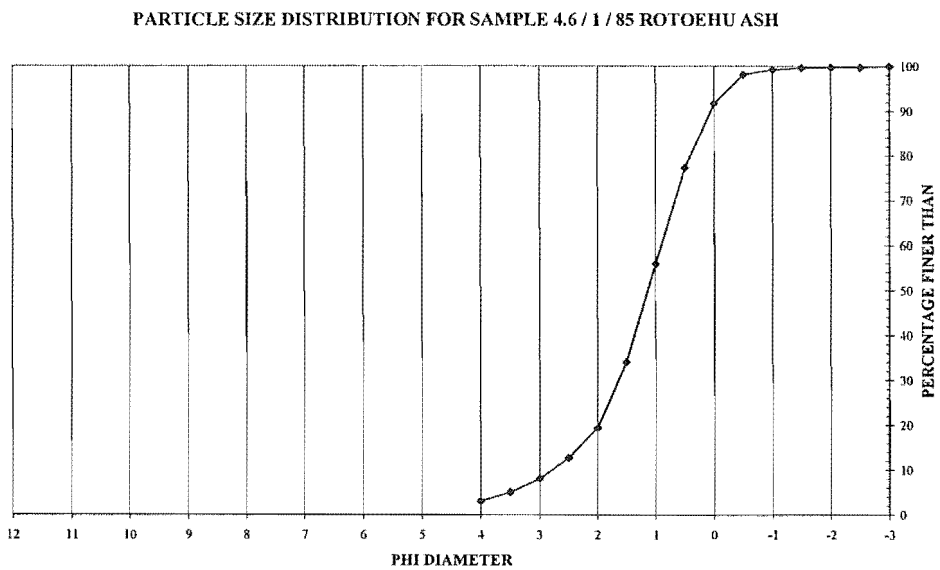

Figure A4.1 Grainsize distribution curve for 4.6 / 1 / 85 which is situated within the Rotoehu Ash.

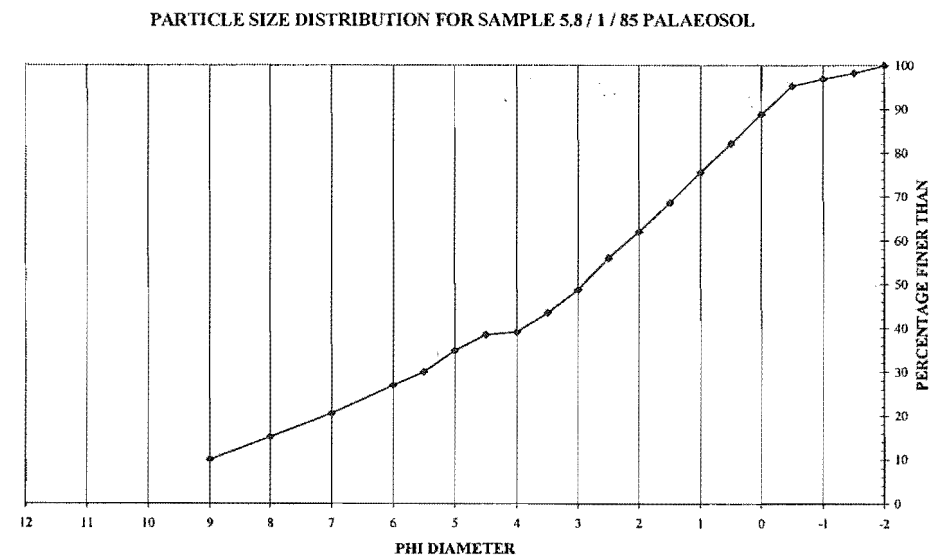

Figure A4.2 Grainsize Distribution curve for 5.8 / 1 / 85 which is situated within the Palaeosol.

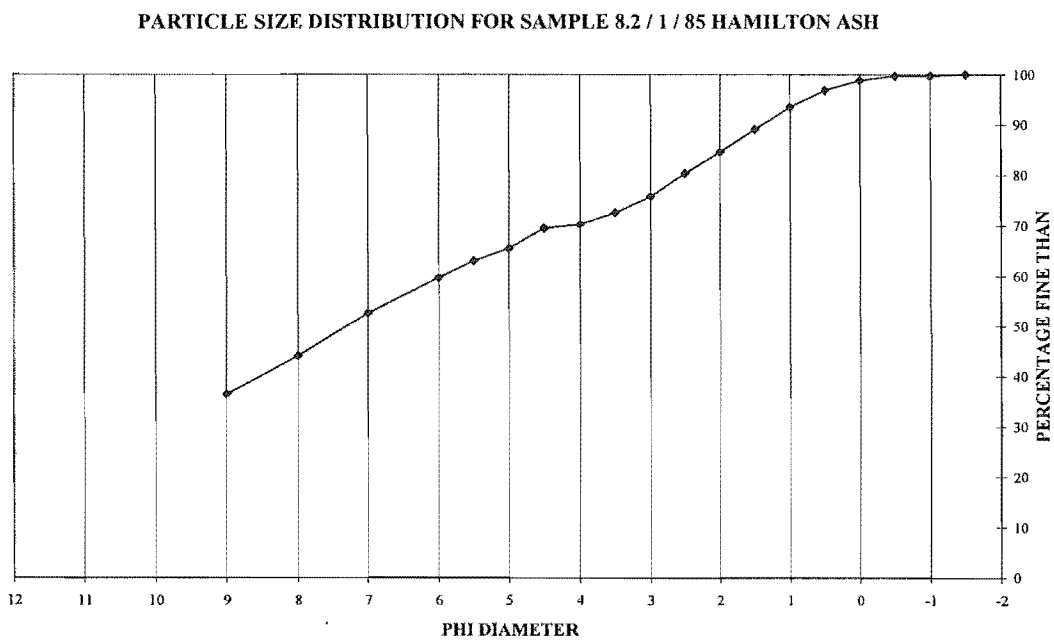

Figure A4.3 Grainsize distribution curve for 8.2 / 1 / 85 which is situated within the Hamilton Ash.

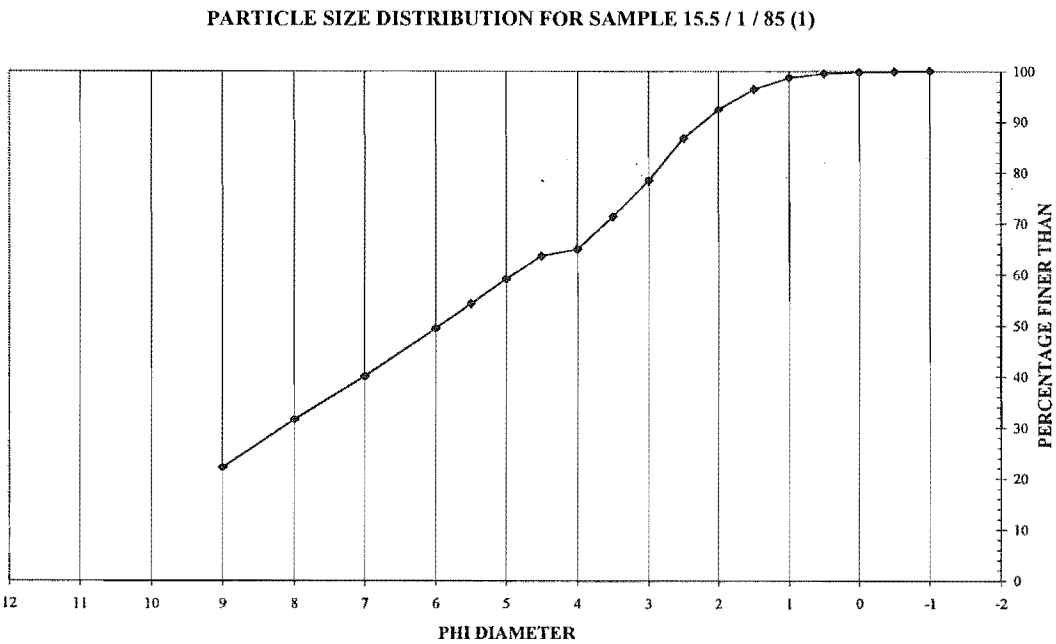

Figure A4.4 Grainsize distribution curve for 15.5 / 1 / 85 (1) which is situated within the cross-bedded section of the Upper Matua Subgroup.

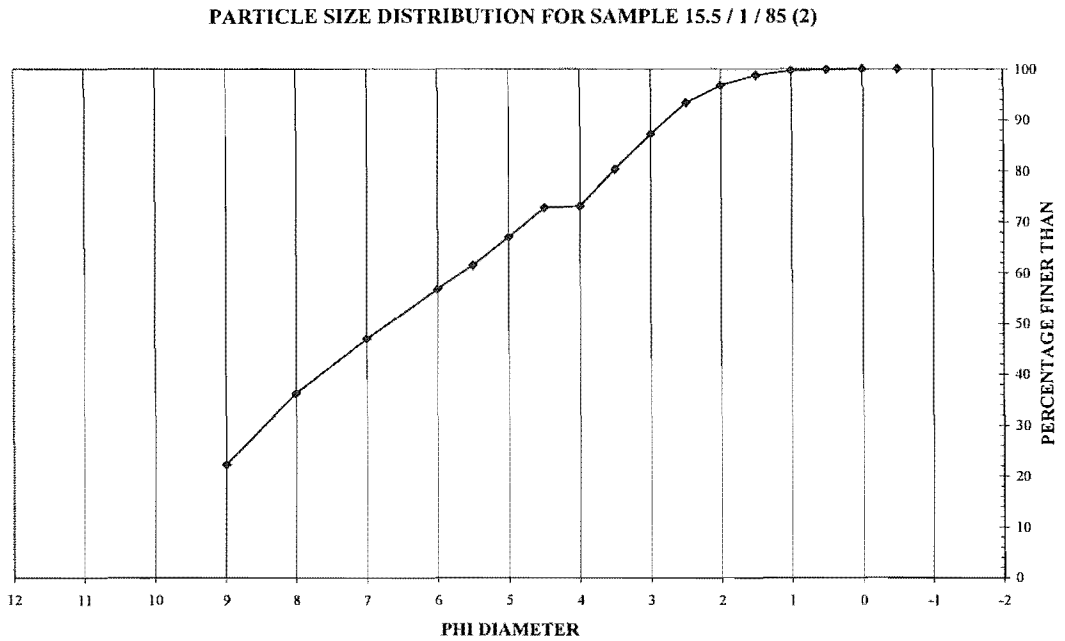

Figure A4.5 Grainsize distribution curve for 15.5 / 1 / 85 (2) which is situated within the cross-bedded section of the Upper Matua Subgroup.

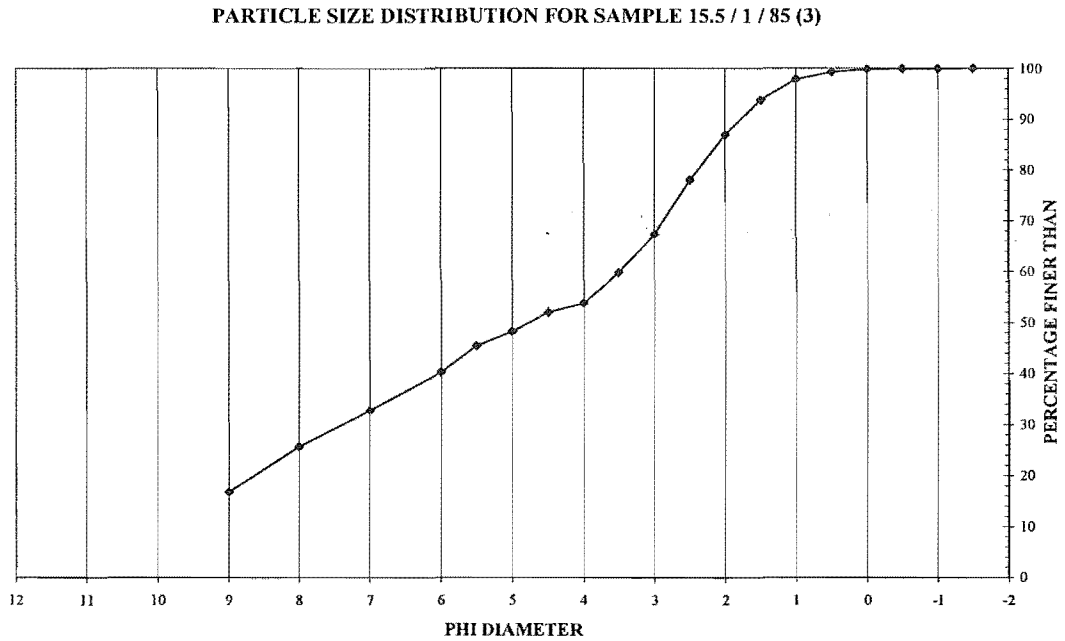

Figure A4.6 Grainsize distribution curve for 15.5 / 1 / 85 (3) which is situated within the cross-bedded section of the Upper Matua Subgroup.

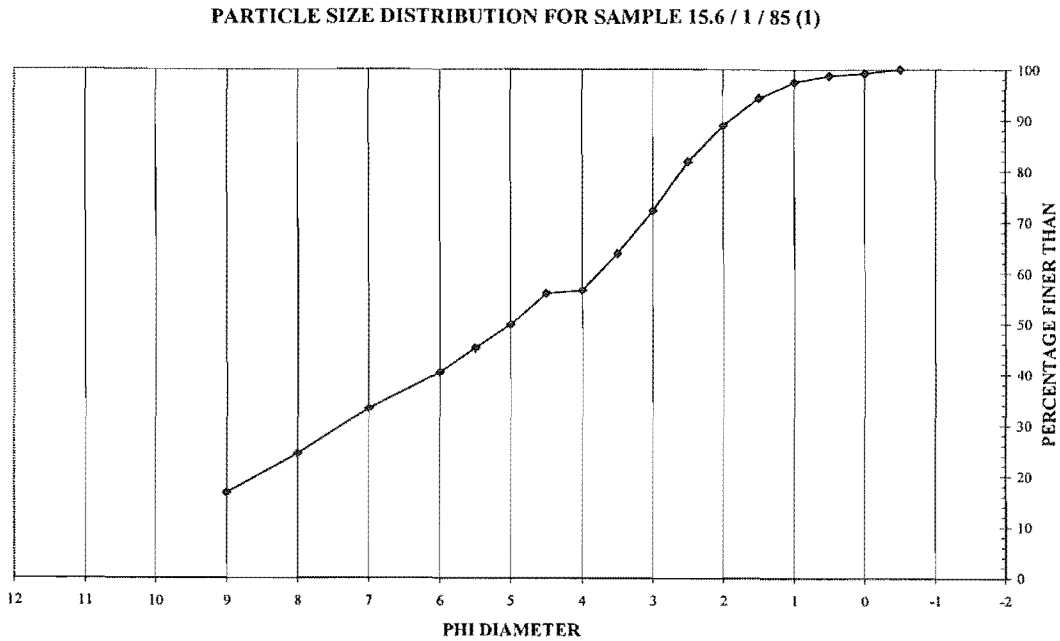

Figure A4.7 Grainsize distribution curve for 15.6 / 1 / 85 which is situated within the cross-bedded section of the Upper matua Subgroup.

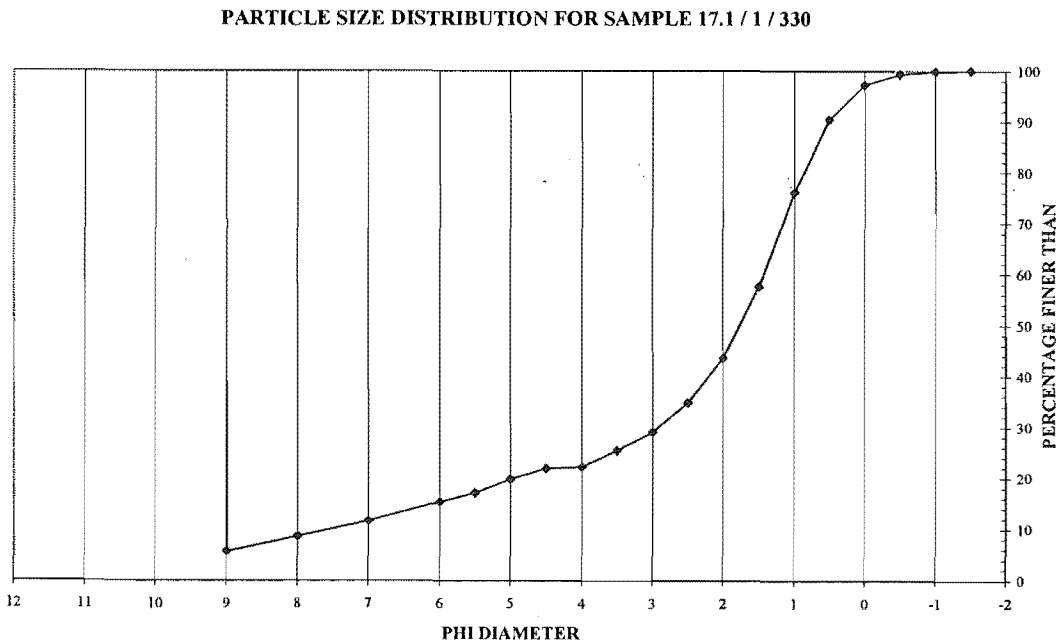

Figure A4.8 Grainsize distribution curve for 17.1 / 1 / 330 which is situated within the aquiferial zone of the Upper matua Subgroup.

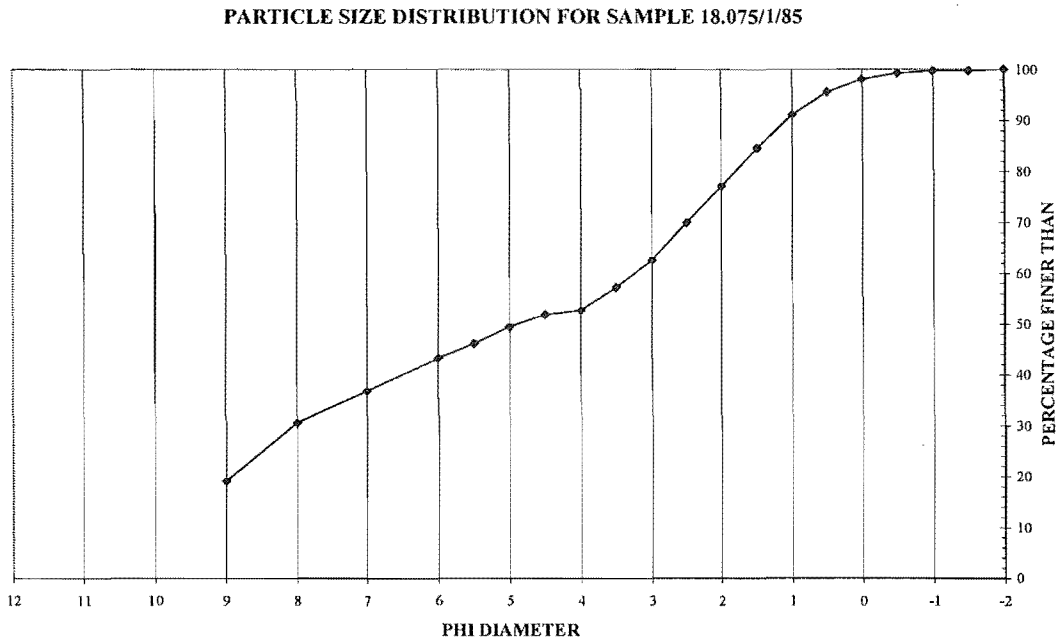

Figure A4.9 Grainsize distribution curve for 18.075/1/85 which is situated within the lower aquitard in the Upper Matua Subgroup.

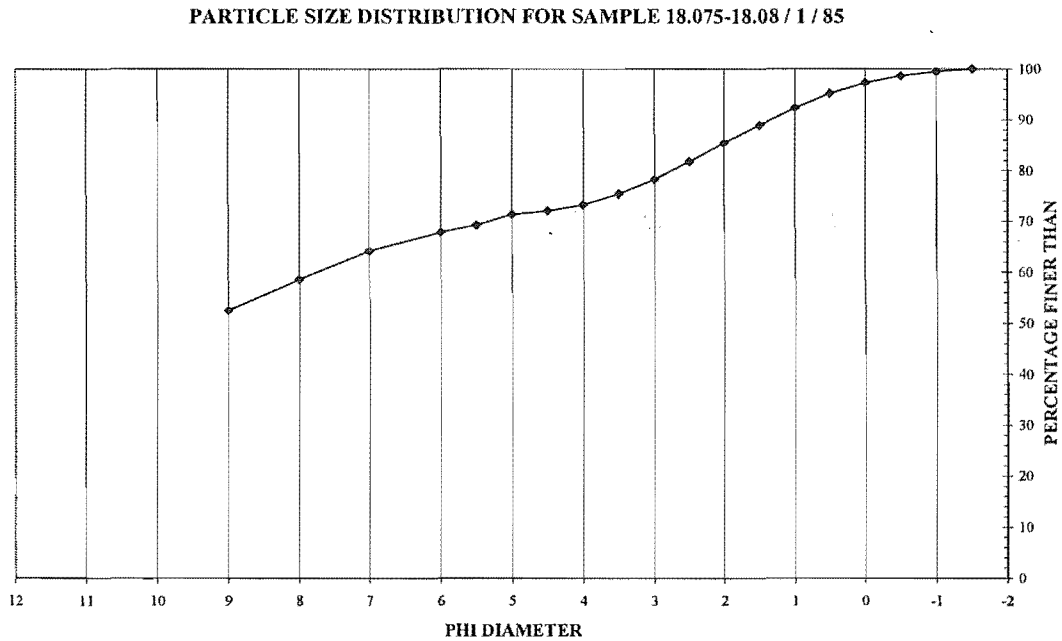

Figure A4.10 Grainsize distribution curve for 18.075-18.08 / 1 / 85 which is situated within the lower aquitard in the Upper Matua Subgroup.

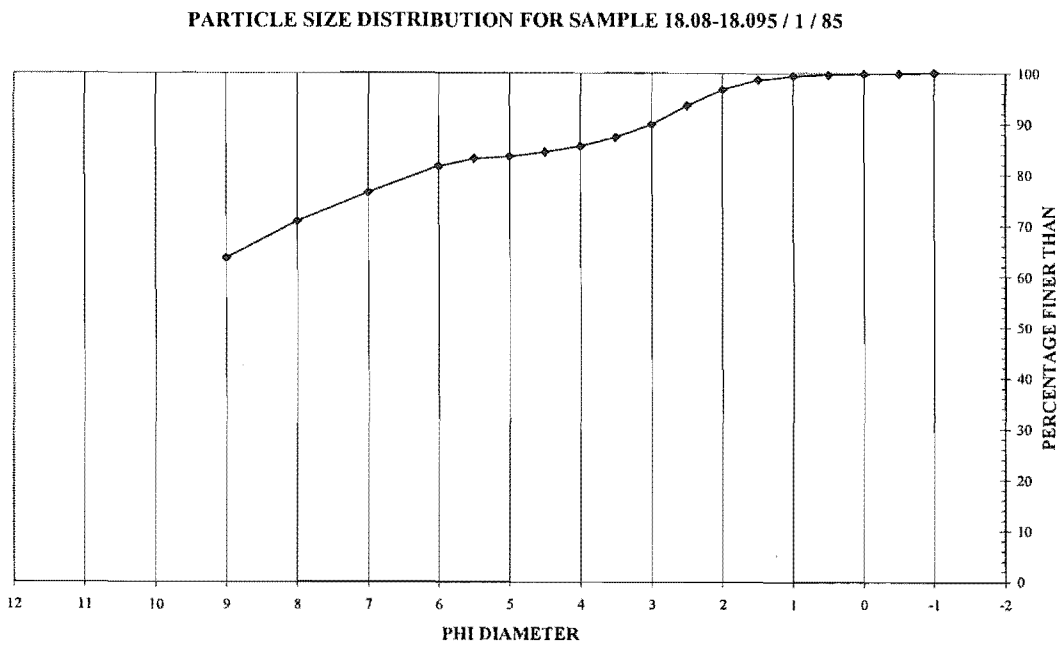

Figure A4.11 Grainsize distribution curve for 18.08-18.095 / 1 / 85 which is situated within the lower aquitard in the Upper Matua Subgroup.

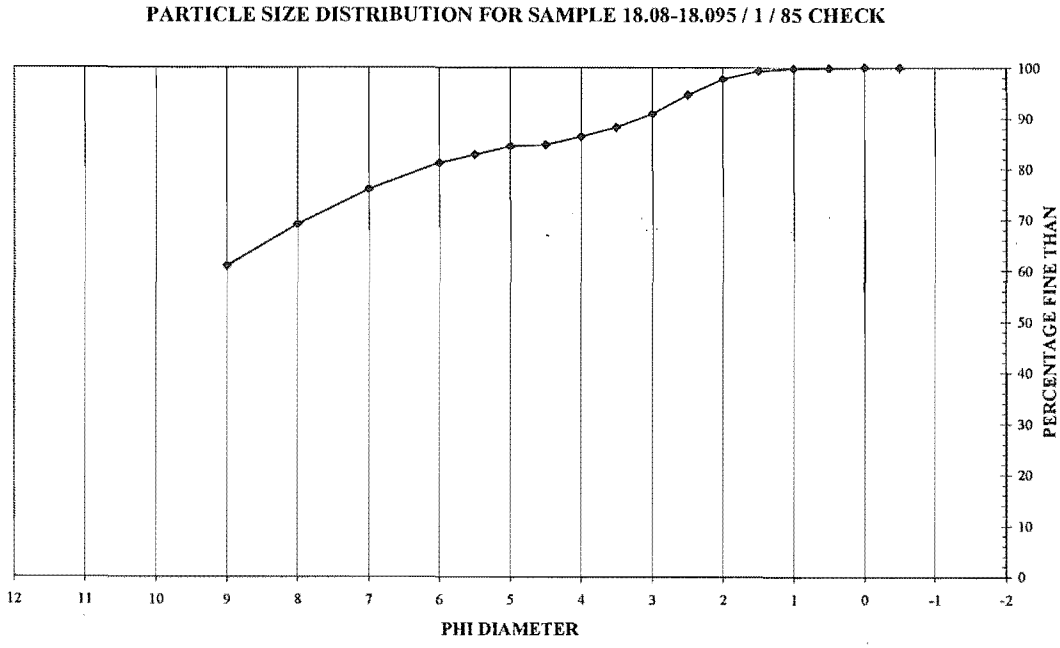

Figure A4.12 Grainsize distribution curve for 18.08-18.095 / 1 / 85 Check, which is situated within the lower aquitard in the Upper Matua Subgroup.

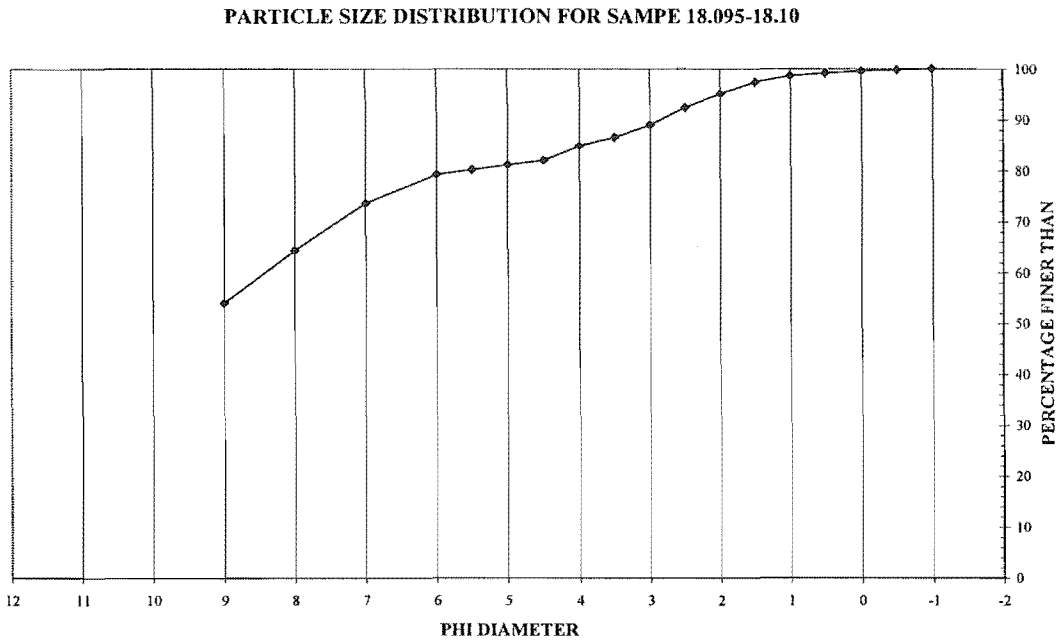

Figure A4.13 Grainsize distribution curve for 18.095-18.10 / 1 / 85 which is situated within the lower aquitard in the Upper Matua Subgroup.

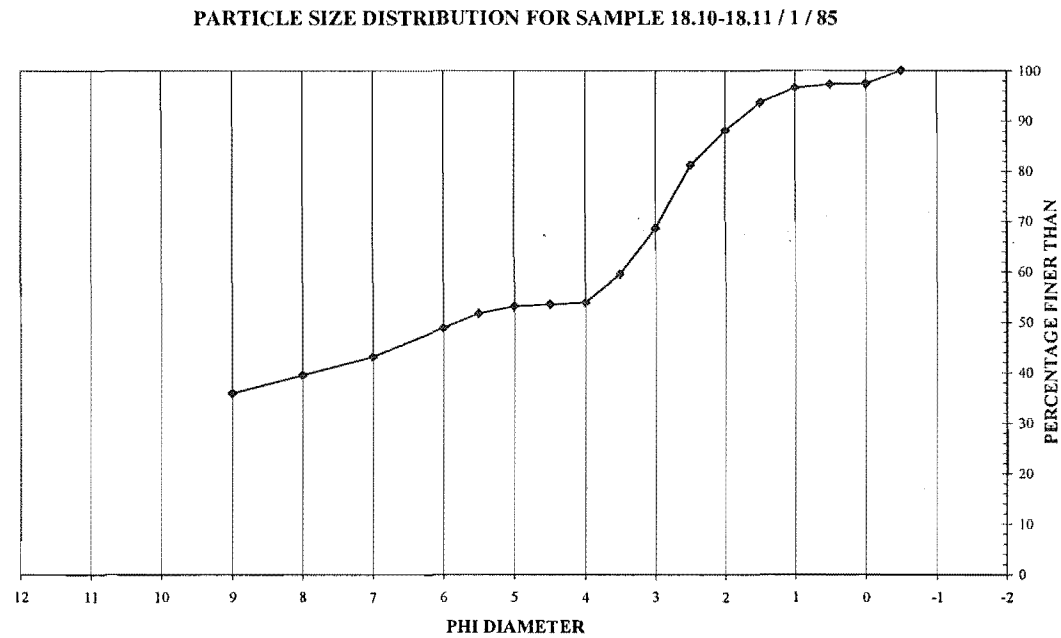

Figure A4.14 Grainsize distribution curve for 18.10-18.11 / 1 / 85 which is situated within the lower aquitard in the Upper Matua Subgroup.

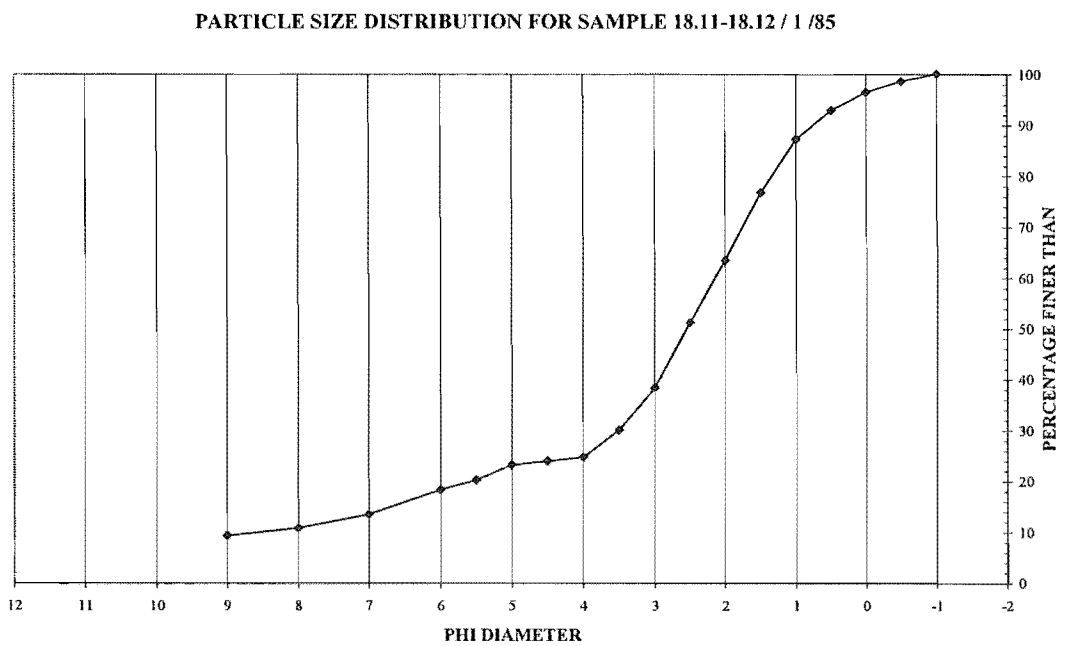

Figure A4.15 Grainsize distribution curve for 18.11-18.12 / 1 / 85 which is situated within the lower aquitard in the Upper Matua Subgroup.

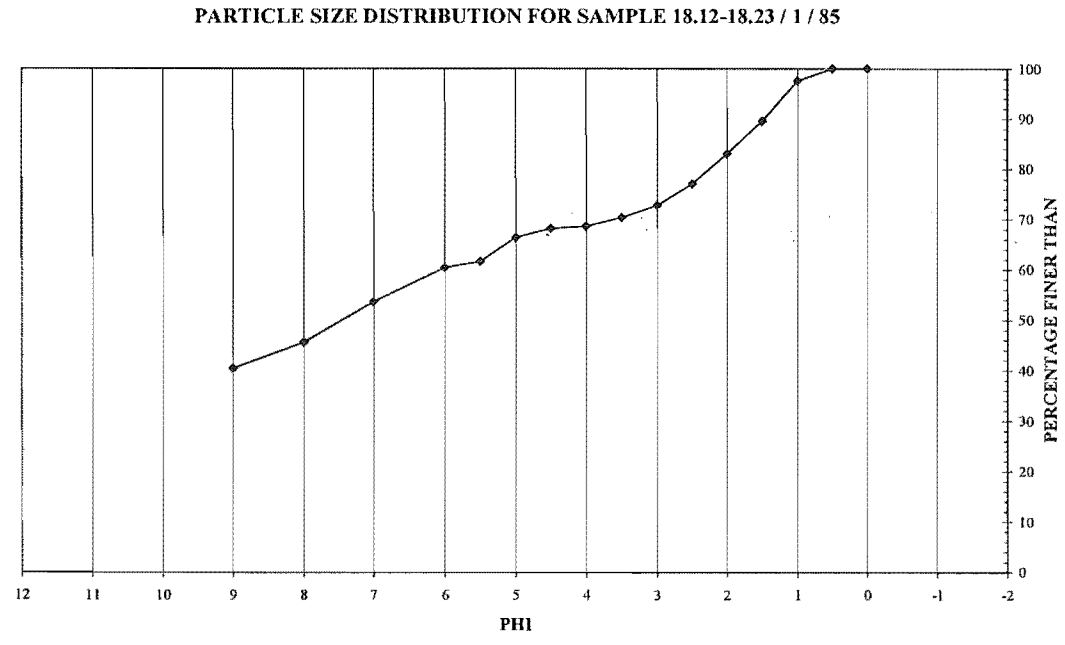

Figure A4.16 Grainsize distribution curve for 18.12-18.23 / 1 / 85 which is situated within the lower aquitard in the Upper Matua Subgroup.

APPENDIX A4.3 X-ray Diffraction and X-ray Fluorescence Analysis

A4.3.1 X-rAY DIFFRACTION ANALYSIS (XRD)

Clay mineralogy is an important aspect to consider when ascessing the geological stability of the soil. Clay samples were collected from grainsize analysis at 8ϕ and 9ϕ intervals, then the slurry was centrifuged and placed on a glass slide. The slides were allowed to partially air-dry under cover in a cool location therefore limiting the amount of alteration of the clay fraction. Analysis involved the use of a Phillips PW1729 X-ray generator connected to a Phillips PW1710 diffractometer control. A Phillips PW1820/00 Goniometer is connected to a 2kW Cpooer target X-ray tube. Operating conditions are: 50kV/40mA with a scanning speed of 1°2θ/minute. Samples were firstly analysised in there natural state, then placed in a solution of ethelene glycol to identify the presents of any swelling clays. The samples were then heated to a temperture above 550 °C for 1 hour to collapse the crystal structure of certain clays such as Kaolinite. From the resulting plots it proved difficult to distingish the difference between Kaolinite and Halloysite. Dr David lowe (Pers. Com. 1997) suggested an intercalation method using Formamide (Churchman et al. 1984) to identify the difference between Halloysite and Kaolinite. This method was however not favoured by the Departments of Geological Science's XRD technican (Steven Brown) due to the difficulties in dealing with Fromamide used for the test method. It was decided that on heating there was a singicant enough difference between the temperatures where the cyrstal structure collasped for Halloysite and Kaolinite that an identification could made. With a new sample, on heating, the temperature was slowly increased to approximately 500 °C where the crystal structure of Hallyosite collasped. The diffractograms obtained are presented on the following pages.

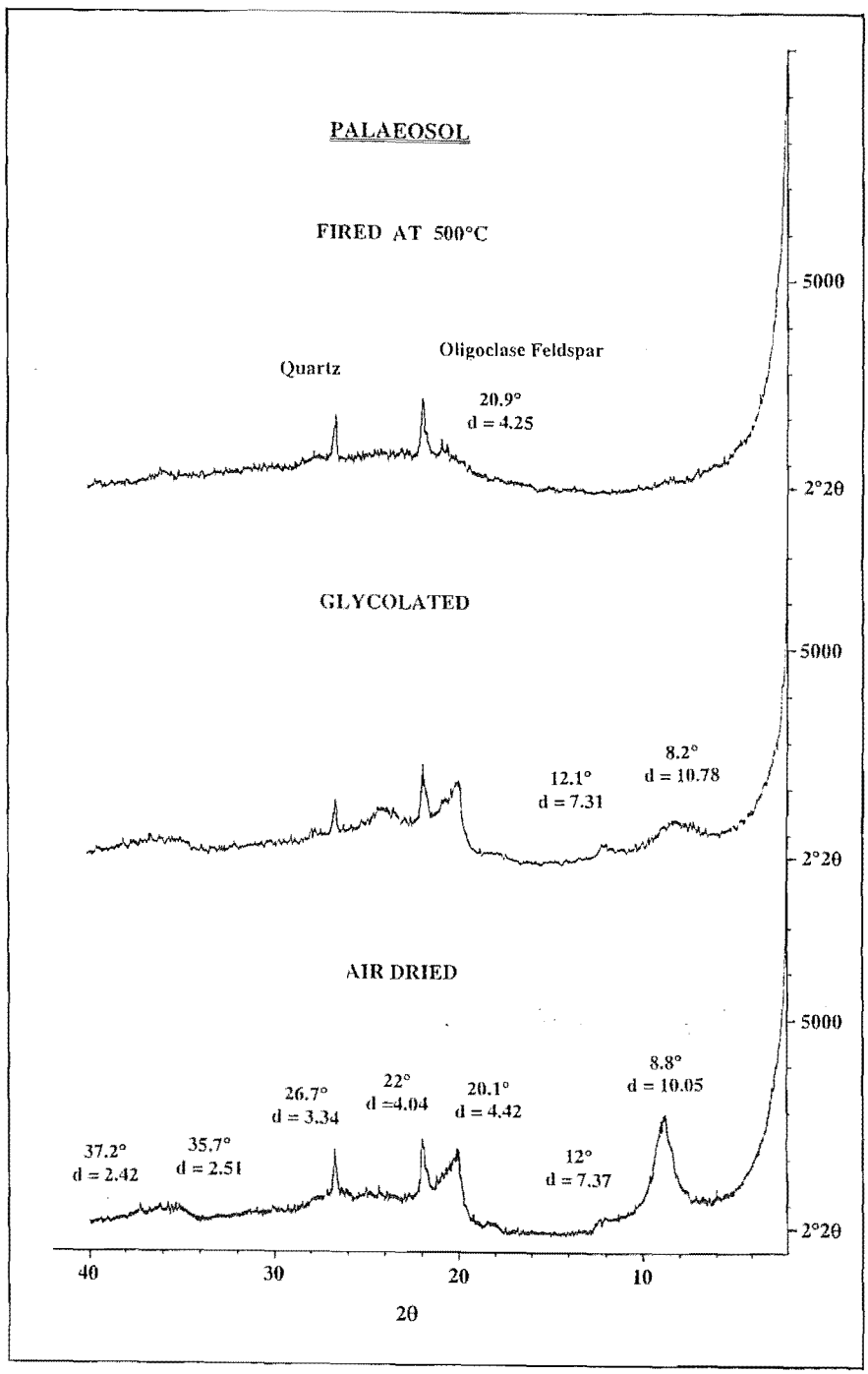

Figure A4.17 XRD profiles for the 9ϕ fraction of the Palaeosol

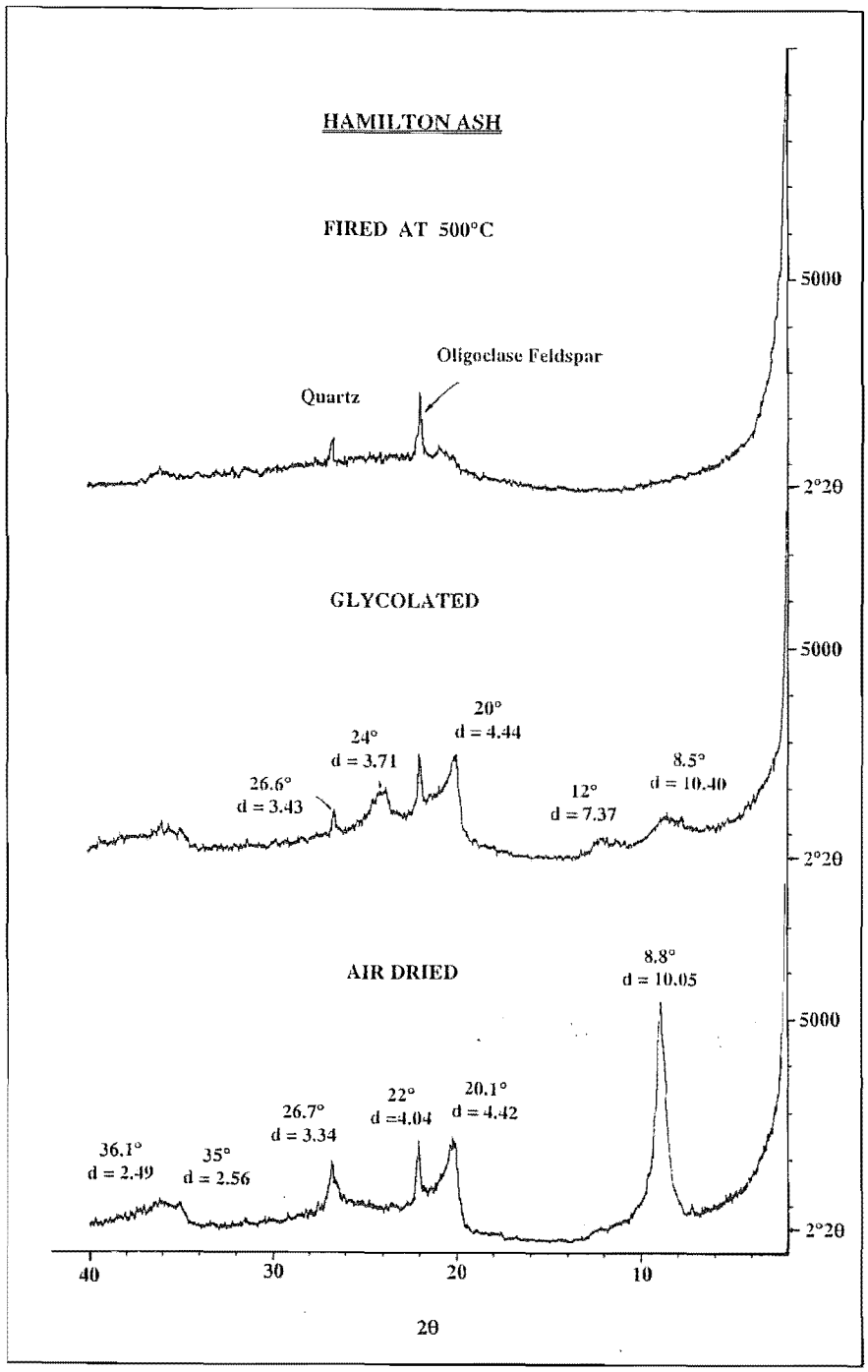

Figure A4.18 **XRD profiles for the 9ϕ fraction of the Hamilton Ash**

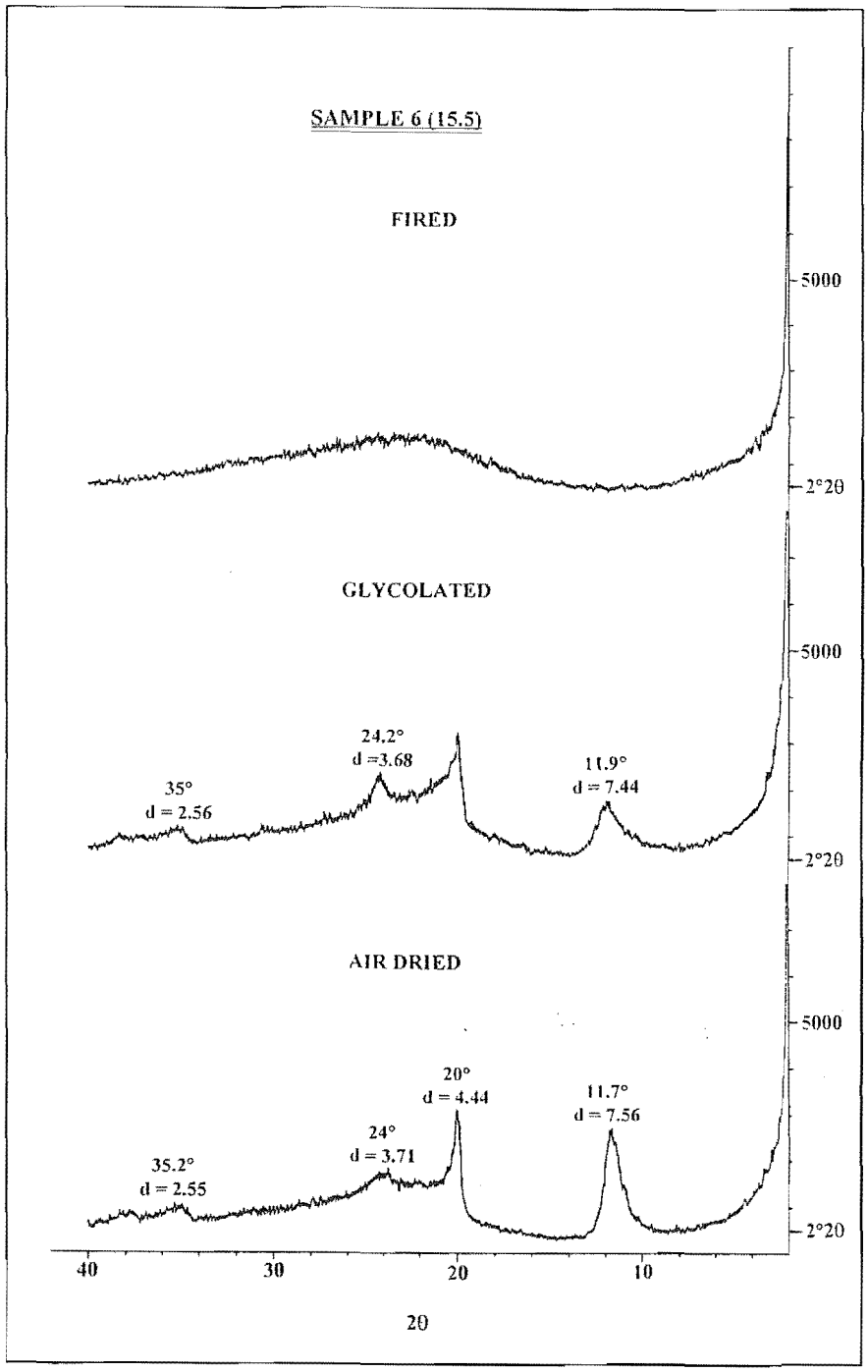

Figure A4.19 XRD profiles for sample 15.5 / 1 / 85 Cross-bedded section of the Upper Matua Subgroup

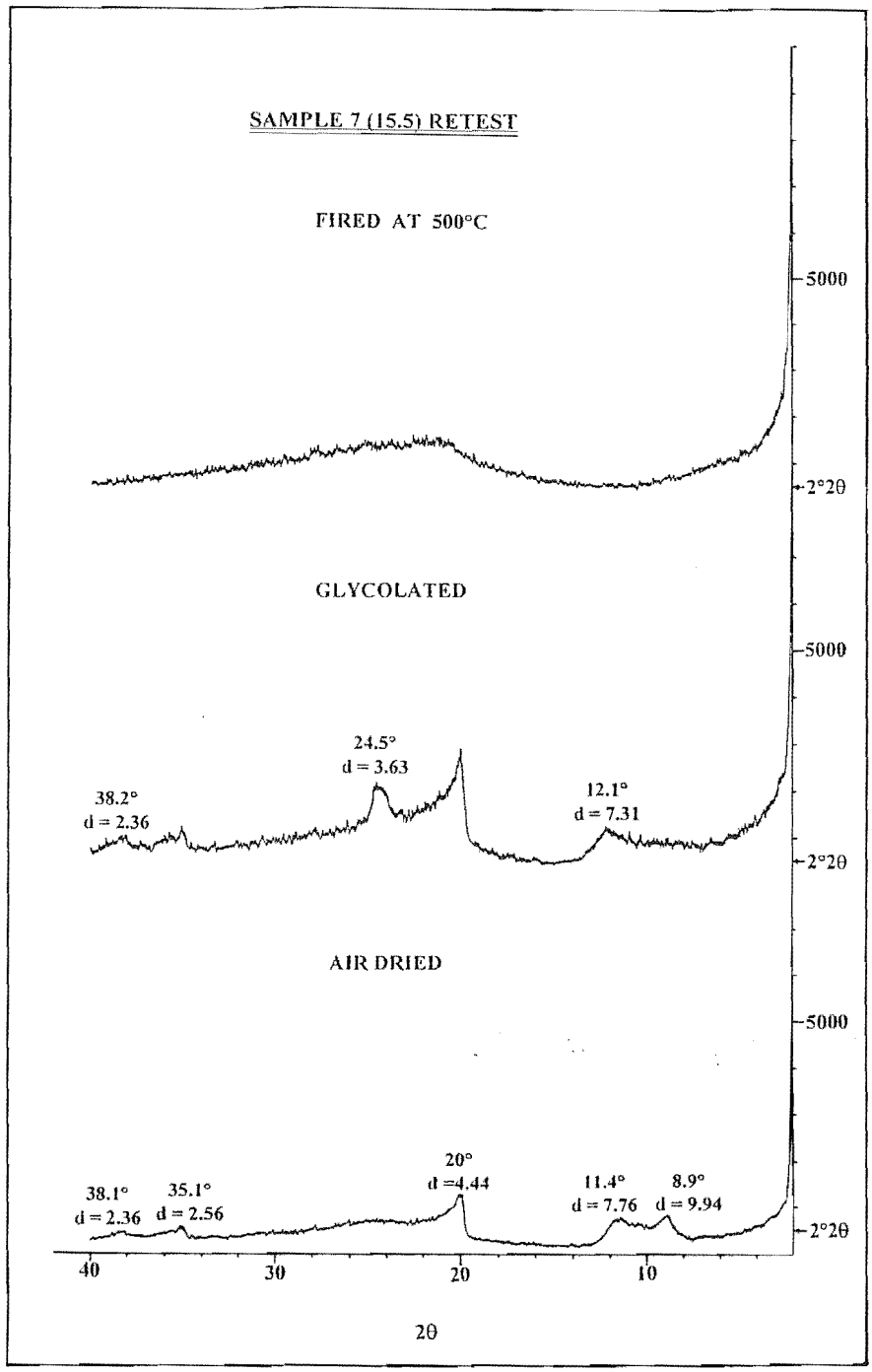

Figure A4.20 XRD retest profiles for the sample fired at 500°C, sample 15.5 / 1 / 85 Cross-bedded section of the Upper Matua Subgroup

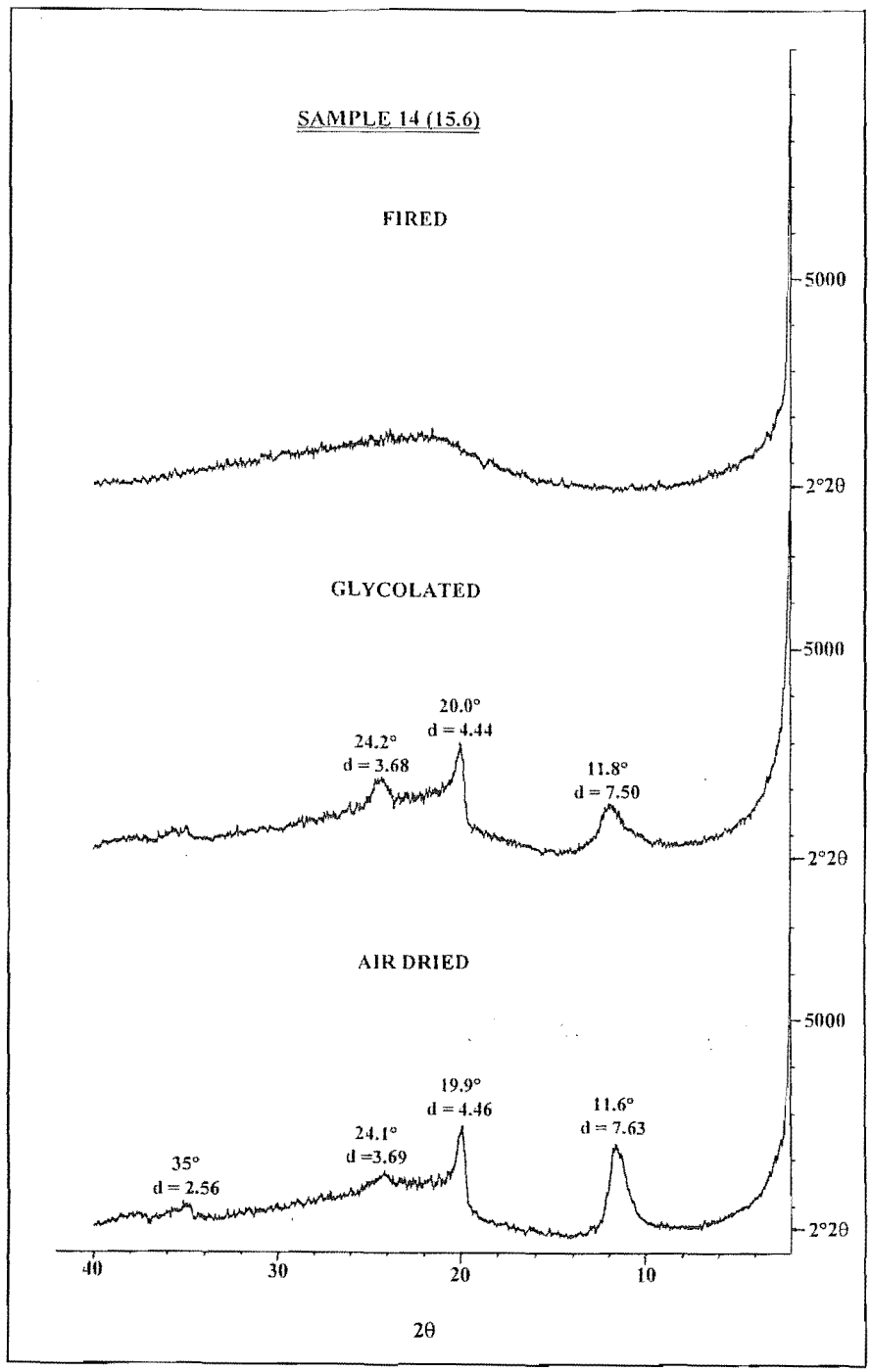

Figure A4.21 XRD profiles for sample 15.6 / 1 / 85 Cross-bedded section of the Upper Matua Subgroup

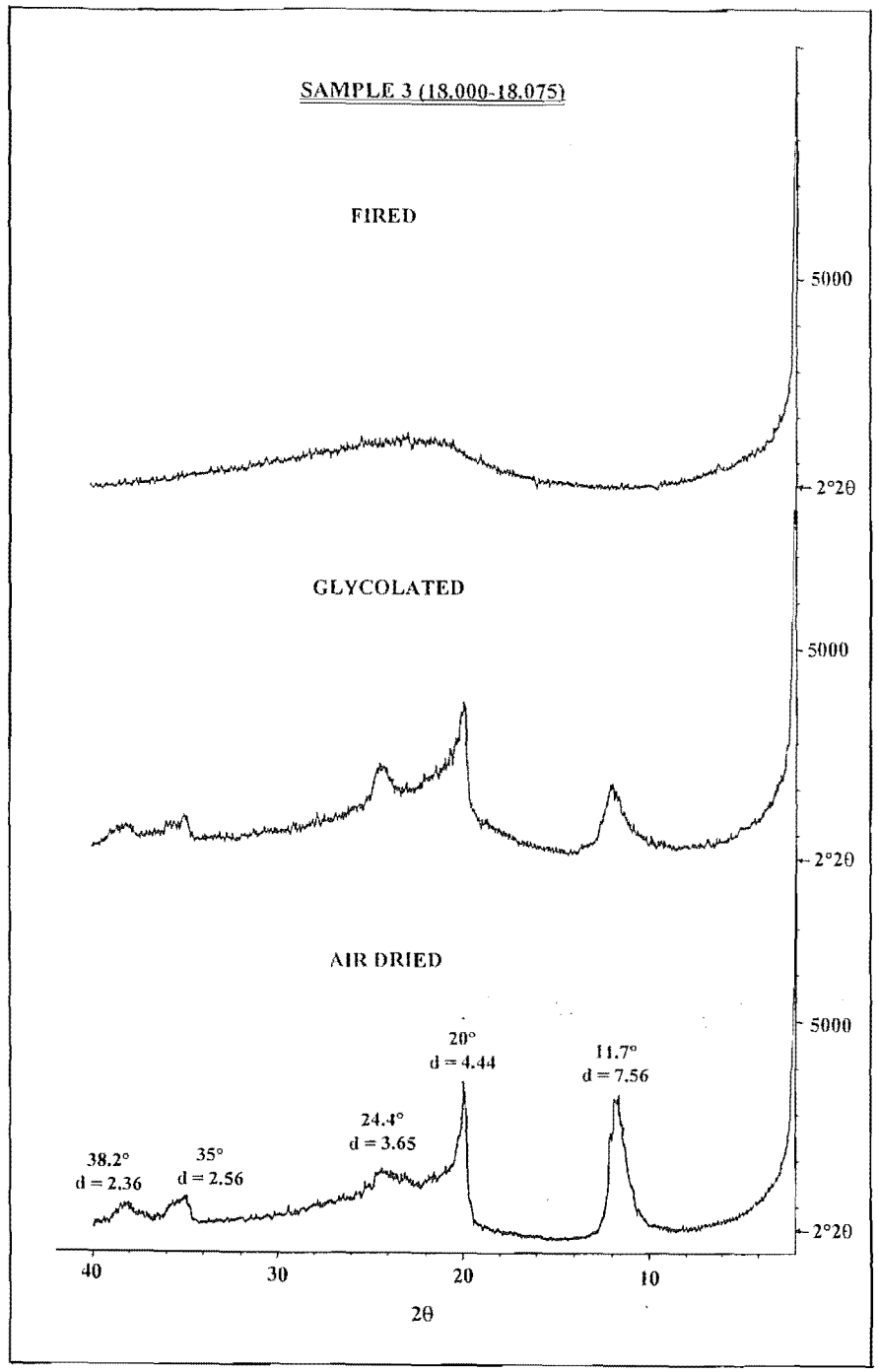

Figure A4.23 XRD profiles for the 9ϕ fraction, sample 18.0-18.075 / 1 / 85 located within the lower bounding aquitard of the Upper Matua Subgroup

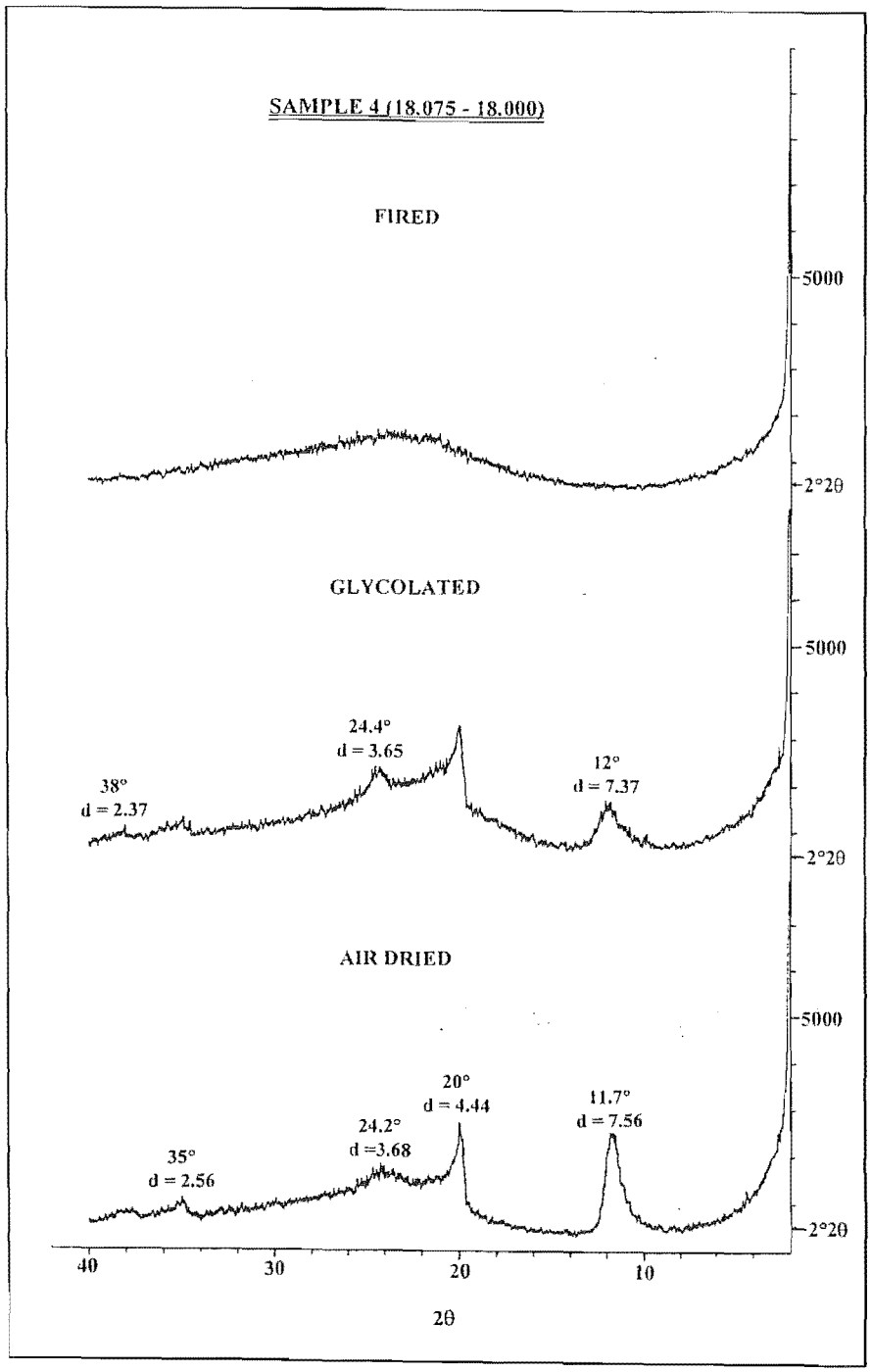

Figure A4.24 XRD profiles for sample 18.075-18.08 / 1 / 85 located within the lower bounding aquitard of the Upper Matua Subgroup

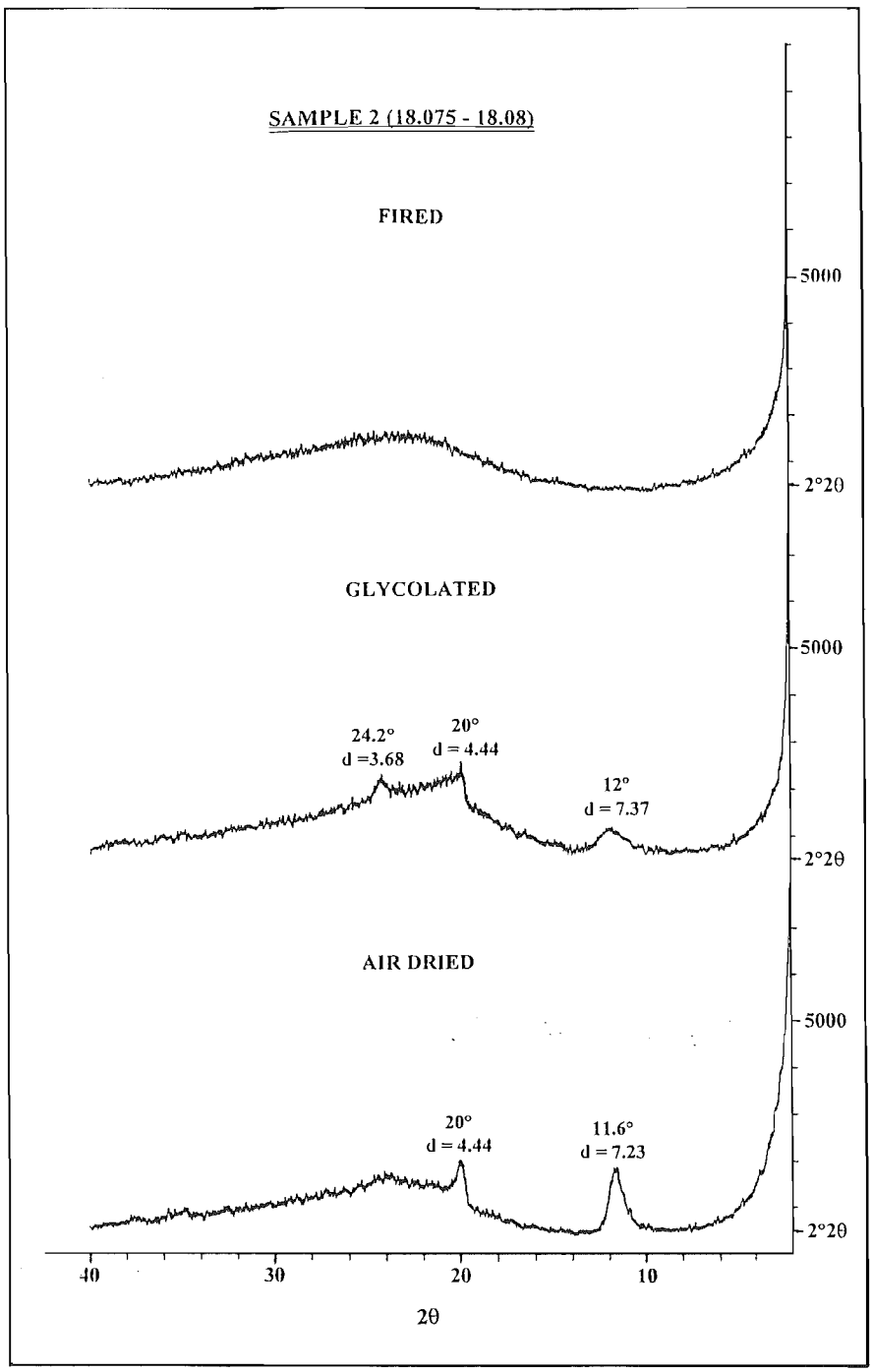

Figure A4.24 XRD profiles for sample 18.075-18.08 / 1 / 85 located within the lower bounding aquitard of the Upper Matua Subgroup

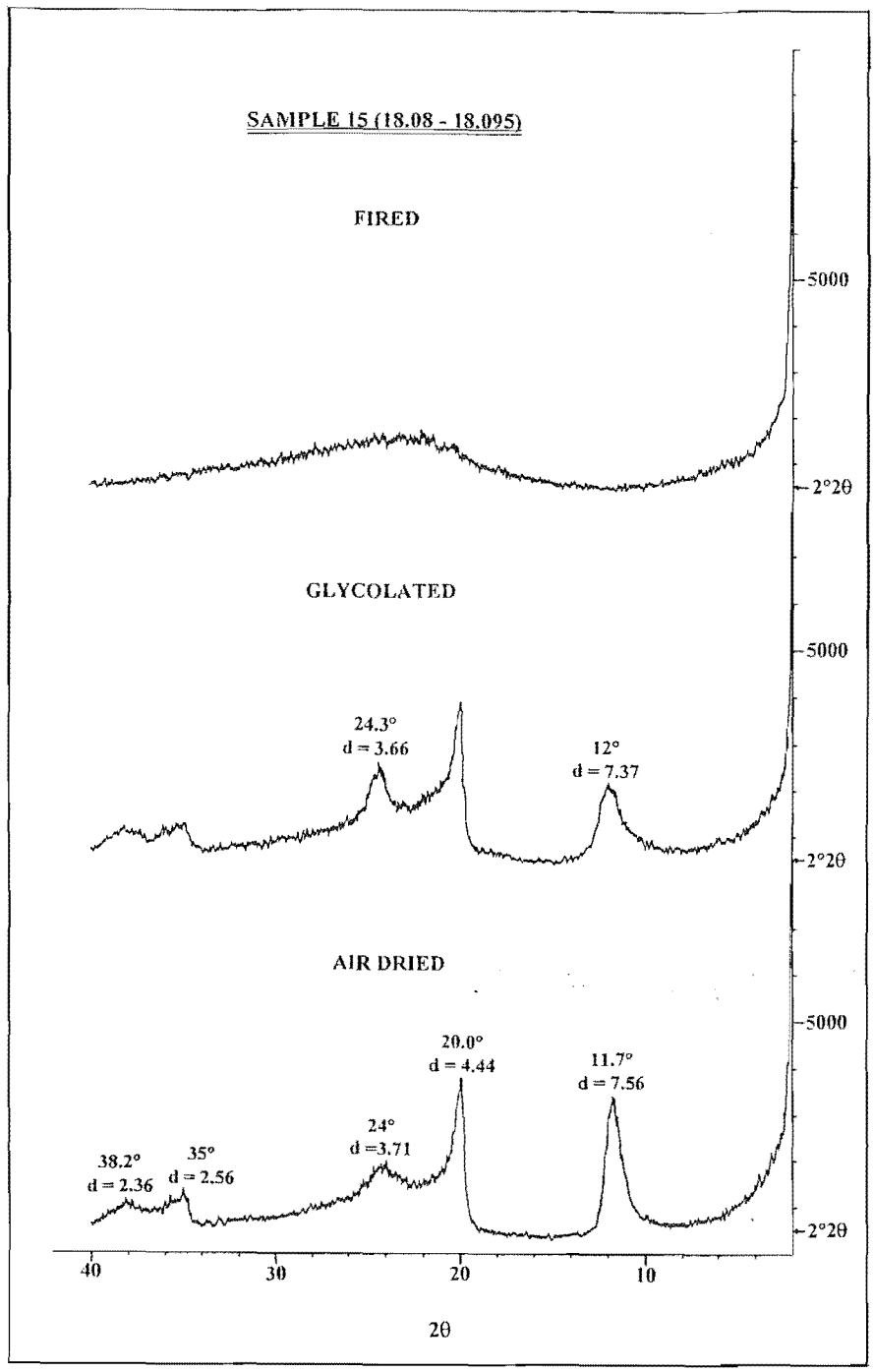

Figure A4.24 XRD profiles for the 8ϕ fraction, sample 18.08-18.095 / 1 / 85 located within the lower bounding aquitard of the Upper Matua Subgroup

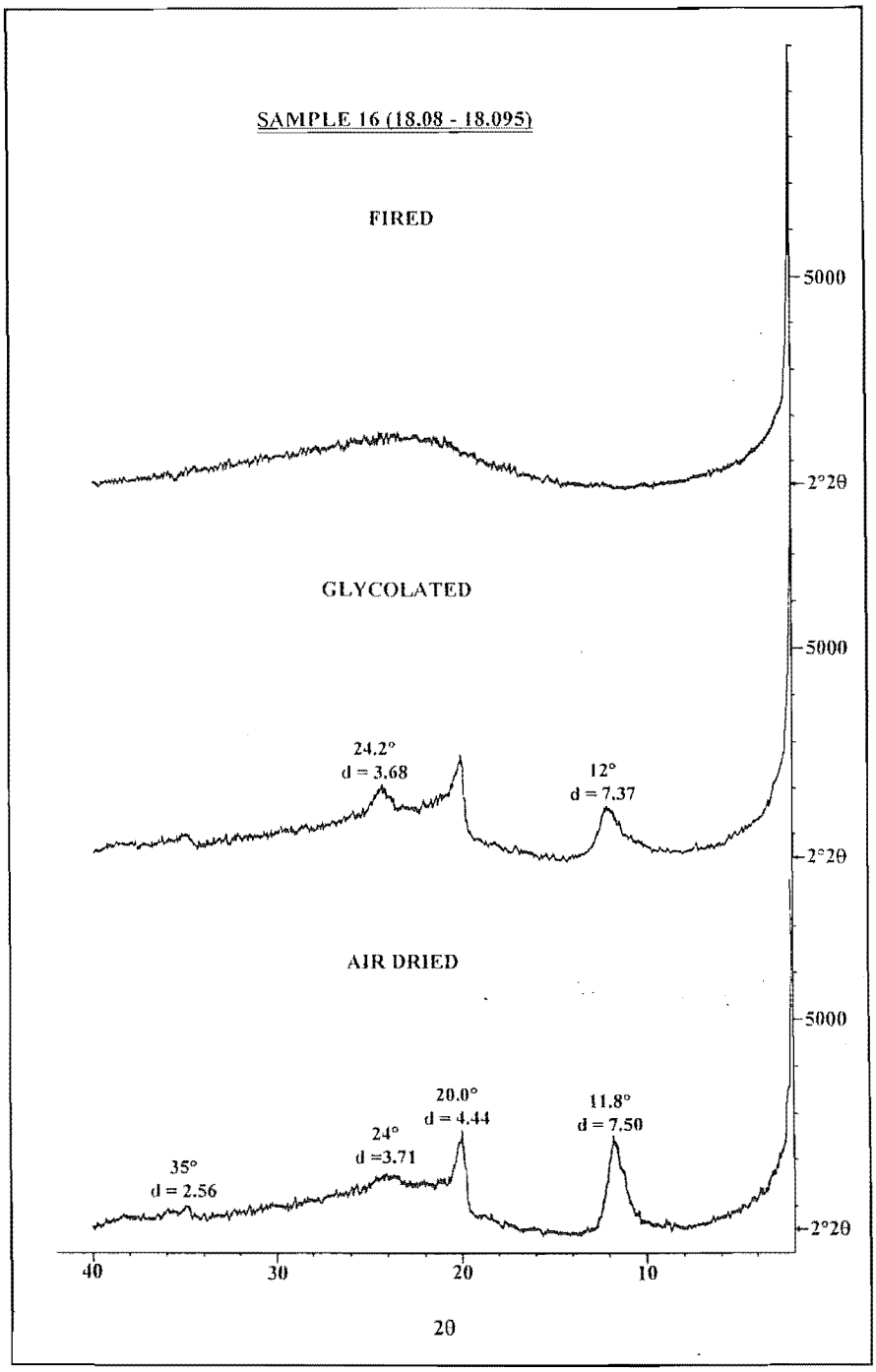

Figure A4.25 XRD profiles for the 9ϕ fraction, sample 18.08-18.095 / 1 / 85 located within the lower bounding aquitard of the Upper Matua Subgroup

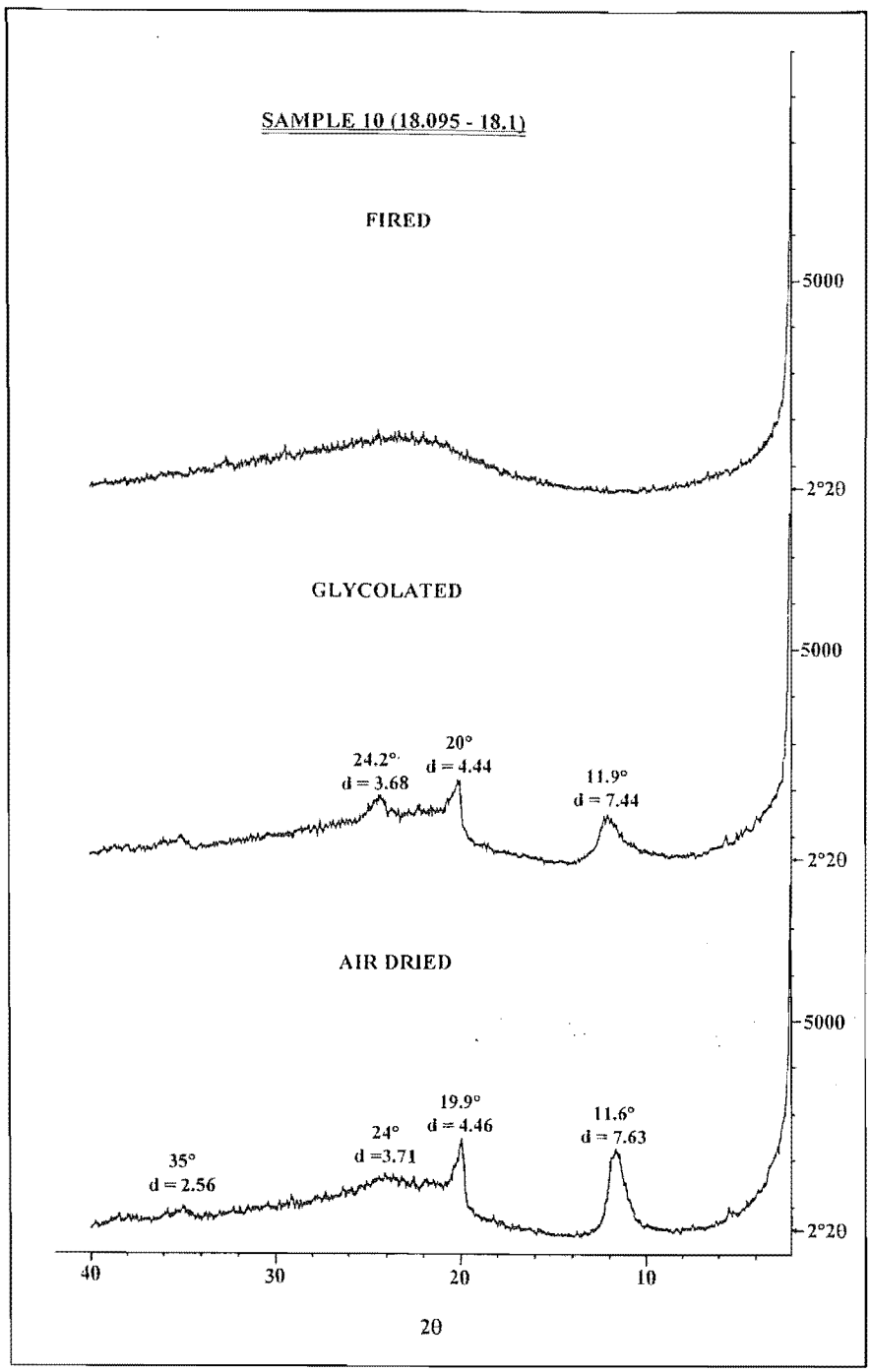

Figure A4.26 XRD profiles for sample 18.095-18.1 / 1 / 85 located within the lower bounding aquitard of the Upper Matua Subgroup

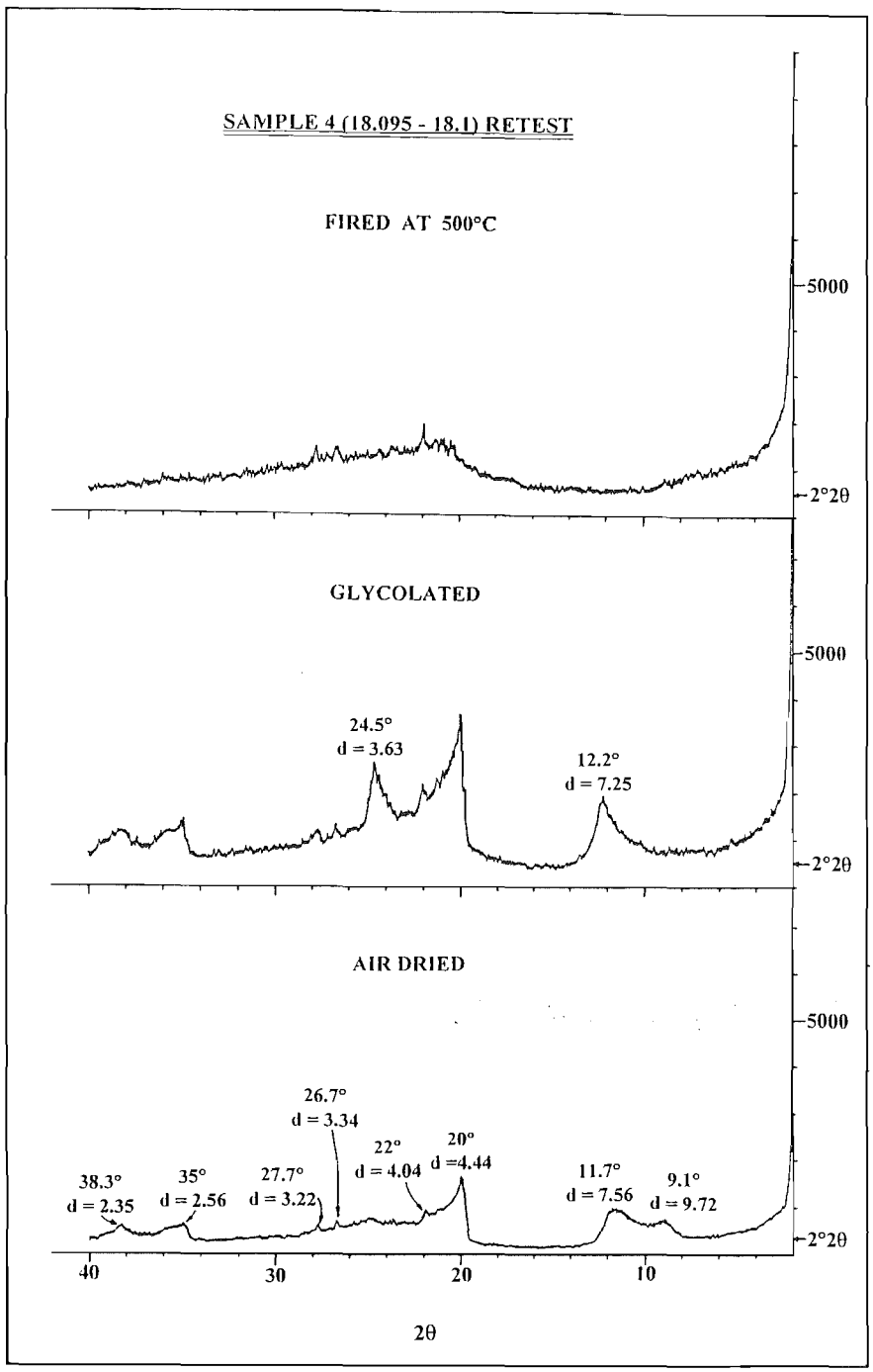

Figure A4.27 XRD retest profiles for the sample fired at 500°C, 18.095-18.1 / 1 / 85 located within the lower bounding aquitard of the Upper Matua Subgroup

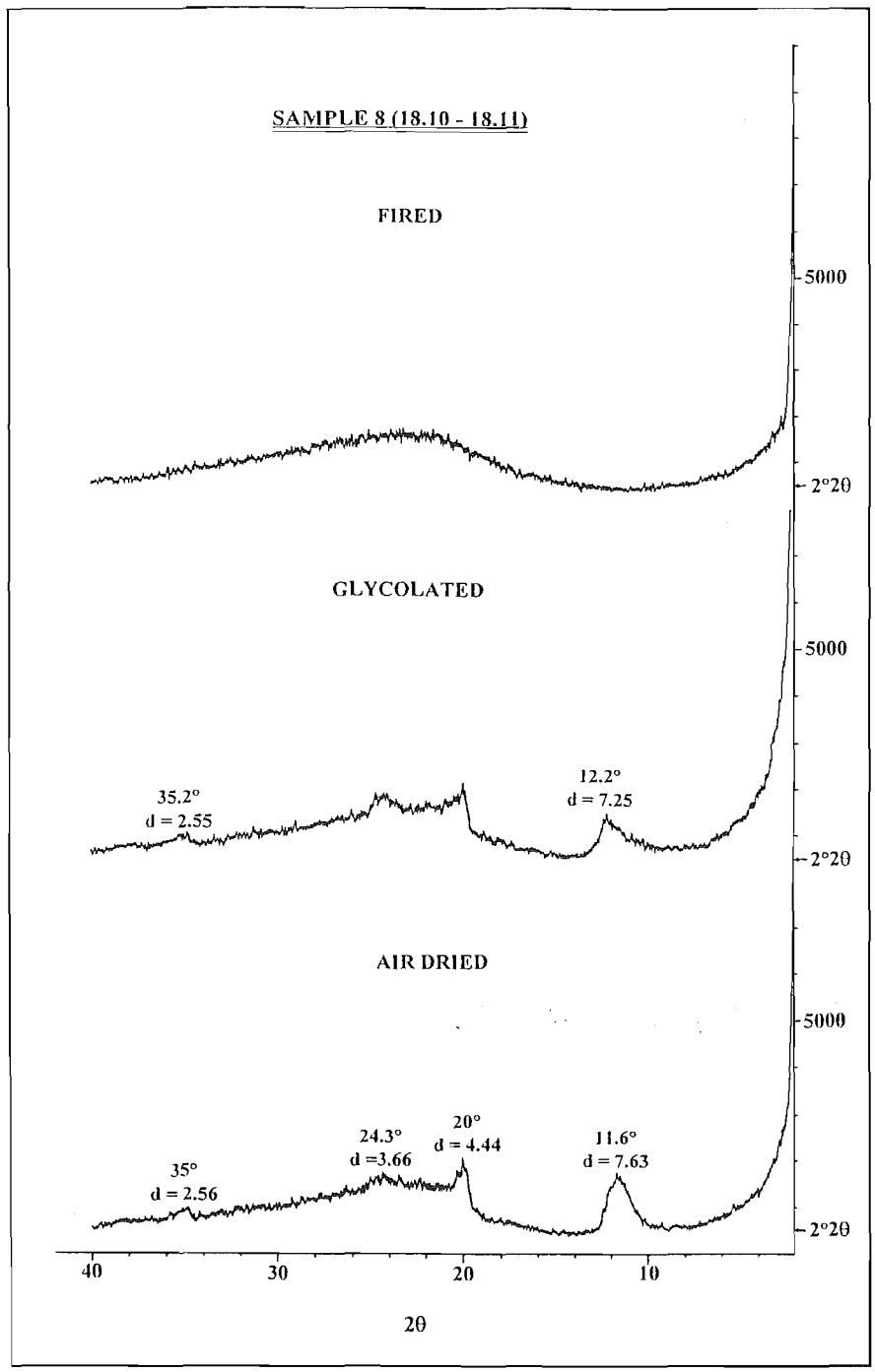

Figure A4.28 XRD for sample 18.10-18.11 / 1 / 85 located within the lower bounding aquitard of the Upper Matua Subgroup

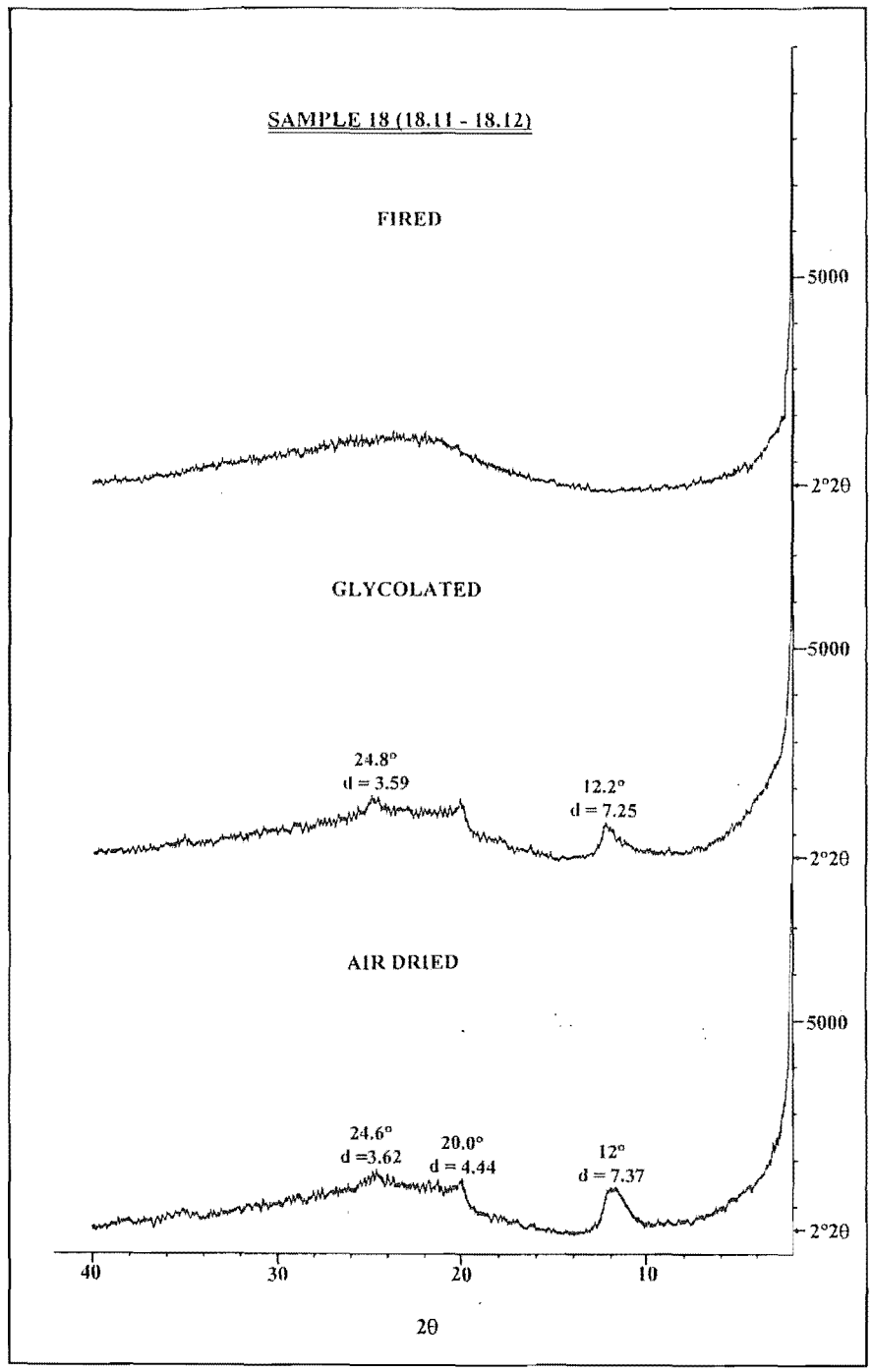

Figure A4.29 XRD profiles for sample 18.11-18.12 / 1 / 85 located within the lower bounding aquitard of the Upper Matua Subgroup

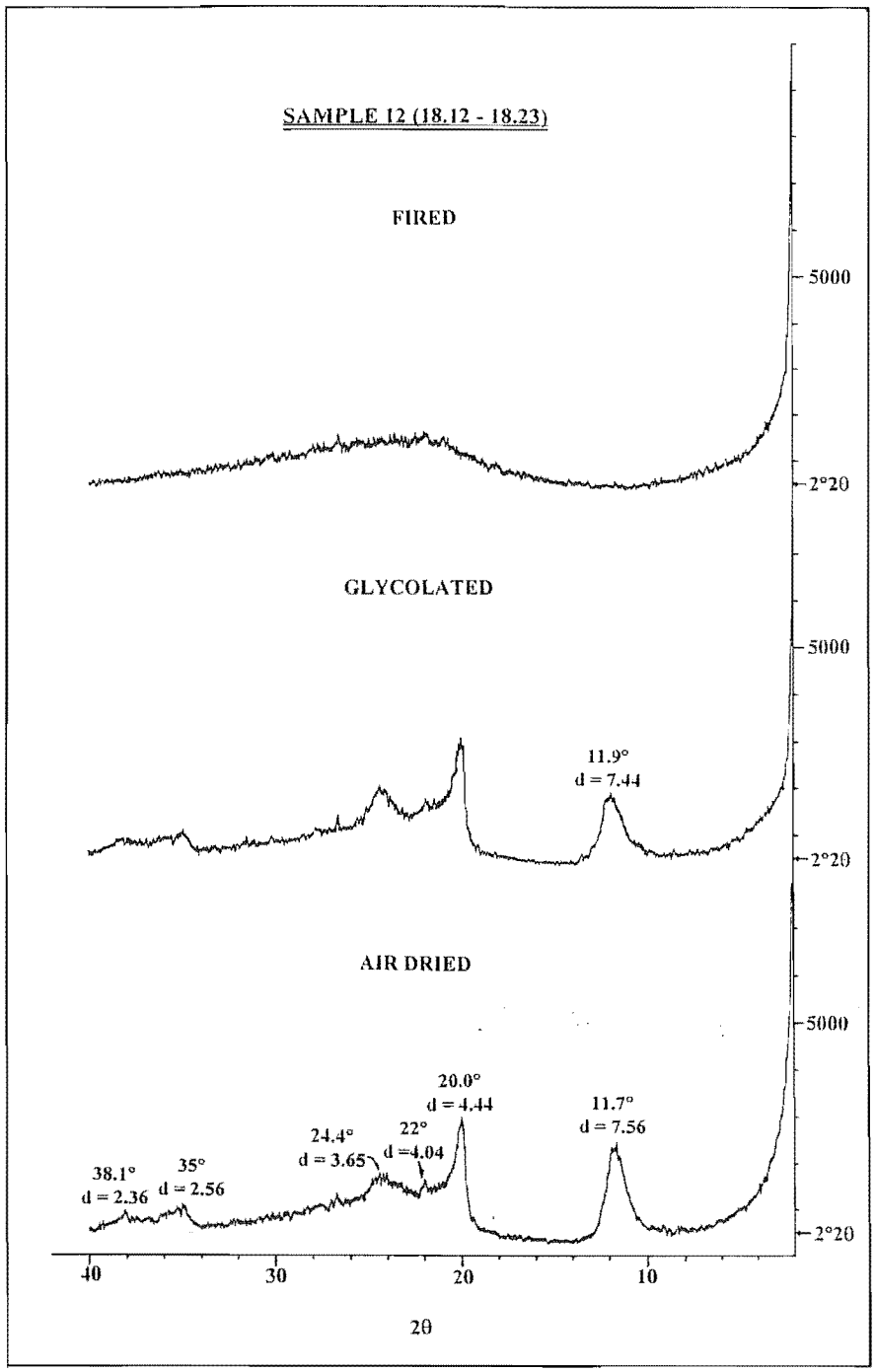

Figure A4.30 XRD profiles for sample 18.12-18.23 / 1 / 85 located within the lower bounding aquitard of the Upper Matua Subgroup

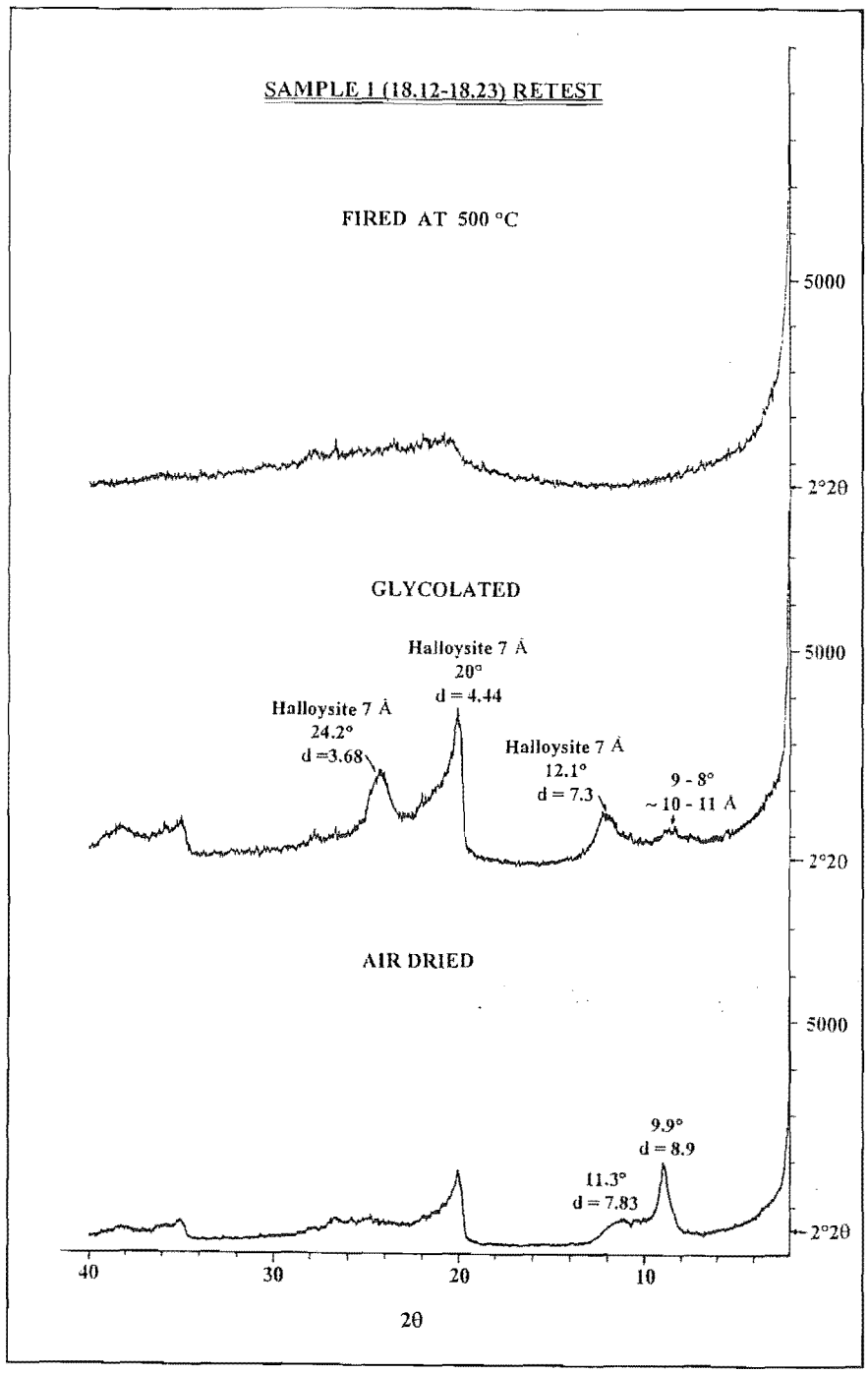

Figure A4.31 XRD retest profiles for the sample fired at 500°C, 18.12-18.23 / 1 / 85 located within the lower bounding aquitard of the Upper Matua Subgroup

A4.3.2 X-Ray Fluorescence Analysis (XRF)

Located thoughout the soil mass are numerous dark coloured greenish black, brownish black, and black grains varing from medium sand to granule in size. XRD analysis was unsucessful at detecting mineral composition due to the large amorphous glass content, and XRD mineral data base consisting of only inorganics compounds. A sampole was prepared according to technicans instructions and analysized using a Philips PW 2400 X-ray Fluorescence spectrometer using a Rhodium tube. On determation of porportions of chemical composition the data was then again run through the XRD data base to try and obtain a possible match. Data is presented in the text.

APPENDIX A4.4 Atterbrg Limits

Atterberg limits represents the liquid limit, plastic limit, and plasticity index of a soil. In this study all soils were passed through a 425 μm sieve and testing conducted according to procedures denoted by BS 1377: Part 2: 1990 for determination of the liquid limit (using the cone penetrometer), plastic limit, and the plasticity index.

The Plasticity Index (PI or I_P) can be calculated from the following expression:

$$PI=w_L-w_P$$

Where w_L=liquid limit and w_P=plastic limit.

The Activity of a clay is related to the amount of water which is attracted to the surfaces of the soil particles. As the surface area per unit of mass increases with decreasing particle size the amount of attracted water will be influenced by the amount of caly, Lambe and Whitman (1979). Therefore the ratio of the plasticity index to the clay fraction can be used to quantify the activity.

$$\text{Activity of a clay} = \frac{\text{Plasticity index}}{\%\text{ by weight finer than } 2\mu m}$$

APPENDIX A4.5 Direct Shear Strength Testing (Shear Box)

Testing involved the use of a Wykeham Farrance WF 25300 stepless & 25 speed drive direct/residual shear box. Testing proceduer used was that specified by the manufacturer using a 100 mm diameter *in-situ* sample.

Inorder to obtain a friction angle and associated cohesion a spread of normal loads had to be calculated. By using a oveburden of 14 m derived from field investigations equating to the approximate height of the aquiferial zone, a range of weights can be obtained for testing.

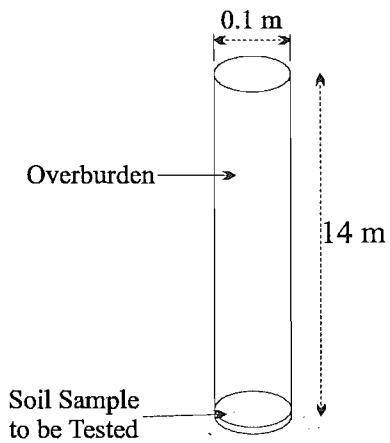

$$Wt = \frac{\pi\left(\frac{d}{2}\right)^2 L\rho}{10}$$

Where Wt Weight on the torque arm equvilent to 14 m of overburden at an average bulk density of 1550 kg/m^3

d diameter of sample = 0.1 m

L depth of overburden = 14 m

ρ bulk density = 1550 kg/m^3

Therefore Wt = 17 kg

Weights of 10, 15 and 20 kg were used to produce three peak shear strengths at overburdens depths of 8.2, 12.3 and 16.4 m respectively.

The *in-situ* sample choosen for testing was placed into the test cradle within the shear box and weight of either 10, 15, or 20 kg placed onto the torque arm. The sample was then left to

consolidate for 24 hrs while the time taken and the amount of consolidation were measured. The normal load and shear strength were calculated as follows:

$$\text{Normal Load} \quad \frac{(\text{Torque arm mass} = (\text{Hanger mass}}{\text{Sample area} \times 1000} \times \qquad G$$

$$\text{Shear Strength} \quad \frac{\text{Peak Load}}{\text{Sample area} \times 1000} \qquad (kN/m^2)$$

Table A4.3 presenting the data produced by direct shear testing

DIRECT SHEAR DATA				
Sample	Weight applied to Torque Arm (kg)	Normal Load kN/m^2	Shear Strength kN/m^2	**Lithological Unit Within The Sample Is Located**
2.7 / 1 / 85	5	62	32	Post-Rotoehu Ash Tephras
	5	62	45	
	10	124	90	
	10	124	94	
	15	186	27	
	15	186	0.4	
12.4 / 1 / 89	5	62	67	Pahoia Tephra (Upper Matua Subgroup)
	10	124	10	
	15	186	6	
	15	186	18	
15.6 / 1 / 85	10	124	87	Cross-bedding (Upper Matua Subgroup)
	15	186	135	
	20	248	175	
16.5 / 1 / 89	10	124	96.3	Cross-bedding (Upper Matua Subgroup)
	15	186	113	
	20	248	169	
17.0 / 1 / 89	10	124	94	Cross-bedding (Upper Matua Subgroup)
	15	186	136	
	20	248	184	
17.1 / 1 / 330	10	124	84	Upper Matua Subgroup
	15	186	135	
	20	248	176	Situated just above aquiferial zone (Upper Matua Subgroup)
18.6 / 1 / 89	10	124	111	
	15	186	170	
	20	248	227	Weakest noticeable unit in the field situated within the aquiferial zone (Upper Matua Subgroup)
Sample 11	10	124	59	
	15	186	81	
	20	248	100	

Plots normal load verse shear strength were graphed to obtained cohesion and friction angle.

PLOT OF NORMAL LOAD Vs. PEAK SHEAR STRENGTH TO DETERMINE ϕ AND c' FOR SAMPLE 2.7 / 1 / 85

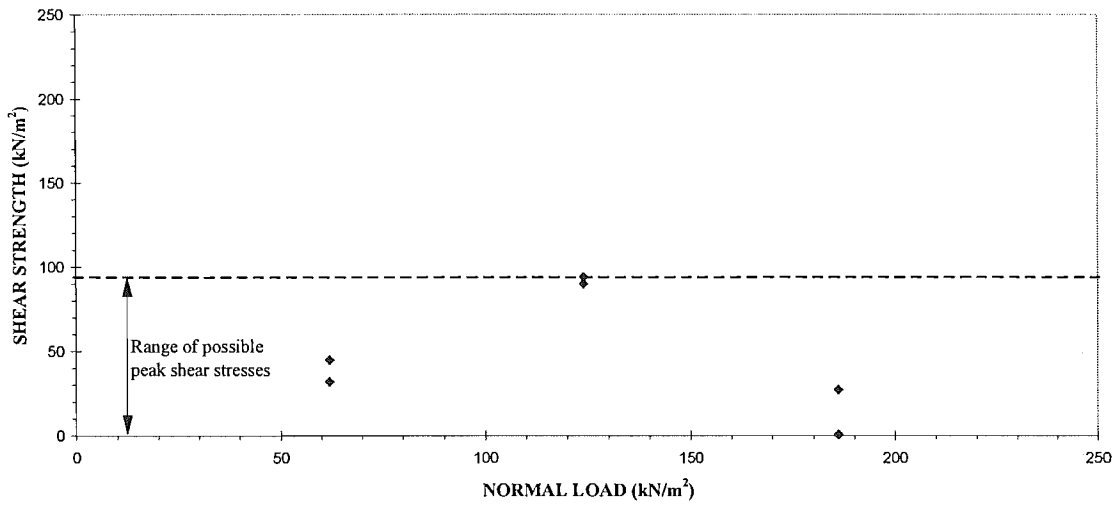

Figure A4.32 demonstrates a range of shear strengths for sample 2.7 / 1 / 85. The main reason in not obtaining a cohesion value or friction angle may be due to the pumicious nature of the sands as well as the wide range of grain sizes. This trend which can be seen above tends to indicate that strength of the soil material is not dependent on the normal load.

PLOT OF NORMAL LOAD Vs. PEAK SHEAR STRENGTH TO DETERMINE ϕ AND c' FOR SAMPLE 12.4 / 1 / 89

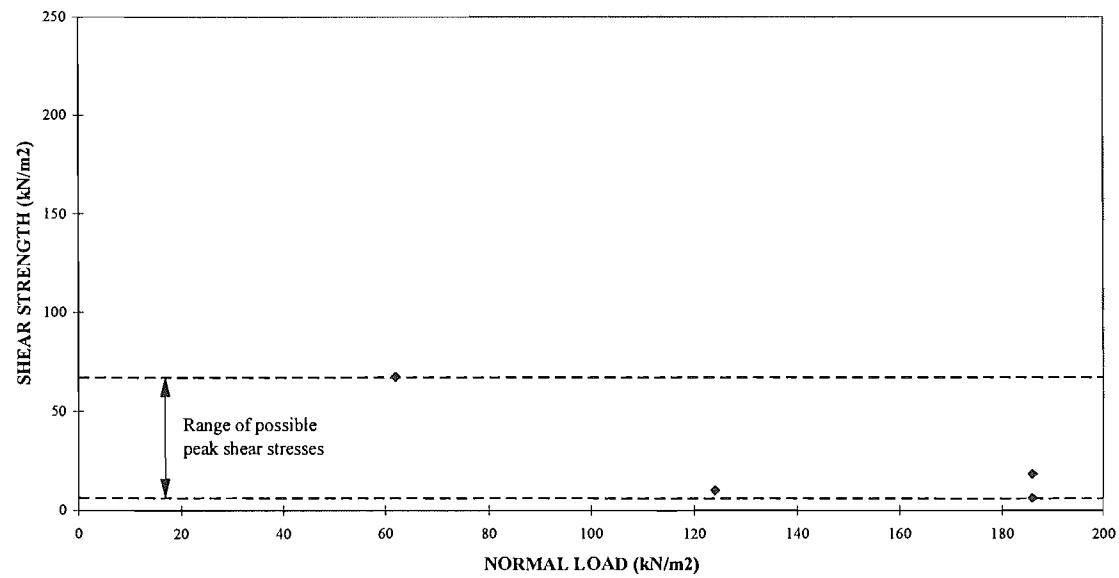

Figure A4.33 present a similar situation as sample 2.7 / 1 / 85 in that the variability in grain size and composition makes it very hard to obtain a representive sample, therefore only a range of

shear strengths resulted. This trend which can be seen above tends to indicate that strength of the soil material is not dependent on the normal load.

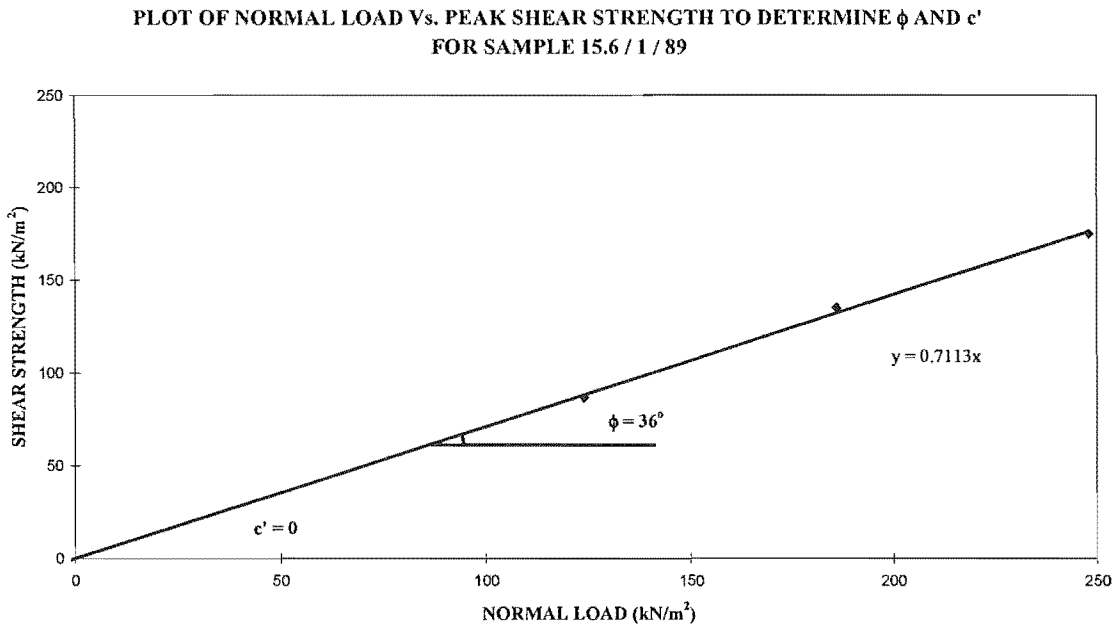

Figure A4.34 presents a cohesion c' = 0 and a friction angle $\phi = 36°$.

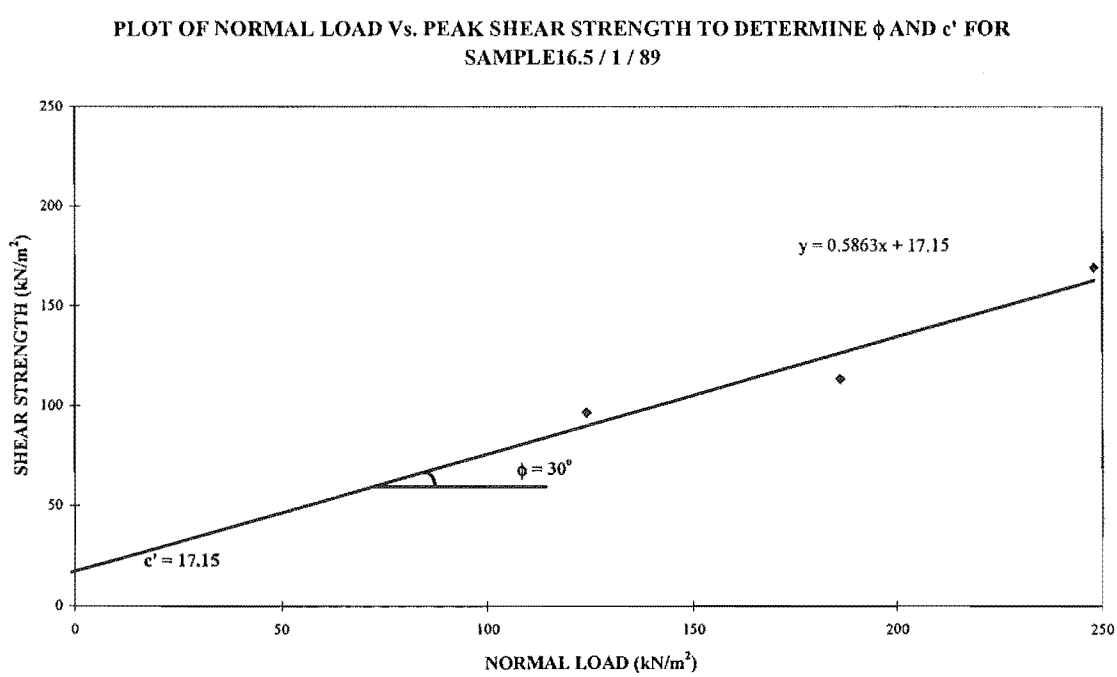

Figure A4.35 presents a cohesion c' = 17.15 and a friction angle $\phi = 30°$.

PLOT OF NORMAL LOAD Vs. PEAK SHEAR STRENGTH TO DETERMINE ϕ AND c' FOR SAMPLE 17.0 / 1 / 89

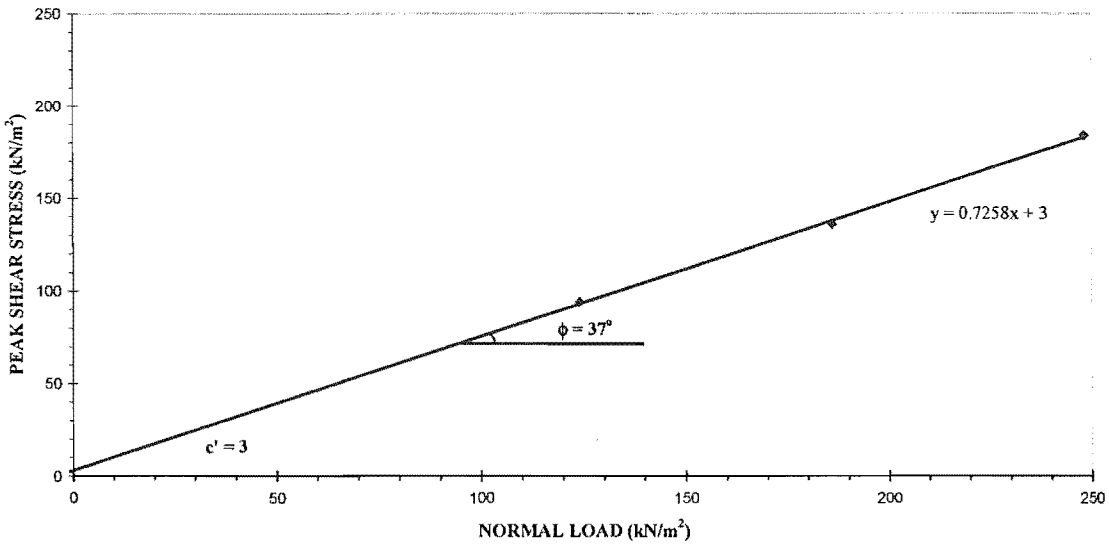

Figure A4.36 presents a cohesion c' = 3 and a friction angle ϕ = 37°.

PLOT OF NORMAL LOAD Vs. PEAK SHEAR STRENGTH TO DETERMINE ϕ AND c' FOR SAMPLE 17.1 / 1 / 330

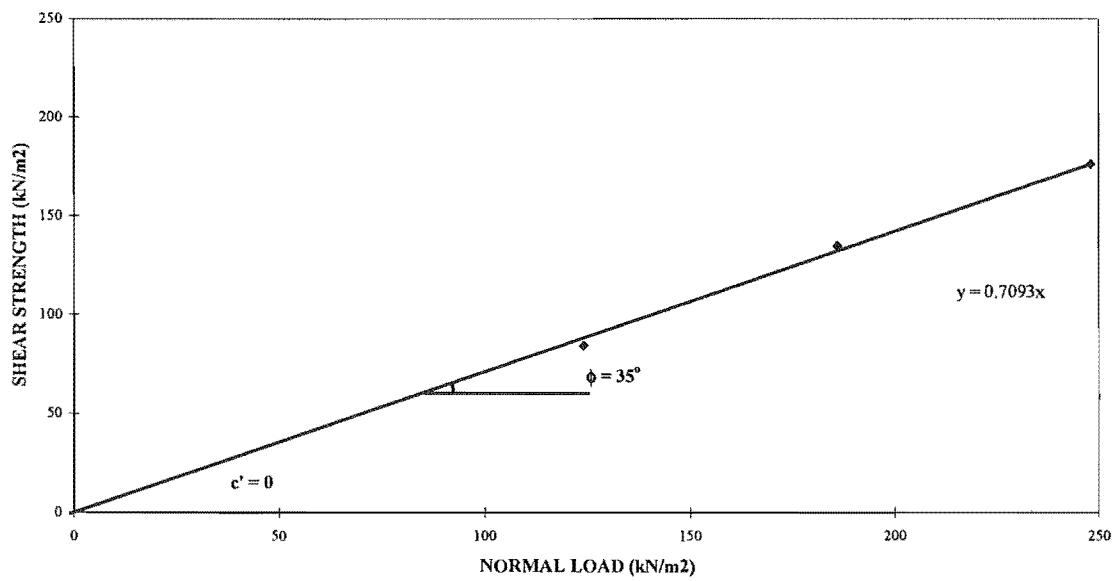

Figure A4.37 presents a cohesion c' = 0 and a friction angle ϕ = 35°.

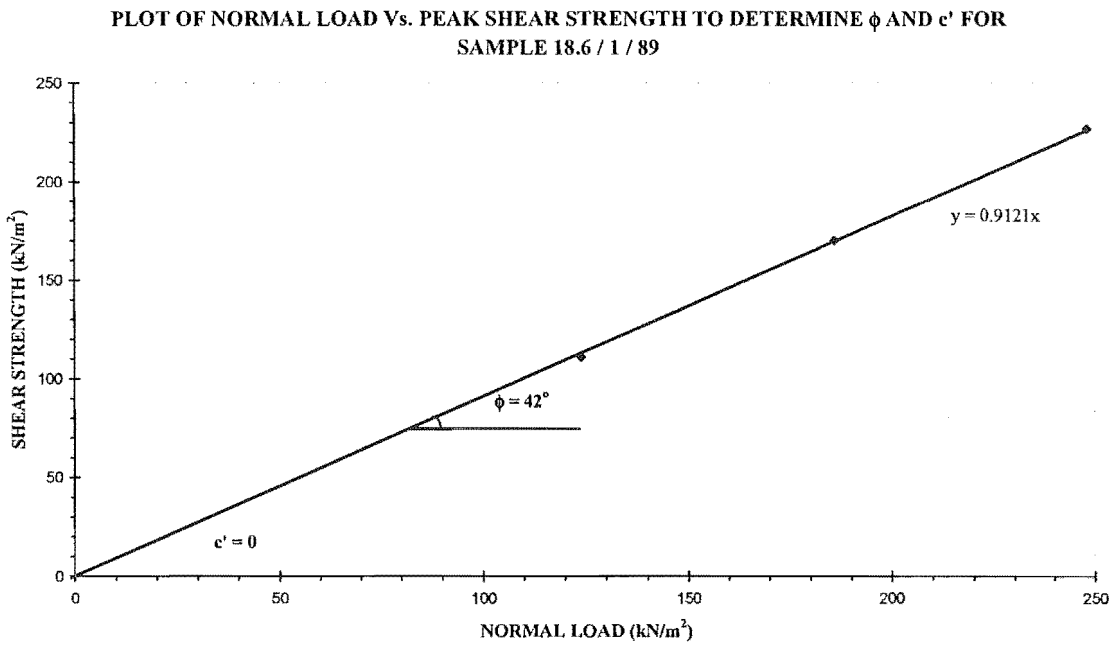

Figure A4.38 presents a cohesion c' = 0 and a friction angle ϕ = 42°.

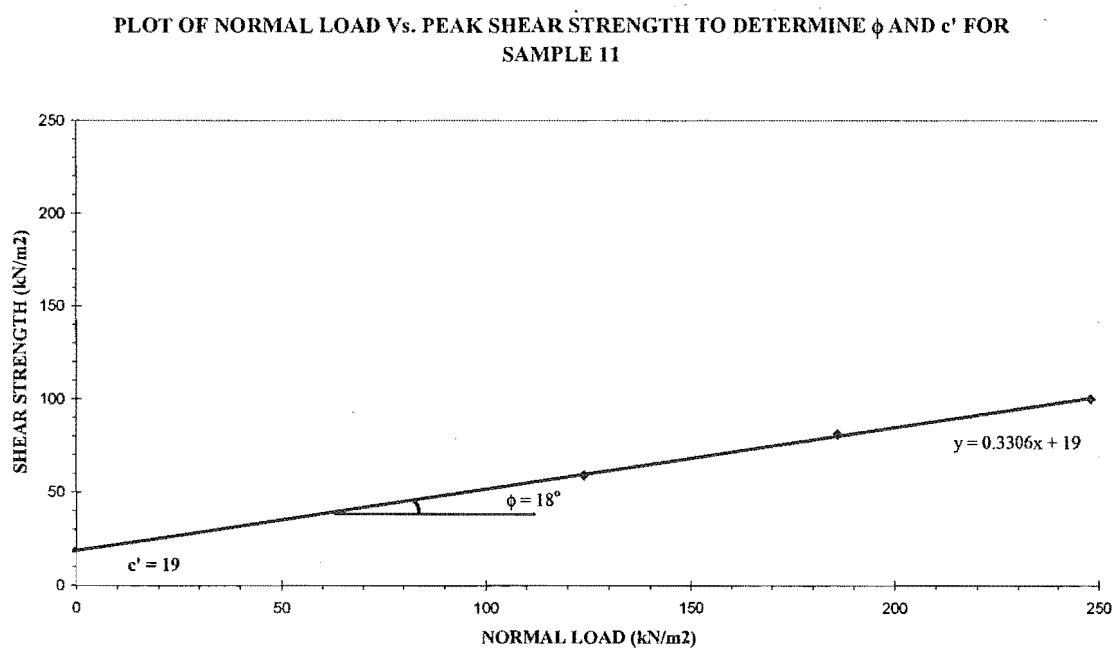

Figure A4.39 presents a cohesion c' = 19 and a friction angle ϕ = 18°.

APPENDIX A4.6 Triaxial Testing

Unconsolidated Undrained Triaxial Testing

All testing was completed in accordance with the NZ Standards NZS 4402: 1986 Test 6.2.1. An *in-situ* sample was obtained in the field by carefully pushing a 38 × 100 mm thin walled stainless steel tube into the desired soil mass. This was in turn tripple bagged to maintain the *in-situ* moisture content. In addition bulk samples were also collected for testing. Tube samples were carefully extruded via a hydrolic ram. These were then assembled in the triaxial cell and filled with water, Figure ? & ?. Three confining pressures (150, 300, 450 kPa) were chosen to provide a spread of strength data. A standard shear rate of 0.2 mm/minute was decided on to best similate failure dynamics of the Maungatapu Slips. Data was then recorded through Visual Basic to a spreadsheet where the deviator stress was calculated. Equations used:

$$\text{Axial Strain } (\varepsilon_1) = \frac{\text{Displacement (mm)}}{\text{Sample Height, Ho (mm)}}$$

$$\text{Adjusted Area} = \text{Ao}\left(\frac{1}{(1-\varepsilon_1)}\right)$$

Where A_O = Initial Area

$$\text{Deviator Stress} = \left(\frac{\text{Axial Load}}{\text{Adjusted Area}}\right) \times 1000(\text{to convert to kPa})$$

From here a maximum deviaror Stresses were calculated and Mohr Circles plotted to obtain maximum and minimum unconsolidated undrained shear strengths. The results are as follows:

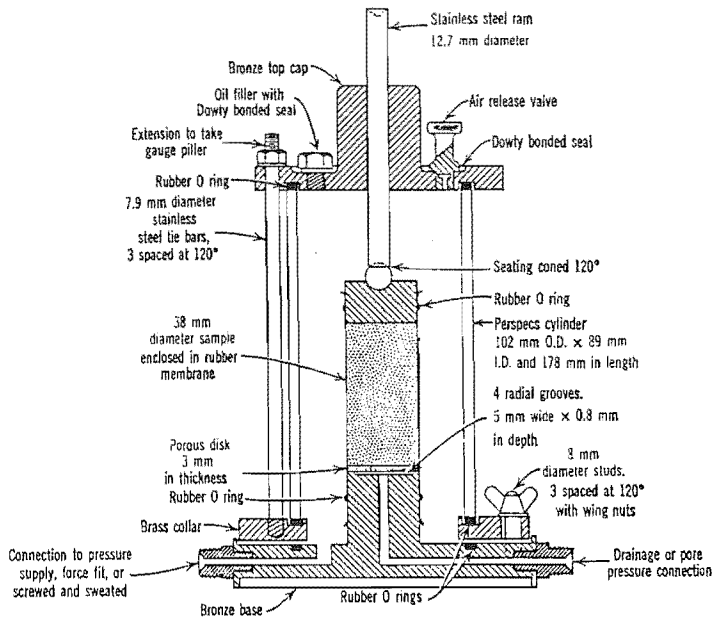

Figure A4.40 Cross section of a Typical Triaxial cell. (From Bishop and Henkel, 1962)

Results are as follows:

TRIAXIAL TESTING INFORMATION FOR SAMPLE 3.1 / 1 / 330

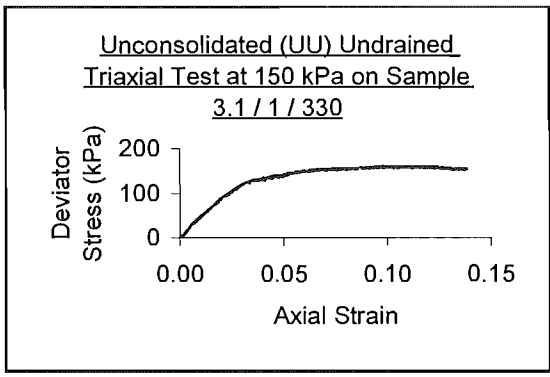

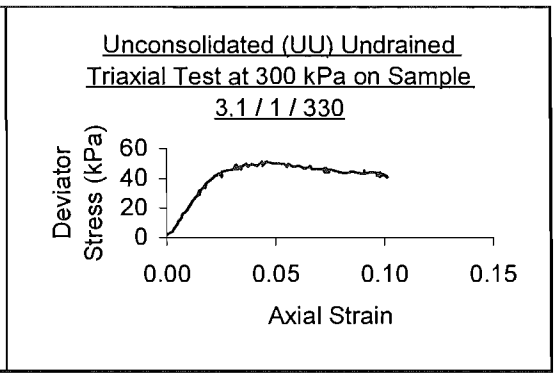

Sample: 3.1 / 1 / 330		
Confining pressure σ_3	Maximum Deviator Stress, $\sigma_1 - \sigma_3$	Principle Stress σ_1
150	160	310
300	51	351
450		

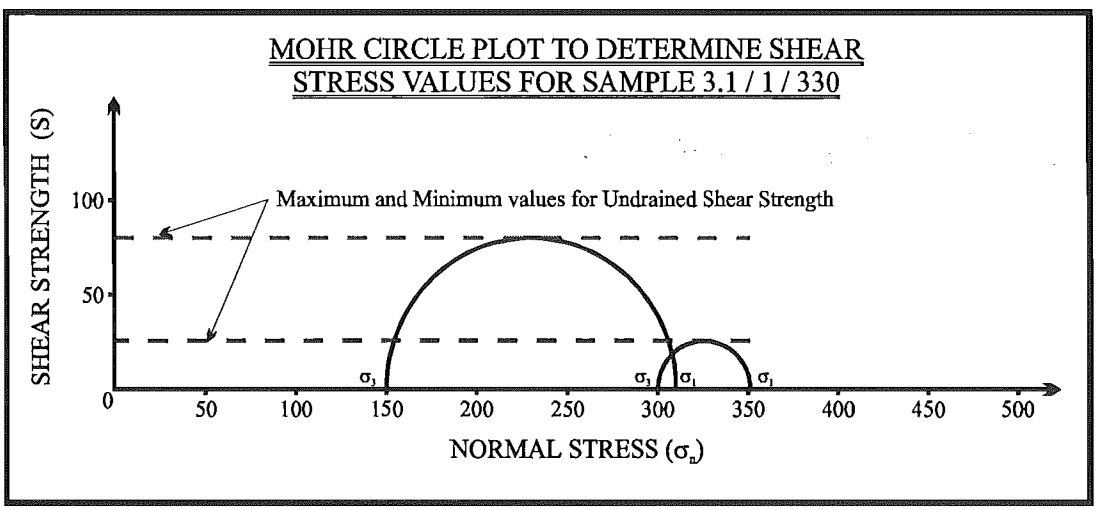

TRIAXIAL TESTING INFORMATION FOR SAMPLE 4.9 / 1 / 85

Unconsolidated (UU) Undrained Triaxial Test at 150 kPa on Sample 4.9 / 1 / 85

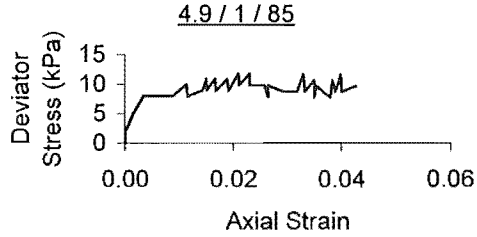

Unconsolidated (UU) Undrained Triaxial Test at 300 kPa on Sample 4.9 / 1 / 85

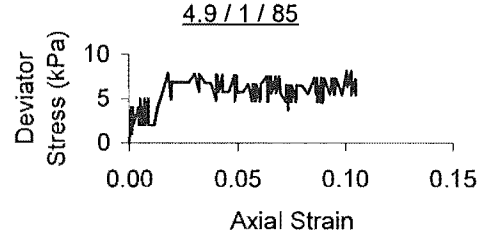

Sample: 4.9 / 1 / 85		
Confining pressure σ_3	Maximum Deviator Stress, $\sigma_1 - \sigma_3$	Principle Stress σ_1
150	12	162
300	8	308
450	4	454

Unconsolidated (UU) Undrained Triaxial Test at 450 kPa on Sample 4.9 / 1 / 85

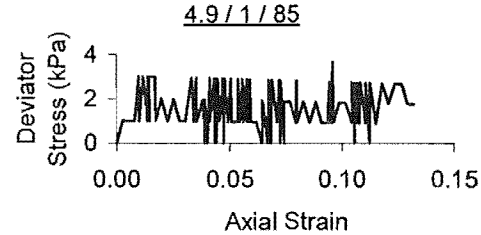

MOHR CIRCLE PLOT TO DETERMINE SHEAR STRESS VALUES FOR SAMPLE 4.9 / 1 / 85

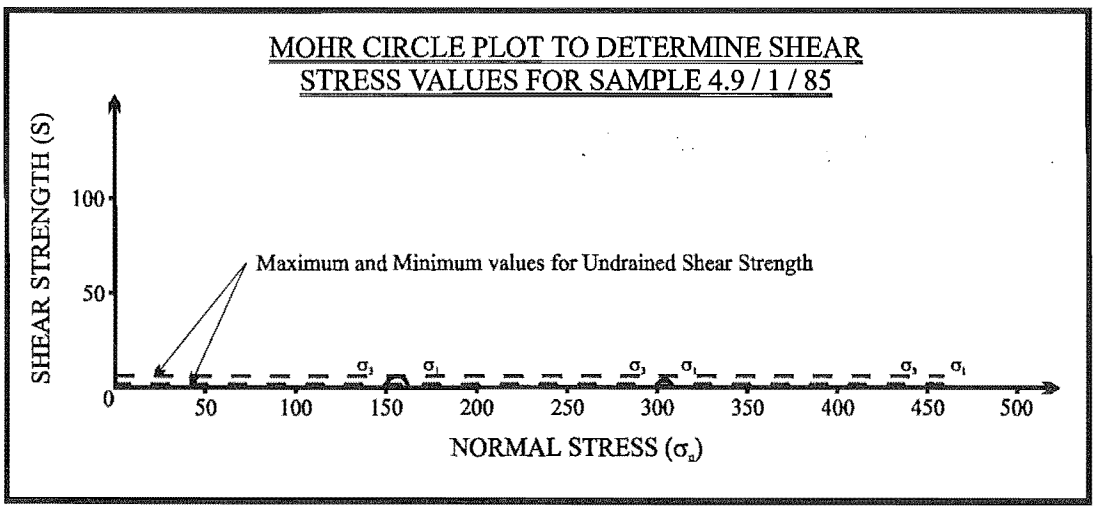

TRIAXIAL TESTING INFORMATION FOR SAMPLE 16 / 1 / 85

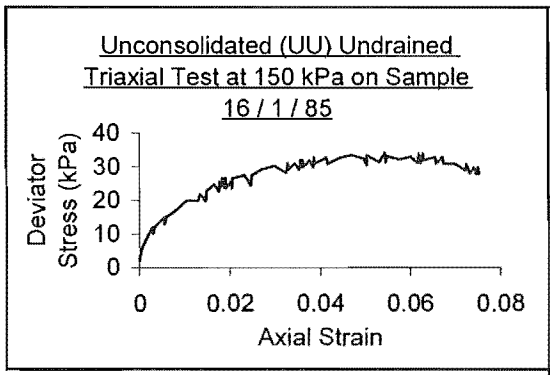

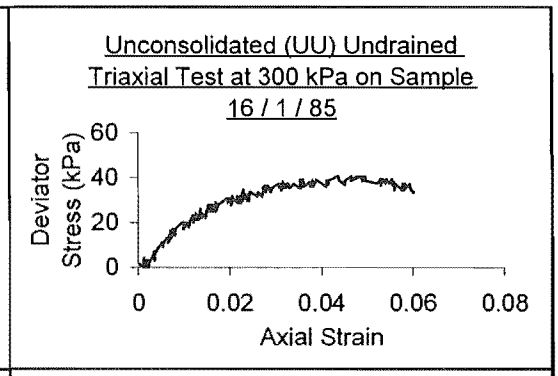

Sample: 16 / 1 / 85		
Confining pressure σ_3	Maximum Deviator Stress, $\sigma_1 - \sigma_3$	Principle Stress σ_1
150	34	184
300	41	341
450	23	473

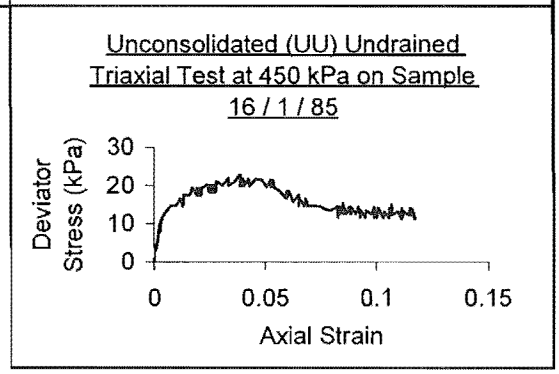

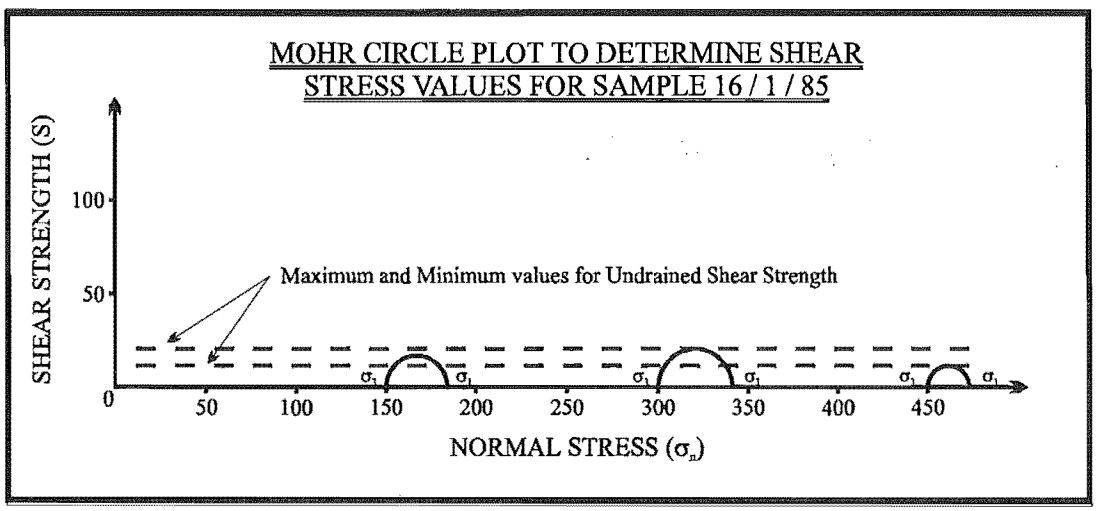

TRIAXIAL TESTING INFORMATION FOR SAMPLE 1

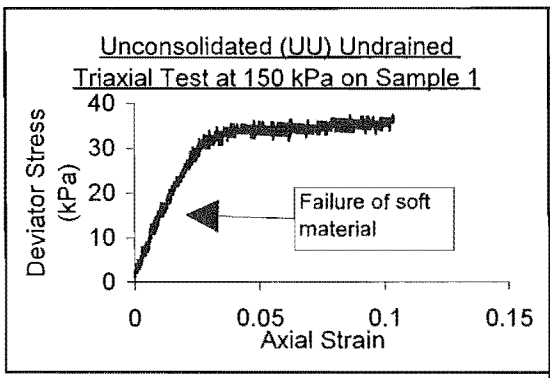

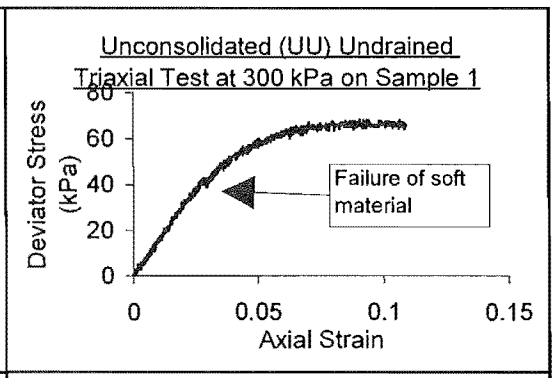

Sample: 1		
Confining pressure σ_3	Maximum Deviator Stress, $\sigma_1 - \sigma_3$	Principle Stress σ_1
150	37	187
300	68	368
450	52	502

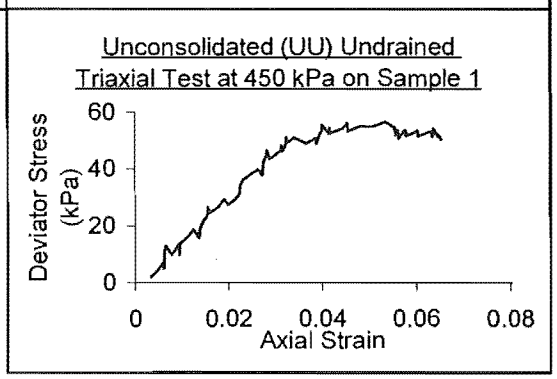

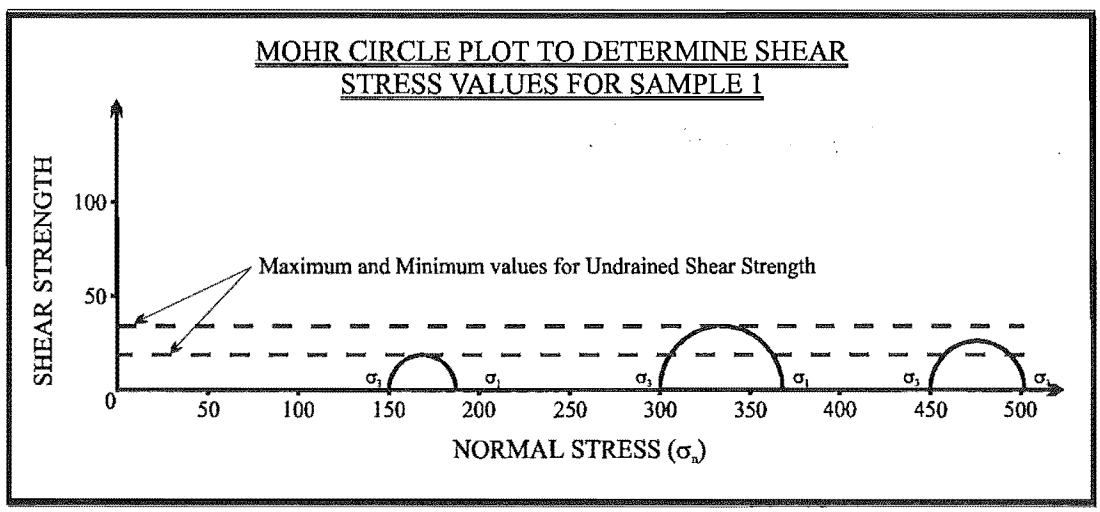

TRIAXIAL TESTING INFORMATION FOR SAMPLE 2TOP

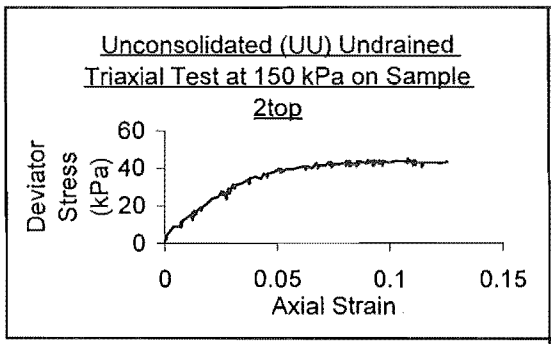

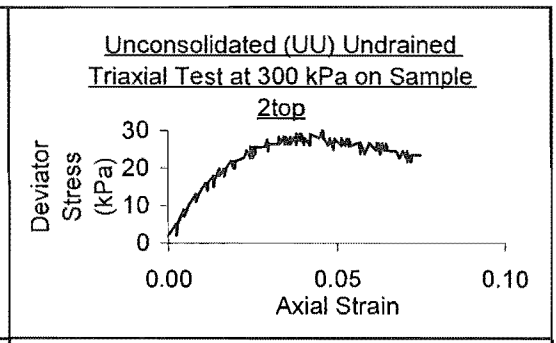

Sample: 2top		
Confining pressure σ_3	Maximum Deviator Stress, $\sigma_1 - \sigma_3$	Principle Stress σ_1
150	45	195
300	30	330
450	24	474

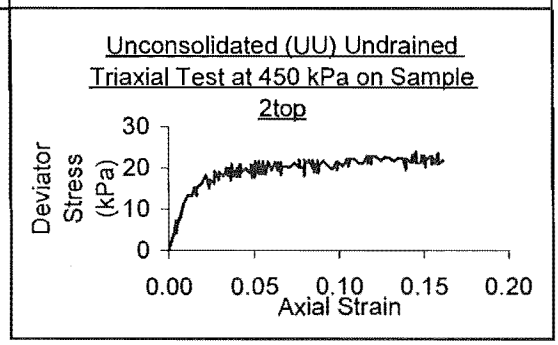

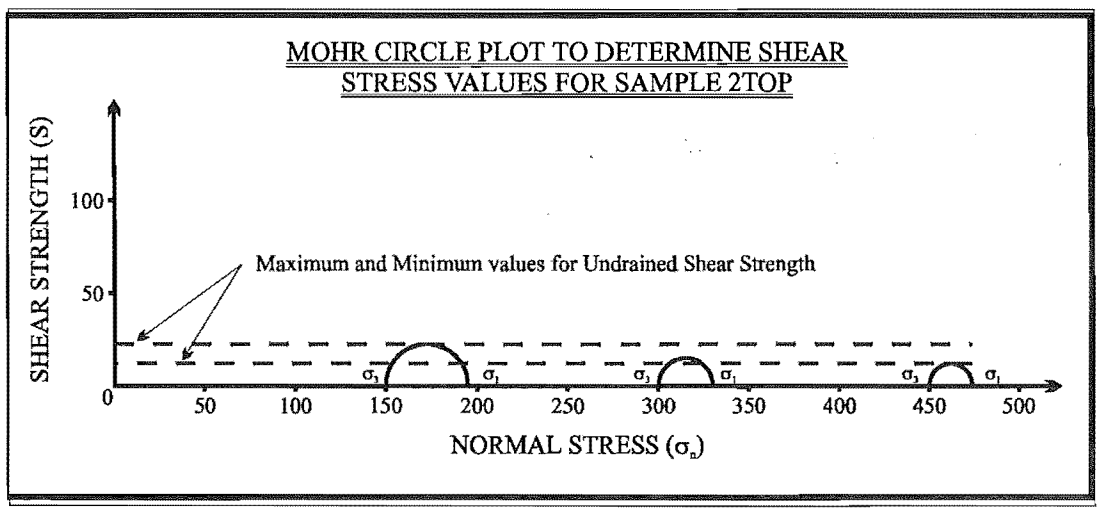

TRIAXIAL TESTING INFORMATION FOR SAMPLE 2BOTTOM

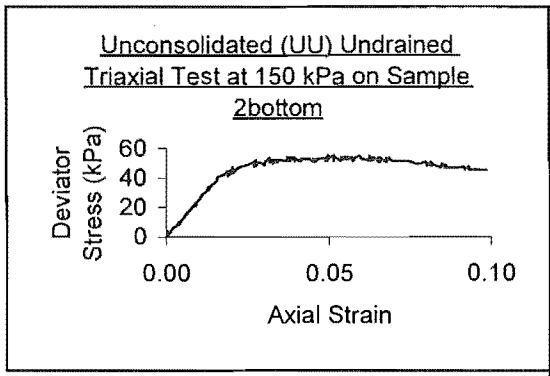

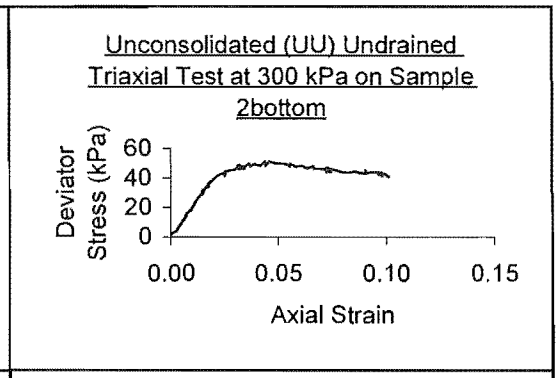

Sample: 2bottom		
Confining pressure σ_3	Maximum Deviator Stress, $\sigma_1 - \sigma_3$	Principle Stress σ_1
150	55	205
300	51	351
450	54	504

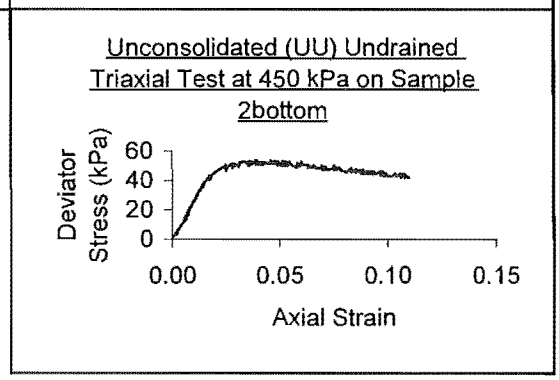

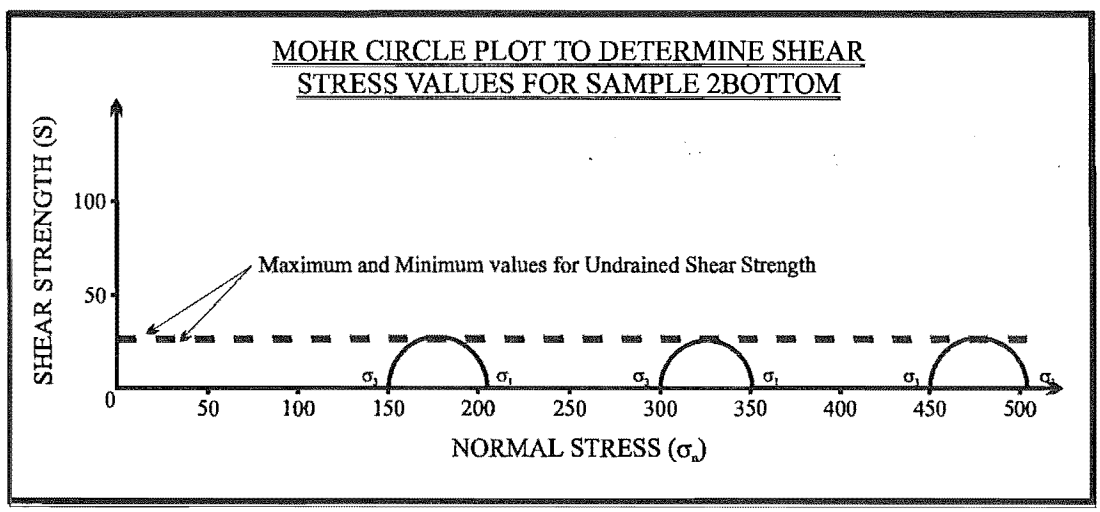

TRIAXIAL TESTING INFORMATION FOR SAMPLE 3TOP

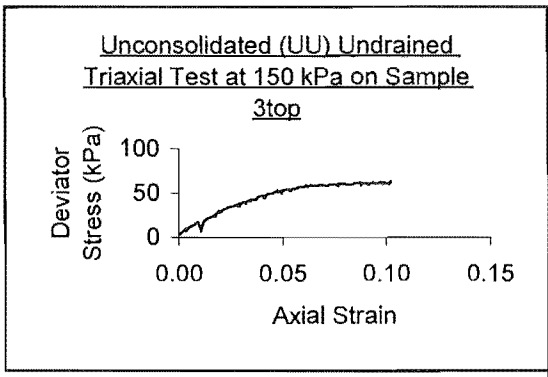

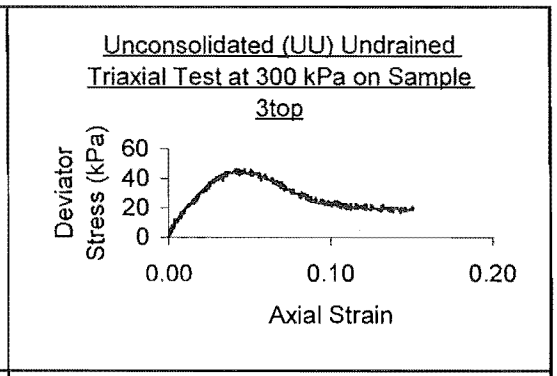

Sample: 3top		
Confining pressure σ_3	Maximum Deviator Stress, $\sigma_1 - \sigma_3$	Principle Stress σ_1
150	62	212
300	46	346
450	46	496

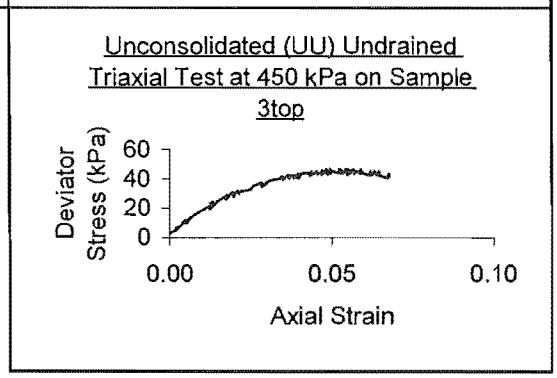

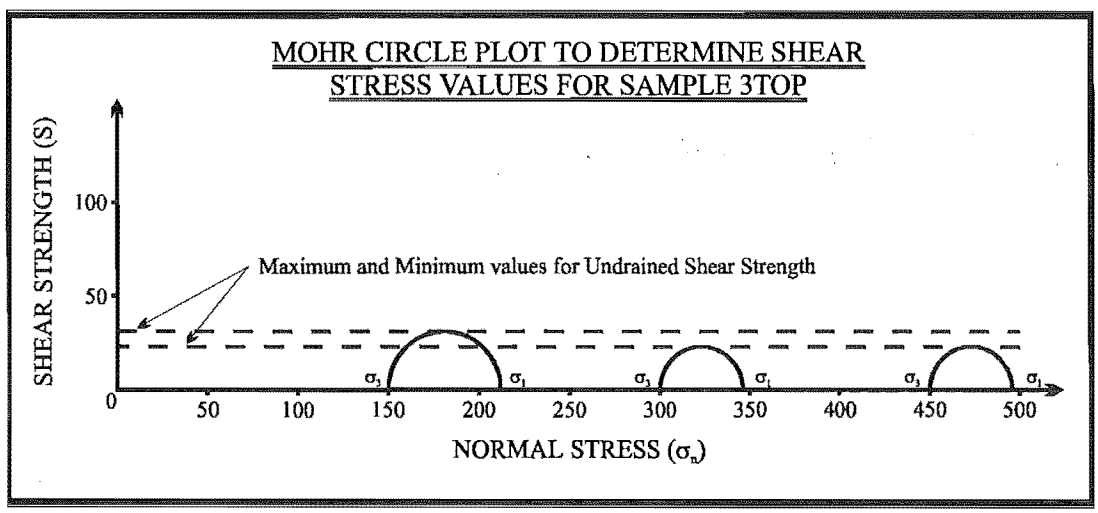

TRIAXIAL TESTING INFORMATION FOR SAMPLE 3BOTTOM

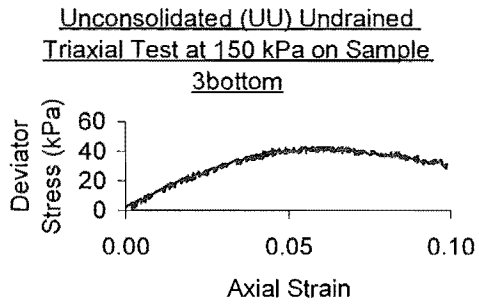

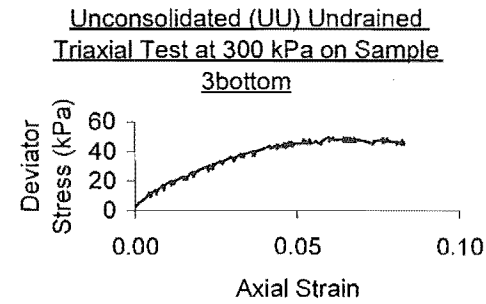

Sample: 3bottom		
Confining pressure σ_3	Maximum Deviator Stress, $\sigma_1 - \sigma_3$	Principle Stress σ_1
150	43	193
300	49	349
450	56	506

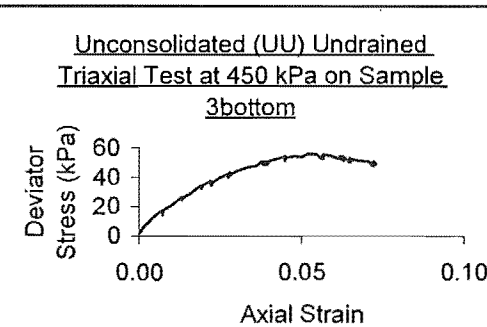

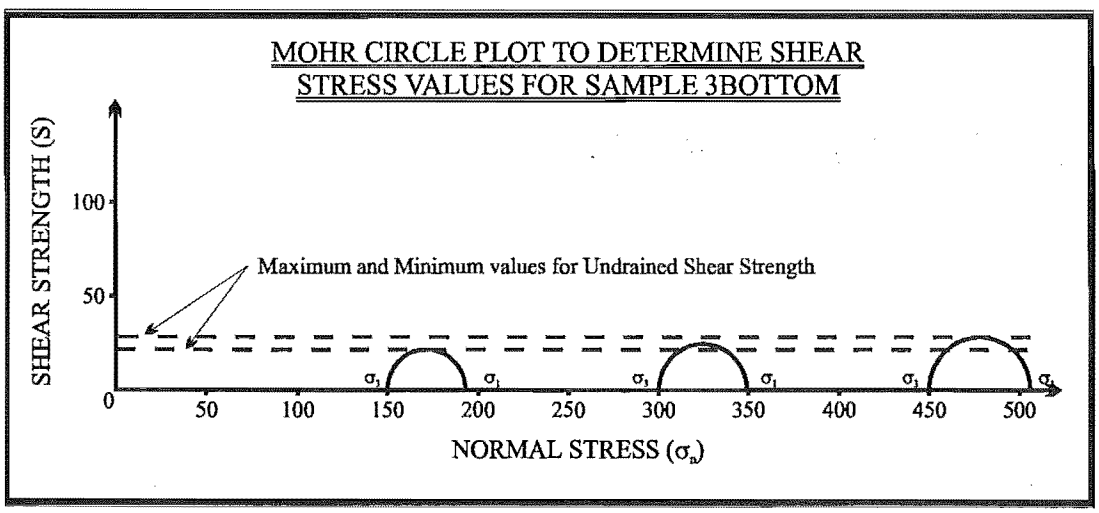

TRIAXIAL TESTING INFORMATION FOR SAMPLE 9

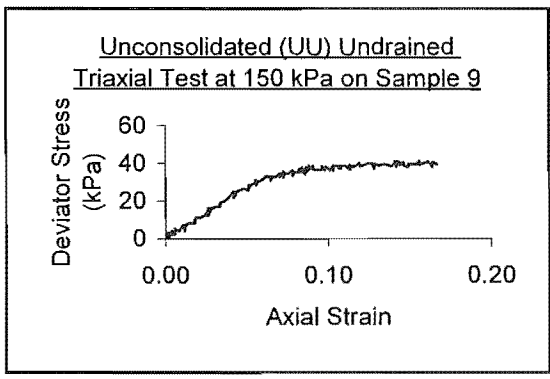

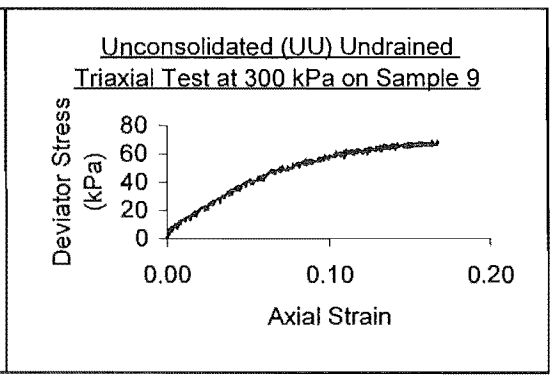

Sample: 9		
Confining pressure σ_3	Maximum Deviator Stress, $\sigma_1 - \sigma_3$	Principle Stress σ_1
150	41	191
300	69	369
450		

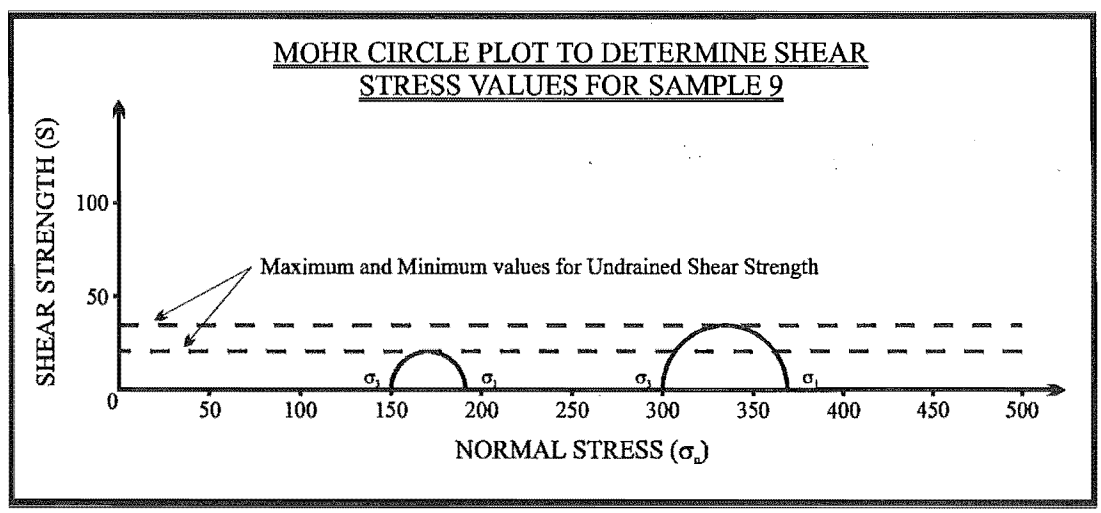

TRIAXIAL TESTING INFORMATION FOR SAMPLE 10

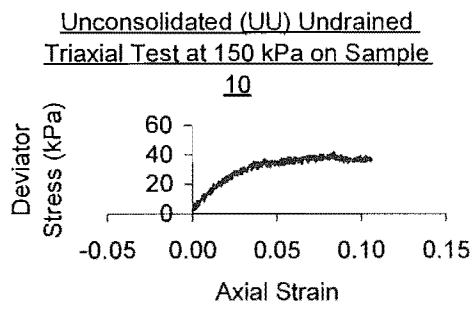

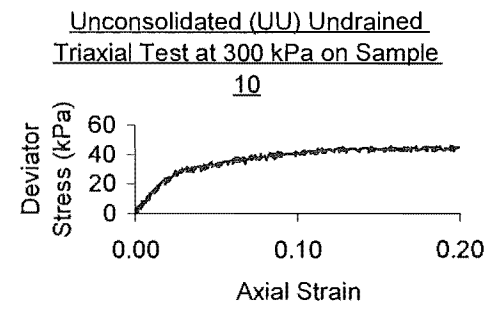

Sample: 10		
Confining pressure σ_3	Maximum Deviator Stress, $\sigma_1 - \sigma_3$	Principle Stress σ_1
150	41	191
300	46	346
450	41	491

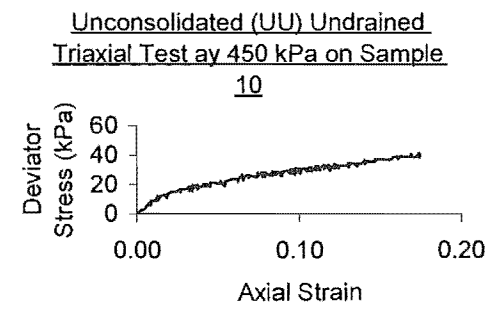

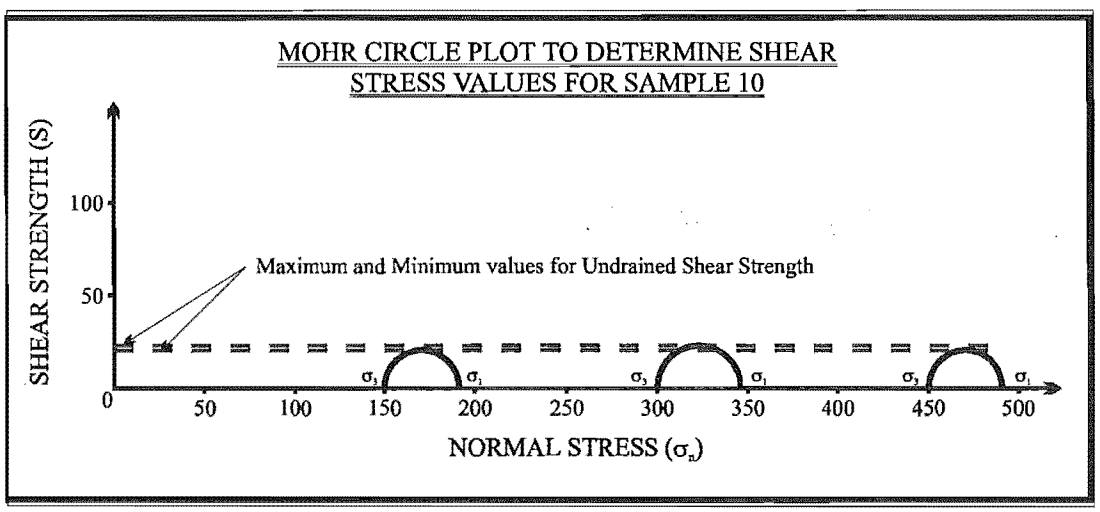

Sample 10 lies within the aquiferial zone. This sample also showed a graditional type failure which is reflected in the UU plots.The strengths ranged from 20.5 - 23 kPa, with failure following a similar path as in sample 1. No picture taken of sample.

APPENDIX A4.7 In-situ Bulk And Dry Density

Method and Calculations

1. *In-situ* samples were collected in 35 mm ϕ × 175 mm long stainless steel tubes. These were in-turn double bag to maintain *in-situ* moisture content.

2. The sample and tube were weigh to an accuracy of 0.05g, and the lenght and diameter of soil in the tube measured.

3. They were then placed in a oven at 105 °C for a minimum of 12 hours.

4. On completion the sample and tube was weigh again as well as measuring the diameter and length of the sample within the tube.

5. The sample was extruded from the tube and the tube weigh.

6. Finially the natural soil water content (M_w), dry state (M_s), water content (w), bulk density (ρ), and the dry density (ρ_d).

7. calaulations used are as follows:

$$\text{Water content} \quad w = \frac{M_w - M_s}{M_s} \times 100 \quad \%$$

$$\text{Bulk Density} \quad \rho = \frac{M_w\left(4\times10^6\right)}{\pi\phi^2 L_{wet}} \quad \text{kg/m}^3$$

$$\text{Dry Density} \quad \rho_d = \frac{M_s\left(4\times10^6\right)}{\pi\varphi^2 L_{dry}} \quad \text{kg/m}^3$$

Results can be view on the following page.

IN-SITU BULK AND DRY DENSITIES													
Sample No.	Stratigraphic position	Soil + Tube (wet)	Soil + Tube (dry)	Tube	Natural soil water Content (M_w)	Dry State (M_s)	Natural water content of soil (w%)	Wet length of soil in tube, L_{wet} (mm)	Dry length of soil in tube, L_{dry} (mm)	Length of tube (mm)	Diameter of tube (mm)	Bulk density (Kg/m3)	Dry Density (Kg/m3)
0.4/1/330	Post-Rotoehu Ash Tephras	345.45	285.65	193.25	152.20	92.40	64.72	119.91	123.71	173.67	35.27	1299.15	764.48
3.1/1/330	Palaeosol	372.15	312.10	192.95	179.20	119.15	50.40	119.70	117.91	175.50	36.86	1402.95	946.98
10.5/1/330	Cross-bedded	478.15	376.20	194.30	283.85	181.90	56.05	174.42	168.37	174.42	35.46	1647.88	1093.96
10.0/1/330	section of the	468.35	384.35	194.55	273.80	189.80	44.26	168.10	167.91	175.10	35.60	1636.35	1135.61
14.2/1/330	Upper Matua	473.30	377.00	193.35	279.95	183.65	52.44	175.30	172.87	175.30	35.59	1605.29	1067.89
14.0/1/330	Subgroup	474.00	384.00	196.15	277.85	187.85	47.91	162.38	161.67	177.47	35.65	1714.23	1164.05
											Averages =	1601.34	1081.70

BULK DENSITIES AQUIRED FROM PINHOLE SAMPLES BEFORE TESTING										
Sample No.	Stratigraphic position	Beaker + Sample (wet)	Beaker + Sample (dry)	Beaker	Natural soil water content, M_w (%)	Dry State, M_s (%)	Water Content, w (%)	Length of wet soil sample, L_{wet} (mm)	Diameter of soil sample (mm)	Bulk Density of soil samples (Kg/m3)
0.4 / 1 / 330	Post-Rotoehu Ash Tephra	136.07	120.81	95.34	40.73	25.48	59.89	31.07	35.81	1301.69
3.1 / 1 / 330	Palaeosol	143.27	127.49	95.36	47.91	32.14	49.08	31.93	35.83	1488.17
9.8 / 1 / 330	Cross-bedded	135.49	117.15	80.04	55.46	37.11	49.43	31.58	35.89	1735.80
10.0 / 1 / 330	section of the	107.52	90.06	50.69	56.83	39.37	44.34	28.38	35.80	1989.45
14.0 / 1 / 330	Upper Matua	148.40	128.88	85.88	62.52	43.00	45.38	35.26	35.80	1761.46
14.2 / 1 / 330	Subgroup	153.53	135.57	96.85	56.68	38.71	46.40	35.83	36.08	1547.19
18.0 / 1 / 330	Aquifer	142.48	133.19	95.34	47.14	37.86	24.53	22.92	35.98	2022.89
18.8 / 1 / 85	Situated below the lower aquitard	150.93	127.36	96.85	54.07	30.51	77.25	30.70	35.93	1737.09
									AVERAGE =	1697.97

Table A4.4 In-situ bulk and dry densities for samples collected during field investigations.

APPENDIX A4.8 Erodibility (Pinhole Test) And Dispersion (Crumb Test)

A 4.6.1 Pinhole Test

Pinhole testing was modified after BS 1377:Part 5, 1990 which is based on the test developed by Sherard (1976). Yetton and Bell (1992) indicated that the pinhole test should be used to defined the erosional characteristics of a soil and not the dispersive nature. Therefore the classification scheme used in this study has been redefined in terms of the erosive potential of a soil instead of the dispersive, e.g. the dispersion classification of D1 is changed to and erosion classification E1, Table ?. Table ? also indicates a colour or cloudiness of the water entering the measuring cylinda. This is interpretated as providing an indication of erosion form the sample and not the dispersive nature of the sample. Yetton and Bell (1992) have proposed a new classification scheme (Table ?) which is similar to the modified British Standards used, Table ?.

Method

1. Field samples were collected in stainless steel tubes approximately 100 mm in lenght bt 35 mm in diameter at *in-situ* moisture content,

2. The sample were trimed to 50 mm in lenght and flush with one of the ends of the tube,

3. A 1mm diameter hole was drilled through the centre of the sample with a counter sunk conical depression. The sample was then setup in the appratus, Figure ?,

4. The inlet vlaue was opened and a stready rate of flow of water was passed through at varying heads of 50, 180, 380, and 1000 mm, with flow rates exiting the outlet pipe being determined,

5. Erosion classes were assigned from Table ?. The British Standards use dispersion classification which has been changed to present an erosion classification E1-NE4.

Table A4.5 Erosion Classification from soil pinhole test data modified from Classification of soils from pinhole test data, American Society for testing and Materials in BS 1377: Part 5: 1990.

Classification Of Soils From Pinhole Test Data					
Erosion Classification	Head	Final Flow Rate Through Specimen	Cloudiness Of Flow At End Of Test		Hole Size after Test
	(mm)	mL/s	From Side	From Top	mm
E1 (D1)	50	> 1.5	dark	very dark	>2.0
E2 (D2)	50	1.0-1.5	moderately dark	dark	>1.5
NE4 (ND4)	50	0.8-1.0	slightly dark	moderately dark	<1.5
NE3 (ND3)	180	1.4-2.7	barely visible	slightly dark	>1.5
NE3 (ND3)	380	1.8-3.2			
NE2 (ND2)	1000	>3.0	clear	barely visible	<1.5
NE1 (ND1)	1000	<3.0	perfectly clear	perfectly clear	1.0
Where (D1-ND1) represent dispersive classification form classification of soils from pinhole test data in BS 1377: Part 5: 1990.					

Table A4.6 Erosional classes proposed by Yetton and Bell (1992) compared to Sherard et al. (1976a) and the modified BS, modified from Yetton and Bell (1992).

Erosional Classes For Pinhole Testing		
Modified British Standards	Sherard (1976a)	Yetton & Bell (1992)
E1	D1	E_{50}
E2	D2	$E_{180\text{-}50}$
NE3	ND4	E_{180}
NE3	ND3	E_{380}
NE2	ND2	E_{1000}
NE1	ND1	$E_{>1000}$

Results of testing follow:

Table A4.7 Pinhole data sheet for sample 0.4 /1/330 indicating colour, particles falling, flow rate, and flow rate distribution plot.

ERODIBILITY - PINHOLE TEST

Location :	Maungatapu Peninsula 330 Maungatapu Road	Borehole / Pit Number :	Face Log	Comment : 1 mm Pinhole appeared to be basically in-tacked, but the sample was completely saturated. No determinable particles could be seen settling through the measuring beaker due to their small grain sizes
Soil Description :	Pumiceous Sand	Sample Number :	0.4 / 1 / 330	
		Depth (m) :	0.4	
Test Method :				

Clock Time		Hydraulic Head, H (mm)	Rate Of Flow		Colour As Seen From Side Of Measuring Beaker					Particles Falling		
Minutes	Seconds		Volume (mL)	Flow Rate, Q (mL/sec)	Dark	Medium	Slight	Barely Visible	Completely Clear	None	Few	Many
1	60	50	30	0.50								
2	120	50	70	0.67								
3	180	50	115	0.75								
4	240	50	150	0.58								
5	300	50	185	0.58								
6	360	50	220	0.58								
7	420	50	260	0.67								
8	480	50	290	0.50								
9	540	50	300	0.17								
10	600	50	320	0.33								
11	660	180	350	0.50								
12	720	180	390	0.67								
13	780	180	400	0.17								
14	840	180	420	0.33								
15	900	180	450	0.50								
16	960	180	480	0.50								
17	1020	180	495	0.25								
18	1080	180	515	0.33								
19	1140	180	535	0.33								
20	1200	180	550	0.25								
21	1260	380	590	0.67								
22	1320	380	630	0.67								
23	1380	380	675	0.75								
24	1440	380	700	0.42								
25	1500	380	730	0.50								
26	1560	380	770	0.67								
27	1620	380	800	0.50								
28	1680	380	830	0.50								
29	1740	380	870	0.67								
30	1800	380	900	0.50								
31	1860	1020	960	1.00								
32	1920	1020	1050	1.50								
33	1980	1020	1150	1.67								
34	2040	1020	1230	1.33								
35	2100	1020	1310	1.33								
36	2160	1020	1390	1.33								
37	2220	1020	1470	1.33								
38	2280	1020	1550	1.33								
39	2340	1020	1630	1.33								
40	2400	1020	1700	1.17								

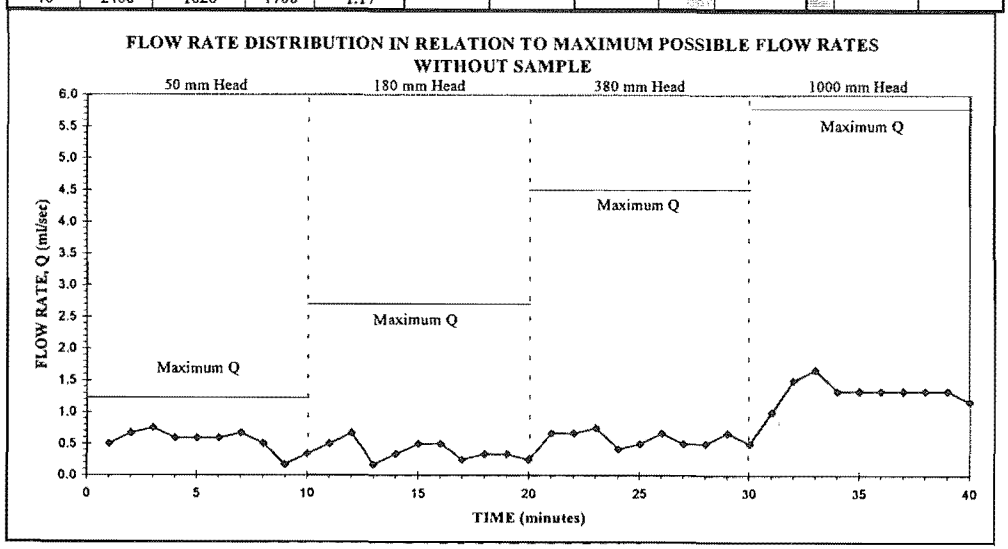

Table A4.8 Pinhole data sheet for sample 3.1 /1/330 indicating colour, particles falling, flow rate, and flow rate distribution plot.

ERODIBLILITY - PINHOLE TEST

Location :	Maungatapu Peninsula 330 Maungatapu Road	**Borehole / Pit Number :**	Face Log	**Comment :** No change was detectable in the diameter of the pinhole, and the had basically stayed at in-situ moisture content measured before testing. This indicated that most of the water had flowed through the pinhole
Soil Description :	Dark Brown Clayey Silt	**Sample Number :**	3.1 / 1 /330	
		Depth (m) :	3.1	
Test Method :				

Clock Time		Hydraulic Head, H (mm)	Rate Of Flow		Colour As Seen From Side Of Measuring Beaker					Particles Falling		
Minutes	Seconds		Volume (ml)	Flow Rate, Q (ml/sec)	Dark	Medium	Slight	Barely Visible	Completely Clear	None	Few	Many
1	60	50	5	0.08								
2	120	50	30	0.42								
3	180	50	50	0.33								
4	240	50	70	0.33								
5	300	50	90	0.33								
6	360	50	105	0.25								
7	420	50	125	0.33								
8	480	50	145	0.33								
9	540	50	160	0.25								
10	600	50	180	0.33								
11	660	180	210	0.50								
12	720	180	260	0.83								
13	780	180	300	0.67								
14	840	180	350	0.83								
15	900	180	400	0.83								
16	960	180	450	0.83								
17	1020	180	500	0.83								
18	1080	180	550	0.83								
19	1140	180	590	0.67								
20	1200	180	640	0.83								
21	1260	380	710	1.17								
22	1320	380	800	1.50								
23	1380	380	895	1.58								
24	1440	380	1000	1.75								
25	1500	380	1090	1.50								
26	1560	380	1190	1.67								
27	1620	380	1270	1.33								
28	1680	380	1380	1.83								
29	1740	380	1450	1.17								
30	1800	380	1550	1.67								
31	1860	1000	1680	2.17								
32	1920	1000	1830	2.50								
33	1980	1000	1975	2.42								
34	2040	1000	2125	2.50								
35	2100	1000	2265	2.33							minor	
36	2160	1000	2350	1.42							minor	
37	2220	1000	2500	2.50								
38	2280	1000	2640	2.33							minor	
39	2340	1000	2790	2.50							minor	
40	2400	1000	2940	2.50							minor	

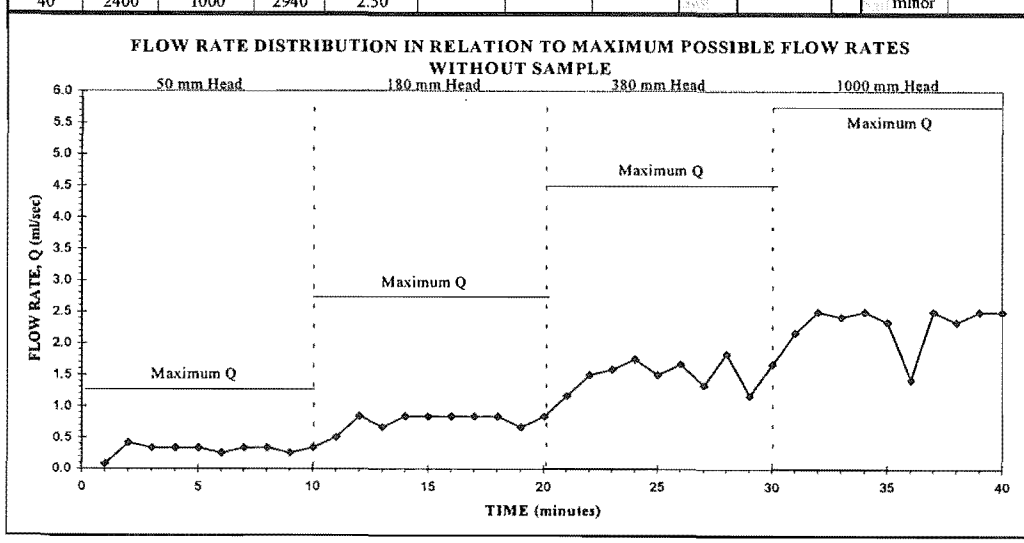

Table A4.9 Pinhole data sheet for sample 9.8/1/330 indicating colour, particles falling, flow rate, and flow rate distribution plot.

ERODIBILITY - PINHOLE TEST

Location : Maungatapu Peninsula 330 Maungatapu Road	**Borehole / Pit Number :**	Face Log	**Comment :** Major blow out occurred during testing which increased the flow rate output considerably. The pinhole closed so water had to flow through the sample mass.
Soil Description : Water has flowed continually through this sample resulting in transportation of the clay fraction along the unit weaken the soil structure.	**Sample Number :**	9.8 / 1 / 330	
	Depth (m) :	9.8	

Test Method :

Clock Time		Hydraulic Head, H (mm)	Rate Of Flow		Colour As Seen From Side Of Measuring Beaker					Particles Falling		
Minutes	Seconds		Volume (ml)	Flow Rate, Q (ml/sec)	Dark	Medium	Slight	Barely Visible	Completely Clear	None	Few	Many
1	60	50	300	5.00	Immediate Blow Out							
2	120	50	650	5.83								
3	180	50	950	5.00								
4	240	50	1260	5.17								
5	300	50	1610	5.83								
6	360	50	1890	4.67								
7	420	50	2200	5.17								
8	480	50	2540	5.67								
9	540	50	2850	5.17								
10	600	50	3200	5.83								
11	660	180										
12	720	180										
13	780	180										
14	840	180										
15	900	180										
16	960	180										
17	1020	180										
18	1080	180										
19	1140	180										
20	1200	180										
21	1260	380										
22	1320	380										
23	1380	380										
24	1440	380										
25	1500	380										
26	1560	380										
27	1620	380										
28	1680	380										
29	1740	380										
30	1800	380										
31	1860	1000										
32	1920	1000										
33	1980	1000										
34	2040	1000										
35	2100	1000										
36	2160	1000										
37	2220	1000										
38	2280	1000										
39	2340	1000										
40	2400	1000										

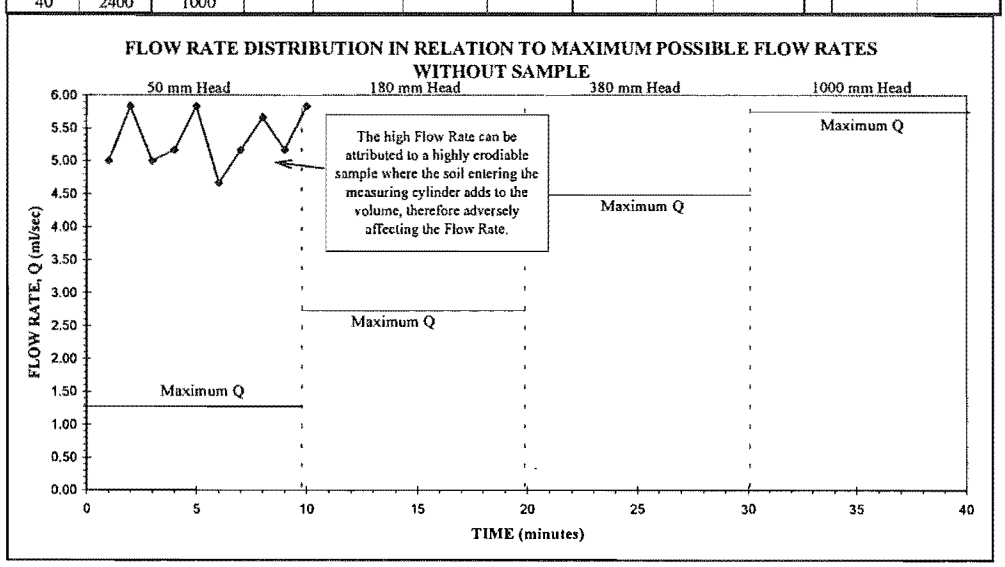

Table A4.10 Pinhole data sheet for sample 10.0/1/330 indicating colour, particles falling, flow rate, and flow rate distribution plot.

ERODIBILITY - PINHOLE TEST

Location :	Maungatapu Peninsula 330 Maungatapu	Borehole / Pit Number :	Face Log	Comment : On inspection the pinhole has appeared to have closed up in sections resulting in the sample becoming saturated. The measuring beaker appears to be quite dark, but the particles are of such a fine fraction that they are hard to see.
Soil Description :	Clayey Sand	Sample Number :	10.0 / 1 / 330	
		Depth (m) :	10	
Test Method :				

Clock Time		Hydraulic Head, H (mm)	Rate Of Flow		Colour As Seen From Side Of Measuring Beaker					Particles Falling		
Minutes	Seconds		Volume (ml)	Flow Rate, Q (ml/sec)	Dark	Medium	Slight	Barely Visible	Completely Clear	None	Few	Many
1	60	50	30	0.5								
2	120	50	60	0.50								
3	180	50	90	0.50								
4	240	50	140	0.83								
5	300	50	170	0.50								
6	360	50	170	0.00								
7	420	50	170	0.00								
8	480	50	170	0.00								
9	540	50	170	0.00								
10	600	50	170	0.00								
11	660	180	175	0.08								
12	720	180	175	0.00								
13	780	180	180	0.08								
14	840	180	180	0.00								
15	900	180	180	0.00								
16	960	180	180	0.00								
17	1020	180	180	0.00								
18	1080	180	180	0.00								
19	1140	180	180	0.00								
20	1200	180										
21	1260	380										
22	1320	380										
23	1380	380										
24	1440	380										
25	1500	380										
26	1560	380										
27	1620	380										
28	1680	380										
29	1740	380										
30	1800	380										
31	1860	1000										
32	1920	1000										
33	1980	1000										
34	2040	1000										
35	2100	1000										
36	2160	1000										
37	2220	1000										
38	2280	1000										
39	2340	1000										
40	2400	1000										

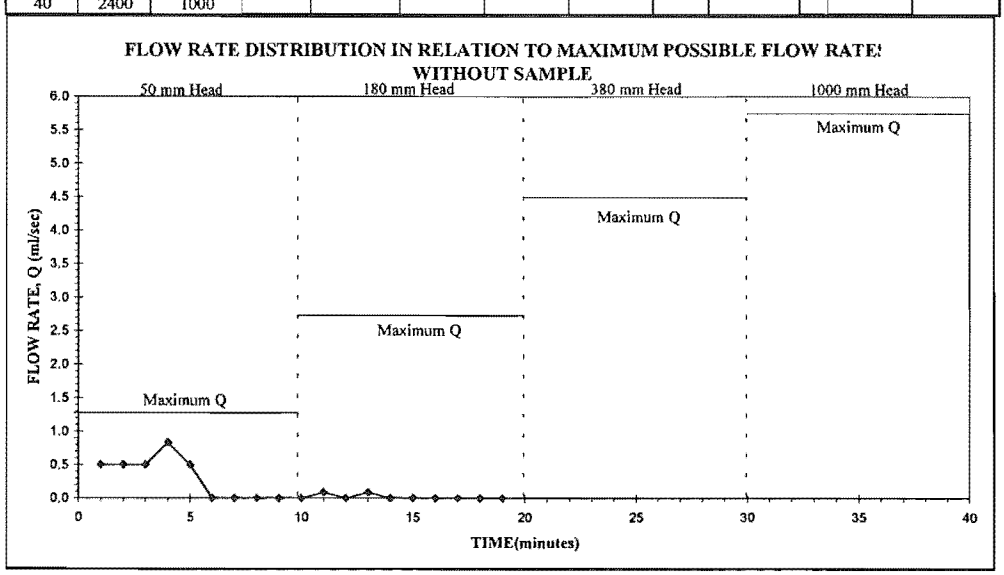

Table A4.11 Pinhole data sheet for sample 14.0/1/330 indicating colour, particles falling, flow rate, and flow rate distribution plot.

ERODIBILITY - PINHOLE TEST

Location :	Maungatapu Peninsula 330 Maungatapu Road	**Borehole / Pit Number :**	Face Log	**Comment :** The sample is completely saturated. The pinhole appears to be in-tacked the entire length of the sample, and has decreased in size due to swelling of walls of the pinhole. This has limited the Flow Rate. The falling particles are to small to see, but can be seen once settled
Soil Description :	Pumiceous Clayey Sand	**Sample Number :**	14.0 / 1 /330	
		Depth (m) :	14	
Test Method :				

Clock Time		Hydraulic Head, H (mm)	Rate Of Flow		Colour As Seen From Side Of Measuring Beaker					Particles Falling		
Minutes	Seconds		Volume (ml)	Flow Rate, Q (ml/sec)	Dark	Medium	Slight	Barely Visible	Completely Clear	None	Few	Many
1	60	50	50	0.83								
2	120	50	90	0.67								
3	180	50	140	0.83								
4	240	50	180	0.67								
5	300	50	220	0.67								
6	360	50	260	0.67								
7	420	50	300	0.67								
8	480	50	360	1.00								
9	540	50	405	0.75								
10	600	50	460	0.92								
11	660	180	480	0.33								
12	720	180	480	0.00								
13	780	180	490	0.17								
14	840	180	495	0.08								
15	900	180	495	0.00								
16	960	180	500	0.08								
17	1020	180	500	0.00								
18	1080	180	505	0.08								
19	1140	180	515	0.17								
20	1200	180	520	0.08								
21	1260	380	525	0.08								
22	1320	380	525	0.00								
23	1380	380	525	0.00								
24	1440	380	530	0.08								
25	1500	380	535	0.08								
26	1560	380	540	0.08								
27	1620	380	540	0.00								
28	1680	380	540	0.00								
29	1740	380	545	0.08								
30	1800	380	545	0.00								
31	1860	1000	550	0.08								
32	1920	1000	555	0.08								
33	1980	1000	560	0.08								
34	2040	1000	565	0.08								
35	2100	1000	570	0.08								
36	2160	1000	575	0.08								
37	2220	1000	580	0.08								
38	2280	1000	590	0.17								
39	2340	1000	595	0.08								
40	2400	1000	600	0.08								

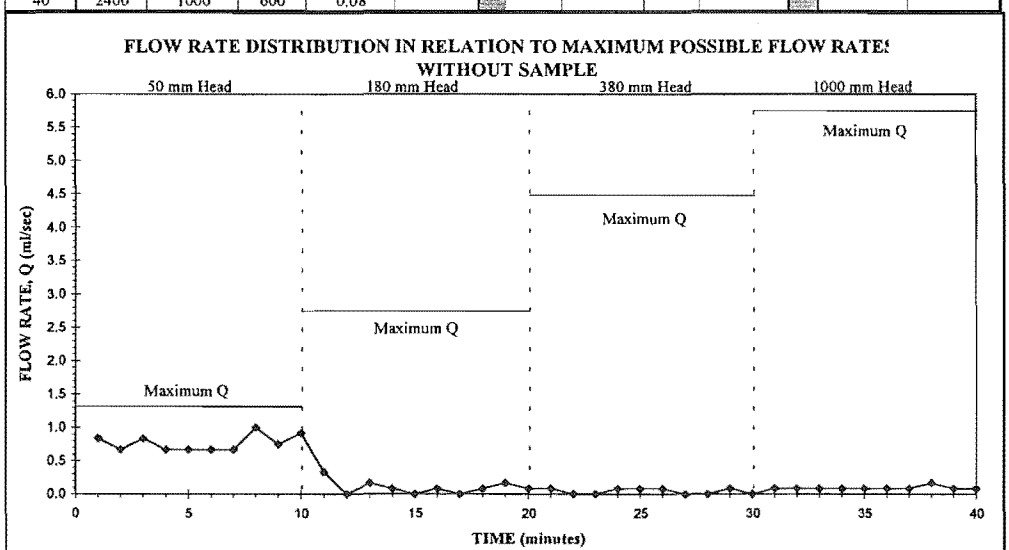

Table A4.12 Pinhole data sheet for sample 14.2/1/330 indicating colour, particles falling, flow rate, and flow rate distribution plot.

ERODIBILITY - PINHOLE TEST

Location :	Maungatapu Peninsula 330 Maungatapu Road	**Borehole / Pit Number :**	Face Log	**Comment :** A large chamber formed inside the sample approximately 15 - 16 mm diameter, running 30 mm in length. The exit point has eroded to a size of 4 × 2 mm. The sample is saturated.
Soil Description :	Pumiceous Clayey Sand	**Sample Number :**	14.2 / 1 330	
		Depth (m) :	14.2	
Test Method :				

Clock Time		Hydraulic Head, H (mm)	Rate Of Flow		Colour As Seen From Side Of Measuring Beaker					Particles Falling		
Minutes	Seconds		Volume (mL)	Flow Rate, Q (mL/sec)	Dark	Medium	Slight	Barely Visible	Completely Clear	None	Few	Many
1	60	50	65	1.08								
2	120	50	150	1.42								
3	180	50	210	1.00								
4	240	50	240	0.50								
5	300	50	275	0.58								
6	360	50	300	0.42								
7	420	50	330	0.50								
8	480	50	360	0.50								
9	540	50	385	0.42								
10	600	50	400	0.25								
11	660	180	430	0.50								
12	720	180	470	0.67								
13	780	180	490	0.33								
14	840	180	515	0.42								
15	900	180	525	0.17								
16	960	180	555	0.50								
17	1020	180	575	0.33								
18	1080	180	595	0.33								
19	1140	180	605	0.17								
20	1200	180	610	0.08								
21	1260	380	625	0.25								
22	1320	380	645	0.33								
23	1380	380	685	0.67								
24	1440	380	710	0.42								
25	1500	380	730	0.33								
26	1560	380	745	0.25								
27	1620	380	765	0.33								
28	1680	380	785	0.33								
29	1740	380	805	0.33								
30	1800	380	815	0.17								
31	1860	1000	845	0.50								
32	1920	1000	885	0.67								
33	1980	1000	925	0.67								
34	2040	1000	980	0.92								
35	2100	1000	1025	0.75								
36	2160	1000	1035	0.17								
37	2220	1000	1045	0.17								
38	2280	1000	1065	0.33								
39	2340	1000	1070	0.08								
40	2400	1000	1095	0.42								

Decrease in Flow Rate could be attributed to swelling or clogging of the pinhole

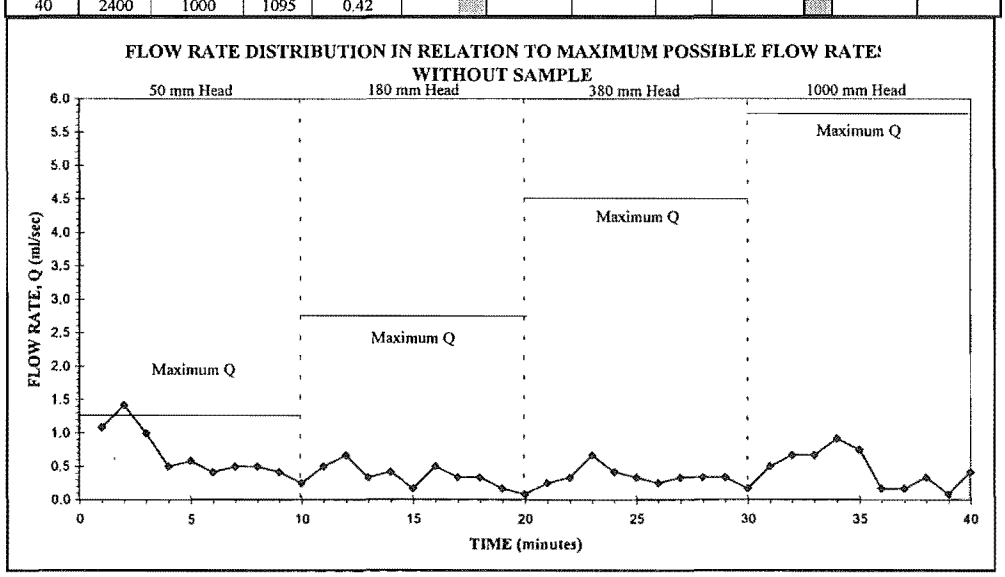

Table A4.13 Pinhole data sheet for sample 18.0/1/330 indicating colour, particles falling, flow rate, and flow rate distribution plot.

ERODIBILITY - PINHOLE TEST

Location :	Maungatapu Peninsula 330 Maungatapu Road	**Borehole / Pit Number :**	Face Log	**Comment :** 1/10 of the original sample has been left in the pinhole tube, the rest has washed out into the measuring cylinder
Soil Description :	Clean Sand where it appears that the Clay fraction has been washed out by the aquiferial flow of water	**Sample Number :**	18.0 / 1 / 330	
		Depth (m) :	18	
Test Method :				

Clock Time		Hydraulic Head, H (mm)	Rate Of Flow		Colour As Seen From Side Of Measuring Beaker					Particles Falling		
Minutes	Seconds		Volume (ml)	Flow Rate, Q (ml/sec)	Dark	Medium	Slight	Barely Visible	Completely Clear	None	Few	Many
1	60	50	90	1.50								
2	120	50	195	1.75								
3	180	50	300	1.75								
4	240	50	400	1.67								
5	300	50	500	1.67								
6	360	50	600	1.67								
7	420	50	700	1.67								
8	480	50	820	2.00								
9	540	50	925	1.75								
10	600	50	1045	2.00								
11	660	180	1275	3.83								
12	720	180	1340	1.08								
13	780	180	1475	2.25								
14	840	180	1600	2.08								
15	900	180	1750	2.50								
16	960	180	1900	2.50								
17	1020	180	2060	2.67								
18	1080	180	2200	2.33								
19	1140	180	2300	1.67								
20	1200	180	2450	2.50								
21	1260	380	2650	3.33								
22	1320	380	2875	3.75								
23	1380	380	3100	3.75								
24	1440	380	3310	3.50								
25	1500	380	3540	3.83								
26	1560	380	3775	3.92								
27	1620	380	4000	3.75								
28	1680	380	4240	4.00								
29	1740	380	4390	2.50								
30	1800	380	4605	3.58								
31	1860	1000	4890	4.75								
32	1920	1000	5210	5.33								
33	1980	1000	5555	5.75								
34	2040	1000	5900	5.75								
35	2100	1000	6190	4.83								
36	2160	1000	6510	5.33								
37	2220	1000	6860	5.83								
38	2280	1000	7200	5.67								
39	2340	1000	7540	5.67								
40	2400	1000	7865	5.42								

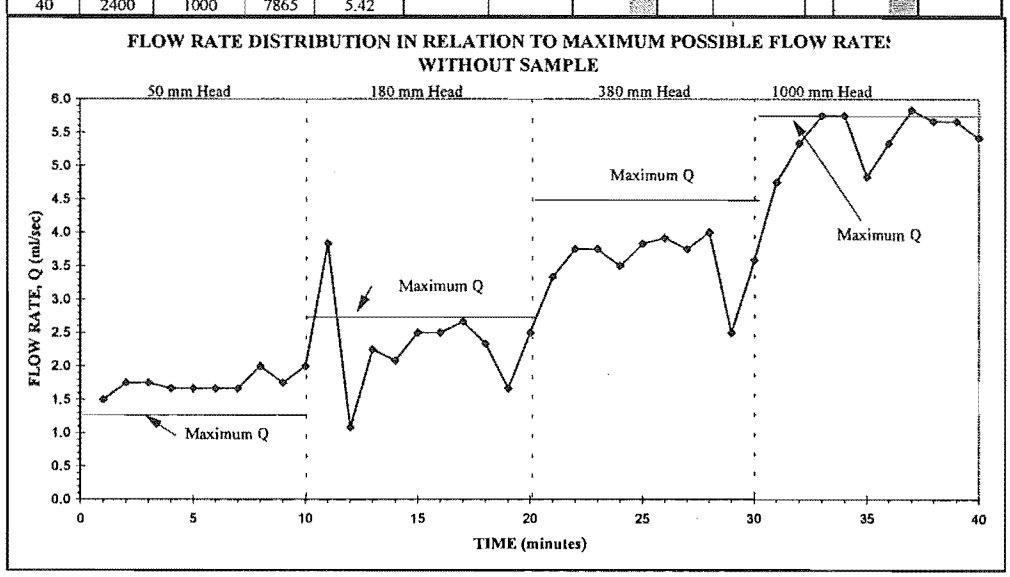

Table A4.14 Pinhole data sheet for sample 18.8/1/330 indicating colour, particles falling, flow rate, and flow rate distribution plot.

DISPERSIBILITY - PINHOLE TEST

Location :	Maungatapu Peninsula 85 Te Hono Street	**Borehole / Pit Number :**	Face Log	**Comment :** Half the sample has evacuate the pinhole tube entering the measuring cydrinda leaving the remaining sample completely saturated
Soil Description :	Saturated Clayey Sand	**Sample Number :**	18.8 / 1 / 85	
		Depth (m) :	18.8	
Test Method :				

Clock Time		Hydraulic Head, H (mm)	Rate Of Flow		Colour As Seen From Side Of Measuring Beaker					Particles Falling		
Minutes	Seconds		Volume (mL)	Flow Rate, Q (mL/sec)	Dark	Medium	Slight	Barely Visible	Completely Clear	None	Few	Many
1	60	50	50	0.83								
2	120	50	115	1.08								
3	180	50	185	1.17								
4	240	50	260	1.25								
5	300	50	330	1.17								
6	360	50	415	1.42								
7	420	50	490	1.25								
8	480	50	580	1.50								
9	540	50	640	1.00								
10	600	50	725	1.42								
11	660	180	855	2.17								
12	720	180	1000	2.42								
13	780	180	1120	2.00								
14	840	180	1280	2.67								
15	900	180	1440	2.67								
16	960	180	1600	2.67								
17	1020	180	1765	2.75								
18	1080	180	1980	3.58								
19	1140	180	2075	1.58								
20	1200	180	2240	2.75								
21	1260	380	2450	3.50								
22	1320	380	2675	3.75								
23	1380	380	2860	3.08								
24	1440	380	3070	3.50								
25	1500	380	3300	3.83								
26	1560	380	3525	3.75								
27	1620	380	3750	3.75								
28	1680	380	3985	3.92								
29	1740	380	4215	3.83								
30	1800	380	4450	3.92								
31	1860	1000	4760	5.17								
32	1920	1000	5080	5.33								
33	1980	1000	5400	5.33								
34	2040	1000	5750	5.83								
35	2100	1000	6150	6.67								
36	2160	1000	6415	4.42								
37	2220	1000	6690	4.58								
38	2280	1000	7030	5.67								
39	2340	1000	7375	5.75								
40	2400	1000	7700	5.42								

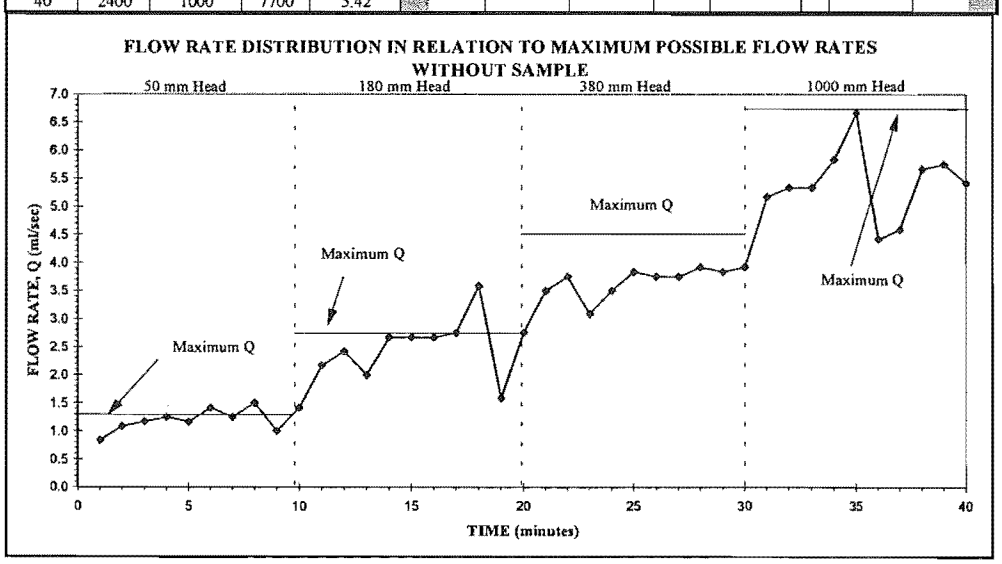

A4.6.2 Emerson Crumb Test

The Emerson Crumb test was modifed by Sherard et al. (1976) from Emerson (1966). It involves a easy to perform short duration testing time of a *in-situ* sample which excludes slaking as a criteria, Yetton (1986).

Method

A crumb of soil between 4-6 mm at *in-situ* moisture content is dropped into a beaker of distilled water and observed for a period of 10 minutes. The degree that the clay fraction forms a colloidal suspension within the water provides an indication of the dispersive nature of the soil. Four classification classes exist:

1. **Class 1**. No Reaction. Crumb may slake and run out on the bottom of the beaker in a flat pile, but no sign of cloudy water caused by colloids in suspension.

2. **Class 2**. Slight Reaction. Slight cloud in the water near the surface of the crumb.

3. **Class 3**. Moderate Reaction. Easily recognisable cloud of colloids in suspension around the sample.

4. **Class 4**. Strong Reaction. Colloidal cloud virtually obscures the whole bottom of the beaker and in extreme cases the whole beaker.

All results are presented in Chapter 4.

APPENDIX A4.9 Falling Head Permeability Testing

Permeability testing was conducted on one of three samples, 1) samples collected *in-situ* during fielding investigations, 2) *in-situ* samples obtained from a bulk sample, and 3) samples that were recompacted in a proctor mould according to NZS 4402: 1986 Test 4.1.1 at three different blow counts providing a range of densities.

Examining the grainsize distribution curves in Appendix 4.9 it was concluded that most of the samples consisted of a higher enough silt-clay content that a falling head permeability test could be conducted. The testing procedure followed was that outlined by Wykeham Farrance and the Department of Civil Engineering- University of Canterbury. Samples for testing were saturated for 3-7 days depending on the clay-silt content, with samples with a higher clay-silt percentages allowed to saturate for a longer time. The coefficient of permeability was obtained from the following furmula

$$k = \frac{aL}{At} Ln\left(\frac{h_0}{h}\right)$$

where

a = Standpipe area

A = Specimen area

t = Elapsed time

L = Specimen thickness

h = Height of water in standpipe

h_0 = Initial height of water in standpipe

Readings were taken at regular intervals and coefficients of permeabilies calculated. Results are as follows:

FALLING HEAD PERMEABILITY TESTING

Sample : 3.2-3.4 / 1 / 89 Post Rotoehu Ash Tephras
Test performed on a in-situ sample

Compaction Cell Bulk Density and Moisture Content Before testing

Bulk Density

Weight of base plate + cell + sample :	2156.4 g		
Weight of base plate + cell :	852.5 g		
Weight of sample :	1303.9 g		1.3039 kg
Sample Diameter :	100 mm	0.1 m	
Sample Length :	130 mm	0.13 m	
Sample Volume :	1021018 mm^3	0.00102 m^3	
Bulk Density :	1277 kg/m^3		

Moisture Content

Beaker + $Sample_{(wet)}$	169.95 g
Beaker + $Sample_{(dry)}$	148.17 g
Beaker	80.02 g
$Sample_{(wet)}$	89.93 g
$Sample_{(dry)}$	68.15 g
Moisture Content :	32 %

Permeability Cell Fully Saturated Bulk Density and Moisture Content After testing

Weight of base plate + cell + sample :	3403.1 g		
Weight of base plate + cell :	1878.8 g		
Weight of sample :	1524.3 g		1.5243 kg
Sample Diameter :	100 mm	0.1 m	
Sample Length :	130 mm	0.13 m	
Sample Volume :	1021018 mm^3	0.00102 m^3	
Bulk Density :	1493 kg/m^3		

Moisture Content

Beaker + $Sample_{(wet)}$	190.701 g
Beaker + $Sample_{(dry)}$	147.944 g
Beaker	80.036 g
$Sample_{(wet)}$	110.665 g
$Sample_{(dry)}$	67.908 g
Moisture Content :	63 %

Falling Head Permeability Test

Test :

Elapsed Time	Height (mm)	Permeability		Formula for Permeability	
0	1051			a=standpipe area	75.43 mm^2
12	61	4.9E-06	m/sec	A=specimen area	7853.98 mm^2
0	1051			t=elapsed time	sec
13	151	3.1E-06	m/sec	L=specimen thickness	130 mm
				h=height of water in	m

Test :

Time (min)	Height (mm)	Permeability			
0	1051			a=standpipe area	0.000075 m^2
13	151	3.1E-06	m/sec	A=specimen area	0.0079 m^2
0	1051			t=elasped time	sec
14	151	2.9E-06	m/sec	L=specimen thickness	0.13 m
				h=height of water in standpipe	m

Average Permeability :	3.5E-06	m/sec

FALLING HEAD PERMEABILITY TESTING

Sample : 2.55-2.75 / 1 / 330 Rotoehu Ash
Test performed on a in-situ sample

Compaction Cell Bulk Density and Moisture Content Before testing

Bulk Density

Weight of base plate + cell + sample :	2117.8 g		
Weight of base plate + cell :	857.6 g		
Weight of sample :	1260.2 g		1.2602 kg
Sample Diameter :	100 mm	0.1 m	
Sample Length :	130 mm	0.13 m	
Sample Volume :	1021018 mm^3	0.00102 m^3	
Bulk Density :	1234 kg/m^3		

Moisture Content

Beaker + $Sample_{(wet)}$	117.26 g
Beaker + $Sample_{(dry)}$	109.14 g
Beaker	57.63 g
$Sample_{(wet)}$	59.63 g
$Sample_{(dry)}$	51.51 g
Moisture Content :	16 %

Permeability Cell Fully Saturated Bulk Density and Moisture Content After testing

Weight of base plate + cell + sample :	3503.2 g		
Weight of base plate + cell :	1901.8 g		
Weight of sample :	1601.4 g		1.6014 kg
Sample Diameter :	100 mm	0.1 m	
Sample Length :	130 mm	0.13 m	
Sample Volume :	1021018 mm^3	0.00102 m^3	
Bulk Density :	1568 kg/m^3		

Moisture Content

Beaker + $Sample_{(wet)}$	198.878 g
Beaker + $Sample_{(dry)}$	168.135 g
Beaker	94.466 g
$Sample_{(wet)}$	104.412 g
$Sample_{(dry)}$	73.669 g
Moisture Content :	42 %

Falling Head Permeability Test

Test : 1

Elapsed Time	Height (mm)	Permeability		Formula for Permeability	
0	1051			a=standpipe area	75.43 mm^2
0.2	53	3.1E-04	m/sec	A=specimen area	7853.98 mm^2
				t=elapsed time	sec
				L=specimen thickness	130 mm
				h=height of water in	m

Test : 2

Time (min)	Height (mm)	Permeability			
0	1051			a=standpipe area	0.000075 m^2
0.2	53	3.1E-04	m/sec	A=specimen area	0.0079 m^2
				t=elasped time	sec
				L=specimen thickness	0.13 m
				h=height of water in standpipe	m

Average Permeability	3.1E-04 m/sec

FALLING HEAD PERMEABILITY TESTING

Sample : 4.3 - 5.0 / 1 / 85
Remoulded with a Blow Count:

Compaction Cell Bulk Density and Moisture Content Before testing

Bulk Density

Weight of base plate + cell + sample :	4599.8 g		
Weight of base plate + cell :	2979.5 g		
Weight of sample :	1620.3 g		1.6203 kg
Sample Diameter :	104.96 mm	0.10496 m	
Sample Length :	115.2 mm	0.1152 m	
Sample Volume :	996759 mm^3	0.00100 m^3	
Bulk Density :	1626 kg/m^3		

Moisture Content

Beaker + $Sample_{(wet)}$	120.15 g
Beaker + $Sample_{(dry)}$	116.18 g
Beaker	89.55 g
$Sample_{(wet)}$	30.60 g
$Sample_{(dry)}$	26.63 g
Moisture Content :	15 %

Permeability Cell Fully Saturated Bulk Density and Moisture Content After testing

Weight of base plate + cell + sample :	5964 g		
Weight of base plate + cell :	3951.2 g		
Weight of sample :	2012.8 g		2.0128 kg
Sample Diameter :	104.96 mm	0.10496 m	
Sample Length :	115.2 mm	0.1152 m	
Sample Volume :	996759 mm^3	0.00100 m^3	
Bulk Density :	2019 kg/m^3		

Moisture Content

Beaker + $Sample_{(wet)}$	138.98 g
Beaker + $Sample_{(dry)}$	128.86 g
Beaker	94.46 g
$Sample_{(wet)}$	44.52 g
$Sample_{(dry)}$	34.4 g
Moisture Content :	29 %

Falling Head Permeability Test

Test : 1

Elapsed Time	Height (mm)	Permeability	
0	1051		
1	992	9.7E-07	m/sec
5	790	7.6E-07	m/sec
10	587	5.0E-07	m/sec
20	287	6.0E-07	m/sec
30	79	7.2E-07	m/sec

Formula for Permeability

a=standpipe area	75.43 mm^2
A=specimen area	8652.42 mm^2
t=elapsed time	sec
L=specimen thickness	115.2 mm
h=height of water in	m

Test : 2

Time (min)	Height (mm)	Permeability	
0	1051		
1	986	1.1E-06	m/sec
5	767	8.4E-07	m/sec
10	555	5.4E-07	m/sec
20	251	6.6E-07	m/sec
30	52	8.8E-07	m/sec

a=standpipe area	0.000075 m^2
A=specimen area	0.0087 m^2
t=elasped time	sec
L=specimen thickness	0.1152 m
h=height of water in standpipe	m

Average Permeability	7.5E-07	m/sec

FALLING HEAD PERMEABILITY TESTING

Sample : 3.1 / 1 / 330 Palaeosol
Remoulded with a Blow Count: 15 Blows

Compaction Cell Bulk Density and Moisture Content Before testing

Bulk Density

Weight of base plate + cell + sample :	6403.7 g		
Weight of base plate + cell :	4747.5 g		
Weight of sample :	1656.2 g		1.6562 kg
Sample Diameter :	105 mm	0.105 m	
Sample Length :	115.3 mm	0.1153 m	
Sample Volume :	998384 mm^3	0.00100 m^3	
Bulk Density :	1659 kg/m^3		

Moisture Content

Beaker + $Sample_{(wet)}$	146.20 g
Beaker + $Sample_{(dry)}$	129.32 g
Beaker	94.45 g
$Sample_{(wet)}$	51.75 g
$Sample_{(dry)}$	34.87 g
Moisture Content :	48 %

Permeability Cell Fully Saturated Bulk Density and Moisture Content After testing

Weight of base plate + cell + sample :	5101.6 g		
Weight of base plate + cell :	3410.4 g		
Weight of sample :	1691.2 g		1.6912 kg
Sample Diameter :	105 mm	0.105 m	
Sample Length :	115.3 mm	0.1153 m	
Sample Volume :	998384 mm^3	0.00100 m^3	
Bulk Density :	1694 kg/m^3		

Moisture Content

Beaker + $Sample_{(wet)}$	126.47 g
Beaker + $Sample_{(dry)}$	116.27 g
Beaker	96.24 g
$Sample_{(wet)}$	30.23 g
$Sample_{(dry)}$	20.03 g
Moisture Content :	51 %

Falling Head Permeability Test

Test : 1

Elapsed Time	Height (mm)	Permeability	
0	1051		
1	861	1.7E-06	m/sec
2	703	8.7E-07	m/sec
4	471	8.6E-07	m/sec
8	227	7.8E-07	m/sec
15	59	7.7E-07	m/sec

Formula for Permeability

a=standpipe area	38.48 mm^2
A=specimen area	8659.01 mm^2
t=elapsed time	sec
L=specimen thickness	115.3 mm
h=height of water in	m

Test : 2

Time (min)	Height (mm)	Permeability	
0	1051		
1	897	1.4E-06	m/sec
2	761	7.0E-07	m/sec
4	543	7.2E-07	m/sec
8	286	6.8E-07	m/sec
15	74	7.7E-07	m/sec

a=standpipe area	0.000038 m^2
A=specimen area	0.0087 m^2
t=elasped time	sec
L=specimen thickness	0.1153 m
h=height of water in	m
standpipe	

Average Permeability	9.2E-07	m/sec

FALLING HEAD PERMEABILITY TESTING

Sample : 3.1 / 1 / 330 Palaeosol
Remoulded with a Blow Count: 27 Blows

Compaction Cell Bulk Density and Moisture Content Before testing

Bulk Density

Weight of base plate + cell + sample :	6396.6 g		
Weight of base plate + cell :	4747.5 g		
Weight of sample :	1649.1 g		1.6491 kg
Sample Diameter :	104.88 mm	0.10488 m	
Sample Length :	115.06 mm	0.11506 m	
Sample Volume :	994030 mm^3	0.00099 m^3	
Bulk Density :	1659 kg/m^3		

Moisture Content

Beaker + $Sample_{(wet)}$	177.65 g
Beaker + $Sample_{(dry)}$	149.11 g
Beaker	94.45 g
$Sample_{(wet)}$	83.20 g
$Sample_{(dry)}$	54.66 g
Moisture Content :	52 %

Permeability Cell Fully Saturated Bulk Density and Moisture Content After testing

Weight of base plate + cell + sample :	5080.1 g		
Weight of base plate + cell :	3408.4 g		
Weight of sample :	1671.7 g		1.6717 kg
Sample Diameter :	104.88 mm	0.10488 m	
Sample Length :	115.06 mm	0.11506 m	
Sample Volume :	994030 mm^3	0.00099 m^3	
Bulk Density :	1682 kg/m^3		

Moisture Content

Beaker + $Sample_{(wet)}$	72.68 g
Beaker + $Sample_{(dry)}$	62.57 g
Beaker	44.23 g
$Sample_{(wet)}$	28.45 g
$Sample_{(dry)}$	18.34 g
Moisture Content :	55 %

Falling Head Permeability Test

Test : 1

Elasped Time	Height (mm)	Permeability	
0	997		
95	743	2.6E-08	m/sec
120	675	6.8E-09	m/sec
390	365	1.3E-08	m/sec

Test : 2

Time (min)	Height (mm)	Permeability	
0	1003		
180	561	2.8E-08	m/sec
780	201	1.1E-08	m/sec

Formula for Permeability

a=standpipe area	38.48 mm^2
A=specimen area	8639.23 mm^2
t=elasped time	sec
L=specimen thickness	115.06 mm
h=height of water in	m
a=standpipe area	0.000038 m^2
A=specimen area	0.0086 m^2
t=elasped time	sec
L=specimen thickness	0.11506 m
h=height of water in	m

Average Permeability	1.7E-08	m/sec

FALLING HEAD PERMEABILITY TESTING

Sample : 3.1 / 1 / 330
Remoulded with a Blow Count: 40 Blows

Compaction Cell Bulk Density and Moisture Content Before testing

Bulk Density

Weight of base plate + cell + sample :	6394.7 g		
Weight of base plate + cell :	4747.5 g		
Weight of sample :	1647.2 g		1.6472 kg
Sample Diameter :	104.9 mm	0.1049 m	
Sample Length :	112.94 mm	0.11294 m	
Sample Volume :	976087 mm^3	0.00098 m^3	
Bulk Density :	1688 kg/m^3		

Moisture Content

Beaker + $Sample_{(wet)}$	159.51 g
Beaker + $Sample_{(dry)}$	137.57 g
Beaker	89.52 g
$Sample_{(wet)}$	69.99 g
$Sample_{(dry)}$	48.05 g
Moisture Content :	46 %

Permeability Cell Fully Saturated Bulk Density and Moisture Content After testing

Weight of base plate + cell + sample :	5086.2 g		
Weight of base plate + cell :	3410.4 g		
Weight of sample :	1675.8 g		1.6758 kg
Sample Diameter :	104.9 mm	0.1049 m	
Sample Length :	112.94 mm	0.11294 m	
Sample Volume :	976087 mm^3	0.00098 m^3	
Bulk Density :	1717 kg/m^3		

Moisture Content

Beaker + $Sample_{(wet)}$	180.91 g
Beaker + $Sample_{(dry)}$	151.78 g
Beaker	89.53 g
$Sample_{(wet)}$	91.38 g
$Sample_{(dry)}$	62.25 g
Moisture Content :	47 %

Falling Head Permeability Test

Test : 1

Elapsed Time	Height (mm)	Permeability	
0	1051		
388	1043	1.7E-10	m/sec
1549	1001	2.2E-10	m/sec
2760	979	6.7E-11	m/sec
			m/sec
			m/sec

Formula for Permeability

a=standpipe area	38.48 mm^2
A=specimen area	8642.53 mm^2
t=elapsed time	sec
L=specimen thickness	112.94 mm
h=height of water in	m

Test : 2

Time (min)	Height (mm)	Permeability	
0	811		
793	801	1.3E-10	m/sec
4039	724	2.1E-10	m/sec
5083	703	4.9E-11	m/sec
			m/sec
			m/sec

a=standpipe area	0.000038 m^2
A=specimen area	0.0086 m^2
t=elasped time	sec
L=specimen thickness	0.11294 m
h=height of water in standpipe	m

Average Permeability	1.4E-10	m/sec

FALLING HEAD PERMEABILITY TESTING

Sample : 8.2 / 1 / 85 Hamilton Ash
Remoulded with a Blow Count: 15 Blows

Compaction Cell Bulk Density and Moisture Content Before testing

Bulk Density

Weight of base plate + cell + sample :	4354.9 g		
Weight of base plate + cell :	2978.2 g		
Weight of sample :	1376.7 g		1.3767 kg
Sample Diameter :	105 mm	0.105 m	
Sample Length :	115.5 mm	0.1155 m	
Sample Volume :	1000116 mm^3	0.00100 m^3	
Bulk Density :	1377 kg/m^3		

Moisture Content

Beaker + $Sample_{(wet)}$	135.01 g
Beaker + $Sample_{(dry)}$	115.65 g
Beaker	89.53 g
$Sample_{(wet)}$	45.48 g
$Sample_{(dry)}$	26.12 g
Moisture Content :	74 %

Permeability Cell Fully Saturated Bulk Density and Moisture Content After testing

Weight of base plate + cell + sample :	3957.9 g		
Weight of base plate + cell :	2519 g		
Weight of sample :	1438.9 g		1.4389 kg
Sample Diameter :	105 mm	0.105 m	
Sample Length :	115.5 mm	0.1155 m	
Sample Volume :	1000116 mm^3	0.00100 m^3	
Bulk Density :	1439 kg/m^3		

Moisture Content

Beaker + $Sample_{(wet)}$	140.24 g
Beaker + $Sample_{(dry)}$	118.1 g
Beaker	89.53 g
$Sample_{(wet)}$	50.71 g
$Sample_{(dry)}$	28.57 g
Moisture Content :	77 %

Falling Head Permeability Test

Test : 1

Elapsed Time	Height (mm)	Permeability	
0	1051		
0.25	903	9.3E-06	m/sec
0.5	771	4.8E-06	m/sec
1	557	5.0E-06	m/sec
2	263	5.7E-06	m/sec
5	78	3.7E-06	m/sec

Formula for Permeability

a=standpipe area	75.43 mm^2
A=specimen area	8659.01 mm^2
t=elapsed time	sec
L=specimen thickness	115.5 mm
h=height of water in	m

Test : 2

Time (min)	Height (mm)	Permeability	
0	1051		
0.25	967	5.1E-06	m/sec
0.5	898	2.3E-06	m/sec
1	755	2.7E-06	m/sec
2	535	2.6E-06	m/sec
5	131	4.3E-06	m/sec

a=standpipe area	0.000069 m^2
A=specimen area	0.0087 m^2
t=elasped time	sec
L=specimen thickness	0.1155 m
h=height of water in standpipe	m

Average Permeability	4.6E-06	m/sec

FALLING HEAD PERMEABILITY TESTING

Sample : 8.2 / 1 / 85 Hamilton Ash
Remoulded with a Blow Count: 27 Blows

Compaction Cell Bulk Density and Moisture Content Before testing

Bulk Density

Weight of base plate + cell + sample :	4401.9 g		
Weight of base plate + cell :	2979.5 g		
Weight of sample :	1422.4 g		1.4224 kg
Sample Diameter :	105 mm	0.105 m	
Sample Length :	115.3 mm	0.1153 m	
Sample Volume :	998384 mm^3	0.00100 m^3	
Bulk Density :	1425 kg/m^3		

Moisture Content

Beaker + $Sample_{(wet)}$	138.57 g
Beaker + $Sample_{(dry)}$	118.25 g
Beaker	94.45 g
$Sample_{(wet)}$	44.12 g
$Sample_{(dry)}$	23.80 g
Moisture Content :	85 %

Permeability Cell Fully Saturated Bulk Density and Moisture Content After testing

Weight of base plate + cell + sample :	3961.3 g		
Weight of base plate + cell :	2521 g		
Weight of sample :	1440.3 g		1.4403 kg
Sample Diameter :	105 mm	0.105 m	
Sample Length :	115.3 mm	0.1153 m	
Sample Volume :	998384 mm^3	0.00100 m^3	
Bulk Density :	1443 kg/m^3		

Moisture Content

Beaker + $Sample_{(wet)}$	66.33 g
Beaker + $Sample_{(dry)}$	56.06 g
Beaker	44.22 g
$Sample_{(wet)}$	22.11 g
$Sample_{(dry)}$	11.84 g
Moisture Content :	87 %

Falling Head Permeability Test

Test : 1

Elapsed Time (min)	Height (mm)	Permeability	
0	1041		
35	938	5.0E-08	m/sec
105	762	3.3E-08	m/sec
145	673	1.4E-08	m/sec

Test : 2

Time (min)	Height (mm)	Permeability	
0	1001		
36	909	4.5E-08	m/sec
82	805	2.5E-08	m/sec
137	692	1.8E-08	
465	211	4.3E-08	

Formula for Permeability

a=standpipe area	75.43 mm^2
A=specimen area	8659.01 mm^2
t=elapsed time	sec
L=specimen thickness	115.3 mm
h=height of water in	m

a=standpipe area	0.000075 m^2
A=specimen area	0.0087 m^2
t=elasped time	sec
L=specimen thickness	0.1153 m
h=height of water in	m

standpipe

Average Permeability = 3.3E-08 m/sec

FALLING HEAD PERMEABILITY TESTING

Sample : 8.2 / 1 / 85 Hamilton Ash
Remoulded with a Blow Count: 40 Blows

Compaction Cell Bulk Density and Moisture Content Before testing

Bulk Density

Weight of base plate + cell + sample :	4445.6 g		
Weight of base plate + cell :	2975.3 g		
Weight of sample :	1470.3 g		1.4703 kg
Sample Diameter :	105 mm	0.105 m	
Sample Length :	115.5 mm	0.1155 m	
Sample Volume :	1000116 mm^3	0.00100 m^3	
Bulk Density :	1470 kg/m^3		

Moisture Content

Beaker + $Sample_{(wet)}$	140.82 g
Beaker + $Sample_{(dry)}$	119.27 g
Beaker	89.54 g
$Sample_{(wet)}$	51.28 g
$Sample_{(dry)}$	29.73 g
Moisture Content :	72 %

Permeability Cell Fully Saturated Bulk Density and Moisture Content After testing

Weight of base plate + cell + sample :	4019.8 g		
Weight of base plate + cell :	2516.3 g		
Weight of sample :	1503.5 g		1.5035 kg
Sample Diameter :	105 mm	0.105 m	
Sample Length :	115.5 mm	0.1155 m	
Sample Volume :	1000116 mm^3	0.00100 m^3	
Bulk Density :	1503 kg/m^3		

Moisture Content

Beaker + $Sample_{(wet)}$	142.33 g
Beaker + $Sample_{(dry)}$	115.54 g
Beaker	80.02 g
$Sample_{(wet)}$	62.31 g
$Sample_{(dry)}$	35.52 g
Moisture Content :	75 %

Falling Head Permeability Test

Test : 1

Elapsed Time	Height (mm)	Permeability	
0	1051		
0.5	1011	1.3E-06	m/sec
1	975	6.1E-07	m/sec
2	910	5.8E-07	m/sec
5	759	6.1E-07	m/sec
10	583	4.4E-07	m/sec
20	357	4.1E-07	m/sec

Test : 2

Time (min)	Height (mm)	Permeability	
0	1051		
1	999	8.5E-07	m/sec
2	951	4.1E-07	m/sec
5	820	5.0E-07	m/sec
10	644	4.1E-07	m/sec
20	391	4.2E-07	m/sec
40	129	4.6E-07	m/sec

Formula for Permeability

a=standpipe area	75.43 mm^2
A=specimen area	8659.01 mm^2
t=elapsed time	sec
L=specimen thickness	115.5 mm
h=height of water in	m

a=standpipe area	0.000075 m^2
A=specimen area	0.0087 m^2
t=elasped time	sec
L=specimen thickness	0.1155 m
h=height of water in	m

standpipe

Average Permeability	5.8E-07	m/sec

FALLING HEAD PERMEABILITY TESTING

Sample : 10.3-10.5 / 1 / 330 Pahoia Tephras
Test performed on a in-situ sample

Compaction Cell Bulk Density and Moisture Content Before testing

Bulk Density

Weight of base plate + cell + sample :	2484.4 g		
Weight of base plate + cell :	850.2 g		
Weight of sample :	1634.2 g		1.6342 kg
Sample Diameter :	100 mm	0.1 m	
Sample Length :	130 mm	0.13 m	
Sample Volume :	1021018 mm^3	0.00102 m^3	
Bulk Density :	1601 kg/m^3		

Moisture Content

Beaker + $Sample_{(wet)}$	192.90 g
Beaker + $Sample_{(dry)}$	158.91 g
Beaker	89.54 g
$Sample_{(wet)}$	103.36 g
$Sample_{(dry)}$	69.37 g
Moisture Content :	49 %

Permeability Cell Fully Saturated Bulk Density and Moisture Content After testing

Weight of base plate + cell + sample :	3543.2 g		
Weight of base plate + cell :	1892.7 g		
Weight of sample :	1650.5 g		1.6505 kg
Sample Diameter :	100 mm	0.1 m	
Sample Length :	130 mm	0.13 m	
Sample Volume :	1021018 mm^3	0.00102 m^3	
Bulk Density :	1617 kg/m^3		

Moisture Content

Beaker + $Sample_{(wet)}$	195.896 g
Beaker + $Sample_{(dry)}$	159.15 g
Beaker	89.53 g
$Sample_{(wet)}$	106.366 g
$Sample_{(dry)}$	69.62 g
Moisture Content :	53 %

Falling Head Permeability Test

Test : 1

Elapsed Time	Height (mm)	Permeability		Formula for Permeability	
0	1051			a=standpipe area	38.48 mm^2
45	729	8.6E-08	m/sec	A=specimen area	7853.98 mm^2
75	553	3.9E-08	m/sec	t=elapsed time	sec
120	351	4.0E-08	m/sec	L=specimen thickness	130 mm
195	99	6.9E-08	m/sec	h=height of water in standpipe	m

Test : 2

Time (min)	Height (mm)	Permeability			
0	1051			a=standpipe area	0.000038 m^2
60	669	8.0E-08	m/sec	A=specimen area	0.0079 m^2
120	343	5.9E-08	m/sec	t=elasped time	sec
180	137	5.4E-08	m/sec	L=specimen thickness	0.13 m
				h=height of water in standpipe	m

Average Permeability	6.1E-08	m/sec

FALLING HEAD PERMEABILITY TESTING

Sample : 16 / 1 / 85
Test performed on a in-situ sample

Compaction Cell Bulk Density and Moisture Content Before testing

Bulk Density

Weight of base plate + cell + sample :	2641.7 g		
Weight of base plate + cell :	853.8 g		
Weight of sample :	1787.9 g		1.7879 kg
Sample Diameter :	130 mm	0.13 m	
Sample Length :	99.92 mm	0.09992 m	
Sample Volume :	1326261 mm^3	0.00133 m^3	
Bulk Density :	1348 kg/m^3		

Moisture Content

Beaker + $Sample_{(wet)}$	201.09 g
Beaker + $Sample_{(dry)}$	165.26 g
Beaker	94.45 g
$Sample_{(wet)}$	106.64 g
$Sample_{(dry)}$	70.81 g
Moisture Content :	51 %

Permeability Cell Fully Saturated Bulk Density and Moisture Content After testing

Weight of base plate + cell + sample :	3649.9 g		
Weight of base plate + cell :	1879.2 g		
Weight of sample :	1770.7 g		1.7707 kg
Sample Diameter :	130 mm	0.13 m	
Sample Length :	99.92 mm	0.09992 m	
Sample Volume :	1326261 mm^3	0.00133 m^3	
Bulk Density :	1335 kg/m^3		

Moisture Content

Beaker + $Sample_{(wet)}$	169.66 g
Beaker + $Sample_{(dry)}$	149.05 g
Beaker	96.24 g
$Sample_{(wet)}$	73.42 g
$Sample_{(dry)}$	52.81 g
Moisture Content :	39 %

Falling Head Permeability Test

Test : 1

Elapsed Time	Height (mm)	Permeability	
0	1051		
5	941	1.1E-07	m/sec
10	841	5.4E-08	m/sec
20	664	5.7E-08	m/sec
40	386	6.5E-08	m/sec
60	183	6.0E-08	m/sec

Test : 2

Time (min)	Height (mm)	Permeability	
0	1051		
5	880	1.7E-07	m/sec
10	819	3.5E-08	m/sec
20	632	6.3E-08	m/sec
40	344	7.3E-08	m/sec
60	142	7.1E-08	m/sec

Formula for Permeability

a=standpipe area	38.48 mm^2
A=specimen area	13273.23 mm^2
t=elapsed time	sec
L=specimen thickness	99.92 mm
h=height of water in	m

a=standpipe area	0.000038 m^2
A=specimen area	0.0133 m^2
t=elasped time	sec
L=specimen thickness	0.09992 m
h=height of water in standpipe	m

Average Permeability	7.6E-08	m/sec

FALLING HEAD PERMEABILITY TESTING

Sample : 13 - Sandy unit situated between cross-bedded sequence and upper aquitard
Test performed on a in-situ sample

Compaction Cell Bulk Density and Moisture Content Before testing

Bulk Density

Weight of base plate + cell + sample :	2283.8 g		
Weight of base plate + cell :	851.7 g		
Weight of sample :	1432.1 g		1.4321 kg
Sample Diameter :	100.14 mm	0.10014 m	
Sample Length :	120.04 mm	0.12004 m	
Sample Volume :	945434 mm^3	0.00095 m^3	
Bulk Density :	1515 kg/m^3		

Moisture Content

Beaker + $Sample_{(wet)}$	50.45 g
Beaker + $Sample_{(dry)}$	40.24 g
Beaker	24.72 g
$Sample_{(wet)}$	25.73 g
$Sample_{(dry)}$	15.52 g
Moisture Content :	66 %

Permeability Cell Fully Saturated Bulk Density and Moisture Content After testing

Weight of base plate + cell + sample :	3322.4 g		
Weight of base plate + cell :	1877.1 g		
Weight of sample :	1445.3 g		1.4453 kg
Sample Diameter :	100.14 mm	0.10014 m	
Sample Length :	120.04 mm	0.12004 m	
Sample Volume :	945434 mm^3	0.00095 m^3	
Bulk Density :	1529 kg/m^3		

Moisture Content

Beaker + $Sample_{(wet)}$	168.53 g
Beaker + $Sample_{(dry)}$	137.37 g
Beaker	89.51 g
$Sample_{(wet)}$	79.02 g
$Sample_{(dry)}$	47.86 g
Moisture Content :	65 %

Falling Head Permeability Test

Test : 1

Elapsed Time	Height (mm)	Permeability	
0	1051		
2	990	5.7E-07	m/sec
5	907	3.4E-07	m/sec
10	781	2.9E-07	m/sec
20	575	2.9E-07	m/sec
40	307	3.0E-07	m/sec
60	156	2.2E-07	

Test : 2

Time (min)	Height (mm)	Permeability	
0	1051		
5	927	4.8E-07	m/sec
10	818	2.4E-07	m/sec
20	639	2.4E-07	m/sec
43	365	2.5E-07	m/sec
60	241	1.3E-07	m/sec

Formula for Permeability

a=standpipe area	75.43	mm^2
A=specimen area	7875.99	mm^2
t=elapsed time		sec
L=specimen thickness	120.04	mm
h=height of water in standpipe		m

a=standpipe area	0.000075	m^2
A=specimen area	0.0079	m^2
t=elasped time		sec
L=specimen thickness	0.12004	m
h=height of water in standpipe		m

Average Permeability =	3.1E-07	m/sec

FALLING HEAD PERMEABILITY TESTING

Sample : 17.1 / 1 / 330 Located within the aquiferial zone
Test performed on a in-situ sample

Compaction Cell Bulk Density and Moisture Content Before testing

Bulk Density

Weight of base plate + cell + sample :	2693.5 g		
Weight of base plate + cell :	1603.4 g		
Weight of sample :	1090.1 g		1.0901 kg
Sample Diameter :	130 mm	0.13 m	
Sample Length :	99.92 mm	0.09992 m	
Sample Volume :	1326261 mm^3	0.00133 m^3	
Bulk Density :	822 kg/m^3		

Moisture Content

Beaker + $Sample_{(wet)}$	48.88 g
Beaker + $Sample_{(dry)}$	43.36 g
Beaker	27.72 g
$Sample_{(wet)}$	21.16 g
$Sample_{(dry)}$	15.63 g
Moisture Content :	35 %

Permeability Cell Fully Saturated Bulk Density and Moisture Content After testing

Weight of base plate + cell + sample :	2920 g		
Weight of base plate + cell :	1603.4 g		
Weight of sample :	1316.6 g		1.3166 kg
Sample Diameter :	130 mm	0.13 m	
Sample Length :	99.92 mm	0.09992 m	
Sample Volume :	1326261 mm^3	0.00133 m^3	
Bulk Density :	993 kg/m^3		

Moisture Content

Beaker + $Sample_{(wet)}$	202.26 g
Beaker + $Sample_{(dry)}$	146.173 g
Beaker	62.515 g
$Sample_{(wet)}$	139.745 g
$Sample_{(dry)}$	83.658 g
Moisture Content :	67 %

Falling Head Permeability Test

Test : 1

Elasped Time	Height (mm)	Permeability		Formula for Permeability	
0	1600			a=standpipe area	132.73 mm^2
0.5	1250	8.2E-06	m/sec	A=specimen area	13273.23 mm^2
1	1095	2.2E-06	m/sec	t=elasped time	sec
2	860	2.0E-06	m/sec	L=specimen thickness	99.92 mm
4	530	2.0E-06	m/sec	h=height of water in	m

Test : 2

Time (min)	Height (mm)	Permeability			
0	1600			a=standpipe area	0.000133 m^2
0.5	1280	7.4E-06	m/sec	A=specimen area	0.0133 m^2
1	1145	1.9E-06	m/sec	t=elasped time	sec
2	915	1.9E-06	m/sec	L=specimen thickness	0.09992 m
4	600	1.8E-06	m/sec	h=height of water in standpipe	m

Average Permeability	3.4E-06	m/sec

FALLING HEAD PERMEABILITY TESTING

Sample : 13 - Sandy unit situated between cross-bedded sequence and upper aquitard
Test performed on a in-situ sample

Compaction Cell Bulk Density and Moisture Content Before testing

Bulk Density

Weight of base plate + cell + sample :	2283.8 g		
Weight of base plate + cell :	851.7 g		
Weight of sample :	1432.1 g		1.4321 kg
Sample Diameter :	100.14 mm	0.10014 m	
Sample Length :	120.04 mm	0.12004 m	
Sample Volume :	945434 mm^3	0.00095 m^3	
Bulk Density :	1515 kg/m^3		

Moisture Content

Beaker + $Sample_{(wet)}$	50.45 g
Beaker + $Sample_{(dry)}$	40.24 g
Beaker	24.72 g
$Sample_{(wet)}$	25.73 g
$Sample_{(dry)}$	15.52 g
Moisture Content :	66 %

Permeability Cell Fully Saturated Bulk Density and Moisture Content After testing

Weight of base plate + cell + sample :	3322.4 g		
Weight of base plate + cell :	1877.1 g		
Weight of sample :	1445.3 g		1.4453 kg
Sample Diameter :	100.14 mm	0.10014 m	
Sample Length :	120.04 mm	0.12004 m	
Sample Volume :	945434 mm^3	0.00095 m^3	
Bulk Density :	1529 kg/m^3		

Moisture Content

Beaker + $Sample_{(wet)}$	168.53 g
Beaker + $Sample_{(dry)}$	137.37 g
Beaker	89.51 g
$Sample_{(wet)}$	79.02 g
$Sample_{(dry)}$	47.86 g
Moisture Content :	65 %

Falling Head Permeability Test

Test : 1

Elapsed Time	Height (mm)	Permeability	
0	1051		
2	990	5.7E-07	m/sec
5	907	3.4E-07	m/sec
10	781	2.9E-07	m/sec
20	575	2.9E-07	m/sec
40	307	3.0E-07	m/sec
60	156	2.2E-07	

Test : 2

Time (min)	Height (mm)	Permeability	
0	1051		
5	927	4.8E-07	m/sec
10	818	2.4E-07	m/sec
20	639	2.4E-07	m/sec
43	365	2.5E-07	m/sec
60	241	1.3E-07	m/sec

Formula for Permeability

a=standpipe area	75.43 mm^2
A=specimen area	7875.99 mm^2
t=elapsed time	sec
L=specimen thickness	120.04 mm
h=height of water in	m

a=standpipe area	0.000075 m^2
A=specimen area	0.0079 m^2
t=elasped time	sec
L=specimen thickness	0.12004 m
h=height of water in standpipe	m

Average Permeability =	3.1E-07	m/sec